

ART 14

FOR  
REFERENCE ONLY



# Derivation of fatality probability functions for occupants of buildings subject to blast loads

Phases 1, 2 & 3

Prepared by  
**WS Atkins Science & Technology**  
for the Health and Safety Executive

CONTRACT RESEARCH REPORT

147/1997



# **Derivation of fatality probability functions for occupants of buildings subject to blast loads**

**Phase 1**

**R M Jeffries, S J Hunt & L Gould**  
WS Atkins Science & Technology  
Woodcote Grove  
Ashley Road  
Epsom  
Surrey  
KT18 5BW

The UK Health and Safety Executive (HSE) are often consulted by local planning authorities on the safety aspects of proposed developments in the vicinity of industrial plant and in addition give advice on the siting of new plant with major hazard potential. A quantified risk assessment approach is used, which may include consideration of the effects of explosions which can cause injury to people through direct effects on the body, secondary effects such as the impact of fragments or partial/total building collapse of buildings or tertiary body translation effects. To date the fatalities have been predicted using a probit based on World War II bomb data. The objective of this project is to develop a procedure for assessing the vulnerability of occupants of different types of buildings subject to overpressures produced from vapour cloud explosions. A methodology has been developed for deriving generic fatality probability functions for different building types based on the primary structural characteristics of the building. This report details Phase 1 of the project and includes an outline of the literature search performed and the preliminary development of the methodology.

This report and the work it describes were funded by the Health and Safety Executive. Its contents, including any opinions and/or conclusions expressed, are those of the authors alone and do not necessarily reflect HSE policy.

**HSE BOOKS**

© Crown copyright 1997  
Applications for reproduction should be made in writing to:  
Copyright Unit, Her Majesty's Stationery Office,  
St Clements House, 2-16 Colegate, Norwich NR3 1BQ

*First published 1997*

ISBN 0 7176 1434 4

All rights reserved. No part of this publication may be reproduced, stored in a retrieval system, or transmitted in any form or by any means (electronic, mechanical, photocopying, recording or otherwise) without the prior written permission of the copyright owner.

## **Note to Readers**

This document is an interim report outlining the results of the first phase of an exercise to develop a methodology for estimating the fatality probability for the occupants of buildings subject to explosions. It was written prior to the completion of the later phases of the project and has been issued in order to make the results of the work speedily available to a wider audience, in advance of the publication of the definitive final report produced at the end of the project. Consequently, many of the results and conclusions are presented in a context which lacks the perspective afforded by the later phases of the work. The contents should therefore be viewed as preliminary information and should not be accredited with the authority of a final report.

## CREDITS

Grateful acknowledgment is made to the following for permission to reproduce material used in creating figures in this report.

**Figure 3.1.** Smith, P.D. and Hetherington, J.G., 'Blast and Ballistic Loading of Structures', Butterworth - Heinemann Ltd. Copyright © Butterworth-Heinemann Ltd. 1994. Reproduced by permission of the author.

**Figure 3.2** Johnson, N.F., in 'The protection of Buildings against Terrorism and Disorder - Discussion', Proc. Instn Civ. Engrs Structs & Bldgs, 1994, 104, Aug, 343-350. Copyright © 1994 The authors and the Institution of Civil Engineers. Reproduced by permission of the author.

**Figure 6.1** Van den Berg, A.C., in 'Guidelines for Evaluating the Characteristics of Vapor Cloud Explosions, Flash Fires and BLEVEs', Center for Chemical Process Safety of the American Institute of Chemical Engineers. Copyright © 1994 American Institute of Chemical Engineers. Reproduced by permission of the author.

**Figure 7.1** Smith, P.D. and Hetherington, J.G., 'Blast and Ballistic Loading of Structures', Butterworth - Heinemann Ltd. Copyright © Butterworth-Heinemann Ltd. 1994. Reproduced by permission of the author.

**Figure 8.2** Biggs, J.M., 'Introduction to Structural Dynamics', McGraw-Hill Inc. Copyright © 1964 McGraw-Hill Inc. Reproduced by permission of McGraw-Hill Inc.

# CONTENTS

		<b>Page</b>
1	INTRODUCTION .....	1
2	PROJECT PROGRAMME .....	3
	2.1 Phase 1 .....	3
	2.2 Phases 2 and 3 .....	4
	2.3 Phase 4 .....	4
3	LITERATURE REVIEW .....	7
	3.1 Sources of data .....	7
	3.2 Effects on humans .....	7
	3.3 Structural loading .....	12
	3.4 Structural response .....	17
	3.5 Conclusions .....	28
4	GENERAL PROCEDURE .....	30
5	BUILDING CATEGORISATION .....	34
6	BLAST OVERPRESSURE .....	48
7	STRUCTURAL LOADS .....	53
	7.1 External loading on the building .....	53
	7.2 Building internal pressure .....	58
8	DYNAMIC RESPONSE .....	62
	8.1 Fundamental natural frequency .....	62
	8.2 Dynamic collapse load .....	63
	8.3 Ductility ratio .....	64
	8.4 Limiting overpressure - graphical method .....	65
	8.5 Structural analysis program .....	68
9	STRUCTURAL PERFORMANCE .....	72
	9.1 Approach adopted for assessing structural strength .....	72
	9.2 Structural calculations .....	73
	9.3 Overall building collapse loads .....	84
10	FATALITY PROBABILITY .....	86
	10.1 Probability of fatality from debris hazard .....	86
	10.2 Possibility of fatality from glazing impact .....	90
	10.3 Fatality probability of occupants to building collapse .....	91
	10.4 Derivation of overall fatality probability curves .....	93
11	REFERENCES .....	111

## LIST OF TABLES

<b>Table</b>	3.1	Blast effects on people [24]
	3.2	Summary of accidental deaths at distance from military explosions/manufacturing accidents [81]
	3.3	Fatality probabilities [81]
	3.4	Fatality probabilities for RISKAT [34]
	3.5	Approximation of blast load [47]
	3.6	Failure pressures for different glazing types
	3.7	Damage pressures for different wall types
	3.8	Damage pressures for different building frame types
	3.9	Damage pressures for fixtures and fittings
	5.1	Common building types & building use matrix
	5.2	Generic building types
	6.1	Overpressures for 1 te propane equivalent
	6.2	Overpressures for 3 te propane equivalent
	6.3	Overpressures for 10 te propane equivalent
	7.1	Structural Load Parameters for Example Calculation
	8.1	Typical periods of vibration of structural elements
	8.2	Dynamic properties
	8.3	Ductility factors for various materials used in the construction industry
	8.4	Comparison of calculated dynamic response against literature values
	8.5	Structural analysis program
	9.1	Limiting dynamic overpressures for reinforced concrete framed buildings
	9.2	Typical failure pressures for reinforced concrete structures
	9.3	Limiting dynamic overpressures for steel framed buildings
	9.4	Typical failure pressures for steel framed structures
	9.5	Typical failure pressures for different particleboard types
	9.6	Historical failure pressures for corrugated steel panels
	9.7	Historical failure pressures for corrugated asbestos-cement panels
	9.8	Damage pressures for concrete walls
	9.9	Limiting dynamic overpressures for brick walls
	10.1	Fatality estimates for collapsed masonry and reinforced concrete buildings
	11.1	List of references obtained in literature search

## LIST OF FIGURES

- Figure** 2.1 Estimating fatality probabilities due to glazing  
2.2 Estimating fatality probabilities for occupants of buildings  
3.1 Diffraction of blast wave around simple geometry target  
3.2 Schematic failure curves for laminated glass pane  
4.1 General Procedure  
4.2 Generic Building Fatality Probability curves  
6.1 TNO Multi-Energy Model  
7.1 Reflection coefficients vs angle of incidence for shock waves and pressure waves  
7.2 Schematic representation of the time-pressure diagram for a finite reflective surface  
7.3 External pressure loads on building periphery  
7.4 Calculated resultant pressure variation on structure  
7.5 Pressure relief on external walls from glazing/cladding failure  
7.6 Blast and internal pressures for a range of building / vent dimensions  
7.7 Building internal pressure as a percentage of applied pressure wave  
8.1 Typical elasto-plastic resistance function  
8.2 Maximum response of elastoplastic one degree of freedom systems due to triangular load pulse with zero rise time  
9.1 Maximum coexistent axial loads and moments for reinforced concrete column  
9.2 Limiting overpressures for different percentages of glazing (or shorter span lengths)  
10.1 Fatality probability for personnel subject to glazing/cladding debris hazard  
10.2 Velocity/Fatality graph for brickwork  
10.3 Fatalities range for brickwork  
10.4 Velocity/Fatality graph for partitions  
10.5 Fatalities range for wooden partitions  
10.6 Velocity/Fatality graph for partitions (based on whole body translation)  
10.7 Fatalities range for wooden partitions (based on whole body translation)  
10.8 Velocity/Fatality graph for cladding  
10.9 Fatalities range for cladding  
10.10 Velocity/Fatality graph for cladding (based on whole body translation)  
10.11 Fatalities range for cladding (based on whole body translation)  
10.12 Velocity/Fatality graph for 4mm glass  
10.13 Fatalities range for glass  
10.14 Fatality Probability of Building Occupants Arising from Glazing Failure  
10.15 Fatality Probability of Building Occupants Arising from Building Collapse  
10.16 Overall Building Occupant Fatality Probability



# 1 INTRODUCTION

The UK Health and Safety Executive (HSE) are often consulted by local planning authorities on the safety aspects of proposed developments in the vicinity of industrial plant, and in addition, give advice on the siting of new plant with major hazard potential. HSE has therefore developed a quantified risk assessment approach to assist in making judgements concerning the appropriate advice to give. This quantified risk assessment may include consideration of the effects of explosions which can cause injury to people either through direct effects on the body, secondary effects such as the impact of fragments or the total/partial collapse of buildings and tertiary body translation effects. In general the secondary effects are the major cause of injury and death.

At present the methods used to assess fatalities due to building collapse do not fully take into account the characteristics of the building or the incident blast wave. Within the computerised analysis tool RISKAT, fatalities due to building collapse caused by overpressure are assessed using a probit derived from World War II flying bomb data.

The objective of this project is to develop a procedure for assessing the vulnerability of occupants of different types of buildings subject to overpressures produced from vapour cloud explosions. This requires the failure sequence of a building subject to increasing blast loads to be determined and the effect on people within the building of either debris generated by the blast load striking them or partial/total collapse of the load bearing structure to be assessed.

As such it involves deriving data similar to those presented in Chapters 2 and 3 of CPR 16E, 1st Edition 1992 [2]. However these data have been extended as outlined in this document to define a procedure for deriving the overall vulnerability of personnel within a particular type of building. The purpose of this approach is to produce a consistent methodology for assessing the comparative vulnerability of occupants of differing types of buildings to blast loads, based on the building's primary constructional characteristics. The method will also take into account the shape of the incident blast wave. This is thought to be an improvement upon the procedures presently available.

The project has therefore sought to produce:

- A procedure for deriving fatality probability/overpressure curves based on the characteristics of a particular building.
- Individual fatality probability functions for particular types of glazing, wall cladding and building frame.
- Generic fatality probability functions for particular building types, where appropriate.

The work involves four phases, and is presented in three reports. This report details Phase 1 of the project, the literature survey and the outline of the methodology. Phases 2 and 3 investigated the importance of various assumptions in terms of their

effect on the methodology's predictions. The results of Phases 2 and 3 are described in the second report of this series. Phase 4 uses the methodology, refined in view of the Phase 2 and 3 results, to produce damage and fatality probability predictions for a wide range of building types. Phase 4 is the subject of the third report. The project programme is described in detail in the next section. It is anticipated that the methodology will require further development as new data become available.

## **2 PROJECT PROGRAMME**

### **2.1 Phase 1**

Phase 1 involved a literature survey, assessing the general procedure to be used to obtain a fatality probability function for a particular building and determining the individual functions for glazing failure, cladding failure and building collapse.

In order to assess the structural behaviour of these buildings with increasing blast loading a procedure is proposed which assesses the structural integrity of the glazing, external wall cladding and load bearing frame. This requires the categorisation of the generic building by the following features:

- Glazing details;
- Construction of the load bearing frame (generally steel or reinforced concrete, or for brick-built structures in which the walls themselves are load bearing, the walls can be said to form the 'frame');
- Construction of the external wall cladding;
- Spacing of load bearing frame;
- Aspect ratio and size of the building.

The building damage predicted for the different categories of building is derived from:

- Calculations based on examples of typical buildings;
- Experimental data on building components subject to blast loads; and
- Historical data on the performance of buildings subject to blast loads.

The effect of building 'failure' on the occupants is assessed by considering the effects of failure of the external cladding/glazing and the progressive collapse of the building frame.

In considering the effects of failure of the wall cladding on the occupants of the building, two types of fragments are considered: penetrating and non-penetrating. Certain types of glazing that shatters produces shards that can penetrate building occupants. Fragments such as pieces of wall cladding are considered as non-penetrating fragments. Calculations on the effect of shards of glazing and wall fragments on people are based on empirical data.

The blast wave also causes varying degrees of collapse to the building itself. The vulnerability of people in damaged buildings is based upon historical data gathered from surveys.

Fatality probability functions are derived for glazing failure, cladding failure and building collapse. As an example, Figure 2.1 shows the approach proposed for deriving the probability of fatality due to glazing. The individual functions are then combined to give an overall fatality probability for a particular building as shown in Figure 2.2.

The procedures and fatality probability curves thus derived are a tool for providing an initial assessment of the anticipated level of damage to buildings, and the resulting effect on their occupants, subject to explosive events. As such they are intended to provide a relatively crude but useful tool for use in the overall risk assessment of occupants of buildings.

## **2.2 Phases 2 and 3**

Phases 2 and 3 involved assessing the sensitivity of the response of the structure (and thus vulnerability of the occupants) to the loading and structural models.

The aim of these Phases was to examine the effects of various aspects of the loading and structural characteristics upon the model predictions. In addition sample calculations were performed to demonstrate the procedure which were validated against relevant historical data.

In particular, the following were examined in Phases 2 and 3:

- the effect of the shape of the pressure pulse on the overall structural response of the building using representative building sizes;
- the effect of pressure relief due to failure of windows and wall cladding on the overall response of the building;
- the effect of pressure relief on the rear of buildings;
- the effect of the negative phase of the explosion.
- the structural characteristics of particular generic building types using historical, experimental and analytical data; and
- a more detailed examination of glass and other fragment effects.

## **2.3 Phase 4**

Phase 4 involved deriving fatality probability relationships for different building types. A provisional list of the building types considered is given in Section 5 of this report.

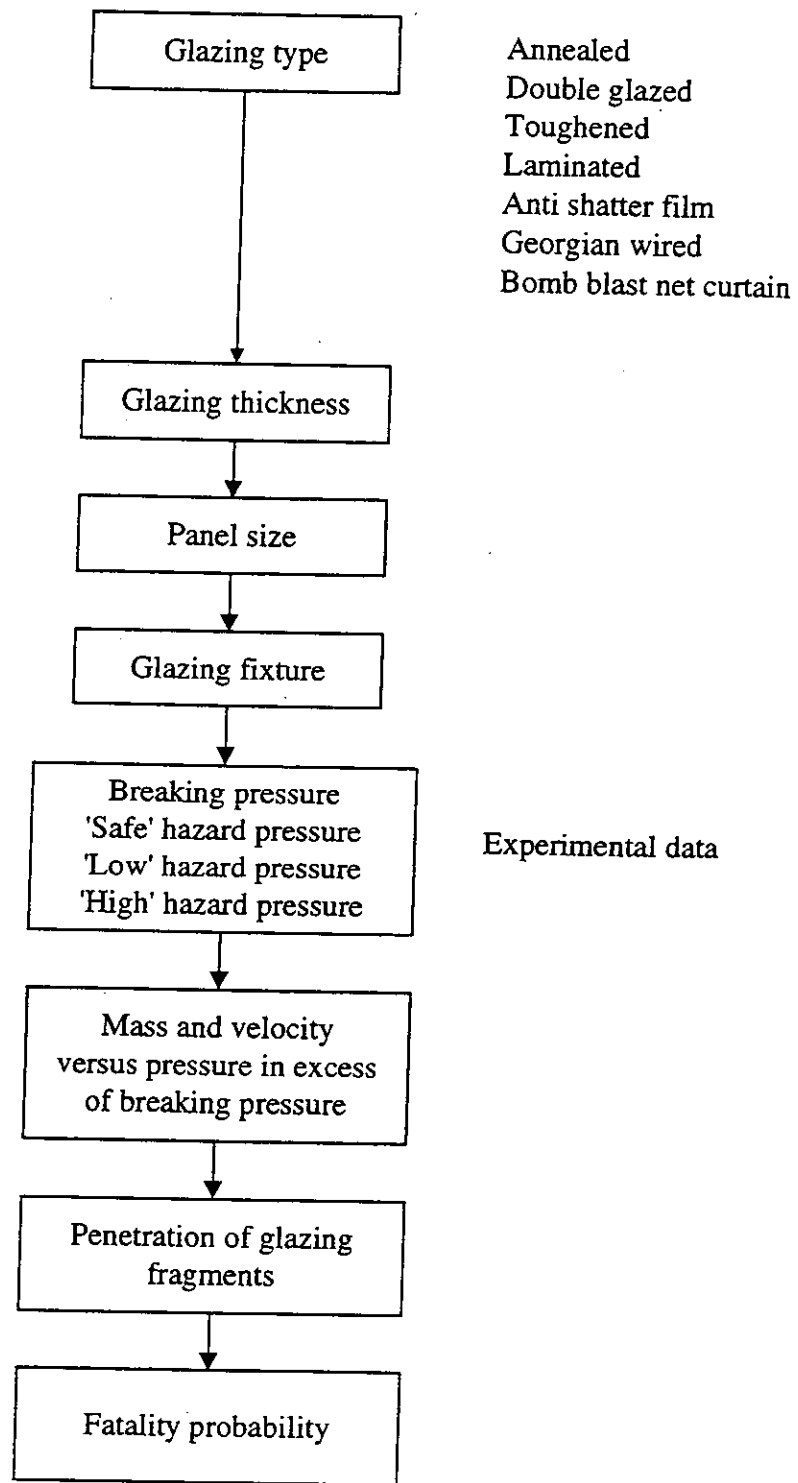


Figure 2.1: Estimating fatality probabilities due to glazing

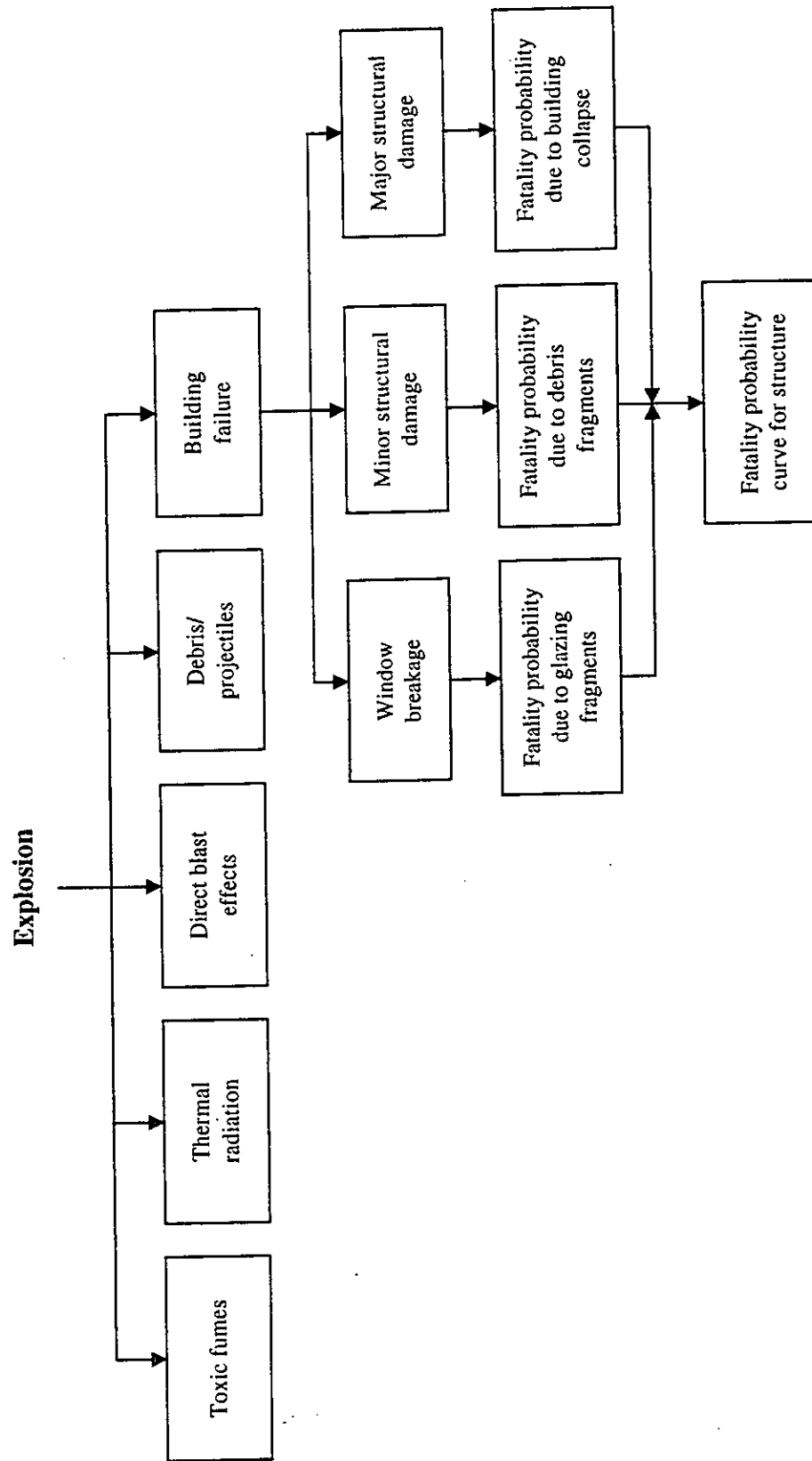


Figure 2.2: Estimating fatality probabilities for occupants of buildings

### 3 LITERATURE REVIEW

#### 3.1 Sources of data

The literature search was based both on a search of databases available through the WS Atkins library plus documents held at the Institution of Civil Engineers and the Institute of Structural Engineers, and references suggested by HSE. The databases searched include general engineering and medical databases as follows:

EI COMPENDEX Plus	1970 - 1995
Energy Sci-Tec	1974 - 1995
NTIS	1964 - 1995
APILIT	1964 - 1994
McGraw Hill Publications Online	1985 - 1995
BIOSIS PREVIEWS	1969 - 1995
Pascal	1973 - 1994
EMBASE	1974 - 1995
MEDLINE	1966 - 1995
Occ.Saf. and Health	1973 - 1994

As a result of the search, using terms such as Blast and Explosion with Buildings and Structures, and also with Human and People, approximately 30 references were identified as being potentially relevant, mainly in relation to the response of buildings to blast loading. However, only a limited number of references relating to the effect of explosions on the occupants of those buildings were found.

A complete list of the references obtained is given in the References (Section 11) at the end of this report.

#### 3.2 Effects on humans

The purpose of this study is to derive a methodology for determining the fatality probability of the occupants of buildings subject to blast loading. This is dependent on the level of blast loading, and the type and construction of the building. The probability of fatality is dependent on the probability of acquiring a specific injury and the probability of that injury being fatal.

In general, three categories of blast induced injury are identified [53]:

- **Primary injury** is due directly to blast wave overpressure and duration. The location of most severe injuries is where the density differences between adjacent body tissues are greatest, i.e. the lungs, the ears, the abdominal cavity, the larynx and trachea.
- **Secondary injury** is due to building collapse and impact by missiles produced as a result of the explosion. This can give rise to laceration, penetration and blunt trauma.

- **Tertiary injury** is due to displacement of the entire body followed by high decelerative impact loading which is when broken or fractured limbs can occur.

Experience indicates that secondary effects are the dominant cause of fatalities. Primary and tertiary injuries are less important at the overpressure levels considered, although impairment of hearing or lung damage may affect the ability of people to escape from collapsed buildings.

A summary of historical data on damage to humans from air blast effects is given in Table 3.1:

Effects on People	Incident Equivalent Peak Overpressure (mbar)
Annoying noise of continuous type at 10-15 Hz and 137 dB	1.4
Loud noise at 143 dB	2.8
Sound 'noted' as an Unusual Event' - An Explosion	0.34
Threshold for temporary loss of hearing	13.8
Threshold for eardrum rupture	138
50% Eardrum rupture threshold	331
Threshold of skin laceration by missiles	69 - 138
Personnel knocked down or thrown to the ground	103 - 200
Possible death by persons being projected against obstacles	138
Low personnel risk when inside a resistant structure	69
50% probability of eardrum rupture	345 - 483
90% probability of eardrum rupture	689 - 1034
Threshold of internal injuries by blast	483
Serious missile wounds giving about 50% fatality	276 - 345
Serious missile wounds of near 100% fatality	483 - 689
Threshold of lung haemorrhage	827 - 1034
50% fatality from lung haemorrhage	1379 - 1724
99% fatality from lung haemorrhage	2068 - 2413
People standing up will be thrown a distance	552 - 1103
People lying flat on the ground are picked up and hurled about	827 - 1655
Immediate blast fatalities	4826 - 13,790

**Table 3.1:**

**Blast effects on people [24]**

The most widely used information concerning the fatality probability for the different types of injury sustained are presented in Baker et al [4]. These data have been compiled from a number of references and curves are presented for whole body translation, lung damage and penetrating and non-penetrating fragment impact. This provides data concerning the vulnerability of humans to:

- **glazing failure:** penetration injuries
- **debris:** blunt trauma
- **direct blast:** lung damage and whole body translation



However, there are few data available for the vulnerability of humans to building collapse. Studies have been performed on the vulnerability of occupants of basement shelters to roof collapse, but in general it has been assumed that the proportion of fatalities is equal to the proportion of collapsed roof [68, 69]. Information can be obtained from references detailing the number of fatalities due to building collapse during earthquakes. In general the data from earthquakes for fatalities due to building collapse is relevant to explosion scenarios, with the following provisos:

- The time taken for a building to collapse in an earthquake may be much longer than in an explosion. In the earthquake case, occupants have more time to leave the building, and they are less likely to be caught in the collapsed structure. The percentage of occupants trapped is dependent on the percentage of the building collapsed and the ability of the occupants to escape. In an earthquake, 30 to 50% of the occupants of a single storey building will be able to escape during the duration of the earthquake. Clearly this is not the case for an explosion in which the loading is potentially severe and relatively short-lived.
- The directional nature of the loading for a blast wave on the side of a building may result in fairly localised collapse, whereas in an earthquake, movement of the foundations may cause global structural collapse. People caught in building collapses suffer a range of types of injury, including traumatic injuries, fractures, crushing, contusions or lacerations of soft tissue and bronchial or thoracic injuries from dust inhalation. Causes of death can depend on the type of building: in masonry buildings, a primary cause of death is often suffocation from the weight and powder of wall or roof material which buries the victim. Suffocation is also a real danger to those trapped inside reinforced concrete structures from the large amount of dust generated by the collapse. A proportion of the occupants are killed outright when collapse occurs. Others are injured to varying degrees of severity. It is suggested [11] that the injury distribution may be a function of the degree of cavitation in collapse, i.e. the void to volume ratio of the rubble and the size of the cavities left within it. It is estimated that in a masonry structure, 20% of the occupants trapped will receive fatal injuries on collapse, whereas in a reinforced concrete structure, 40% of the injuries received will be fatal [11]. This assumes complete collapse of the structure, whereas in an explosion scenario, it may be more appropriate to factor these numbers by the proportion of the building which has collapsed.
- Post-collapse, those people trapped in the rubble will die if they are not rescued and given medical treatment. In an earthquake, the fatalities post-collapse are largely dependent on the speed at which emergency rescue services can be facilitated. This is potentially less of a problem in an explosion scenario where the damage is relatively localised and rescue efficiency is expected to be high.

In the casualty model presented by Coburn et al [11], the number of people killed due to building collapse is estimated from:

$$\text{Fatality rate} = \frac{\text{Building}}{\text{Occupancy}} \times \% \text{ occupants trapped} \times \left( \text{mortality at collapse} + \text{mortality post collapse} \right)$$

There appears to be little further information available in the literature relating to experimental work on human response, although further information may be obtained from descriptions of the results of terrorist bombs and accidental or military explosions. The information available concerning the effects of terrorist bombs focuses mainly on the extent of damage and the numbers of casualties and fatalities, but little information is given concerning the causes of injury or death or the locations of the fatalities. The St Mary Axe bomb [63], a car bomb containing 1300lbs of home-made high explosive, resulted in 3 deaths, 37 serious injuries and 130 minor injuries. Of the three fatalities, two were in the street and only one was in a building. However, the bomb was detonated outside working hours and most of the buildings in the locality were offices: hence it is difficult to draw any conclusions concerning the vulnerability of the occupants of those buildings to the blast. For the bomb explosion in Bologna, Italy [77] there is a considerable amount of information concerning the injuries sustained, but very little information concerning the causes of fatalities in the 84 deaths. The bomb was sited in the waiting room of Bologna's central station, and the report attributes the devastating effects of the explosion partly to the large number of people at the station and partly to the construction of the station building, which resulted in a high level of fragmentation. In addition, parts of the station building collapsed, crushing people to death or causing severe injuries. However, there is no information concerning the distribution of injury with distance from the bomb, so again it is difficult to draw any conclusions concerning the relationship of fatality probability to overpressure.

An investigation into the probability of fatality within buildings subjected to blast loading has been performed by Hewkin [81]. A summary of deaths at various distances from accidental military explosions and other fatal manufacturing accidents is presented in the report and is reproduced in Table 3.2, together with equivalent overpressures calculated from the Henrych formulae given in [53].

Explosion Site	NEQ (kg)	Approx Scaled Distance for Farthest Fatality	Approx overpressure (calculated) (mbar)
Rotherwas	136	4.8	343
Offley	2358	9.4	120
Soham	5216	1.1	6419
Bootle	8482	3.2	703
Gascoigne Wood	12250	5.9	245
Anes B Abs 2	499K	2.5	1123
Burton-on-Trent	2423K	5.7	259
Bishopston	1700	1.4	3737
Stevenston	820	1.4	3737
Bridgwater	450	1.3	4402
Ardeer	210	8.4	142
Rainbow Ltd.	45	28	~ 30
AWRE	23	23?	~ 40 ?

**Table 3.2:**

**Summary of accidental deaths at distance from military explosions/manufacturing accidents [81]**

The proposed fatality probabilities in [81] relate to military explosions and are approximately as given in Table 3.3:

Scaled distance	Approximate overpressure (mbar)	Fatality probability (%)
3	792	100
5	321	15
10	110	0.75
20	40	0.04
30	30	0.01

**Table 3.3:**

**Fatality probabilities [81]**

This compares with the values used in the HSE code RISKAT as follows [34]:

Approximate Overpressure (mbar)	Fatality probability (%)
600	30
140	0.2
70	0.0

**Table 3.4:**

### **Fatality probabilities for RISKAT [34]**

These data can be used as a comparison to corroborate the assumptions and predictions made of fatalities due to accidental explosions.

## **3.3 Structural loading**

As we are primarily interested in fatalities among occupants of buildings, it is important to assess the effects of the blast load on the building, the likelihood of structural failure and of building collapse. In order to do this, it is necessary first to characterise the blast load itself, and then to assess the interaction of that load with the various structural components. In this section, methods for calculating the loading on the structure are investigated.

### **3.3.1 Vapour Cloud Explosion (VCE)**

The majority of information available on the form of the blast waves arising from explosive events relates to condensed high explosives which detonate to create shock waves [38, 60]. For these types of explosion, a reasonable estimate of the blast wave properties can be made, based on published blast data, provided the amount and type of explosive are known. By comparison, the amount of material in a cloud undergoing VCE has to be estimated from the stored amount, as it is dependent on the explosion mechanisms and the levels of evaporation and dispersion [78]. In the vast majority of accidental VCEs, a flame propagates as a deflagration, i.e. the flame front propagates through the unburnt gas at a velocity less than the speed of sound in the unburned gas, but at a rate such that a significant overpressure is produced. There is no universally accepted definition of what constitutes a 'significant' overpressure. Theoretically, deflagrations can produce pressures up to 8-10 bar, though evidence from actual incidents suggests that pressures in VCEs are usually much less. A detonation could produce pressures in excess of 15 bar, but evidence from actual incidents suggests that propagation of a detonation throughout an entire cloud, or even a significant portion thereof, is extremely rare [42].

The role and importance of obstacles and confinement in driving a vapour cloud ignition incident into a VCE are well documented, and a summary is given in [42]. The level of congestion at the explosion site greatly affects the maximum overpressure within the cloud and hence the pressures experienced at some distance from the

explosion centre. For highly congested areas, it appears that a maximum overpressure of 1 bar within the cloud is a reasonable estimate, whereas for completely flat, unobstructed areas a maximum overpressure of 0.1 bar may be a reasonable value.

Several different methods are available for estimating the strength of a blast, varying from simple TNT equivalence techniques to computational fluid dynamics (CFD) techniques. Compared to blast waves from high explosives, pressure waves from VCEs are characterized by a slower rise time, longer duration, lower peak pressure near the blast centre, slower decay with distance and more significant negative pressure phase in some cases [42]. The use of TNT equivalence methods in application to VCEs is therefore thought to be of questionable validity. While methods based on CFD offer a potentially powerful approach to accurate site-specific modelling, they are numerically intensive and require large computing resources. Other available calculation techniques are described in [42]. These define the size of the cloud according to the congested region of the release site and decay with distance outside the cloud. The difference between the techniques is in the parameter required to set the peak pressure within the cloud: either the peak pressure itself is estimated (Hemispherical Equivalent Method) or the blast intensity (Multi Energy Method) or flame speed mach number are used in conjunction with curves plotting dimensionless overpressure or impulse against combustion energy scaled distance to give an estimate of the pressure within the cloud.

### **3.3.2 Blast wave form and simplification**

For a typical pressure wave from a VCE, the maximum overpressure does not occur at the location of the wave front, but slightly behind it. As the wave travels away from the blast centre, the higher velocity particles behind the wave front travel quicker than the front itself, and the wave gradually 'shocks up' [53].

It is very common to simplify the pressure-time variation by a straight line graph. The implications of this are discussed in [47], and are summarised in Table 3.2. The governing factor is the ratio of the pulse duration,  $t_p$ , to the natural period of the structure,  $T$ : if the duration of the load is significantly less than the natural period, high loads can be tolerated since the structure has insufficient time to fully respond, so the loading is termed 'impulsive', i.e. dependent on the impulse. If the load duration is much longer than the natural period, the full effect of the load is felt and the loading is termed 'quasistatic', i.e. damage is determined by the peak load value. In between these two extremes, loading is termed dynamic and damage is dependent on both peak pressure and impulse. Studies appear to indicate that response to a blast load with an appreciable rise time is usually in the dynamic to quasistatic regime and rarely in the impulsive.

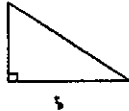
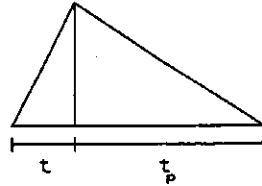
Feature	Nature of Blast Load		
	Impulsive $t_p/T < 0.4$	Dynamic $0.4 < t_p/T < 2.0$	Quasistatic $t_p/T > 2.0$
Peak Value	Preserving the exact peak value is not critical	Preserve peak value - increase/decrease in this quantity will result in a similar increase/decrease in response	
Duration	Preserving the exact load duration is not critical	Preserve load duration since in this range it is close to the natural period of the structure. Even slight changes may affect the response.	Load duration is not too important if response is purely elastic, but it becomes significant when response is plastic.
Impulse	Accurate representation of the impulse is important, with negative impulse included in some cases	Accurate representation of the impulse is not too critical, although better results would be achieved if some attempt were made to estimate this quantity	Accurate representation of the impulse is not important
Rise Time	Preserving rise time is not important	Preserving rise time is very important: not doing so can significantly affect the response.	
General Shape	General shape of idealised load is a right-angle triangle of the form: 	General shape of idealised load is a triangle of the form:  A tri- or tetra-linear form can be used to more accurately represent the rise and decay of the load, predicting slightly better response	

Table 3.5:

### Approximation of blast load [47]

In idealising the pressure wave, the negative phase is often disregarded [2], but it is important to note that such an assumption may lead to an overprediction of the structural load [47].

### 3.3.3 Structural Loads

The pressure field within an explosion rarely represents the net load imposed on a structure within it. The blast wave generated by the explosion impinges on the front face of the structure and undergoes reflection. The result is an increase in the pressure experienced by the structure, the actual magnitude being determined by the type of reflection, i.e. normal, oblique or Mach [47]. On reflection of the blast wave, rarefaction waves are formed at the edges of the reflecting surface which progress towards the centre of the surface. As a result, the pressure on the surface decreases to a value equal to the incident wave pressure at that moment plus the dynamic pressure. The pressure differential between the front and rear faces of the structure produces an initial lateral load. As the wave travels forward it is diffracted around and/or through the structure, imposing loads on the sides, top and eventually the rear face, while the pressure on the front face drops. The net load is again dependent on the amount of blast energy reflected, which will increase for structures offering a high resistance to flow through them in the direction of the oncoming wave. In addition, if a structure is engulfed in a sufficiently long duration blast wave such that the impulsive changes have had time to relax, then it will experience drag or dynamic loading due to the passing gas flow. This is illustrated in Figure 3.1.

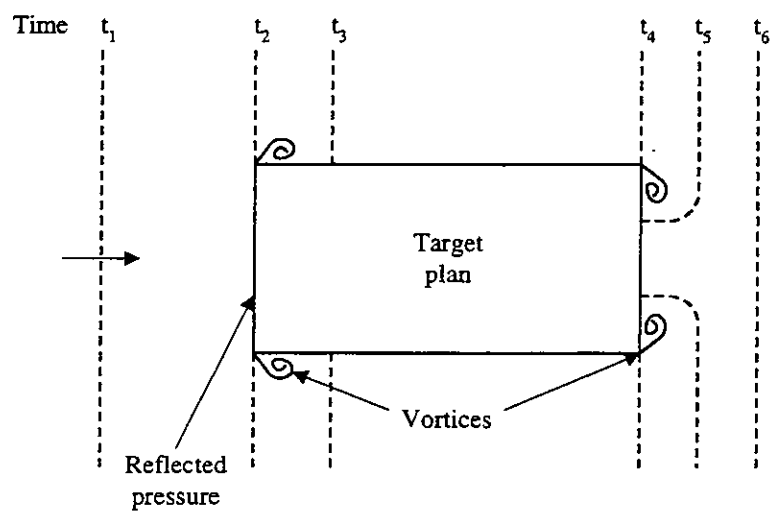
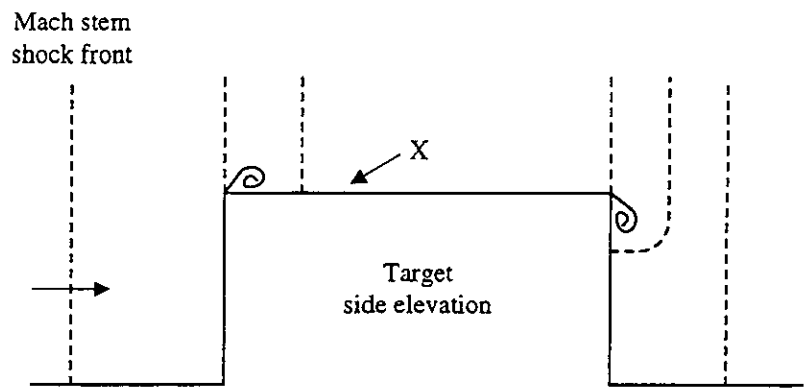


Figure 3.1:

Diffraction of blast wave around simple geometry target



In the case of an incident pressure wave, rarefaction waves will again develop. Due to the slower build-up of pressure produced by an incident pressure wave, the reflected pressure acting on a finite surface will be so much relieved that the resulting pressure will not be higher than the peak incident pressure plus the dynamic pressure [2].

In order to determine the loads, it is necessary to know the shape of the structure, its resistance to flow and the detailed pressure and velocity time history in the incident wave [49]. The effects of congestion around an explosion centre have been noted by Jenkins [63]. In his report he describes the effects of the St Mary Axe bomb, noting the 'unpredictability of the effects, with buildings out of the line of sight damaged and others in the same street untouched'. This is of particular concern in built-up residential areas where it is important to predict the extent of the blast loading.

Predictive methods for calculating structural loading can be divided into simple hand calculation techniques as described in Glasstone [29] and CPR16E [2], and complex numerical simulation methods. A variety of 3-dimensional numerical models are available which solve a complete set of governing equations and which are able to simulate the frictional effects due to turbulence and hence predict the drag components of loading in both steady and transient flows. Examples of such codes are GECCO, FLOW3D and COBRA [49].

#### **3.3.4 Summary**

The physical parameters influencing the structural loading due to a VCE can be summarised as follows:

- spatial and temporal gradients of overpressure and the resulting pressure differentials, giving rise to net directional load components;
- drag forces due to blast wind;
- interaction between blast waves and the structure, i.e. reflection and diffraction around and through the structure; and
- interaction between adjoining structures.

Several techniques are available for assessing the structural loading due to an explosion; the choice of method is largely dependent on the data available and the accuracy required.

#### **3.4 Structural response**

In order to assess the fatality probability for occupants of buildings, it is necessary to understand the structural properties of the building in which they are housed and the way in which it responds to the blast loading. Techniques for calculating structural response vary from single degree of freedom dynamic models to non-linear finite element codes [53]. In addition, some historical and experimental data are available

in the literature with which to validate the calculations. The principal sources of data are reports of World War II bomb damage [60], reports of terrorist bomb damage [63, 74, 77], nuclear explosion tests [64] and accident reports [55, 82]. The data available appear to be extensive, but unfortunately, many of the data are not directly useful for deriving structural failure pressures. In addition, the pressure data are not necessarily relevant to vapour cloud explosions, owing to the different blast wave characteristics for high explosives and VCEs. However, the data do provide some qualitative indication of the structural response and the levels of damage to be expected for different structures exposed to blast loading.

In the progressive collapse of a structure, the weakest components closest to the source of the blast can be assumed to fail first. In most buildings, this will be the glazing, which fails at fairly low overpressures, followed by either the walls or the building frame, dependent on the type of construction and the materials used.

### 3.4.1 Glazing

The overpressures at which glazing fails are dependent on a number of factors, including:

- Material type;
- Thickness;
- Pane dimensions;
- Rate of loading; and
- Frame construction.

Failure pressures for different types and dimensions of glass are given in Table 3.5 [50, 39, 40, 41]. For the plate/sheet glass single panes and bonded double glazed units (the lower number in the table is for plate glass, and the higher for sheet glass) [50], the values are based on the design criteria for glazing in CP 152 for durations typical of gas explosions, and verified against a series of explosion tests performed by the British Ceramic Research Association [56]. In these tests, explosions took place within a building, and hence the glazing was close to the centre of the explosion. For the polycarbonate [39], tempered glass [40] and laminated thermally tempered glass [41], the results have been extracted from the curves presented for durations of 100ms. These curves are based on model predictions for design purposes, and present the overpressures at which the probability of failure of the panel is 0.001. This implies that the actual failure pressure is likely to be somewhat higher than the values given, an implication which is upheld by the comparison of the values for tempered glass with the values for sheet/plate glass. For the tempered glass, the design predictions are compared against experiment, although the comparison is somewhat inconclusive. In almost all cases, the glass had not failed at the design failure pressure in the experiments. Experimental tests on hardened glass are described in Nowee, 1985 [33]. For a 6mm pane, 1650 x 1100 mm in dimension, the average measured dynamic failure pressure was 133 mbar for a positive phase duration of the shock load of 30 ms, compared with a value of 56 mbar for unhardened glass. This compares with a value of 65 mbar for sheet glass given in reference [50] and 69 mbar for tempered glass, given in [40] for a similar phase duration.

While the data in the table are generally of interest, the values in the last three columns are not directly useful unless some indication of the factor of safety can be derived. However, in the majority of urban residential buildings, the glazing is most likely to be plate or sheet glass, and the first two columns are then relevant.

Aspect Ratio	Length x width (in)	Thick-ness (in)	Failure pressure (mbar)				
			Plate/sheet glass - single panes [50]	Plate/sheet glass - bonded double glazed units [50]	Poly - carbonate [39]	Tempered glass [40]	Laminated thermally tempered glass [41]
1.0	18 x 18	0.1875	210 / 250	> 250	-	-	-
1.0	36 x 36	0.1875	50 / 66	85 / 120	-	-	-
1.0	60 x 60	0.1875	18 / 23	35 / 45	-	-	-
1.0	36 x 36	0.25	90 / 125	160 / 250	62.0	106.9	-
1.0	60 x 60	0.25	33 / 45	65 / 95	9.0	42.7	-
1.0	36 x 36	0.50	> 250	-	324.0	386.1	-
1.0	60 x 60	0.50	115 / > 250	-	148.2	165.5	-
1.0	36 x 36	1.50	-	-	2413	3206	2310
1.0	60 x 60	1.50	-	-	1034	1172	827.4
1.5	24 x 36	0.25	150 / 200	> 250	110.3	172.4	-
1.5	24 x 36	1.00	-	-	1793	1931	1358
2.0	18 x 36	0.25	> 250	> 250	144.8	162.0	-
2.0	18 x 36	1.00	-	-	1724	2717	1917

**Table 3.6:**

**Failure pressures for different glazing types**

The values given in Table 3.5 are for loading durations of the order of 100ms. Strengths are highly dependent on the loading duration: for durations longer than one second, the strength appears to decrease by about 15% for each increase of an order of magnitude in the duration. For shorter durations, there is an increase in strength of between 20 and 25% for each reduction of an order of magnitude in the duration from 1 second [50].

The mode of failure is also different for different glazing types. An example of this is laminated glass, for which schematic P-I failure curves are presented in Figure 3.2 [62]. The left-hand curve corresponds to cracking a sheet of glass acting as a plate in bending, whereas the right hand curve represents the equivalent membrane action of the lamination. For this particular example, a blast pressure of 1 bar can be withstood,

provided it is of less than 10ms duration, whereas for longer durations, the peak overpressure drops (400 mbar at 40ms duration)

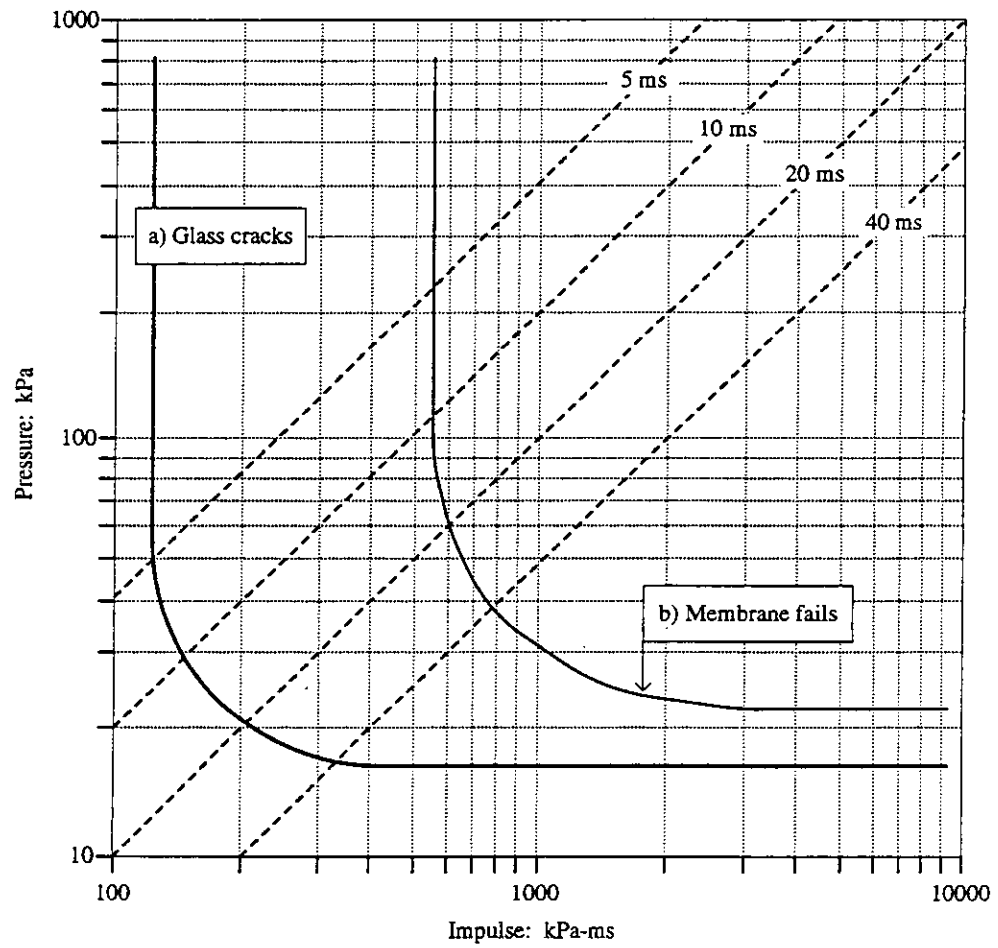


Figure 3.2:

Schematic P-I failure curves for laminated glass pane

The strength of glass and polycarbonate glazing is highly variable, and in particular degrades with age. These figures do not take this into account. When glass has been in place for some time, its strength may be reduced by atmospheric corrosion, surface abrasion or pre-straining by warping of the frame. Polycarbonate degrades due to ultraviolet radiation [39]. In addition, the explosive pressure acting on the window or cladding as a whole may similarly reduce the effective strengths of individual panes of glass by inducing strains additional to those induced by the pressure acting directly on the panes [50].

### 3.4.2 Wall components

The local behaviour of a structure is dependent on the wall panel construction, the edge restraint provided at the connection to the frame and the size of the bays across which the wall panels are spanning. Typical wall construction materials are as follows:

- **wood:** failure pressures identified in the literature correspond to failure of the connections allowing whole panels to be blown in [56], at pressures between 69 and 138 mbar.
- **brick/block:** a wide range of failure pressures have been identified in the literature for brick wall panels and brick walls. The pressure is dependent on the wall thickness and the level of precompression in the wall, and despite some discrepancies between the references, the consensus of opinion is that the onset of collapse occurs at overpressures of the order of 150 mbar.
- **concrete:** more consistency is seen in the failure pressures for concrete panels. Typical failure pressures lie in the range 140 to 400 mbar, although again, the thickness of the wall and level of reinforcement is important.
- **corrugated asbestos panels:** complete demolition of corrugated asbestos panels is observed at overpressures greater than 65 mbar.
- **corrugated steel or aluminium panels:** failure of corrugated steel or aluminium panels is observed at pressures greater than 200 mbar, although failures of the connections at the edge of the panels are observed at much lower overpressures (69 to 138 mbar).

Failure pressures for these components have been extracted from the literature and are shown in Table 3.7.

Structure	Over - pressure (mbar)	Description of damage	Comments	Ref.
Corrugated asbestos siding	69 - 138	Shattering	Values from nuclear tests for brittle failure i.e. not dependent on blast duration.	29
Corrugated asbestos cement panels	6 - 30 30 - 65 > 65	Slight cracking and deflection Parts blown out Complete demolition	Only applicable where the duration of loading is long compared with the natural period. Based on design wind loads, experimental tests and engineering judgement	78
Corrugated steel or aluminium panelling	69 - 138	Connection failure followed by buckling	Values from nuclear tests for brittle failure i.e. not dependent on blast duration.	29
Corrugated steel panels	80 - 200 200 - 350 > 350	Slight cracking and deflection Parts blown out Complete demolition	Only applicable where the duration of loading is long compared with the natural period. Based on design wind loads, experimental tests and engineering judgement	78
Frameless steel panel building	207 - 276	Demolished	No information given concerning source of data	24
Cladded steel frame target - 6 m x 3 m 0.70 mm BS steel plastisol coated sheeting attached to galvanised purlins and sheeting rails	67  109  118	Corner flashing detached and propelled 15 m. Front face pushed in 0.5 m. Cladding and purlins creased and deformed.  Front wall pushed in 0.3 m and impacted against transducer support.  Front wall pushed in 0.04 m. Minor deformation of cladding and purlins.	Vented dust explosions	84
Brick wall panel, 8 in or 12 in thick (not reinforced)	207 - 552	Shearing and flexure failures	Values from nuclear tests for brittle failure i.e. not dependent on blast duration.	29
External house walls	138 - 241	Partial demolition	No information given concerning source of data	24
Brick wall panels 9 in thick	172 - 276	Collapse		
Brick wall panels - 13.5 in thick	483 - 621	Collapse		
Brick walls, 20 - 30 cm thick	500	Collapse	No source of data given - probably relates to reference 29.	79

Structure	Over - pressure (mbar)	Description of damage	Comments	Ref.
8 in brickwork walls	300 - 400 400 - 800 > 800	Slight cracking and deflection Parts blown out Complete demolition	Only applicable where the duration of loading is long compared with the natural period Based on design wind loads, experimental tests and engineering judgement	78
Brickwork: 50 mm cavity wall - outer wall 'common' bricks, internal wall thermalite blocks.	< 142  161  340	Damage largely superficial - cracking of brick mortar joint.  Front wall pushed in by 100 mm. Brick and mortar joint cracks up to 12 mm wide on all walls. Top 2 courses of internal blockwork displaced and held by roof ties.  Wall collapsed.	Vented dust explosions	84
Wood siding panels	69 - 138	Failure at main connections allowing whole panels to be blown in	Values from nuclear tests for brittle failure i.e. not dependent on blast duration.	29
12 in thick cement breeze block wall panels	200 - 248	Rupture	No information given concerning source of data	24
Concrete or cinder block wall panels, 8 in or 12 in thick (not reinforced)	103 - 380	Shattering of the wall	Values from nuclear tests for brittle failure i.e. not dependent on blast duration.	29
Concrete block wall	150 - 200	Collapse	No source of data given - may relate to reference 29.	79
0.15m thick concrete walls	100 - 230 230 - 400 > 400	Slight cracking and deflection Parts blown out Complete demolition	Only applicable where the duration of loading is long compared with the natural period Based on design wind loads, experimental tests and engineering judgement	78
0.25m thick concrete walls	300 - 650 650-1800 > 1800	Slight cracking and deflection Parts blown out Complete demolition		78
Roof structures	65 - 180 180 - 400 > 400	Slight cracking and deflection Parts blown out Complete demolition	Only applicable where the duration of loading is long compared with the natural period Based on design wind loads, experimental tests and engineering judgement	78

Structure	Over - pressure (mbar)	Description of damage	Comments	Ref.
Blast wall panel	500 - 800	Failure	'Typical' values - no source given	83
Steel framed blast wall	200 - 400	Whole wall yield line failure		83

**Table 3.7:**

### **Damage pressures for different wall types**

Unfortunately, few extensive test data have been uncovered in the literature search, and the historical data available are incomplete concerning panel dimensions and connection details. Information given in the Zeeuwen and Schippers report [78], is based on failure pressures estimated from calculations and compared against experimental evidence where available. However, the majority of the data come from Glasstone [29], and relate to observed damage at specific overpressure levels, i.e. they are not necessarily failure pressures. In addition, the typical durations of the blast load for the nuclear explosions are of the order of 1 second or longer, which is considerably longer than expected for a VCE. For a very long duration load, the time taken for the pulse to travel around a structure may be lower than the time for the pulse to pass the front face, in which case the structure will experience load on all sides. Alternatively, if the pulse passes the front face before the rear face becomes loaded, the structure may experience a travelling load, which may be less damaging to the overall structure. In addition, if the duration is long compared with the natural period of the structural component, it will respond in a quasistatic manner. The failure pressures may therefore be higher for the short duration VCE than for the long duration nuclear explosion.

#### **3.4.3 Building frames**

The response of complete buildings to blast loadings is dependent for framed buildings on the resistance of the building frame, in addition to that of the wall cladding. The governing factor is primarily whether the walls fail before the building frame, releasing the pressure load that the frame experiences. In this case, the failure pressures for the frame are high. If the walls are high strength, and the wall-frame connections are sufficiently strong, then failure of the building can occur at lower pressures as less pressure relief occurs. Clearly for buildings with load bearing walls, such as brick buildings, collapse of the walls leads to collapse of structure.

Data for wood, brick, concrete and steel framed buildings have been extracted from the literature and are presented below. A wide range of damage with distance from the source of an explosion has been observed in a congested area [60, 75]; even if the initial blast pressure has a relatively small variability, the effect of reflections and shielding on the overpressures experienced by the buildings give rise to a wide scatter in the structural response. Hence these values (Table 3.8) are only indicative of the pressure levels at which failure should be expected:



Structure	Over - pressure (mbar)	Description of damage	Comments	Ref.
2 storey wooden framed house	110	11% damaged, i.e. window breakage, caved - in doors and slight roof damage	Source of data is Wilton, C. and Gabrielsen, B., 'House damage assessment', 14th Annual Explosives Safety Seminar, 1972. - No detail given in 79 concerning test details	79
	340	82% damaged, i.e. collapsed		
1 storey wooden house with concrete floor	131	12% damaged - as above		79
	352	82% damaged - as above		
Wood frame building, 1 or 2 storeys	70	Windows and doors blown in, interior partitions cracked	Nuclear tests of duration ~ 1 second 'Structure primarily affected by diffraction loading', i.e. maximum overpressure more important than duration.	29
	123	Wall framing cracked, roof severely damaged, interior partitions blown down		
	181	Frame shattered - almost complete collapse		
House	70	Partial demolition - uninhabitable	'Typical' value - no source given	37
Brick-built houses	10 - 15	Damage to roofs, ceilings, minor crack formation in plastering, more than 1% damage to glass panels	No source or experimental details given for data.	79
	30	Minor structural damage		
	70 - 150	25% wall failure		
	350	50 - 75% outer walls damaged		
	700	More than 75% of all outer walls collapsed		
2 storey brick built house	352	81% collapsed	Source of data is Wilton, C. and Gabrielsen, B., 'House damage assessment', 14th Annual Explosives Safety Seminar, 1972. - No detail given in 79 concerning test details	79
2 storey brick built house with supporting walls - no windows in side walls	593	53% collapsed		79
Brick apartment house, up to 3 storeys	70	Windows and doors blown in, interior partitions cracked	Nuclear tests of duration ~ 1 second 'Structure primarily affected by diffraction loading', i.e. maximum overpressure more important than duration.	29
	185	Exterior walls severely cracked, interior partitions severely cracked or blown down		
	253	Collapse of bearing walls resulting in total collapse of structure		
Reinforced concrete building with concrete walls, small window area, 3 to 8 storeys	70	Windows and doors blown in, interior partitions cracked	Nuclear tests of duration ~ 1 second 'Structure primarily affected by diffraction loading', i.e. maximum overpressure more important than duration.	29
	370	Exterior walls severely cracked, interior partitions severely cracked or blown down, structural frame permanently distorted, extensive spalling of concrete		
	471	Walls shattered, severe frame distortion, incipient collapse		

Structure	Over - pressure (mbar)	Description of damage	Comments	Ref.
Reinforced concrete frame office building, 3 to 10 storeys, lightweight low strength walls which fail quickly	70	Windows and doors blown in, light siding ripped off, interior partitions cracked	Based on observations of nuclear tests of duration ~ 1 second 'Structure primarily affected by drag loading', i.e. duration of blast load is important. Ranges refer to the ranges of yield applicable?	29
	554 - 615	Frame distorted moderately, interior partitions blown down, some spalling of concrete		
	688 - 760	Severe frame distortion, incipient collapse		
Multistorey reinforced concrete building with reinforced concrete walls, blast resistant design, high strength walls which do not fail quickly, no windows	70	Some cracking of concrete walls and frame	Nuclear tests of duration ~ 1 second 'Structure primarily affected by diffraction loading', i.e. maximum overpressure more important than duration.	29
	534	Walls breached or on the point of being so, frame distorted, entrances damaged, doors blown in or jammed, extensive spalling of concrete		
	724	Walls shattered, severe frame distortion, incipient collapse		
Steel frame	80 - 100 200	Minor damage Collapse	No source given for data - may come from reference 29.	79
Steel Girder framed building	500	Collapse	'Typical' value - no source given	37
Light steel frame industrial building, single storey, with up to 5 ton crane capacity, low strength walls which fail quickly	70	Windows and doors blown in, light siding ripped off	Nuclear tests of duration ~ 1 second	29
	431 543	Minor to major distortion of frame Severe distortion or collapse of frame		
Heavy steel frame industrial building, single storey, 60 to 100 ton crane capacity, lightweight low strength walls which fail quickly	70	Windows and doors blown in, light siding ripped off	'Structure primarily affected by drag loading', i.e. duration of blast load is important.	29
	492 615	Minor to major distortion of frame Severe distortion or collapse of frame		
Multistorey steel frame office building, 3 to 10 storeys, lightweight low strength walls which fail quickly	70	Windows and doors blown in, light siding ripped off, interior partitions cracked	'Structure primarily affected by drag loading', i.e. duration of blast load is important.	29
	677 - 738 832 - 905	Frame distorted moderately, interior partitions blown down Severe frame distortion, incipient collapse		

**Table 3.8:**

**Damage pressures for different building frame types**

The values in the above table are subject to the same comments as Table 4.7. The majority of the information comes from reference 29, and the duration of the blast load needs to be considered when using these values.

#### **3.4.4 Fixtures and fittings**

In terms of risk to humans, the possibility of equipment within buildings being dislodged under pressure is another important aspect. Data concerning this are limited, although for a specific building, displacement pressures could be calculated from a detailed knowledge of the equipment design and connection details. Some data have been identified in the literature, in particular in [19], where interior and exterior service pipes were observed to be intact at an overpressure of 345 mbar, and domestic appliances were also not affected. The majority of damage appears to be caused by failure of the supporting structure, i.e. walls and floors.

#### **3.4.5 Miscellaneous items**

In addition to the building contents, data have been extracted for a number of miscellaneous items as outlined in Table 3.9.

Structure	Overpressure (mbar)	Description of damage	Comments	Ref.
Steel chimney	345 - 483	Collapse	No information given concerning source of data	24
Brick chimney	2068 - 4137	Major damage		
Oil storage tank	200	rupture		
Storage tank (petroleum, oil, lubricant)	70	lifting of tank from foundation, failure of joints, leakage	No information given concerning source of data	2
Pipe-bridge	350	displaced, breakage of piping		
Horiz. pressure vessel	400	moves, pipes break	No data source given	24
Spherical tank	500 1100	moves, pipes break overturns		
Water sealed gasholder	690	severe damage		
Elevated water tanks	690	heavily damaged		
Pipework for bulk storage and filling plant	345	superficial damage	Data based on observations for nuclear explosions with durations of ~ 1 second or greater.	29
Heavy machine tools (3.5 tons)	689.5	moved and badly damaged		
Wooden telephone pole	345 - 758	Snapped		
Cars and Trucks	552 - 827 1379 - 2068	Blown over Severe damage		
Trees	69 - 103 117 - 159 166 - 255 241 - 414	Minor damage Leaves and branches blown off 30% large trees blown down 90% large trees blown down		
Bridge	345 - 1034	Movement of bridge members on abutments and some distortion of bridge members		

**Table 3.9:  
Damage pressures for miscellaneous items**

### 3.5 Conclusions

The historical and experimental data available on the effects of explosions on structures and on humans is limited. In terms of experimental data for structural components, the majority of references relate to the work by Glasstone and Dolan [29] on the effects of nuclear explosions on structures. This data needs to be treated with caution, for two reasons. Firstly, in some cases, the pressures given are based on observed levels of damage at particular overpressures and durations, and are not necessarily failure pressures. Secondly, the durations of the nuclear explosions are far longer than for a typical VCE, which implies that the nature on the loading on the structures is different, and the failure pressures may not be applicable. In addition, there has been some experimental work on the effects of explosions on load-bearing

brick structures by Astbury et al [56], and other work by Jarrett and Wilton and Gabrielsen [2].

As regards hazards to humans, information available is summarised in Baker et al [4], and little additional information has been discovered in the literature search. Detailed documentation of accidental and terrorist explosions could provide a useful insight into the distribution of injuries and fatalities, but accident reports appear to focus on the numbers of casualties rather than the causes of injury or fatality. Further literature searches have been undertaken in this area. Information relating to earthquakes is also of interest, but care must be taken when interpreting it, as the difference in duration of the earthquake and the explosion means that there is more chance for occupants to escape from collapsing buildings in an earthquake. Counteracting this is the fact that post collapse, emergency rescue services are likely to provide a more rapid and efficient response in an explosion compared with an earthquake where the damage is likely to be widespread.

The paucity of useful data means that it is necessary to estimate failure pressures by calculating the limiting loads for the different structural components and develop a consistent set of failure pressures for different building and load types. The available data can then be used to validate and support the calculations.

## 4 GENERAL PROCEDURE

It is necessary to construct a consistent methodology for assessing the capacities of buildings subject to blast loading, and the consequential vulnerability of the occupants of those buildings. The general procedure for doing this is based on an assessment of the pressure loads, the structural response, the structural capacity and the human vulnerability for generic building types, as outlined below:

### - **Building types**

The first action is to investigate the buildings existing in the UK, typical of development proposals to be considered in planning applications around a major on-shore hazardous installation. This includes residential properties, together with offices, retail developments, hospitals, schools and leisure centres, and covers the whole range of building types and geometries. From this wide range, a list of typical structures has been derived, as described in Section 5. Another important issue is location of buildings (offices, control rooms etc.) on major hazard sites. The list has been expanded to include such buildings.

### - **Blast loads**

Having decided what types of buildings are important, it is then necessary to determine the ranges of blast loading of interest for a vapour cloud explosion scenario. This includes maximum overpressures, pulse shape and duration, together with the corresponding dynamic pressures, for a range of typical combustion energies. The relevant pressure loads are outlined in Section 6.

### - **Structural loads**

The load experienced by a structure as a result of an incident blast wave is a complex function of the incident pulse, the building length and breadth and the vented areas. These are combined in Section 7 to provide an overall estimate of the loading on the structure.

### - **Dynamic response**

Having determined the loading on the structure, it is then necessary to assess its dynamic behaviour and the way in which it responds to the incident blast wave. This depends on the natural frequency of the building and the elastic limit of the structural components. The response is assessed in Section 8 using a non-linear single degree of freedom elasto-plastic model to represent the structure, and derives maximum displacements, velocities and accelerations in the structure under a prescribed pressure load. If the maximum displacement of the structure is known, this methodology can then be used to predict the maximum overpressure that can be tolerated for a particular pulse duration.

- **Structural capacity**

The method for assessing dynamic response is then applied to specific structural components in order to assess the maximum overpressure ranges for those components. The literature review revealed very few additional data to those presented in the classical texts on the subject of blast analysis such as Glasstone and Dolan [29] and Baker et al [4]. Consequently, in some cases, component capacities have been calculated based on the static allowables in design guides, and compared against historical or experimental data where available, taking into account the provisos on the experimental data given in Section 3. These calculations are outlined in Section 9.

- **Fatality probability**

Finally the fatality probability of the building occupants can be assessed, based on a knowledge of the behaviour of the structure, the failure capacities of the various components and the vulnerability of people to glazing, debris and building collapse. The methodology for calculating fatality probabilities is outlined in Section 10.

This general procedure, which is presented schematically in Figure 4.1, will be applied to variations within a particular generic building type in order to derive upper and lower bound fatality probability curves for the generic building as defined in Figure 4.2.

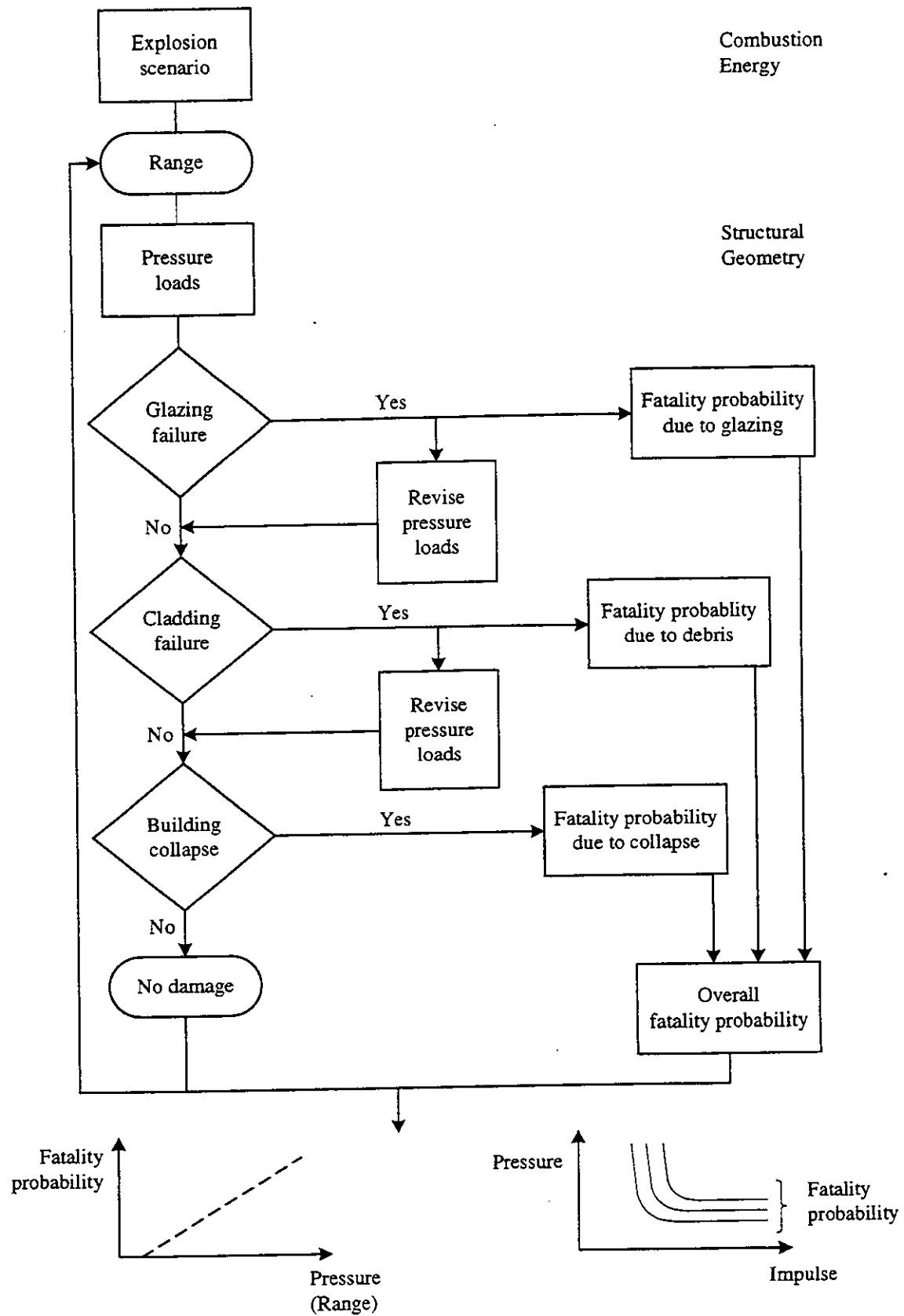


**Figure 4.1:**  
**General procedure**



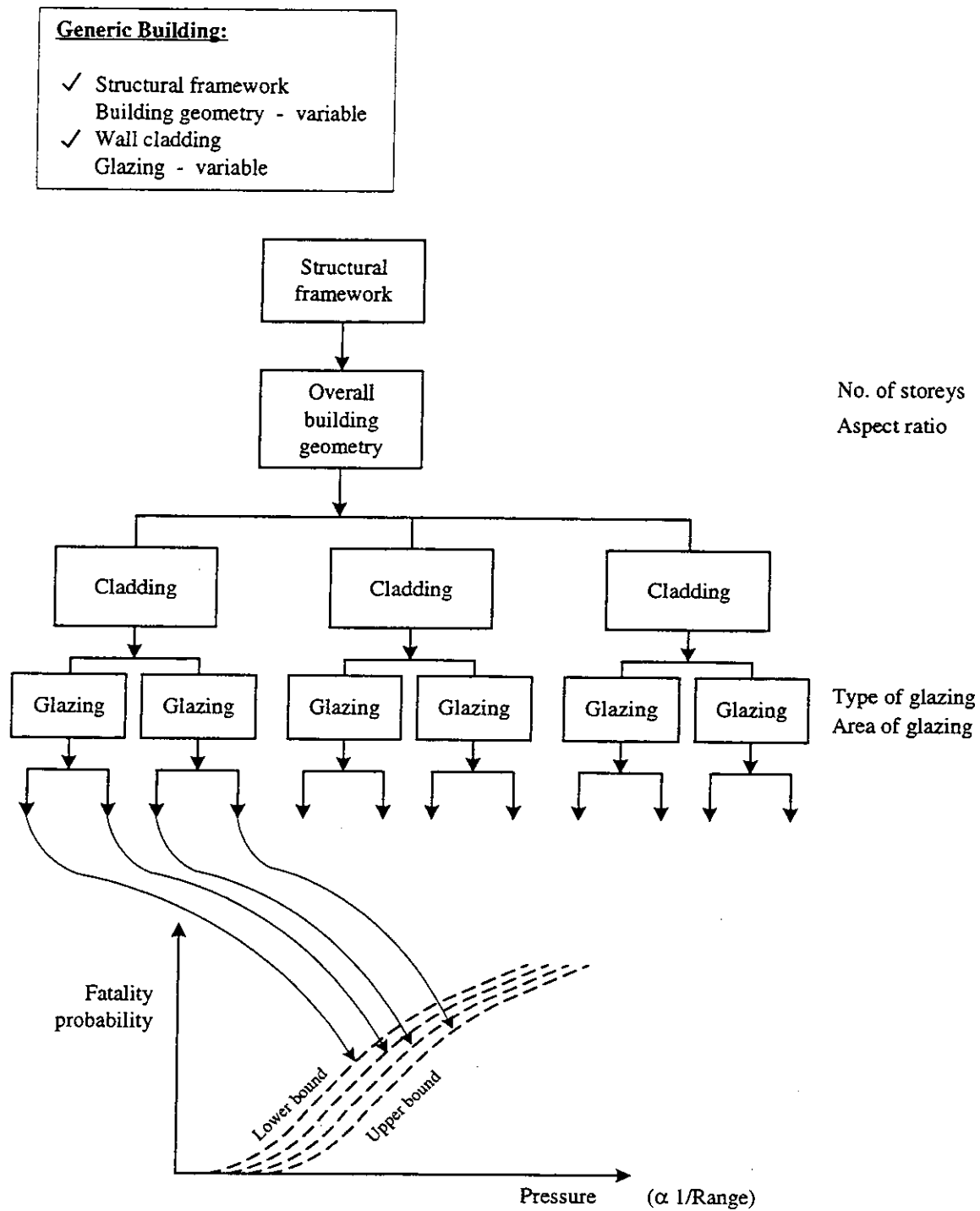


**Figure 4.2**

**Generic building fatality probability**

## 5 BUILDING CATEGORISATION

A common building type and building use matrix has been developed for the following building types (Table 5.1):

Portacabin/timber building	(B1)
Brick building	(B2)
Concrete framed building	(B3)
Steel framed building	(B4)
Special types	(B5)
- long span	
- tall buildings	
- hardened structures: on site blast - resistant design	

In order to assess the structural behaviour of these buildings with increasing pressure a procedure which assesses the integrity of the various structural components needs to be developed (e.g. glazing, external wall cladding, load bearing frame). This requires the categorisation of the building by the following features:

- Glazing area and type;
- Construction and spacing of load bearing frame;
- Construction of external wall cladding; and
- Dimensions of building.

Two lists have been compiled as shown on the following pages. Table 5.1 summarises the probable combinations of building materials, frame type, building height and aspect ratio. It is not all inclusive but it represents a fairly wide range of typical, i.e. common, buildings found in the UK. It also represents possible combinations of materials and framing for new buildings. However, in order to rationalise the building types and to develop generic fatality probability functions for particular building types, the types shown in Table 5.2 have been considered. The building types which have the larger aspect ratios have tended to be highlighted as the response of these buildings with blast loads applied along the two building axes will tend to envelope the behaviour of the buildings with intermediate aspect ratios, although the most realistic layouts have also been taken into consideration.

The data used for these two tables are based on WS Atkins' experience in the building sector and from previous work on similar subjects. Certain characteristics regarding overall size, aspect ratio and building height have been extracted from publications such as Tutt and Adler [9] and the DOE/PSA Technical Guides 1 & 2 [10].

No.	Type	Building use	No. of storeys	Aspect ratio	Frame type	Floor const. (elevated)	Roof constr.	Wall Const.	Glazing type
1		SC/TE/FBE	1	3:1	Timber	-	Timber	Timber Panels	Sing e
2	Portacabin	SC/TE/FBE	1	2:1	Timber	-	Timber	Timber Panels	Sing c
3	(B1)	SC/TE/FBE	2	3:1	Timber/Steel	Timber	Timber	Timber Panels	Sing e
4		SC/TE/FBE	2	2:1	Timber/Steel	Timber	Timber	Timber Panels	Sing e

**Table 5.1:**

**Common building types & building use matrix**

No.	Type	Building use	No. of storeys	Aspect ratio	Frame type	Floor const. (elevated)	Roof constr.	Wall const.	Glazing type
1		RH/SC	1	1:1	Timber/Steel	-	Timber	Brick/Block	Single
2		RH/SC	1	2:1	Timber/Steel	-	Timber	Brick/Block	Single
3		RH/SC/FBO	1	3:1	Load Bearing	-	Timber	Brick/Block	Double
4		RH/RF	2	1:1	Brick/Block	Timber	Timber	Brick/Block	Single
5		RH/RF/SC	2	2:1	Brick/Block	Timber	Timber	Brick/Block	Single
6		RH/RF/SC	2	3:1	Brick/Block	Timber	Timber	Brick/Block	Double
7	Brick	RH/RF/SC	3	1:1	Brick/Block	Timber	Timber	Brick/Block	Single
8	(B2)	RH/RF/SC	3	2:1	Brick/Block	Timber	Timber	Brick/Block	Single
9		RH/RF/SC	3	3:1	Brick/Block	Timber	Timber	Brick/Block	Double
10		RH/SC/HO/RF	2	1:1	Brick/Block	Conc	Timber	Brick/Block	Single
11		RH/SC/HO/RF	2	2:1	Brick/Block	Conc	Timber	Brick/Block	Single
12		RH/SC/HO/RF	2	3:1	Brick/Block	Conc	Timber	Brick/Block	Double
13		RH/SC/HO/RF	3	1:1	Brick/Block	Conc	Timber	Brick/Block	Single
14		RH/SC/HO/RF	3	2:1	Brick/Block	Conc	Timber	Brick/Block	Double
15		RH/SC/HO/RF	3	3:1	Brick/Block	Conc	Timber	Brick/Block	Double

Table 5.1 (cont'd):

Common building types & building use matrix

No.	Type	Building use	No. of storeys	Aspect ratio	Frame type	Floor const. (elevated)	Roof constr.	Wall conc.	Glazing type
1		RF/RH/HO/SC/CO	2	2:1	MRF	Concrete	Concrete	Brick/Block	Double
2		RF/RH/HO/SC/CO	2	3:1	MRF	Concrete	Concrete	Brick/Block	Double
3		RF/RH/HO/SC/CO	2	4:1	MRF	Concrete	Concrete	Brick/Block	Double
4		RF/RH/HO/SC/CO	2	5:1	MRF	Concrete	Concrete	Brick/Block	Double
5		RF/RH/HO/SC/CO	2	6:1	MRF	Concrete	Concrete	Brick/Block	Double
6		RF/RH/HO/SC/CO	2	2:1	MRF	Concrete	Concrete	Concrete Panels	Double
7	RC Concrete	RF/RH/HO/SC/CO	2	3:1	MRF	Concrete	Concrete	Concrete Panels	Double
8	(B3)	RF/RH/HO/SC/CO	2	4:1	MRF	Concrete	Concrete	Concrete Panels	Double
9		RF/RH/HO/SC/CO	2	5:1	MRF	Concrete	Concrete	Concrete Panels	Double
10		RF/RH/HO/SC/CO	2	6:1	MRF	Concrete	Concrete	Concrete Panels	Double
11		RF/HO/CO	3	2:1	Braced Frame	Concrete	Concrete	Brick/Block	Double
12		RF/HO/CO	3	3:1	Braced Frame	Concrete	Concrete	Brick/Block	Double
13		RF/HO/CO	3	4:1	Braced Frame	Concrete	Concrete	Brick/Block	Double
14		RF/HO/CO	3	5:1	Braced Frame	Concrete	Concrete	Brick/Block	Double
15		RF/HO/CO	3	6:1	Braced Frame	Concrete	Concrete	Brick/Block	Double

Table 5.1 (cont'd):

Common building types & building use matrix

No.	Type	Building use	No. of storeys	Aspect ratio	Frame type	Floor const. (elevated)	Roof const.	Wall conc.	Glazing type
16		RF/HO/CO	3	2:1	Braced Frame	Concrete	Concrete	Concrete	Double
17		RF/HO/CO	3	3:1	Braced Frame	Concrete	Concrete	Concrete	Double
18		RF/HO/CO	3	4:1	Braced Frame	Concrete	Concrete	Concrete	Double
19		RF/HO/CO	3	5:1	Braced Frame	Concrete	Concrete	Concrete	Double
20		RF/HO/CO	3	6:1	Braced Frame	Concrete	Concrete	Concrete	Double
21		RF/HO/CO	4	2:1	Braced Frame	Concrete	Concrete	Concrete	Double
22	RC Concrete	RF/HO/CO	4	3:1	Braced Frame	Concrete	Concrete	Brick/Block	Double
23	(B3)	RF/HO/CO	4	4:1	Braced Frame	Concrete	Concrete	Brick/Block	Double
24		RF/HO/CO	4	5:1	Braced Frame	Concrete	Concrete	Brick/Block	Double
25		RF/HO/CO	4	6:1	Braced Frame	Concrete	Concrete	Brick/Block	Double
26		RF/HO/CO	4	2:1	Braced Frame	Concrete	Concrete	Concrete	Double
27		RF/HO/CO	4	3:1	Braced Frame	Concrete	Concrete	Concrete	Double
28		RF/HO/CO	4	4:1	Braced Frame	Concrete	Concrete	Concrete	Double
29		RF/HO/CO	4	5:1	Braced Frame	Concrete	Concrete	Concrete	Double
30		RF/HO/CO	4	6:1	Braced Frame	Concrete	Concrete	Concrete	Double

Table 5.1 (cont'd):

Common building types & building use matrix

No.	Type	Building use	No. of storeys	Aspect ratio	Frame type	Floor const. (elevated)	Roof constr.	Wall constr.	Glazing type
1		CI/RE/LB/FBN	1	1:1	MRF	-	Clad	Clad	Double
2		CI/RE/LB/FBN	1	2:1	MRF	-	Clad	Clad	Double
3		CI/RE/LB/FBN	1	3:1	MRF	-	Clad	Clad	Double
4		CI/RE/LB/FBN	1	4:1	MRF	-	Clad	Clad	Double
5		CI/RE/LB/FBN	1	5:1	MRF	-	Clad	Clad	Double
6	Steel	CI/RE/LB/FBN	1	1:1	MRF	-	Clad	Clad	Double
7	(B4)	CI/RE/LB/FBN	1	2:1	MRF	-	Clad	Clad	Double
8		CI/RE/LB/FBN	1	2:1	MRF	-	Clad	Clad	Double
9		CI/RE/LB/FBN	1	4:1	MRF	-	Clad	Clad	Double
10		CI/RE/LB/FBN	1	5:1	MRF	-	Clad	Clad	Double
11		CI/RE/LB/FBN	1	1:1	Braced	-	Clad	Clad	Double
12		CI/RE/LB/FBN	1	2:1	Braced	-	Clad	Clad	Double
13		CI/RE/LB/FBN	1	3:1	Braced	-	Clad	Clad	Double
14		CI/RE/LB/FBN	1	4:1	Braced	-	Clad	Clad	Double
15		CI/RE/LB/FBN	1	5:1	Braced	-	Clad	Clad	Double
16		CI/RE/LB/FBN	1	1:1	Braced	-	Clad	Clad	Double
17		CI/RE/LB/FBN	1	2:1	Braced	-	Clad	Clad	Double

Table 5.1 (cont'd):

Common building types & building use matrix

No.	Type	Building use	No. of storeys	Aspect ratio	Frame type	Floor const. (elevated)	Roof const.	Wall const.	Glazing type
18		CI/RE/LB/FBN	1	3:1	Braced	-	Clad	Clad	Double
19		CI/RE/LB/FBN	1	4:1	Braced	-	Clad	Clad	Double
20		CI/RE/LB.FBN	1	5:1	Braced	-	Clad	Clad	Double
21		CO/CI/RE/LB	2	1:1	Braced	PC Units	Clad	Brick/Block	Double
22		CO/CI/RE/LB	2	2:1	Braced	PC Units	Clad	Brick/Block	Double
23		CO/CI/RE/LB	2	3:1	Braced	PC Units	Clad	Brick/Block	Double
24		CO/CI/RE/LB	2	4:1	Braced	PC Units	Clad	Brick/Block	Double
25	Steel	CO/CI/RE/LB	2	5:1	Braced	PC Units	Clad	Brick/Block	Double
26	(B4)	CO/CI/RE/LB	2	1:1	Braced	PC Units	Clad	Concrete Panels	Double
27		CO/CI/RE/LB	2	2:1	Braced	PC Units	Clad	Concrete Panels	Double
28		CO/CI/RE/LB	2	3:1	Braced	PC Units	Clad	Concrete Panels	Double
29		CO/CI/RE/LB	2	4:1	Braced	PC Units	Clad	Concrete Panels	Double
30		CO/CI/RE/LB	2	5:1	Braced	PC Units	Clad	Concrete Panels	Double
31		CO/RE	3	1:1	Braced	PC Units	Tiles	Brick/Block	Double
32		CO/RE	3	2:1	Braced	PC Units	Tiles	Brick/Block	Double

Table 5.1 (cont'd):

Common building types & building use matrix



No.	Type	Building use	No. of storeys	Aspect ratio	Frame type	Floor const. (elevated)	Roof constr.	Wall constr.	Glazing type
33		CO/RE	3	3:1	Braced	PC Units	Tiles	Brick/Block	Double
34		CO/RE	3	4:1	Braced	PC Units	Tiles	Brick/Block	Double
35		CO/RE	3	5:1	Braced	PC Units	Tiles	Brick/Block	Double
36		CO/RE	3	1:1	Braced	PC Units	Tiles	Concrete Panels	Double
37		CO/RE	3	2:1	Braced	PC Units	Tiles	Concrete Panels	Double
38		CO/RE	3	3:1	Braced	PC Units	Tiles	Concrete Panels	Double
39		CO/RE	3	4:1	Braced	PC Units	Tiles	Concrete Panels	Double
40	Steel	CO/RE	3	5:1	Braced	PC Units	Tiles	Concrete Panels	Double
41	(B4)	CO	4	1:1	Braced	PC Units	Tiles	Brick/Block	Double
42		CO	4	2:1	Braced	PC Units	Tiles	Brick/Block	Double
43		CO	4	3:1	Braced	PC Units	Tiles	Brick/Block	Double
44		CO	4	4:1	Braced	PC Units	Tiles	Brick/Block	Double
45		CO	4	5:1	Braced	PC Units	Tiles	Brick/Block	Double
46		CO	4	1:1	Braced	PC Units	Tiles	Concrete Panels	Double

**Table 5.1 (cont'd):**

**Common building types & building use matrix**

No.	Type	Building use	No. of storeys	Aspect ratio	Frame type	Floor const. (elevated)	Roof constr.	Wall constr.	Glazing type
47		CO	4	2:1	Braced	PC Units	Tiles	Concrete Panels	Double
48		CO	4	3:1	Braced	PC Units	Tiles	Concrete Panels	Double
49		CO	4	4:1	Braced	PC Units	Tiles	Concrete Panels	Double
50		CO	4	5:1	Braced	PC Units	Tiles	Concrete Panels	Double

Table 5.1 (cont'd):

Common building types & building use matrix

No.	Type	Building use	No. of storeys	Aspect ratio	Frame type	Floor const. (elevated)	Roof constr.	Wall constr.	Glazing type
1	Long Span	LB	1	2:1	Braced Steel	-	Clad	Clad	Double
2	Long Span	LB	1	3:1	Braced Steel	-	Clad	Clad	Double
3	Tall Buildings	RF/CO	5-20	1:1	Coupled Shear Walls	Concrete	Concrete	Concrete Panels	Double
4	Tall Buildings	RF/CO	5-20	2:1	Coupled Shear Walls	Concrete	Concrete	Concrete Panels	Double
5	Tall Buildings	CO	5-20	3:1	Coupled Shear Walls	Concrete	Concrete	Curtain Walling	Double
6	Hardened Structure	CI	1	2:1	Braced Steel	Concrete	Concrete	Concrete Panels	None

**Note:**

1. Data from previous work and from "New Metric Handbook Planning and Design Data" by P Tutt & D Adler [9].
2. Tall building data from DoE/PSA Technical Guides 1 x 2 on Shear Walls & Box Frame Design of Buildings [10].

**BUILDING USE CODE**

RH: Residential Housing	CO: Commercial/Office	FBO: Factory Building Old
RF: Residential	CI: Commercial/Industrial	FBN: Factory Building New
HO: Hospital	RE: Retail/Hypermarket	FBE: Factory Building Ext
SC: School	LB: Leisure Building	TE: Temporary Building

**Table 5.1 (cont'd):**

**Common building types & building use matrix: special types**

Building type	Building use	No. of storeys	Aspect ratio	Frame type	Floor construction (elevated)	Roof construction	Wall construction	Glazing type
Portacabin (B1)	SC/TE/FBE	1	2:1	Timber	-	Timber	Timber panels	Single
	SC/TE/FBE	2	3:1	Timber/steel	Timber	Timber	Timber panels	Single
Brick Built (B2)	RH/SC	1	2:1	Timber/steel	-	Timber	Brick/block	Single
	RH/SC	2	2:1	Brick/block	Timber	Timber	Brick/block	Single
	RH/SC	3	2:1	Brick/block	Timber	Timber	Brick/block	Single
	RH/SC/HO/RF	3	3:1	Brick/block	Concrete	Timber	Brick/block	Double

**BUILDING USE CODE**

RH:	Residential Housing	CO:	Commercial/Office	FBO:	Factory Building Old
RF:	Residential	CI:	Commercial/Industrial	FBN:	Factory Building New
HO:	Hospital	RE:	Retail/Hypermarket	FBE:	Factory Building Ext
SC:	School	LB:	Leisure Building	TE:	Temporary Building

**Table 5.2:**

**Generic building types**

Building type	Building use	No. of storeys	Aspect ratio	Frame type	Floor construction (elevated)	Roof construction	Wall construction	Glazing type
Concrete frame (B3)	RF/RH/HO/SC/CO	2	4:1	MRF	Concrete	Concrete	Brick/block	Double
	RF/RH/HO/SC/CO	2	4:1	MRF	Concrete	Concrete	Concrete panels	Double
	RF/HO/CO	4	4:1	Braced frame	Concrete	Concrete	Brick/block	Double
	RF/HO/CO	4	4:1	Braced frame	Concrete	Concrete	Brick/block	Double

**BUILDING USE CODE**

RH:	Residential Housing	CO:	Commercial/Office	FBO:	Factory Building Old
RF:	Residential	CI:	Commercial/Industrial	FBN:	Factory Building New
HO:	Hospital	RE:	Retail/Hypermarket	FBE:	Factory Building Ext
SC:	School	LB:	Leisure Building	TE:	Temporary Building

**Table 5.2:**

**Generic building types**

Building type	Building use	No. of storeys	Aspect ratio	Frame type	Floor construction (elevated)	Roof construction	Wall construction	Glazing type
Steel frame (B4)	CI/RE/LB/FBN	1	5:1	MRF	-	Clad	Clad	Double
	CI/RE/LB/FBN	1	5:1	Braced	-	Clad	Clad	Double
	CO/CI/RE/LB	2	5:1	Braced	PC units	Tiles	Brick/block	Double
	CO/CI/RE/LB	2	5:1	Braced	PC units	Clad	Concrete panels	Double
	CO	4	2:1	Braced	PC units	PC units	Brick/block	Double
	CO	4	2:1	Braced	PC units	PC units	Concrete panels	Double
	LB	1	2:1	Braced steel	-	Clad	Clad	Double
	LB	1	3:1	Braced steel	-	Clad	Clad	Double
Special long span								

**BUILDING USE CODE**

RH:	Residential Housing	CO:	Commercial/Office	FBO:	Factory Building Old
RF:	Residential	CI:	Commercial/Industrial	FBN:	Factory Building New
HO:	Hospital	RE:	Retail/Hypermarket	FBE:	Factory Building Ext
SC:	School	LB:	Leisure Building	TE:	Temporary Building

**Table 5.2:**

**Generic building types**

Building type	Building use	No. of storeys	Aspect ratio	Frame type	Floor construction (elevated)	Roof construction	Wall construction	Glazing type
Special: Tall building	RF/CO	5-20	1:1	Coupled shear walls	Concrete	Concrete	Concrete panels	Double
	RF/CO	5-20	2:1	Coupled shear walls	Concrete	Concrete	Concrete panels	Double
	CO	5-20	3:1	Coupled shear walls	Concrete	Concrete	Curtain walling	Double
Special hardened structure	CI	1	2:1	Braced steel	Concrete	Concrete	Concrete panels	None

**BUILDING USE CODE**

RH:	Residential Housing	CO:	Commercial/Office	FBO:	Factory Building Old
RF:	Residential	CI:	Commercial/Industrial	FBN:	Factory Building New
HO:	Hospital	RE:	Retail/Hypermarket	FBE:	Factory Building Ext
SC:	School	LB:	Leisure Building	TE:	Temporary Building

**Table 5.2:**

**Generic building types**

## 6 BLAST OVERPRESSURE

A range of free-field side-on overpressures and positive phase durations have been determined using the TNO Multi-Energy Model (Figure 6.1). This model offers a range of curves from which the data may be read. Curve 1 equates to laminar burning and Curve 10 to a gas-phase detonation. Curve 7 is widely used for the kind of explosions of interest in this study, and will be used here to indicate the pressures and durations of interest for given combustion energies. Two pressure profiles will be used in this study, the shock wave and the pressure wave, although Curve 7 indicates that the profile will be a combination of the two. The range of combustion energies of interest are between  $4.65 \times 10^{10}$  J to around  $4.65 \times 10^{11}$  J (equivalent to 1 te and 10 te of propane respectively). The range of combustion energy scaled distances to be considered would be between 0.3 and 30 (the side-on overpressure at a scaled distance of 3 being about 0.7 kPa). Examples of the overpressure - distance, and positive phase duration - distance values obtained for three different combustion energies are shown in Tables 6.1 to 6.3.

The pressure loads experienced by the structure are dependent on the type of wave, the incident overpressure and the angle of incidence, as the reflected pressure load may be higher than the incident pressure. In addition to the pressure rise, blast is accompanied by air displacement in the direction of the blast wave, which produces extra loading on a reflective surface. Values for this additional dynamic pressure are also given in Tables 6.1 to 6.3.

The Multi-Energy Model is being used solely to define the range of pressures and impulses potentially of interest for this study, and the results from the study will thus not be linked specifically to this model, but will be relevant to any vapour cloud explosion for which the peak overpressures, wave form and blast durations are known.



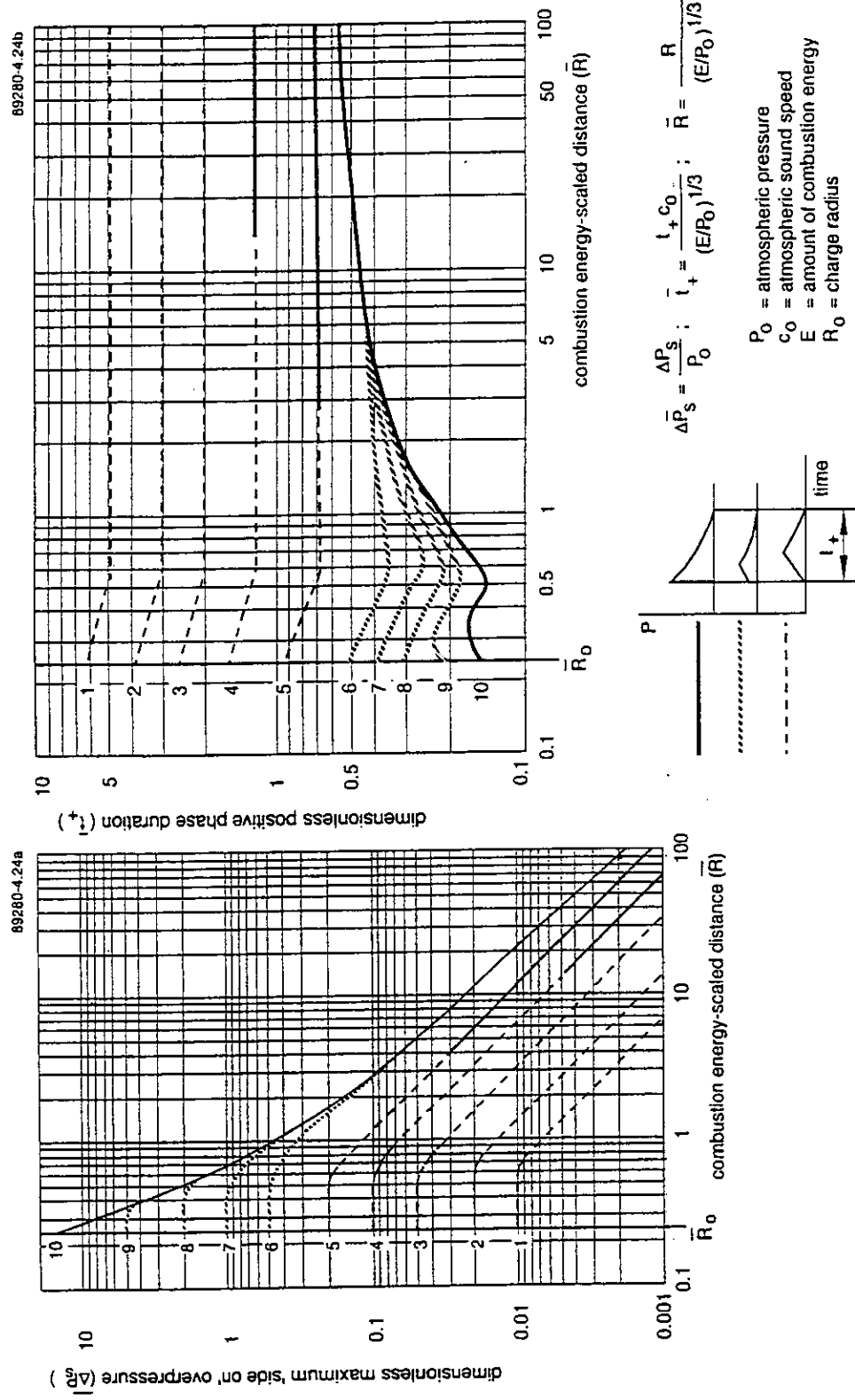


Figure 6.1 TNO Multi-Energy Model

Overpressures for 1 te propane equivalent (4.65E+10 J)							
Scaled distance R	Distance (m)	Scaled pressure	Side-on pressure (kPa)	Scaled dynamic pressure	Dynamic pressure (kPa)	Scaled t+	t+ (ms)
0.3	23.14018	1.0	101.325	0.595	60.28838	0.368353	83.5661
0.4	30.85357	1.0	101.325	0.550	55.72875	0.324539	73.62644
0.5	38.56696	0.940567	95.30297	0.380	38.50350	0.285114	64.68218
0.6	46.28036	0.825371	83.63074	0.235	23.81138	0.265829	60.30718
0.7	53.99375	0.710137	71.95461	0.152	15.40140	0.26535	60.19845
0.8	61.70714	0.608877	61.69444	0.105	10.63913	0.280759	63.69434
0.9	69.42053	0.524040	53.09833	0.078	7.90335	0.293782	66.64859
1	77.13393	0.454179	46.01968	0.060	6.07950	0.305083	69.21239
2	154.2679	0.164167	16.63425	0.00885	0.89673	0.370057	83.9527
3	231.4018	0.094133	9.538036	0.00275	0.27864	0.400898	90.94954
4	308.5357	0.065822	6.669409	0.0	0.0	0.420211	95.33091
5	385.6696	0.051201	5.187953	0.0	0.0	0.43406	98.47287
6	462.8036	0.041701	4.225343	0.0	0.0	0.444813	100.9123
7	539.9375	0.035058	3.552223	0.0	0.0	0.4536	102.9057
8	617.0714	0.030165	3.056463	0.0	0.0	0.461038	104.5931
9	694.2053	0.026419	2.676928	0.0	0.0	0.467495	106.058
10	771.3393	0.023464	2.377539	0.0	0.0	0.473207	107.3539
20	1542.679	0.017533	1.776562	0.0	0.0	0.509969	115.6937
30	2314.018	0.006813	0.690294	0.0	0.0	0.530841	120.429

**Table 6.1:**  
**Overpressures for 1 te propane equivalent**

Overpressures for 3 te propane equivalent (1.395E+11 J)							
Scaled distance R	Distance (m)	Scaled pressure	Side-on pressure (kPa)	Scaled dynamic pressure	Dynamic pressure (kPa)	Scaled t+	t+ (ms)
0.3	33.37391	1.0	101.325	0.595	60.28838	0.368353	120.5232
0.4	44.49855	1.0	101.325	0.550	55.72875	0.324539	106.1877
0.5	55.62319	0.940567	95.30297	0.380	38.50350	0.285114	93.28784
0.6	66.74782	0.825371	83.63074	0.235	23.81138	0.265829	86.97801
0.7	77.87246	0.710137	71.95461	0.152	15.40140	0.26535	86.82119
0.8	88.99710	0.608877	61.69444	0.105	10.63913	0.280759	91.86313
0.9	100.1217	0.52404	53.09833	0.078	7.90335	0.293782	96.12390
1	111.2464	0.454179	46.01968	0.060	6.07950	0.305083	99.82153
2	222.4927	0.164167	16.63425	0.00885	0.89673	0.370057	121.0808
3	333.7391	0.0941331	9.538036	0.00275	0.27864	0.400898	131.1719
4	444.9855	0.065822	6.669409	0.0	0.0	0.420211	137.4910
5	556.2319	0.051201	5.187953	0.0	0.0	0.43406	142.0225
6	667.4782	0.041701	4.225343	0.0	0.0	0.444813	145.5407
7	778.7246	0.035058	3.552223	0.0	0.0	0.4536	148.4158
8	889.9710	0.030165	3.056463	0.0	0.0	0.461038	150.8494
9	1001.217	0.026419	2.676928	0.0	0.0	0.467495	152.9621
10	1112.464	0.023464	2.377539	0.0	0.0	0.473207	154.8311
20	2224.927	0.017533	1.776562	0.0	0.0	0.509969	166.8593
30	3337.391	0.006813	0.690294	0.0	0.0	0.530841	173.6886

**Table 6.2:**

**Overpressures for 3 te propane equivalent**

Overpressures for 10 te propane equivalent (4.65E+11 J)							
Scaled distance R	Distance (m)	Scaled pressure	Side-on pressure (kPa)	Scaled dynamic pressure	Dynamic pressure (kPa)	Scaled t+	t+ (ms)
0.3	49.8540	1.0	101.325	0.595	60.28838	0.368353	180.0377
0.4	66.4720	1.0	101.325	0.550	55.72875	0.324539	158.6234
0.5	83.0900	0.940567	95.30297	0.380	38.50350	0.285114	139.3535
0.6	99.7080	0.825371	83.63074	0.235	23.81138	0.265829	129.9279
0.7	116.326	0.710137	71.95461	0.152	15.40140	0.265350	129.6936
0.8	132.944	0.608877	61.69444	0.105	10.63913	0.280759	137.2253
0.9	149.562	0.52404	53.09833	0.078	7.90335	0.293782	143.5900
1	166.180	0.454179	46.01968	0.060	6.07950	0.305083	149.1136
2	332.360	0.164167	16.63425	0.00885	0.89673	0.370057	180.8706
3	498.540	0.094133	9.538036	0.00275	0.27864	0.400898	195.9449
4	664.720	0.065822	6.669409	0.0	0.0	0.420211	205.3842
5	830.900	0.051201	5.187953	0.0	0.0	0.434060	212.1534
6	997.080	0.041701	4.225343	0.0	0.0	0.444813	217.4089
7	1163.26	0.035058	3.552223	0.0	0.0	0.453600	221.7037
8	1329.44	0.030165	3.056463	0.0	0.0	0.461038	225.3390
9	1495.62	0.026419	2.676928	0.0	0.0	0.467495	228.4950
10	1661.80	0.023464	2.377539	0.0	0.0	0.473207	231.2869
20	3323.60	0.017533	1.776562	0.0	0.0	0.509969	249.2546
30	4985.40	0.006813	0.690294	0.0	0.0	0.530841	259.4563

**Table 6.3:**  
**Overpressures for 10 te propane equivalent**

## 7 STRUCTURAL LOADS

Having defined the structures of interest (Section 5) and the incident pressure pulse (Section 6), it is necessary to investigate how that pulse interacts with the structure, as described in Section 3, and to estimate the actual loads that the structure experiences.

A method of determining the forces acting on a building due to a blast wave has been developed from existing work [2]. This enables the horizontal loading on the building in the direction of the shock wave to be calculated with respect to time, as the blast wave passes over the building. In addition, the pressure rise within a building due to a blast wave entering through an open area has been considered, to give some idea of the pressure relief that can be expected for different vent area/volume ratios. These calculations are outlined in the following sections.

### 7.1 External loading on the building

The horizontal loading on the building structure is defined as being a combination of three blast wave effects, which can be combined to form an overall loading curve with respect to time:

#### - Loading on front face

In the case of an incident shock wave, the primary loading on the front face of the building comes from the reflected pressure,  $P_r$ , which has a value considerably higher than the peak incident overpressure. The reflected value is dependent on the incident overpressure, the pulse shape and the angle of incidence. Values for reflection coefficients (ratio of reflected and incident overpressure) for incident shock waves are presented in Figure 7.1. This primary loading is initially at a peak value, but reduces to zero at a steady rate as the blast wave leaves the front face of the building. However, as mentioned in Section 3, in the case of an incident pressure wave, the maximum pressure experienced by the front face of the building is just the sum of the peak incident pressure and the dynamic pressure.

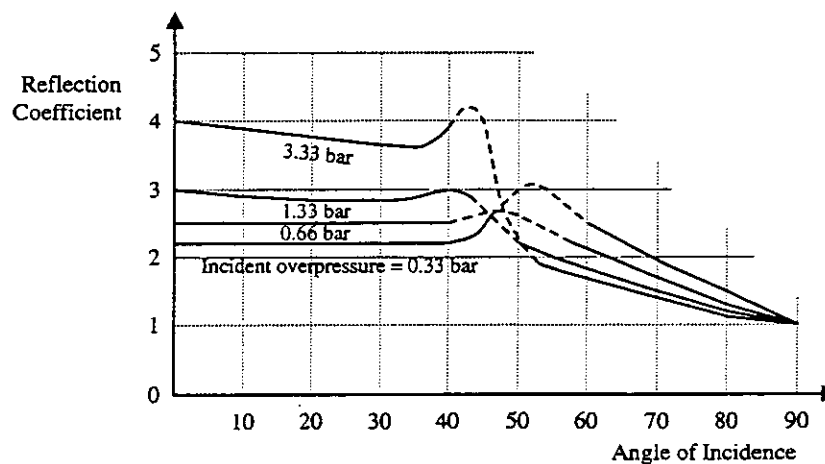


Figure 7.1:

Reflection coefficient vs angle of incidence for varying values of incident overpressure (low pressure range)

### Peak overpressure/drag

The secondary loading arises from a combination of the peak overpressure and the building drag as air is displaced around the building. This loading comes into effect when the initial reflected pressure falls to a value that is lower than the secondary pressure. The secondary pressure lasts for the duration of the blast wave during which time it diminishes to zero at a steady rate. This dynamic pressure can be calculated from the equation:

$$Q_D = C_D \times Q$$

where  $C_D$  is the drag coefficient of the building and  $Q$  is the blast pressure, calculated from the incident pressure,  $P_s$  and the atmospheric pressure,  $P_o$  as:

$$Q = \frac{5}{2} \times \frac{P_s^2}{7P_o + P_s}$$

This equation is appropriate for shock waves, but in comparison with the Multi-Energy Method underestimates the dynamic pressure associated with a pressure wave, close to the source of the blast.

The combination of the initial reflected pressure and the secondary dynamic pressure results in a pressure load of the shape shown in Figure 7.2.

### Loading on rear face

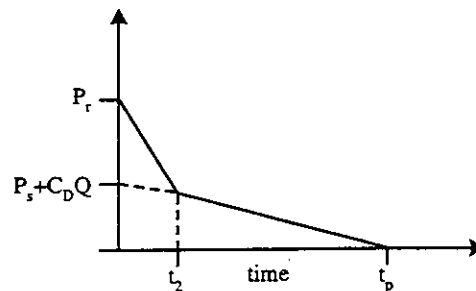
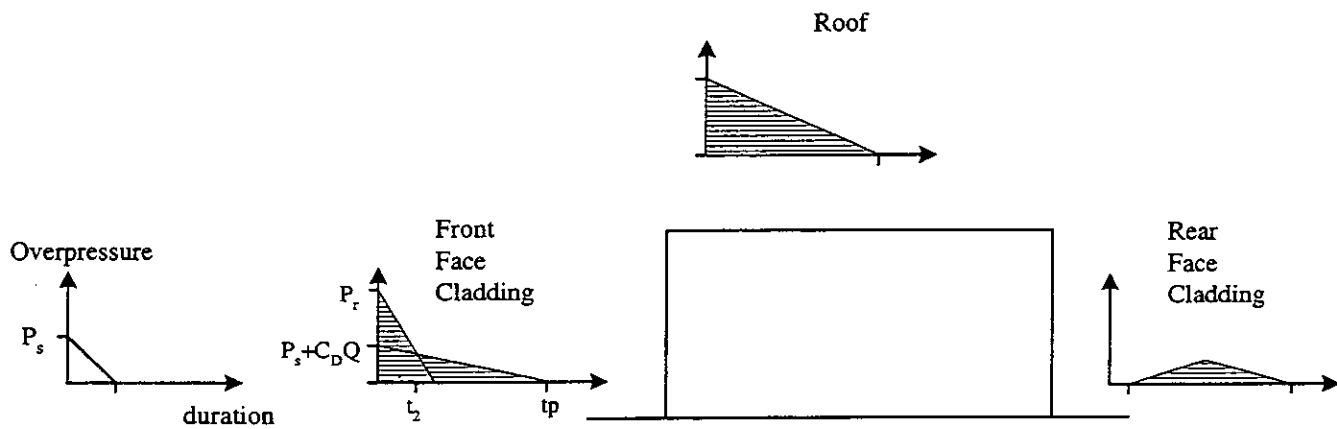


Figure 7.2:

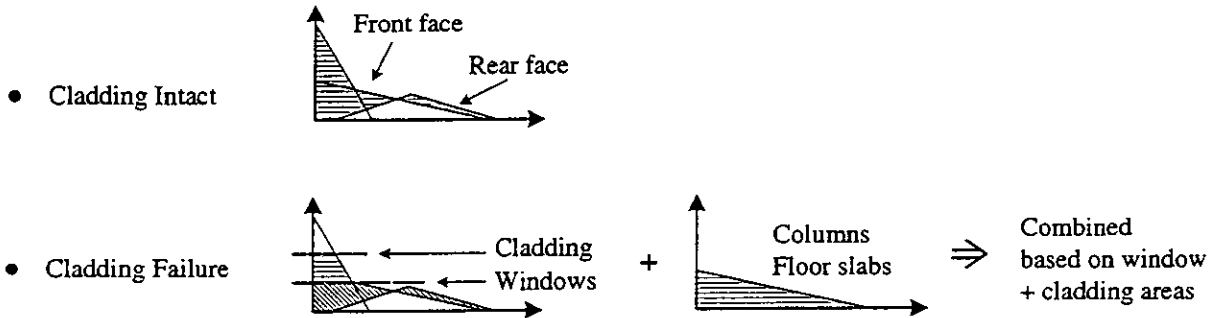
Schematic representation of the time-pressure diagram  
for a finite reflective surface

The third contribution to loading arises when the blast wave reaches the rear of the building. As the wave travels across the rear face, there is a corresponding increase in pressure, as a larger area of the face is covered by the blast wave. This opposes the pressure on the front face, and has the effect of reducing the overall translational load. As soon as the blast wave passes the rear of the building, loading returns to zero.

The pressures acting on the front and rear faces of the building are converted into forces by multiplying them by the total area of the building face. The total loading of the building with respect to time can then be determined. However, the loading will be modified by the failure of any of the structural components, such as windows, cladding or structural frame. This is illustrated in Figure 7.3, which shows the external pressure loads on the building for both the cladding intact and the cladding failed scenarios.



**Overall Building Framework**



**Note**

- Structural resistance of ext. cladding > int. partitions
- Pressure pulses function of geometry of building

**Figure 7.3:**

**External pressure loads on building periphery**

### 7.1.1 Load calculations

As an example, a typical rectangular building structure has been considered. This building was modelled as a block with a defined height, width and length. It was considered to be positioned so that the blast wave would strike the front face and pass around and over the building. For analysis of the loading on the structure, only the forces acting in the direction of the blast wave were considered, as forces on the sides of the building cancel each other out and therefore do not affect the loading on the structural frame. Pressure loading on the roof of the building acting vertically does not have an effect in the direction of the blast wave. It was also assumed for the purpose of these calculations that no cladding failure occurred: internal pressure is considered in Section 7.2.

The blast wave was defined in terms of its peak overpressure, and its duration. The shape of the wave was considered to be a triangular pulse with a typical duration of 0.1 to 0.2 seconds, and an amplitude of up to 1 bar.

The pressure variation on the front face of the building was calculated in accordance with Section 7.1 as the combination of the reflected pressure and the dynamic pressure. The initial value of pressure is equal to the peak reflected pressure  $P_r$ , calculated from the equation:

$$P_r = 2P_s + \frac{(\gamma + 1)P_s^2}{[(\gamma - 1)P_s] + 2\gamma P_o}$$

where  $P_s$  is the peak incident side-on overpressure and  $\gamma$  is the ratio of the specific heat at constant pressure to that at constant volume and is equal to 1.4 for air at fairly low pressures.  $P_o$  is atmospheric pressure.

This peak initial pressure decays down to a value equal to the incident side-on overpressure plus the dynamic pressure in a time  $t_2$ :

$$t_2 = \frac{3S}{U}$$

where  $S$  is a building dimension equal to half the width, or the height, whichever is the smaller, and  $U$  is the velocity of the wavefront, calculated from:

$$U = a_o \frac{\sqrt{1 + 6P_s}}{7P_o}$$

where  $a_o$  is the speed of sound at atmospheric pressure.

Once the pressure reaches a value equal to the incident pressure and the dynamic pressure, it decays to zero over a time equal to  $t_p - t_2$  where  $t_p$  is the positive phase pulse duration. The resulting pressure variation is similar to that shown in Figure 7.2.



The blast wave reaches the rear face of the building after a time  $t_{back} = L/U$  where  $L$  is the length of the building. The pressure then builds up over a time  $t_{maxp} = 4S/U$ , at which point it reaches a maximum value assumed to be equal to the peak incident overpressure  $P_s$ . The pressure at the rear face then decreases such that it reaches zero at a time  $t_p + L/U$  where  $t_p$  is the pulse duration.

For a building of dimensions 20 x 20 x 10 m, subject to a shock load with a maximum overpressure of 500 mbar and a duration of 100 ms, the calculated parameters are as follows:

Parameter	Value
Reflected pressure, $P_r$	1183 mbar
Dynamic pressure, $Q_D$	80 mbar
Velocity of wave-front, $U$	410 m/s
Time for initial pressure to decrease to incident and dynamic value, $t_2$	0.075 s
Time required for pulse to reach back face, $t_{back}$	0.05 s
Time taken for pressure to reach a maximum at rear face, $t_{maxp}$	0.099 s
Time at which pressure reaches zero at rear face	0.15 s

**Table 7.1**

**Structural Load Parameters for example calculation**

The resultant pressure on the building arising from the combined front and rear face pressures is as shown in Figure 7.4.

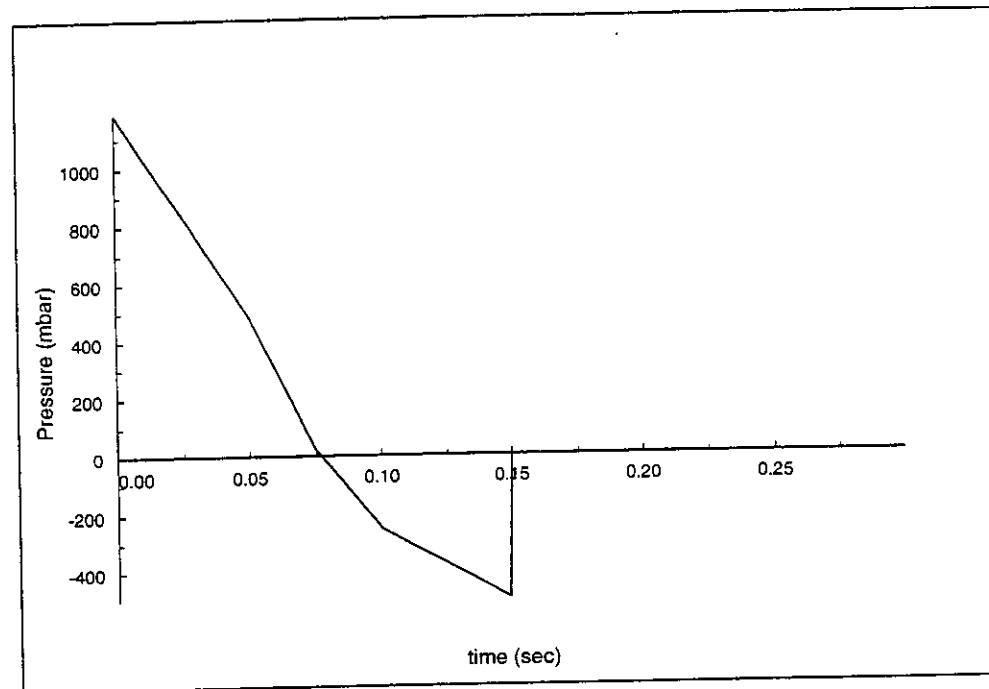


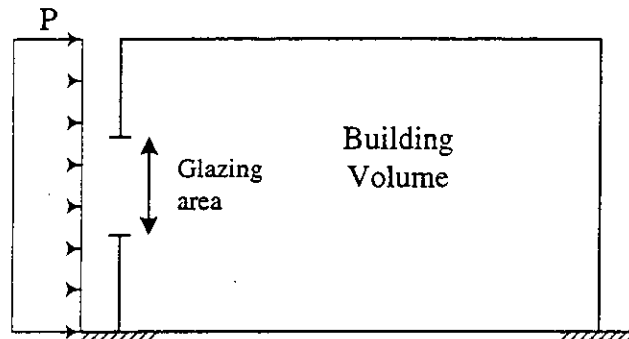
**Figure 7.4:**

### **Calculated resultant pressure variation on structure**

As can be seen from the figure, the initial peak of positive pressure falls away rapidly until it reaches the secondary loading curve. Pressure then falls less rapidly until pressure reaches the back face. Once the blast wave has reached the back face, it opposes the front face pressure, and overall loading on the structure is reduced further, becoming negative in most cases. As the back pressure falls away, the loading returns to zero. The combination of the above pressure loads on different buildings produce curves which tend to follow the same basic pattern.

## **7.2 Building internal pressure**

In these calculations, the pressure rise within a building due to a blast wave entering through open areas has been considered, in order to simulate the case in which windows or cladding have failed, and the pressure or shock wave enters the building, relieving the pressure on the exterior. The pressure relief which occurs when glazing or cladding fails is dependent on the rate of pressure rise within the building and the final pressure which occurs. This is in turn dependent on the pressure differential across the opening, the area of the opening and the volume of the building, as summarised in Figure 7.5.



Pressure relief is dependent upon:

- Pressure in building
- Time to develop pressure within building

Average pressure increases within a structure are given by [17]:

$$\Delta P_i = C_L \frac{A_0}{V_0} \Delta t$$

where:

- $\Delta P_i$  = internal pressure increment, psi
- $C_L$  = leakage pressure coefficient (function of pressure difference,  $P - P_i$ )
- $A_0$  = area of openings,  $\text{ft}^2$
- $V_0$  = volume of structure,  $\text{ft}^3$
- $\Delta t$  = time increment, ms

Limitations: small area of opening / volume ratios applied  
Pressure < 150 psi

**Figure 7.5:**

**Pressure relief on external walls from glazing/cladding failure**

The following geometries were considered:

<b>Building Geometry:</b>	<b>Vent Area:</b>	
5 x 5m x 4m high	0.1 m <sup>2</sup>	(32 x 32 cm) i.e one small window
Volume = 100m <sup>3</sup>	0.5 m <sup>2</sup>	(64 x 78 cm)
(Typical of a room)	1.0 m <sup>2</sup>	(1.0 x 1.0 m)
	5.0 m <sup>2</sup>	(3.0 x 1.67 m)
	10.0 m <sup>2</sup>	(4.0 x 2.5 m)
	15.0 m <sup>2</sup>	(4.5 x 3.33m) i.e. nearly the whole of one side open

In order to cover a range of likely scenarios, four blast waves were considered, a pressure wave, and a shock wave, each of 0.1 and 0.2 second duration.

The change of average pressure within the building was plotted for each of these different geometries and these results are presented in Figure 7.6 for the 100ms duration shock wave (shown as the dotted line on the figure). In addition, this information was used to determine curves for maximum internal pressure as a percentage of the peak blast pressure for each of the different pulse types. These curves are presented in Figure 7.7.

It can be seen from the figures that the most important aspect for determining the peak pressure inside the building is the ratio of open wall area to the volume of the building. As expected, for the small window, virtually no pressure relief can be claimed from venting through the window, whereas where one wall of the room is almost completely missing, the calculations predict that the pressure rise is very similar to the input shock pulse. Figure 7.7 shows that the greatest relief occurs for a long duration pressure wave, whereas the shorter duration shock wave shows lower internal pressure rise for the same open area/volume ratio.

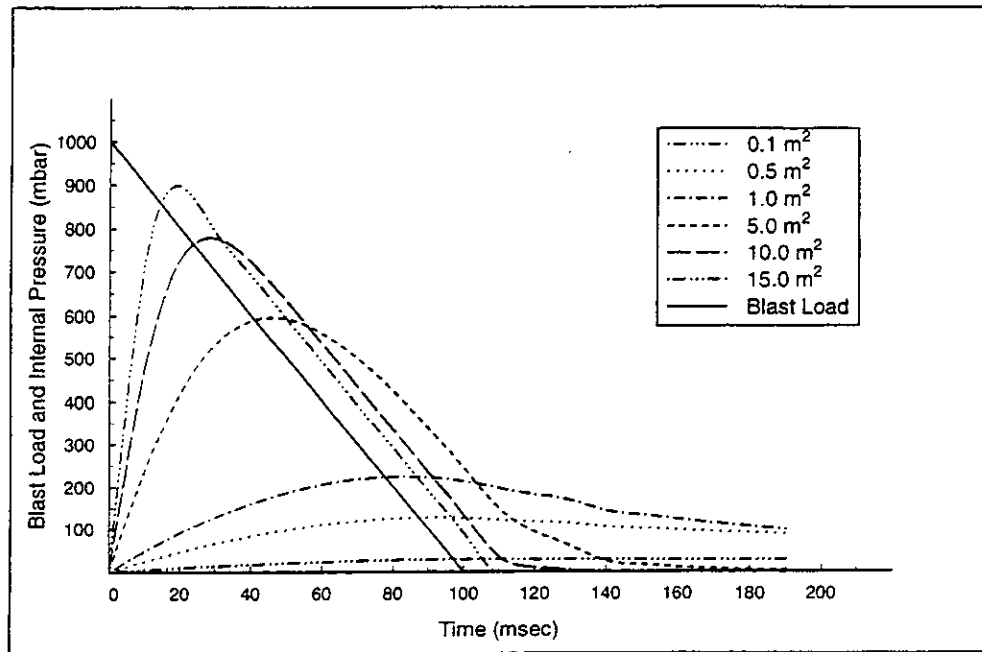


**Figure 7.6:**

**Blast and internal pressure for buildings with different vent areas**

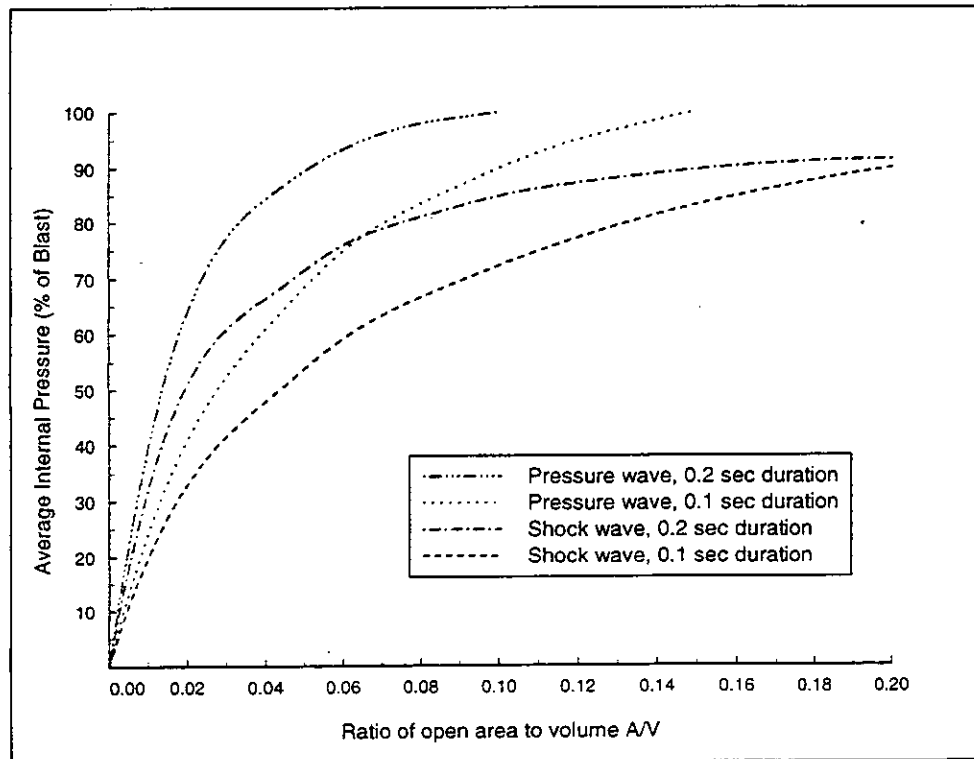


**Figure 7.7:**

**Building internal pressure as a function of applied pressure**

## 8 DYNAMIC RESPONSE

In order to assess the ability of a structure to withstand a load, it is first necessary to predict the response of the structure to the dynamic loading and the maximum displacements and forces caused by the load. This is a potentially complex task, and much time could be devoted to addressing this problem alone, using dynamic finite element and other numerical modelling techniques. However, for this study, the problem has been simplified and the structure considered as a single degree of freedom elasto-plastic system. In this case, the numerical analysis is presented in Biggs [23], and is outlined in Section 8.4.

The following key features of the structure define the limiting overpressure and pulse duration that the structure or component of the structure can withstand:

- The fundamental natural frequency of the structure.
- The dynamic collapse load of the structure.
- The ductility inherent in the type of construction.

The above characteristics, and the way in which they affect the dynamic response of the structure, are outlined below:

### 8.1 Fundamental natural frequency

The response of a structure to a dynamic load is highly dependent on the ratio of the duration of the impulse to the natural period of the structure. If the natural period of the structure is long compared with the impulse duration, the structure does not have time to respond to the impulse before it has died away. Alternatively, if the natural period is very short compared with the impulse duration, the loading can be considered to be quasistatic, and the structure undergoes a number of vibrations while the blast loading is still present. In this latter case, the ratio of the dynamic displacement to the static displacement is large, and the load on the structure is more onerous.

The fundamental natural period of the building (T) can be estimated, assuming that it is a one degree of freedom system and a 'reasonably modern building', using the following equation [3]:

$$T = 0.05 \times \left[ \frac{H}{\sqrt{B}} \right]$$

where

- H = height of building (ft)
- B = breadth of building (facing blast front) (ft)

The fundamental natural periods of the individual components of the building such as walls, floors, etc. have been estimated from experimental data [1, 6], and are given in Table 8.1.

Local		Period (ms)	References
Walls	Timber panels	40 - 90	6
	Brick/block	20 - 40	1, 84
	PC panels (concrete)	10 - 30	1, 84
	Cladding	60 - 100	6, 84
Roofs/Floors	Timber	10 - 30	1
	Concrete		
	Tiled		
	Clad		
	PC units		

**Table 8.1:**

**Typical periods of vibration of structural elements**

**8.2 Dynamic collapse load**

The dynamic collapse load is based on the static collapse load for a component, but taking statistical and dynamic variations into account. Both types of variation represent increases in strength over minimum guaranteed values.

The static collapse load can either be obtained from experimental or historical data, or can be estimated using design codes and structural calculations. Due to the lack of data discovered in the literature search, it is necessary to calculate values and use any available experimental or historical data for corroboration, and typical calculations are outlined in Section 9. The ultimate static collapse load is assessed in the following way:

- the static load capacity for the individual structural components is determined based on the normal design load with the load and material factors removed. For ultimate limit state design calculations and for a structure subject to dead (i.e. self-weight) and wind loads, the load factor on the self-weight of the structure and wind loading is in both cases 1.4. If other loads like imposed floor loads need to be considered in conjunction with dead and wind loads, then a factor of 1.2 is recommended in BS8110: Part 1: 1985 'Structural Use of Concrete'. The use of load and material factors of 1.0 implies that there are no margins of safety included in the calculations i.e. these are capacity calculations rather than design calculations. This assessment is independent of the actual construction details.
- typical component dimensions are assumed and the ultimate static collapse load for the complete building determined. Frame collapse is based upon the pressure exerted on an intact wall, which thereafter is transmitted to the frame. In addition, a reduction in capacity of the walls and columns is

incorporated to allow for other normal loads. This assessment is dependent on building specific factors such as structural connection details and frame spacing.

The static collapse load is multiplied by a material factor and a dynamic increase factor to take both the statistical and the dynamic increases into account. The statistical increase in strength is the difference between the actual value of a material property and the lower bound or minimum guaranteed value assumed in conventional design. References quote the average yield strength for steel being ~ 25% greater than the quoted values and for concrete an increase of ~ 10 - 30% is observed [19]. In addition to increases due to 'real' strengths, the yield strength of a material is dependent on the strain rates induced during loading. An increase in yield strength with increasing strain rate is well established for steel and concrete, and dynamic increase factors are recommended in [19], to take this into account.

The material and dynamic factors for the range of materials considered in this report are summarised in Table 8.2. Where values are not available in the literature, they have been inferred from comparison with the values for other materials.

Material	Material Factor	Dynamic Increase Factor	Overall
Glazing	1.20	1.00	1.20
Timber	1.20	1.00	1.20
Masonry	1.20	1.0*	1.20
Concrete	1.20	1.25	1.50
Steel	1.25	1.20	1.50

\* Reference 1

**Table 8.2:**

**Dynamic properties**

**8.3 Ductility ratio**

The ductility ratio (ratio of deformation at failure/deformation at initial "yield") represents the post yield capacity of the structure, i.e. the quantity of deformation possible after yield but before complete collapse, and it is used together with the ratio of the duration of the load to the natural period of the structure to derive the maximum overpressure range that the structure can withstand for that duration. The ductility factors used for the various types of construction are as given in Table 8.3:



Construction	Ductility ratio		Ref.
<b>Wall construction</b>			
Glazing	2		21
Timber panels	10		21
Brick/block	5		21
PC panels	10		21
Cladding	1.75 - 10 (dependent on fixture)		4 - 22
<b>Frame construction</b>	Local (flexure)	Global (buckling)	
Timber	10	1.5	19/20
RC MRF	10	1.5	19/20
Steel braced	20	5.0	19/20
MRF	20	5.0	19/20

**Table 8.3:**

**Ductility ratios for various materials used in the construction industry**

**8.4 Limiting overpressure - graphical method**

For a single degree of freedom system, it is possible to develop parametric curves relating the response to the dynamic properties of the system. The equation of motion for an undamped system is:

$$m\ddot{x} = f(t) - R$$

where  $m$  is the mass of the system,  $x$  is the displacement of the mass,  $f(t)$  is the loading and  $R$  is the resistance. If the impulse time history and the resistance functions are known, this equation can be solved either directly or by using numerical methods.

The simplest form of resistance function is that for a linear elastic system, in which case the resistance is a linear function of the displacement. However, the majority of structures exhibit some kind of ductility, in which case it is more appropriate to assume that the behaviour is elasto-plastic, with a resistance function similar to that shown in Figure 8.1. The resistance function and the blast load function both exhibit discontinuities, and the above equation can be split into 6 different equations, according to the time elapsed and the deflection. These six equations are:

$$\begin{aligned}
m\ddot{x} &= f(t) - kx && \text{for } t < t_d, x < x_e \\
m\ddot{x} &= f(t) - Rm && \text{for } t < t_d, x > x_e \\
m\ddot{x} &= -kx && \text{for } t > t_d, x < x_e \\
m\ddot{x} &= Rm && \text{for } t > t_d, x > x_e \\
m\ddot{x} &= f(t) - k[x_e - (x_m - x)] && \text{for } t_d > t > t_m \\
m\ddot{x} &= -k[x_e - (x_m - x)] && \text{for } t > t_m \text{ and } t > t_d
\end{aligned}$$

where  $t_m$  is the time when the maximum displacement is reached and  $t_e$  is the time when the maximum elastic deflection is reached. The first two equations relate to the response of the system while the load is applied under elastic and plastic conditions respectively. The third and fourth equations are similar, but describe the response once the load has ended. The final two equations describe the behaviour after the maximum displacement has been reached, during the load and after the pulse has finished.

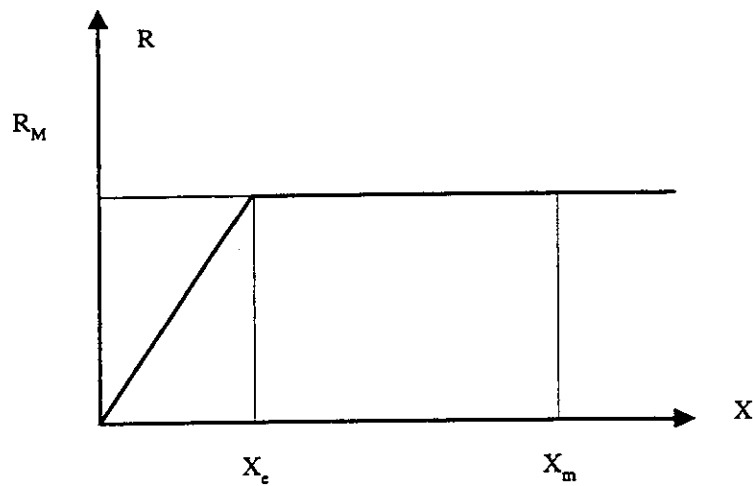


Figure 8.1:

### Typical elasto-plastic resistance function

The response is determined by integrating the above equations with time. The order in which the equations are solved depends on the values of  $t_e$  and  $t_m$ . Parametric curves can be developed which relate the ratio of the pulse duration to the natural period ( $t_d/T$ ) and the ductility ratio ( $x_m/x_e$ ) to the ratio of the maximum resistance to the peak overpressure ( $R_m/F_1$ ) dependent on the shape of the pulse and the resistance function. For simple pulse shapes, such as triangular or rectangular or a gradually applied load, graphs representing the relationship between these values are available in several references, including Biggs [23] and the ASCE Manual and Report on Engineering Practice No. 58 - 'Structural Analysis and Design of Nuclear Plant Facilities' [19]. As an example, the curve for a triangular load is reproduced in Figure 8.2. This shows that for a ductility ratio,  $\mu$ , of 10, and a natural period,  $T$ ,

of 50ms (typical values for a timber panel), then for a shock pulse of duration 50ms ( $t_d/T = 1.0$ ), the ratio of the maximum resistance, or dynamic collapse load,  $R_m$ , to the limiting overpressure,  $F_1$  is:

$$\frac{R_m}{F_1} \approx 0.51$$

This implies that the limiting overpressure is approximately twice the dynamic collapse load for this example.

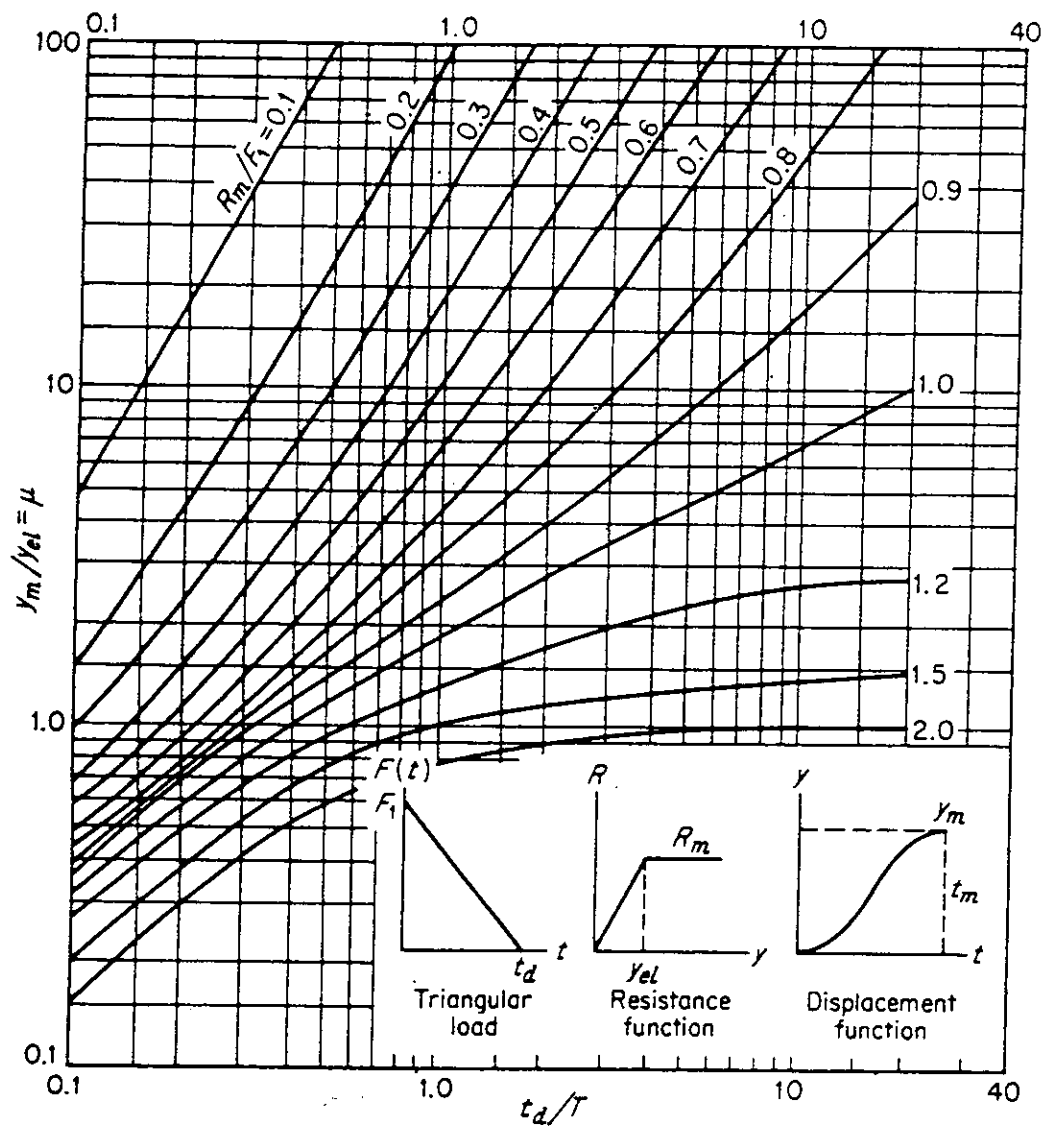


Figure 8.2:

Maximum response of elasto-plastic one degree of freedom systems due to triangular load pulses with zero rise time

## 8.5 Structural analysis program

In Section 7 of this report, it was shown that the load on a structure is a combination of the loads on the different faces and the resulting pulse shape is fairly complex. In this case, it is not possible to use the graphs directly to derive the limiting overpressure range, but instead the theory behind the derivation of the graphs can be used to obtain the structural response and hence the load capacity.

This has been done using a Q BASIC program written to calculate the dynamic response of a structure when subjected to a time-varying load [12].

The building is modelled as a single degree of freedom system incorporating a mass, stiffness and damping ratio to represent the resistance of the building to the applied load. In order to make the response of the building more realistic, an elastic limit has been incorporated which allows the building to have both an elastic and plastic response to any deflection, according to the amount of distortion that is encountered. This arrangement allows for complex motion in which the building may move into and out of the plastic region several times during a particular loading cycle.

The initial input data required for the program consists of the following:

- building stiffness and elastic limits;
- building mass; and
- damping ratio for dynamic response.

These properties are calculated for an individual building based on a knowledge of the building dimensions, construction method and material specification. The building stiffness is defined as a bi-linear function of the displacement of the building in order to represent the elasto-plastic behaviour (Figure 8.1). The elastic limit,  $x_e$ , is assumed to correspond to the displacement at the calculated dynamic collapse load, with failure occurring once the displacement reaches a value equal to the elastic limit multiplied by the ductility. It is conservative to assume that the damping ratio for the structure is 0%, as this maximises the structural displacement.

Any appropriate force time history can then be input into the code, which calculates the limiting elastic displacement, the maximum displacement, and the natural period of the structure under that particular load scenario, together with velocities and accelerations. By comparing the degree of calculated elastic and plastic displacement with the allowable values, the ability of the building to withstand the blast can be determined.

The program has been tested against the curves presented in the literature for two types of triangular pulse load, and a gradually applied load with a range of mass and stiffness values. The maximum deflections of the masses for each load case were noted, and it was found that the program produced results that were in good agreement with the values from the curves [23]. Typical results are shown in Table 8.4.

Structural Properties			Pulse Properties			Derived Parameters		Output	
Mass (kg)	Stiff- ness (N/m)	Dynamic Load Capacity, $R_m$ (N)	Duration, $t_d$ (s)	Maximum Load, $F_1$ (N)	Shape	$R_m/F_1$	$t_d/T$	$y_m/y_{el}$ Calculated	$y_m/y_{el}$ Literature
$1 \times 10^5$	$3.553 \times 10^7$	$3.553 \times 10^5$	1.0	$5.9218 \times 10^5$	Triangular equilateral	0.6	3.0	20.9	21.0
2533	1000	1000	1.0	1000	Triangular - zero rise time	1.0	0.1	0.31	0.32
1000	9869.6	1200	1.0	1000	Gradual rise	1.2	0.5	1.76	1.75

**Table 8.4:**

**Comparison of calculated dynamic response against literature values**

This technique provides a means of assessing the response of a structure to pulse shapes other than the simple triangular and rectangular shapes presented in the literature, provided that the structural mass, stiffness and elastic limit can be determined.

A listing of the program is given in Table 8.5, overleaf.

```

100 CLS
110 PRINT "INPUT MASS (KG)          ";
111 INPUT M
112 PRINT "INPUT STIFFNESS (N/M)    ";
113 INPUT K
114 PRINT "RATIO OF CRITICAL DAMPING ";
115 INPUT B
116 PRINT "POSITIVE YIELD (EG 2000000) (N) ";
117 INPUT R0
118 PRINT "NEGATIVE YIELD (EG -2000000) (N)";
119 INPUT R1
120 DOO = 0
126 Z = K / M
127 Y = 2 * SQR(K * M)
128 C = B * Y
130 PRINT "INPUT TIME STEP";
131 INPUT T1
132 C1 = .5 * T1
133 C2 = T1 * T1 / 6
134 C3 = 1 / (M + .5 * T1 * C)
135 C4 = 1 / (1 + K * C2 * C3)
136 C5 = C2 * C4
137 C6 = 2 * C2
138 C7 = C2 * C3
139 C8 = 1 / (M + .5 * T1 * C + C2 * K)
140 D = 0
141 V = 0
142 A = 0
143 T = -T1
200 REM
205 LOCATE 17, 36: PRINT "          "
210 T = T + T1
220 LOCATE 17, 1: PRINT "FORCING FUNCTION AT TIME ="; T; "SECONDS";
221 INPUT F
222 D1 = D
223 V1 = V
224 A1 = A
225 IF T = 0 THEN 270 ELSE 226
226 IF T > 10 THEN 1000 ELSE 230
230 A = C8 * (F - C * (V1 + C1 * A1) - K * (D1 + V1 * T1 + C6 * A1 - DOO))
240 V = V1 + C1 * (A + A1)
250 D = D1 + V1 * T1 + C6 * A1 + C2 * A
251 F1 = K * (D - DOO)
252 IF F1 > R0 THEN 256 ELSE 253
253 IF F1 < R1 THEN 258 ELSE 254
254 LOCATE 8, 1: PRINT "***** ELASTIC REGION *****";
      GOTO 280
256 LOCATE 8, 1: PRINT "***** POSITIVE YIELD *****";
      R = R0
257 GOTO 262
258 LOCATE 8, 1: PRINT "***** NEGATIVE YIELD *****";
      R = R1

```

**Table 8.5:**

**Structural analysis program**

```

262 A = C3 * (F - C * (V1 + C1 * A1) - R)
263 V = V1 + C1 * (A + A1)
264 D = D1 + V1 * T1 + C6 * A1 + C2 * A
265 IF R > 0 THEN 268 ELSE 266
266 DOO = D - R1 / K
267 GOTO 280
268 DOO = D - R0 / K
269 GOTO 280
270 A = F / M
280 F1 = F * (D - DOO)
281 F2 = C * V
282 LOCATE 10, 1: PRINT "TIME (SECONDS)      ACCELERATION (M/S^2)  VELOCITY
(M/S)      DISPLACEMENT (M)": LOCATE 13, 1: PRINT "SPRING FORCE (N)  FORCE IN
DASH (N)    FORCE APPLIED"
283 LOCATE 11, 1: PRINT "                                ":
LOCATE 11, 1: PRINT ; T
284 LOCATE 11, 22: PRINT ; A
285 LOCATE 11, 45: PRINT ; V
286 LOCATE 11, 65: PRINT ; D
287 LOCATE 14, 1: PRINT "                                ":
LOCATE 14, 1: PRINT ; F1
288 LOCATE 14, 22: PRINT ; F2
289 LOCATE 14, 45: PRINT ; F
290 GOTO 200
1000 END

```

Table 8.5 (cont'd)

## **9 STRUCTURAL PERFORMANCE**

The methodology for assessing the load capacity of individual structural components and complete buildings is described in Section 8. In this section, this approach is used to calculate the load capacities of a range of components under different loading conditions.

### **9.1 Approach adopted for assessing structural strength**

Structural damage can be predicted for the differing categories of building using the following sources of data:

- Calculations based on examples of typical buildings.
- Experimental data on building components subject to blast loads.
- Historical data on the performance of buildings subject to blast loads.

All the above sources of data have inherent uncertainties which need to be considered when deriving damage data. These include:

- The performance of a particular building when subject to blast loads is complicated and dependent upon many features which are difficult to define. The calculation of generic building performance cannot be predicted definitely and any results must be viewed in light of the assumptions made.
- When designing a building to resist blast loads the engineer builds in conservatism which mean that, whilst the margins of safety are significantly reduced from those used for normal loads, the assessed load capacity constitutes a design value rather than a best estimate of the actual collapse load. In producing the data and procedures for calculating vulnerability no margins of safety have been included on either the material properties or the loads, since this report is regarded as providing risk assessment information not design guidelines.
- Experimental data only relate to the actual configurations tested and the type of explosives used. Often the literature does not clearly define all the relevant data.
- Historical data depend on the rigorousness of any survey performed and how estimates of the loading have been obtained.

The structural calculations have primarily been used as the basis of the assessment of the structural strengths with validation being based on a comparison with experimental and historical data. Any discrepancies highlighted in the results obtained from the above sources will be reviewed and if necessary engineering judgement used to derive vulnerability data, bearing in mind that the purpose of this work is not to provide a design guide but rather to provide data for a risk assessment for existing or proposed buildings.



## 9.2 Structural calculations

The structural performance of both load bearing frames and typical non loadbearing external cladding has been examined. The design codes used for assessing the static structural capacity for the various construction materials are:

- Concrete	BS 8110
- Steel	BS 5950
- Brick/Block	BS 5628
- Timber	BS 5268
- External Cladding	BS 8200
Aluminium corrugated and trough	CP 143: Part 1: 1958
Galvanised corrugated steel	CP 143: Part 10 : 1973
Corrugated asbestos cement	BS 5247: Part 14: 1973
Precast concrete	BS 8297: 1995

Having established the static load capacity using the above codes the dynamic load capacity has been determined as described in Section 8.

### 9.2.1 Reinforced concrete frame

The static capacity of a reinforced concrete frame has been assessed based on BS 8110. Dimensions for a typical concrete column have been assumed to be 305mm x 305mm with 4 reinforcement bars, one in each corner, diameter 15.4mm and under 35 mm cover. This represents a slender column with nominal reinforcement. The height of the column has been assumed to be 4.6m and frame spacing of the concrete frame has been assumed to be 5.62m in one direction and 3.46m in the other direction.

The ultimate capacity of this typical column has been assessed under a range of axial loads and moments, with material and load safety factors removed. The resulting curve of maximum co-existent axial loads and moments is shown in Figure 9.1.

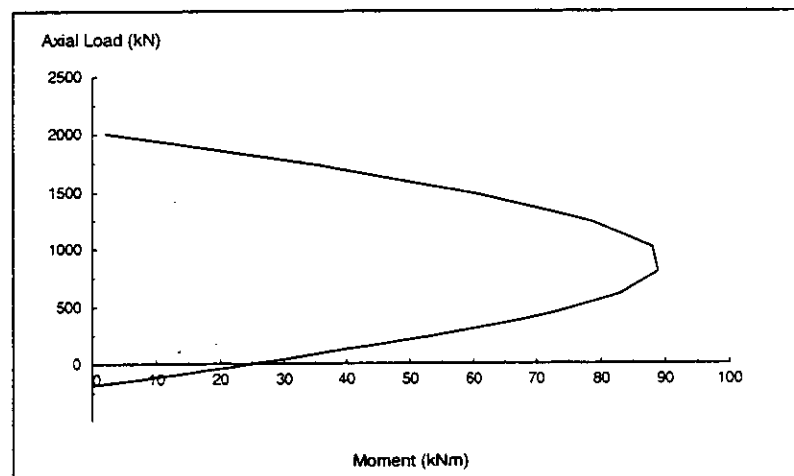


Figure 9.1:

Maximum coexistent axial loads and moments in reinforced concrete column

The maximum moment capacity for this column can be obtained from the curve as 89 kNm, which is relatively low, owing to the section and reinforcement used. The moment capacity has been used to derive a static collapse load for the column of 310 kN, based on the plastic collapse of a fixed-fixed beam under uniform loading, with the formation of one hinge at the mid height. The overpressure at which this load is experienced by the column is dependent on the degree of pressure relief present. If the walls are intact then it is assumed that the full span area transmits its load into the column. In this case the differential pressure across the wall required to cause static collapse is 120 mbar for a span length of 5.62m and 195 mbar for a span length of 3.46m. Alternatively, if all the walls are removed, then the only area to transmit load into the column is the area of the column itself. In this case, the differential pressure across the column required to cause static collapse is ~ 2.2 bar.

The dynamic load capacity has been calculated based on Section 8, for different wall types - brick/block, precast concrete panels/diaphragm walls and cladding/block walls, assuming a wall span length of 3.46m and a 100 ms duration pulse. Assuming that the walls remain intact, the limiting overpressures for a dynamic load for two different shaped pressure pulses are as given in Table 9.1. The ranges shown in the table represent the uncertainty in the natural frequency of the walls. The pressure values given correspond to the differential pressures across the wall required to cause failure.

Wall type	Limiting overpressure (mbar)	Limiting overpressure (mbar)
	Pressure wave	Shock wave
Brick/Block	384 - 450	332 - 390
Precast Concrete Panels/Diaphragm Walls	348 - 362	304 - 322
Cladding/Block	384 - 472	332 - 450

**Table 9.1:**

**Limiting overpressures for reinforced concrete framed buildings**

In reality, however, some pressure relief will occur due to glazing failure. The limiting overpressures assuming different percentages of glazing (i.e. different load span lengths) have been calculated for the brick/block example and are presented in Figure 9.2. For 50% glazing failure (or 50% shorter load span width) the range of limiting overpressure is doubled i.e. 472 - 900 mbar for a pressure pulse.

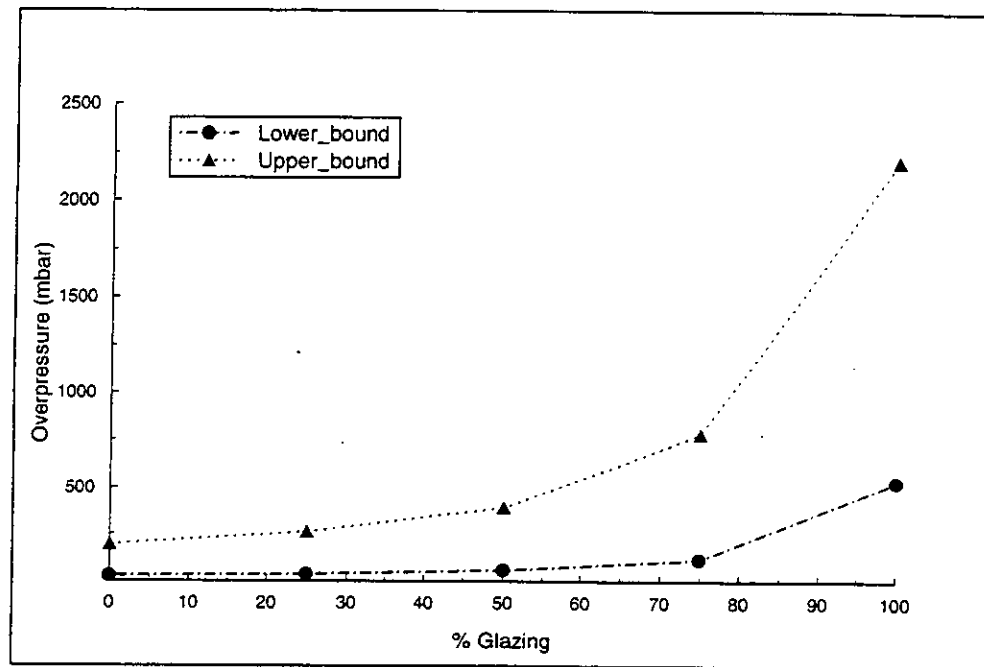


**Figure 9.2:**

**Limiting overpressures for different percentages of glazing  
(or shorter span lengths)**

Typical experimental and historical data are summarised in Table 9.2 for reinforced concrete framed buildings, based on observations of the extent of damage to typical buildings following a nuclear explosion [29]. The typical durations of these loadings are 1 second or longer, and it would be expected that the calculated failure pressures would be higher than these observed values. However the calculated values are if anything lower than the literature values (for a load duration of 500ms a limiting differential pressure for a pressure pulse of 332 - 348 mbar is calculated for a brick/block wall). This reflects the choice of column used in the calculations, which has only nominal reinforcement. In addition, as shown above the effects of pressure relief due to glazing failure increases the limiting overpressure to values which are closer to the historical values, particularly for the first two building types. For the blast-resistant design, it is likely that the frame members are rather more substantial than the typical member assessed here.

Structure	Side-on pressure (mbar)	Description of damage	Reference
Reinforced concrete building with concrete walls, small window area, 3 to 8 storeys	70	Windows and doors blown in, interior partitions cracked	29
	370	Exterior walls severely cracked, interior partitions severely cracked or blown down, structural frame permanently distorted, extensive spalling of concrete	
	471	Walls shattered, severe frame distortion, incipient collapse	
Reinforced concrete frame office building, 3 to 10 storeys, lightweight low strength walls which fail quickly	70	Windows and doors blown in, light siding ripped off, interior partitions cracked	29
	554 - 615	Frame distorted moderately, interior partitions blown down, some spalling of concrete	
	688 - 760	Severe frame distortion, incipient collapse	
Multistorey reinforced concrete building with reinforced concrete walls, blast resistant design, high strength walls which do not fail quickly, no windows	70	Some cracking of concrete walls and frame	29
	534	Walls breached or on the point of being so, frame distorted, entrances damaged, doors blown in or jammed, extensive spalling of concrete	
	724	Walls shattered, severe frame distortion, incipient collapse	

**Table 9.2:**

**Typical failure pressures for reinforced concrete structures**

**9.2.2 Steelwork frame**

Steel frames were assessed for their static capacity, based on BS 5950 part 1. Two typical frames were considered, both of universal columns (203 x 203 x 46). one being 3.2m in height and spaced 3.6m apart, the other being 3.2m in height and spaced 6m apart.

Each vertical steel member was assumed to carry an axial load amounting to 60% of its capacity. This lowered the ability of the member to resist horizontal loading to approximately 65% of its original limit. Blast loading was assumed to be transmitted to the column as a uniformly distributed load via the walls/cladding that exists between the members. An assumption was made that the walls/cladding would not fail and therefore allow pressure relief, resulting in reduced loading on the frame. As with the reinforced concrete frame however, some pressure relief would occur from failing windows and panels and this would substantially increase the collapse load of the structure.

With the walls/cladding intact, the static failure load was calculated as 339 mbar for the universal column framework with 3.6m spacing, and 203 mbar for the framework with 6m spacing. A variety of infill materials were considered for the building, to determine a realistic range for the load capacity under dynamic load.

The load capacity for dynamic loading has been calculated without safety factors for different wall types including diaphragm wall panels, pre-cast concrete panels, cladding walls and brick/block walls. These were assessed for their effect on the steel frame when exposed to two triangular pressure pulses, one with an instantaneous rise time i.e. a shock pulse, the other a triangular pulse (pressure pulse). The results of this analysis are shown in Table 9.3 below. The ranges evident in the table are again due to uncertainty in the natural frequencies of the walls.

Frame type	Wall type	Limiting overpressure (shock wave)	Limiting overpressure (pressure wave)
UC (203 x 203 x 46): 3.6m span	Diaphragm wall panels / Pc panels	552 - 584 mbar	634 - 706 mbar
UC (203 x 203 x 46): 3.6m span	Cladding walls	612 - 862 mbar	726 - 1016 mbar
UC (203 x 203 x 46): 3.6m span	Brick / Block walls	612 - 726 mbar	726 - 876 mbar
UC (203 x 133 x 30): 6m span	Diaphragm wall panels / Pc panels	332 - 350 mbar	382 - 412 mbar
UC (203 x 133 x 30): 6m span	Cladding walls	368 - 516 mbar	434 - 610 mbar
UC (203 x 133 x 30): 6m span	Brick / block walls	366 - 436 mbar	436 - 526 mbar

**Table 9.3:**

**Limiting overpressures for steel framed buildings**

Typical historical and experimental data are summarised in Table 9.4 overleaf. Generally good agreement is seen between the calculations for the universal column framed structures and those given in the table, although insufficient data are available to make a more detailed comparison. As for the reinforced concrete frame described in Section 9.2.1 above, the majority of the data relate to observations from nuclear explosions, which are much longer duration pulses than of interest here.

Structure	Side-on overpressure (mbar)	Description of damage	Reference
Steel frame	80 - 100 200	Minor damage Collapse	2
Steel Girder framed building	500	Collapse	37
Light steel frame industrial building, single storey, with up to 5 ton crane capacity, low strength walls which fail quickly	70 431 543	Windows and doors blown in, light siding ripped off Minor to major distortion of frame Severe distortion or collapse of frame	29
Heavy steel frame industrial building, single storey, 60 to 100 ton crane capacity, lightweight low strength walls which fail quickly	70 492 615	Windows and doors blown in, light siding ripped off Minor to major distortion of frame Severe distortion or collapse of frame	29
Multistorey steel frame office building, 3 to 10 storeys, lightweight low strength walls which fail quickly	70 677 - 738 832 - 905	Windows and doors blown in, light siding ripped off, interior partitions cracked Frame distorted moderately, interior partitions blown down Severe frame distortion, incipient collapse	29

**Table 9.4:**

**Typical failure pressures for steel framed structures**

**9.2.3 External cladding**

The design requirements for the non-loadbearing external cladding of building enclosures is specified in BS 8200 : 1985. This specifies the strength requirements for normal loads (wind, fixtures and operational forces), impacts and explosive forces. An assessment of the design strength of external cladding subject to pressure loads can be made based upon the design wind loads defined as follows:

*"Wind load should be calculated using the basic wind speed in accordance with CP3: Chapter V: Part 2. In determining ground roughness, factor S2, class A should be used. It should be noted that higher pressure coefficients are used at the corners of each elevation".*

Using CP3 the maximum design loads are:

- Wall: 32 mbar
- Roof: 71 mbar

The design criterion specified for external cladding is that:

*"The external vertical enclosure should be capable of resisting and transmitting to its points of support all static and dynamic design loads without fracture or permanent deterioration of its performance. There should be no significant irreversible deformation of surfaces resulting from such design loads".*

This implies that the external cladding is designed to respond in an elastic manner.

In addition to the above wind loads, the roof cladding has to be capable of resisting the dead and imposed loads defined in BS 6399: Part 1: 1984 'Design loading for buildings'. For flat roofs an imposed load (including snow load) of 15mbar is specified. Thus the most critical component with respect to the integrity of the external skin of a clad building is the front wall, for the following reasons:

- the normal design loads on the roof are approximately double those on the walls;
- the reflected pressure wave on the front of the building can be up to double the incident overpressure; and
- the whole of the front face of the building is subject to the reflected pressure reasonably instantaneously, whereas the side walls and roof are subject to a travelling load.

Therefore, with respect to the external cladding, the likely failure sequence is as follows:

- front wall;
- side walls; and
- rear wall/roof.

Clearly, the extent of failure once the front wall fails depends on the overpressure and the pressure relief generated.

Using the design pressure on the wall as an indication of the typical strength of external cladding then it is normal practice to factor the wind load by an appropriate load factor. Using load factors specified in BS 8110: Part 1: 1985, the design pressures become:

- wall:  $1.4 \times 32 = 45$  mbar; and
- roof:  $1.4 \times 71 = 99$  mbar (more onerous than imposed + wind loads).

These are treated as equivalent static design loads. Using these pressures as indicative of the ultimate static collapse capacity of the cladding, then the equivalent dynamic load capacity becomes:

- wall: 62 - 102 mbar; and
- roof: 136 - 158 mbar.

These are differential pressures across the section of interest. Thus if the pulse is reflected at the wall, the limiting overpressure will be half this value.

Clearly the codes require that the cladding support has equivalent structural strength. The fixings are also designed to resist a negative suction pressure. During a blast scenario, the rear wall is subject to an external suction load plus internal leakage pressure which will tend to pull the cladding from the building framework. If this occurs then there will be some relief on the loading on the building frame but this will not generate any significant debris within the building envelope. There may be a debris hazard to persons outdoors in the vicinity of the building, however.

Typical structural characteristics for the different cladding types are calculated as follows:

- **wood based panel products:** BS 5268: Part 2 specifies 9 strength classes, SC1 to SC9, which group together species and grades of timber with similar structural properties. The majority of common softwoods fall into strength classes SC3 to SC5. For SC4 the permissible bending stress parallel to the grain is  $7.5 \text{ N/mm}^2$ .

To provide a homogeneous material, wood based panels such as plywood and particleboard are manufactured. A common commercial size of plywood sheet is 2.4m by 1.2m, with commonly available thicknesses ranging from 3 to 25mm.

The bending strengths of different types of particleboard are given in [32] and have been used to calculate static failure pressures for a 1.2m spanning panel of 12.5mm thickness. The static failure pressures and corresponding failure pressures under dynamic loading are shown below.



Type of board	Bending strength (psi)	Static failure pressure (mbar)	Failure pressure under dynamic load (mbar)
Particleboard (1 - M - 3)	2400	29	46 - 82
Hardboard	3000	37	58 - 102
Shortleaf pine plywood	4250	52	82 - 146
Shortleaf pine	8250	101	158 - 280

**Table 9.5:**

**Typical failure pressures for different particleboard types**

This compares with historical failure pressures of 69 - 138 mbar for failure at the main connections allowing panels to be blown in [56].

- **aluminium corrugated and troughed sheet roof and wall coverings:** CP 143: Part 1: 1958 specifies maximum recommended loading for corrugated and troughed sheeting. A typical pressure is 24 mbar, which is based upon a factor of safety of 2.0 on the 0.1% proof stress of the material. This is consistent with a static collapse load of 48 mbar. The corresponding overpressure range for a dynamic load is 70 - 108 mbar.

This compares with historical failure pressures of 69 - 138 mbar for connection failure followed by buckling in corrugated steel or aluminium panelling.

- **galvanised corrugated steel sheet roof and wall coverings:** CP 143: Part 10: 1973 gives section moduli for corrugated sheets of galvanised steel. From these values and the yield stress, a plastic moment capacity of 4.8 kNm has been calculated for a corrugated sheet, 127mm pitch corrugation and gauge 14. The plastic collapse load has then been calculated for a sheet measuring 3.5m x 1.0m (3.5m is the maximum unsupported span length for this type of corrugated sheet), assuming that the sheet acts as a pinned or fixed ended beam. This gives a static collapse load of 31 mbar for pinned edge connections and 62 mbar for fixed edge connections. The corresponding overpressure range for a dynamic load is 48 - 150 mbar. This is a wide range, owing to the uncertainty in the natural period of the panel which is assumed to be between 10 and 60 ms.

Values from the literature are shown in Table 9.6. These values appear to be somewhat higher than the calculated values, although of the three references, the first refers to data from nuclear tests, the second gives no data source and the third is based on calculations and engineering judgement. No information is given concerning panel size or fixing conditions.

Structure	Side-on overpressure (mbar)	Description of damage	Reference
Corrugated steel or aluminium panelling	69 - 138	Connection failure followed by buckling	29
Frameless steel panel building	207 - 276	Demolished	24
Corrugated steel panels	80 - 200 200 - 350 > 350	Slight cracking and deflection Parts blown out Complete demolition	78

**Table 9.6:**

**Historical failure pressures for corrugated steel panels**

- **corrugated asbestos-cement sheet roof and wall coverings:** BS 5247 Part 14: 1975 gives fixing details and minimum purlin spacings for asbestos cement panels up to wind suction loadings of 15 mbar. Taking this as a static collapse load, the corresponding collapse load under dynamic loading is calculated as 14 - 40 mbar. This is a very conservative estimate as can be seen from a comparison with the historical values presented in Table 9.7.

Structure	Overpressure (mbar)	Description of damage	Reference
Corrugated asbestos siding	69 - 138	Shattering	56
Corrugated asbestos cement panels	6 - 30 30 - 65 > 65	Slight cracking and deflection Parts blown out Complete demolition	78

**Table 9.7:**

**Historical failure pressures for corrugated asbestos-cement panels**

- **non-loadbearing precast concrete panels:** standard precast concrete panels are designed based on the recommendations of BS 8110: Part 1 with characteristic wind loads calculated in accordance with the recommendations for class A structures of CP 3: Chapter V: Part 2: 1972 using the pressure coefficients in Table 7 of that standard. They are then tested subject to 1.5 times the design wind pressure.

Based on a design wind pressure of  $31 \times 1.5 = 46.5$  mbar, the limiting blast overpressure range for dynamic loading is 66 - 68 mbar. This is considerably lower than the values experienced historically (Table 9.8).

Structure	Side-on overpressure (mbar)	Description of damage	Reference
12 in thick cement breeze block wall panels	200 - 248	Rupture	24
Concrete or cinder block wall panels, 8 in or 12 in thick (not reinforced)	138 - 207	Shattering of the wall	56
Concrete block wall	150 - 200	Collapse	2
0.15m thick concrete walls	100 - 230 230 - 400 > 400	Slight cracking and deflection Parts blown out Complete demolition	78
0.25m thick concrete walls	300 - 650 650 - 1800 > 1800	Slight cracking and deflection Parts blown out Complete demolition	78

**Table 9.8:**

**Damage pressures for concrete walls**

In the special circumstance of blast designed buildings, then precast reinforced concrete panels are often used for the external skin. In these circumstances the precast panel can be designed to provide the required blast resistance.

**9.2.4 Brickwork**

In the case of a brickwork building, the situation is slightly different than for the steel or reinforced concrete framed buildings described above. For a framed building, the mode of failure tends to be dependent on the cladding: if the cladding fails quickly, pressure relief occurs on the frame, and global collapse is unlikely to occur. For a brickwork building however, the walls are loadbearing, and form the 'framework' of the building: if the walls fail then structural collapse will follow.

The static collapse loads have been assessed for a range of brickwork, using information from the Structural Masonry Designers Manual [30]. Typical wall thicknesses of 8.5" (215mm), 9" (229mm) and 12" (305mm) have been considered. A wall was modelled as being 3m high and 6.3m wide, with the sides of the wall fixed, the base pinned, and the top edge unrestrained. As the construction of brick walls is subject to considerable variation in terms of materials used, geometry, restraint and quality of construction, average values were assumed for the material properties, and a typical section considered.

The average strength of the material was increased by a factor of 1.6, consistent with the design limits for accidental wind loading [35].

Static collapse loads for the walls were found to be in the range of 120 to 245 mbar, increasing with wall thickness. Walls were considered to be subject to a direct blast with a duration of 100 ms, with two variations in blast wave shape. The first pressure pulse considered was triangular with zero rise time, the second being a triangular pressure pulse with a rise time of half the positive phase duration. The maximum response of the wall was determined for the four possible combinations of the above loading conditions.

Wall thickness (inches)	Static collapse load (mbar)	Limiting overpressure under dynamic loading (mbar) (shock wave)	Limiting overpressure under dynamic loading (mbar) (pressure wave)
8.5	120	150 - 162	178 - 196
9.0	138	168 - 184	202 - 220
12.0	245	314 - 342	376 - 410

**Table 9.9:**

**Limiting overpressures under dynamic loading for steel framed buildings**

The ranges observed in the above calculations are due to uncertainties in the wall properties, in particular the natural period.

These values are in reasonable agreement with historical data. From Table 3.7, collapse of 9 in brick walls is observed at 172 - 276 mbar and 13.5 in walls at 483 - 621 mbar, although no source is given for this data, and there is no indication of pulse duration or wall fixing conditions. The results obtained from the calculations are the pressures required to initiate failure, as they are based on a design code. The actual degree of failure is unspecified, but will not necessarily mean that the wall would be completely demolished. Variations in wall geometry or construction, and the level of precompression, would significantly affect the failure pressure.

**9.3 Overall building collapse loads**

The assessment of overall building collapse was performed in Phases 2 and 3. In assessing the behaviour of the building frame, the following effects are considered:

- the interaction between non load bearing walls and the load bearing frame
- the brittle nature of shear failure compared to bending failure in frames.

The global building behaviour is dependent upon whether the wall cladding constitutes a stronger or weaker component than the load bearing frame. If the wall construction is weaker than the framing then the failure of the wall will relieve the pressure load on the frame. Collapse then refers to the loss of the walls, with the frame and floors

remaining intact. If the wall construction is the stronger element then the frame will fail with probable collapse of the floors. In the case of structures where the walls provide the load-bearing frame, such as typical masonry structures, collapse of the walls will probably cause global collapse of the building.

For framed structures, structural calculations do not tend to take into account the effect of infill walls on the overall behaviour due to the complexity of the calculations required [15, 16]. However experience has indicated that the response of both reinforced concrete and steel framed structures to extreme dynamic loads can be significantly affected by the strong interaction between the frames and infill walls.

The beneficial effects of infill walls are:

- both overall stiffness and lateral resistance of buildings increase considerably after the addition of infills;
- there is an increase of energy dissipation capacity of buildings due to infills (cracking of infills, friction between the infill and the surrounding frame, etc.) provided that premature damage of RC columns due to local interaction effects has been avoided;
- well constructed infill walls may decrease the probability of collapse of a building, even in case of defectively constructed frames.

On the other hand;

- local damage may be observed in frame elements (either near beam-column joints, or at mid-height of columns) due to the frame/infill interaction; while
- the combination of low lateral stiffness frames with stiff but low quality infills may lead to premature failure and subsequent collapse of infills. Failure of brittle unreinforced masonry infills is of an explosive type and is responsible for many casualties and injuries during earthquakes.

Clearly the effect of infill walls could account for a significant difference between structural calculations and experimental/historical experience.

## 10 FATALITY PROBABILITY

People in the vicinity of an explosion may be adversely affected by:

- |   |                      |   |  |
|---|----------------------|---|--|
| 1 | Toxic Fumes          | - | Inhalation of noxious gases                |
| 2 | Fire                 | - | Thermal radiation effects                  |
| 3 |                      | - | Secondary fires due to explosive damage    |
| 4 | Direct Blast Effects | - | Personal injury such as ruptured eardrums  |
| 5 | Debris/projectiles   | - | Injury due to flying glass, brickwork etc. |
| 6 | Building collapse    | - | Direct blast loads                         |
|   |                      | - | Tertiary effects - body translation        |
| 7 |                      | - | Ground shock                               |

A summary of the levels of damage at different pressure levels is given in Table 3.1.

The first three items, fatality arising from toxic fumes, thermal radiation and fires, and the final item, ground shock, have not been considered explicitly in this report. In addition, the direct blast effects associated with vapour cloud explosions on personnel within buildings are not of direct concern in this report, since the explosions are assumed not to give rise to overpressures above 1000 mbar. The effects on humans of the debris, glazing and building collapse have been used to produce an overall blast fatality probability.

The approaches detailed in this chapter will be subject to refinement on the basis of the results of later phases of the project. Figures 10.2 - 10.13 should therefore be considered as being indicative only.

### 10.1 Probability of fatality from debris hazard

The primary causes of injury to personnel within buildings subject to blast loading are impact from debris, either from glazing or from internal partitions or external walls. The probability of fatality from debris is dependent on the failure pressure of the section and the level at which the incident overpressure is higher than that failure pressure causing acceleration of fragments into the building. The methodology for deriving this fatality probability is illustrated schematically in Figure 10.1.

Failure pressures for different structural sections have been estimated in Section 9 of this report, and compared with historical and experimental values obtained through the literature search (Section 3). From the calculations and the historical data, the following conservative estimates for side-on overpressures typical of the onset of failure have been extracted:

- |   |                       |                |
|---|-----------------------|----------------|
| - | Glazing (6 mm thick): | 100 mbar       |
| - | Wooden Partitions:    | 100 mbar       |
| - | Cladding:             | 140 mbar       |
| - | Brickwork:            | 200 - 300 mbar |

In this section, calculations to determine the velocities and ranges of objects accelerated by a blast wave, with blast overpressures varying from 0 to 1000 mbar

above failure are described. It was assumed for the purpose of these calculations that larger fragments were more likely to cause fatalities than smaller ones, and for this reason, fragments of the largest estimated realistic size were used in the determination of the fatality probability curves for each of the debris types. This was assumed to provide a limiting case that covered all fragment sizes up to the one chosen, but has been studied further in subsequent phases. The three types of explosion debris considered are listed below.

- Brickwork (density, 2000 kg/m<sup>3</sup>; sizing, up to 1m<sup>2</sup>);
- Internal room partition (density 500 kg/m<sup>3</sup>; sizing, up to 4m<sup>2</sup>); and
- Aluminium cladding (density, 2800 kg/m<sup>3</sup>; sizing, up to 4m<sup>2</sup>).

Glazing is considered separately in Section 10.2.

Determination of the probability of fatality of people within the vicinity of the debris was carried out by calculating the velocity with respect to distance for each of the debris types due to the blast overpressure experienced.

In this phase, the initial horizontal velocities of fragments accelerated by a blast wave were determined at the point of failure based on calculations from [4]. Assuming that the panel behaves as a rigid body, that none of the blast wave energy is absorbed in breaking the panel from its fixings or deforming it elastically or plastically and that gravity effects can be ignored during the accelerative phase of the motion, the equation of motion is simply:

$$m\ddot{x} = Af(t)$$

where A is the area of the panel and f(t) is the net pressure load. Assuming that the object is at rest initially, this can be solved directly to give:

$$\dot{x} = \frac{A}{m} i_d$$

where  $i_d$  is the total drag and diffraction impulse on the panel (i.e. the area under the pressure time history curve). This calculated velocity is the velocity at the end of the pulse, and is taken as the velocity at the point of failure. Reduction of velocity with distance was determined from the drag forces acting on the object in flight, which are dependent on the shape of the object.

As soon as a fragment is freed from its fixings, it accelerates under gravitational forces, and assuming that lift forces are unimportant, the time that the fragment takes to hit the ground is dependent only on the height at which it starts. In order to determine the range of fragments the maximum starting height was considered to be 4m above floor level, giving a flight time, i.e. the time to hit the ground, of approximately 0.9 seconds. The furthest horizontal distance travelled can then be calculated from the initial velocity and the flight time, taking drag forces into account. i.e.:

$$Range = \dot{x}t - \frac{1}{2} \left[ \frac{C_D Q A_D}{m} \right] t^2$$

where  $t$  is the time to hit the ground,  $C_D$  is the drag coefficient,  $Q$  is the dynamic pressure,  $A_D$  is the area of the fragment and  $m$  is the mass of the fragment.

The probability of fatality of people struck by debris was determined from the mass and velocity of the object [4], by using the vulnerability criterion presented in Baker et al [4]. This identifies the critical velocity for a fragment of given mass to cause a particular probability of fatality. By combining this with the data obtained from the velocity and range calculations, fatality probability against distance curves were plotted. The limiting range at which fragments would cause fatal injuries was determined by comparing the range of the fragments with the velocity. Fragments were considered not to cause fatal injuries if either their velocity had dropped below the critical level for injuries, or they had reached their maximum range. Although fragments would continue to travel after impact with the floor, it was assumed that kinetic energy would be sufficiently reduced to prevent fatal injuries beyond this point.

#### 10.1.1 Probability of fatality due to impact by brickwork

Failure pressures for typical brick walls have been assessed in Section 9.4.1. Based on a comparison of the calculated values and the historical values, initial failure has been assumed to occur at an overpressure of 200 - 300 mbar. This is assumed to be a conservative estimate of the pressure at which fragments of debris may be produced.

For the purposes of this phase, a section of brickwork 2m high and 0.5m wide was considered as the largest fragment to be accelerated by the blast wave. Although the wall would probably fragment into small pieces, this size was chosen as it would ensure that a fragment of it would hit a target the size of a person. Due to its high mass, brickwork did not achieve velocities sufficient to cause fatal injuries unless the side-on overpressure was in excess of 440 mbar. Figure 10.2 shows a comparison between velocities achieved by the section of brickwork against the velocities necessary to cause various degrees of injury. This is only considering injuries caused by brickwork travelling horizontally from the point of failure, and causing injury by its subsequent impact at that angle. For a more realistic assessment, a 60% fatality probability area up to 4m behind the wall has been included, based on the probability of survival during building collapse. This was to take into account the most likely cause of injury, that of sections of the wall falling on top of people behind it. The lower value for the initiation of wall collapse was taken as 200 mbar, with complete collapse at 400 mbar in accordance with the failure pressure range associated with brick walls. These pressures are the differential pressures across the wall, i.e. the difference between the consultant external and the internal pressures. As drag forces are insignificant compared with the inertia of the brickwork, the maximum distance for fatalities to occur is determined by the range of the brickwork rather than the velocity. The graph of fatalities range against overpressure is shown in Figure 10.3.



### **10.1.2 Probability of fatality due to impact by internal partitions/wooden panels**

The probability of fatality of people due to sections of internal partitions accelerated by a blast wave increases with increasing section size, as the critical velocity required to cause fatality is reduced for larger sections. For this reason a section 2m wide and 2m high was chosen for this phase, being the largest realistic size. Failure pressures for various particleboard types have been estimated in Section 9.4.4., and a side-on failure pressure of 100 mbar was selected.

Two assessments of the probability of fatality of people from panelling impact were carried out, as it was considered that the criteria for assessing the critical velocity to cause fatalities based on the mass and velocity of an object alone was unduly conservative. The initial assessment (Figures 10.4 and 10.5) was based on the criteria for fatality arising from non-penetrating fragment impact [4] and did not take into account the ability of the material to flex, break or rotate on impact, which would apply the loading to a person in a gradual, and therefore less severe way. The second assessment (Figures 10.6 and 10.7) was based on the fatality probability of fatality of people who are carried by a blast wave and collide with stationary objects. This second assessment took into account the random nature of an impact, and the overall vulnerability of the whole body. This gave higher critical velocities for fatalities to occur.

Drag forces are significant for this type of panel, and this can be seen in Figures 10.4 and 10.6, where drag forces reduce the velocity and limit the degree of fatalities that could occur. Distances for fatalities to occur are considerably higher than for the brickwork for any particular pressure. However, the comparison would be somewhat different if a smaller mass of brick had been considered. This is due to the lower mass of the panelling, which experiences much greater acceleration. It was noted that increasing fatality probability levels experienced a shift that was more vertical than horizontal on the fatalities range graph, indicating that panels travel to the maximum range without falling below the critical velocity. This is especially noticeable in Figure 10.7, where once a sufficiently high pressure has accelerated the panel to the critical velocity, only a small further increase is required to overcome the drag forces and carry it to the maximum range. This is due to the high velocity and relatively high mass of the panel, which for increasing overpressures is more significant than the drag effects.

### **10.1.3 Probability of fatality due to cladding impact**

As with the internal partitions, the initial velocity of sheets of cladding depended on their size. For this reason, a similar section 2m high and 2m wide was used. This was considered to be the largest realistic section to be accelerated by a blast wave. An aluminium section 2mm thick was chosen, in order to bound a large variety of cladding types. Thinner sections produced larger initial accelerations, but the total range was reduced for each fatality level due to the higher drag to mass ratio, whilst thicker sections had a much lower initial acceleration. Failure pressures have been calculated in Section 9.2.3, and a side-on value of 140 mbar was used for this external cladding.

As with the panelling, two assessments were carried out to account for deformation of the panel on impact, and the random nature of the collision with a person. The results of the more conservative assessment are shown in Figures 10.8 and 10.9, whilst the less conservative one can be seen in Figures 10.10 and 10.11.

Drag forces were very large compared with the mass of the section, resulting in rapid slowing down of the section with distance. This became increasingly significant as the initial velocity due to the impulse increased with increasing overpressure. This can be seen in Figures 10.8 and 10.10, where at maximum range, the final velocity is reduced to below the 10% fatality level. This high initial acceleration and rapid slowing down resulted in a fatalities graph in which the range of fatalities from the point of failure was dependent on the velocity of the section rather than the overall range. This can be seen in Figures 10.9 and 10.11. As with the panelling, the cladding experiences very high accelerations even for very low pressures, which cause fatal injuries. This is however offset by the rapid reduction in velocity, which limits the range for fatalities to occur. It is noted that increasing fatality probability levels experience a shift which is more horizontal than vertical on the fatalities range graph, indicating that panels are falling below the critical velocity before they can reach their maximum range. This is especially noticeable in Fig. 10.10, where for a few meters into the building a relatively low pressure can cause 100% fatality, but even at the highest pressure of 1000 mbar this level of fatality does not occur at the maximum range. This is due to the high velocity and low mass of the cladding, for which drag effects become very significant with increasing overpressures.

It has been assumed that these panels travel face-on to the blast i.e. that they do not rotate in flight. Rotation would lead to a reduction in the drag force and consequently a higher velocity and greater hazard. This has been considered in subsequent phases.

## **10.2 Possibility of fatality from glazing impact**

The hazard to personnel from glazing is dependent on the failure pressure of the glazing and the nature, size and velocity of fragments produced on failure. A considerable amount of data have been generated relating to failure pressures for different types of glazing, largely driven by the requirement to design blast- and ballistic-resistant structures for defence or anti-terrorist purposes [39, 40, 41, 50]. Typical failure pressures for different types of glazing and different pane sizes have been extracted as part of the literature search and are given in Table 3.2. The failure pressures are highly dependent on the pane size. Pressures range from 23 mbar for large panes (60" x 60") of 3/16" sheet glass up to values greater than 3 bar for smaller panes of tempered glass. These values are for load durations greater than or equal to 1 second. For a pane of plate glass or sheet glass, dimensions 1.1m x 0.8m x 6.4mm thick, a failure pressure of 92 - 130 mbar is given for a duration of 1s [50]. For a 100ms pulse, this should be increased by a factor of 1.15 to give a range of 100 - 144 mbar. This compares with a value of 98 mbar for a similarly dimensioned pane (63" x 42" x 0.25" thick) of tempered glass [40]. A value of 100 mbar is thus assumed to be representative of a 6 mm thick pane of glass.

Calculating the probability of fatality of people subject to glazing hazard requires a slightly different approach from other debris, as the type of injury caused is not based

on the mass and velocity of the fragments alone. Calculations were based on [18], which examined glass breakage in detail. Fatalities from failed glazing are assumed to occur due to fracture of the skull by fragments accelerated by the blast wave. An important consideration is the size of these fragments, which varies according to the differential pressure experienced by the glass. For varying pressures, initial velocities and sizes of glass fragments were determined, and a similar approach to that taken for the other debris types used to determine the maximum range and change of velocity with distance. From the velocity/fatality graph (Figure 10.12), it can be seen that glass causes considerably more casualties than any of the other debris types, with fatalities occurring at considerable distances for relatively low pressures. The criteria used to determine fatality was skull fracture [18]. Use of this criterion is reviewed in later phases of the project.

Due to the low drag to mass ratio, the limiting factor on the distance from the point of failure at which fatalities could occur is the maximum range of fragments before impact with the floor. This can be seen in Figure 10.13 where the final velocity at maximum range is still higher than the critical velocity to cause fatalities. It was noted that fatality probability from glass reduced slightly with increasing glass thickness, although this was most noticeable for thicknesses below 4mm. For a general assessment of fatality probability, it can be assumed that negligible spread of glass fragments occurs, so that the glass travels only in a direction normal to the plane of the original pane.

For a glazed building, the overall fatality probability is also dependent on the percentage of the building which is glazed, and the dimensions of the building, which govern the probability of the occupants being within range of the windows. This is illustrated schematically in Figure 10.14. This also applies to the probability of fatality arising from debris impact, which is similarly dependent on the percentage of the building which is not glazed.

### **10.3 Fatality probability of occupants to building collapse**

Assessment of the fatality probability of occupants to building collapse has been made by anticipating the number of fatalities due to building collapse during earthquakes [8, 11].

Factors affecting the number of dead/injured are:

- building occupancy;
- time of day when event occurred;
- proportion of occupants trapped by collapse:

In single storey buildings 30 to 50% will be able to escape during an earthquake. This will not be the case for buildings subject to blast loads. This proportion is dependent upon how collapse is defined. Collapse could equate to partial failure of a building or complete demolition. In addition, the volumetric reduction in building form could be considered in defining the extent of entrapment. This is illustrated schematically in Figure 10.15;

- the type of injuries those trapped received:

There is evidence that different buildings cause different injuries. The amount of injury is affected by the 'cavity potential' of the building. There is evidence that masonry leads to suffocation due to the weight of the building materials and dust whilst reinforced concrete leads to more suffocation from dust; and

- response rate of rescuers.

The number of people killed in the collapse of any particular building type can then be estimated as follows:

$$\% \text{ Fatalities} = M3 * (M4 + M5)$$

Where:

M3 = Number trapped by collapse

M4 = Fatalities at collapse

M5 = Fatalities post-collapse

Table 10.1 gives estimates for masonry and reinforced concrete buildings [11].

		Masonry	R C Frames
Percentage trapped	(M3)	%Collapse Vol.	%Collapse Vol.
Fatalities at Collapse	(M4)	20%	40%
Fatalities post Collapse	(M5)	36%	42%
% Fatalities		56%	82%

**Table 10.1:**

**Fatality estimates for collapsed masonry and reinforced concrete buildings**

These estimates will tend to be high as a blast event is localised compared to an earthquake and thus one would anticipate an effective emergency response. Given that the fatalities of earthquake victims as a result of building collapse are between 30 and 50%, the following formula is used for all building categories other than the Portacabin and Brick Building types.

**Fatality rate due to building collapse = 80% x proportion of volume collapsed.**

For a Portacabin type building (B1) the fatality probability of people due to debris alone is used, with no additional fatality probability due to entrapment. This is because the structure consists of fairly light walls which are assumed not to present a significant fatality mechanism.

For a brick building (B2) in which the roof is supported by brick structures alone, failure is characterised by brittle fracture of the supporting structures (unlike a steel

or concrete framed structure where the frame may remain essentially intact). In this case, there may be little available void space within the collapsed structure, and in addition, quantities of dust released may be large. For this reason, a fatality probability due to building collapse of 60% is assumed for brick buildings.

#### **10.4 Derivation of overall fatality probability curves**

The overall probability of fatality of building occupants as a result of building damage due to blast loads is based on the summation of the effects of glazing, wall debris and collapse. The fatality rates predicted from earthquake data make no allowance for the pressure effects on walls causing debris to be projected at the occupants. The fatality probability curve for a given building may be constructed using the following method (Figure 10.16):

At relatively low overpressures, the variation in strength of different types of glazing is significant. The breaking pressure of the glazing in the building to be assessed is likely to mark the point at which the fatality probability curve begins, this point will move depending on the glazing used.

As the pressure is increased the fatality probability due to glazing is assessed by considering the speed at which fragments are travelling. For any particular building the effect of the amount of glazing can be taken into account by calculating the proportion of glazing compared to the total length of the perimeter of the building. The values of glazing fatality probability are then multiplied by this factor, hence occupants of buildings with a small proportion of glazing will have reduced fatality probability to glazing failure.

Fatality probability due to debris other than glazing is considered next. In this case, the point at which the fabric of the building starts to fail is estimated and at pressures above this failure level fatality probability due to debris is estimated. This fatality probability level is then factored by the proportion of wall material compared to the total perimeter of the building (i.e. 1 - proportion of glazing) to take account of the amount of external perimeter of the building which is not glazed. Fatality probability due to dense material such as brickwork and due to less dense material such as wood panelling need to be considered. The type of debris likely to be produced by a particular building should be considered, for instance a Portacabin might be expected to produce only panelling type debris while other constructions might produce only dense, brick type debris or a combination of both.

Finally, for buildings other than the Portacabin type, collapse of the building is considered. Having estimated how much of a building might collapse, the fatality probability of occupants is calculated by assuming that 100% of those trapped will be killed (60% for the Brick Building).

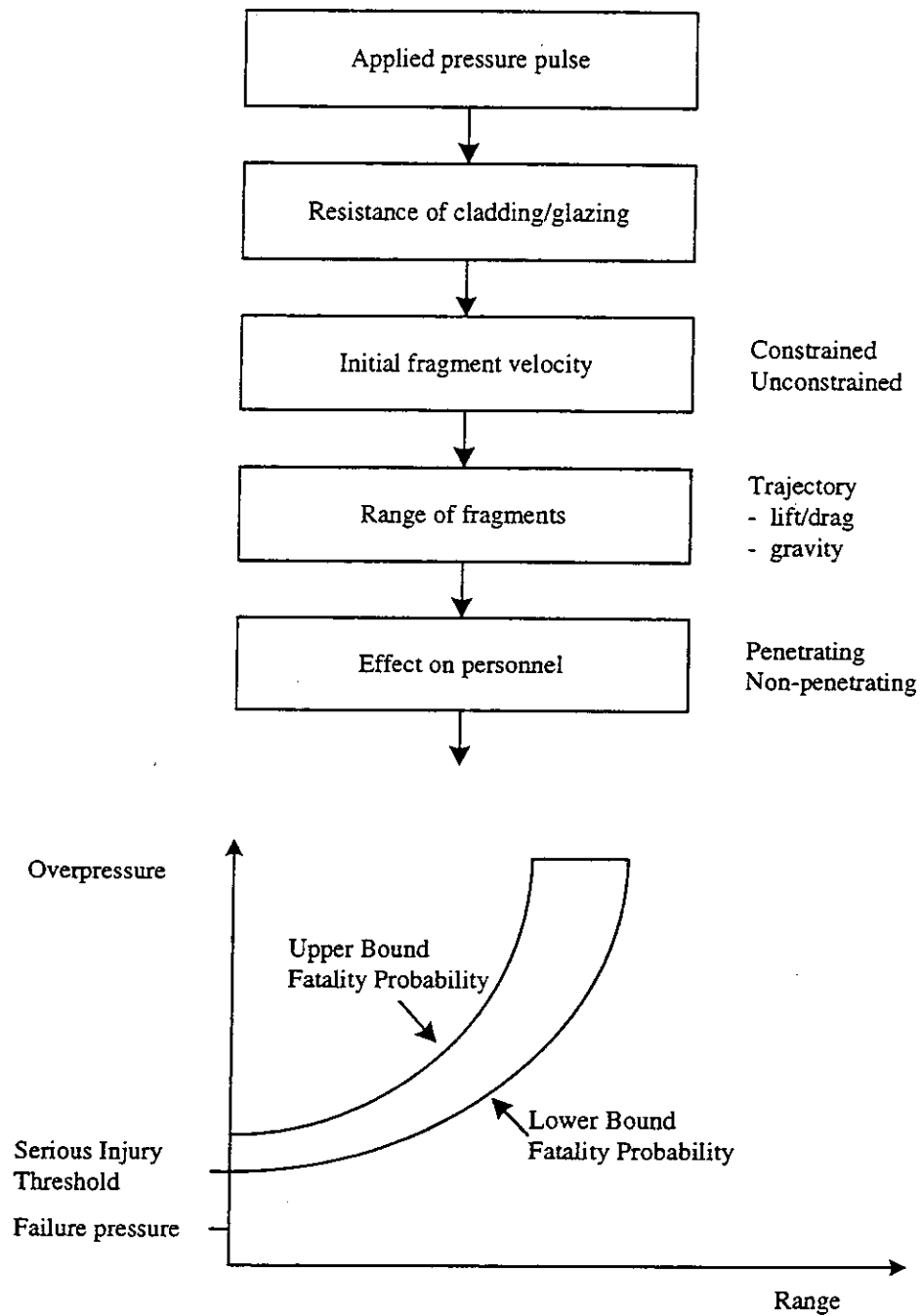
Overall fatality probability curves are a combination of these 3 main areas: in order to prevent double counting of fatalities, the following formula may be used:

**Overall fatality probability,**

$$p_t = p_g + p_d + p_c - (p_g * p_d) - (p_g * p_c) - (p_d * p_c) + (p_g * p_d * p_c)$$

where

- $p_t$  = Total probability of fatality
- $p_g$  = Probability of fatality due to glazing failure  
= Fatality probability due to glazing x % glazing in building
- $p_d$  = Probability of fatality due to debris  
= Fatality probability due to debris x % wall in building
- $p_c$  = Probability of fatality due to building collapse



Variations

Cladding/Brick/Timber panels/partition walls/glazing

**Figure 10.1: Fatality probability of personnel subject to glazing/cladding debris hazard**

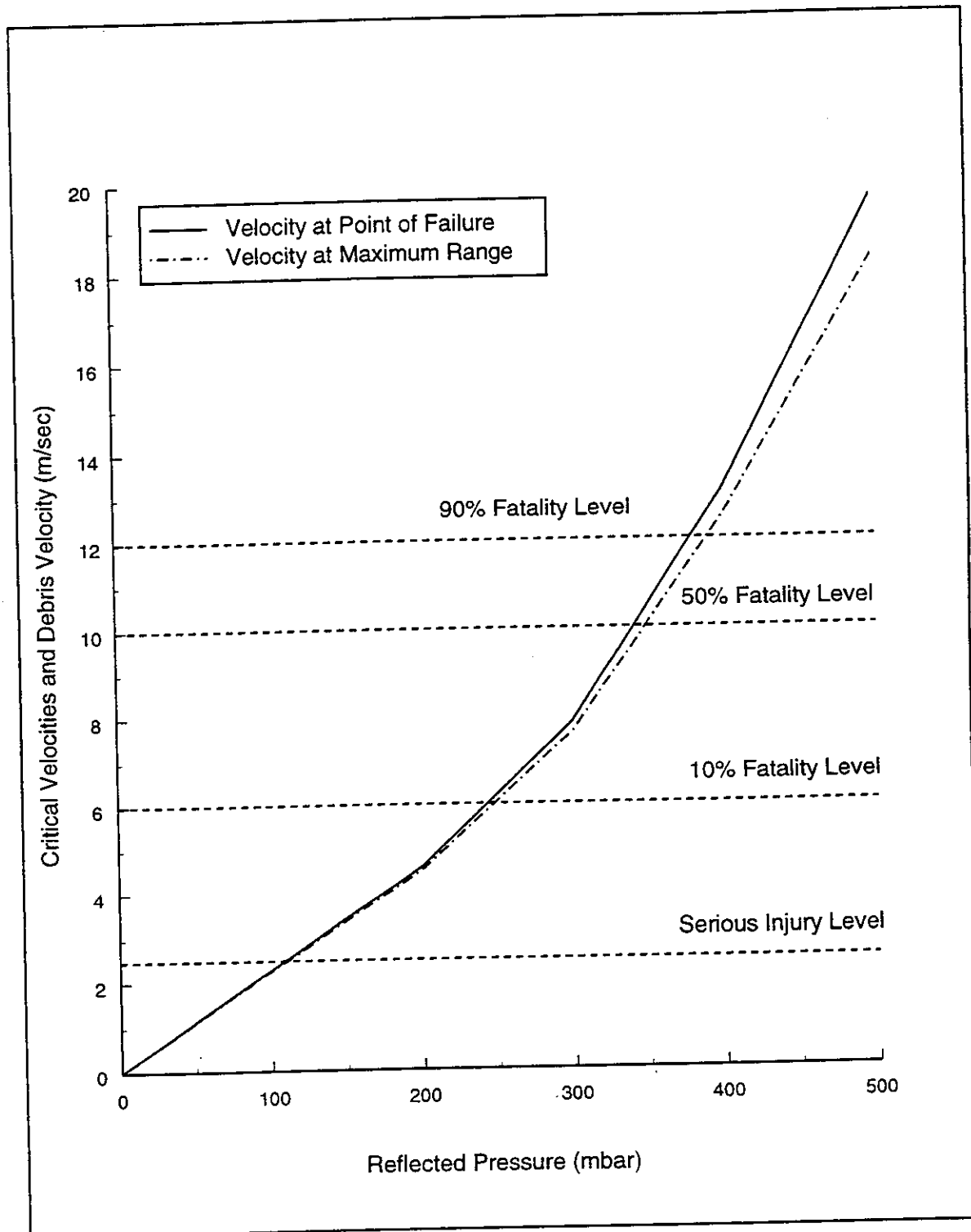
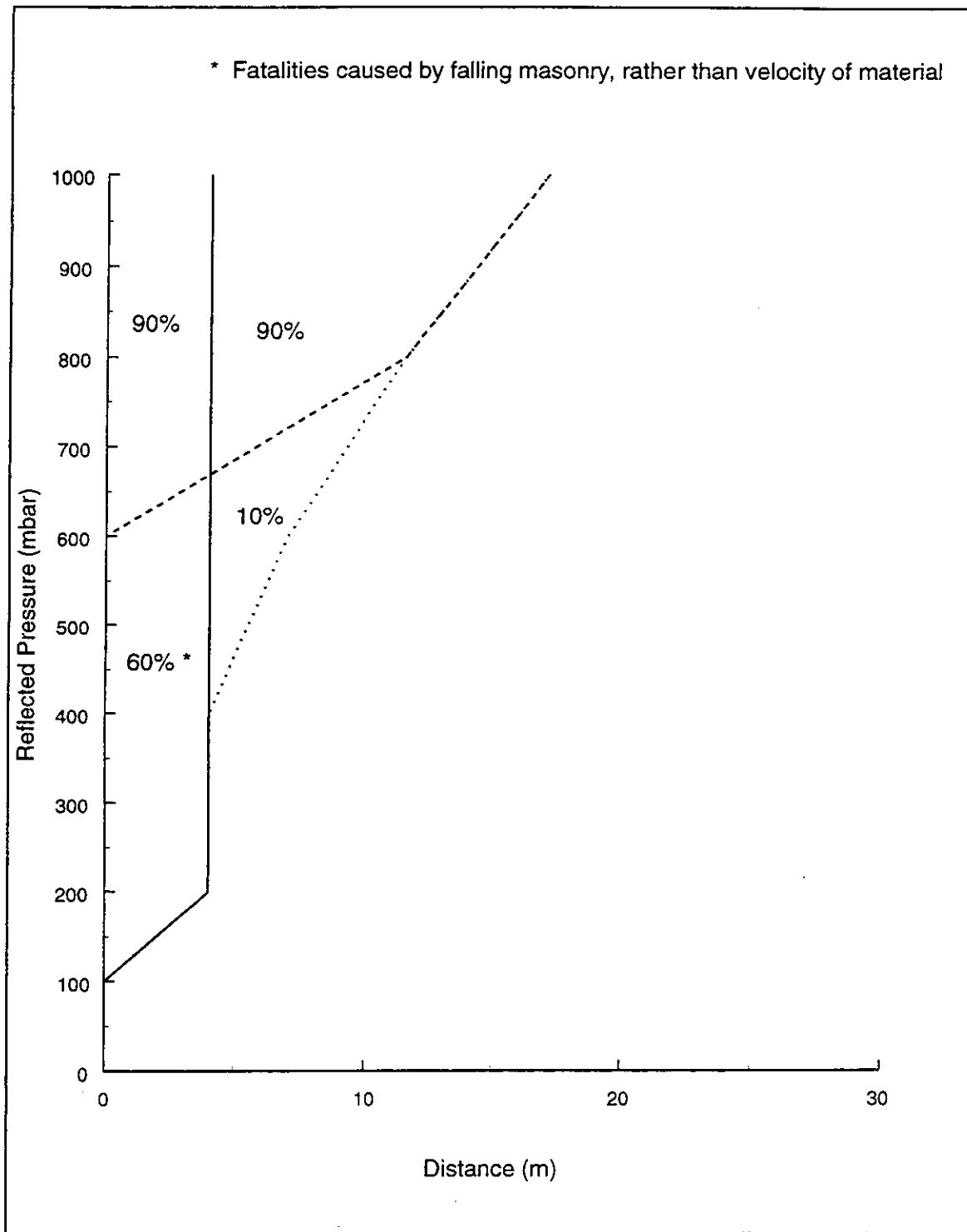


Figure 10.2: Velocity/fatality graph for brickwork





**Figure 10.3: Fatalities range for brickwork**

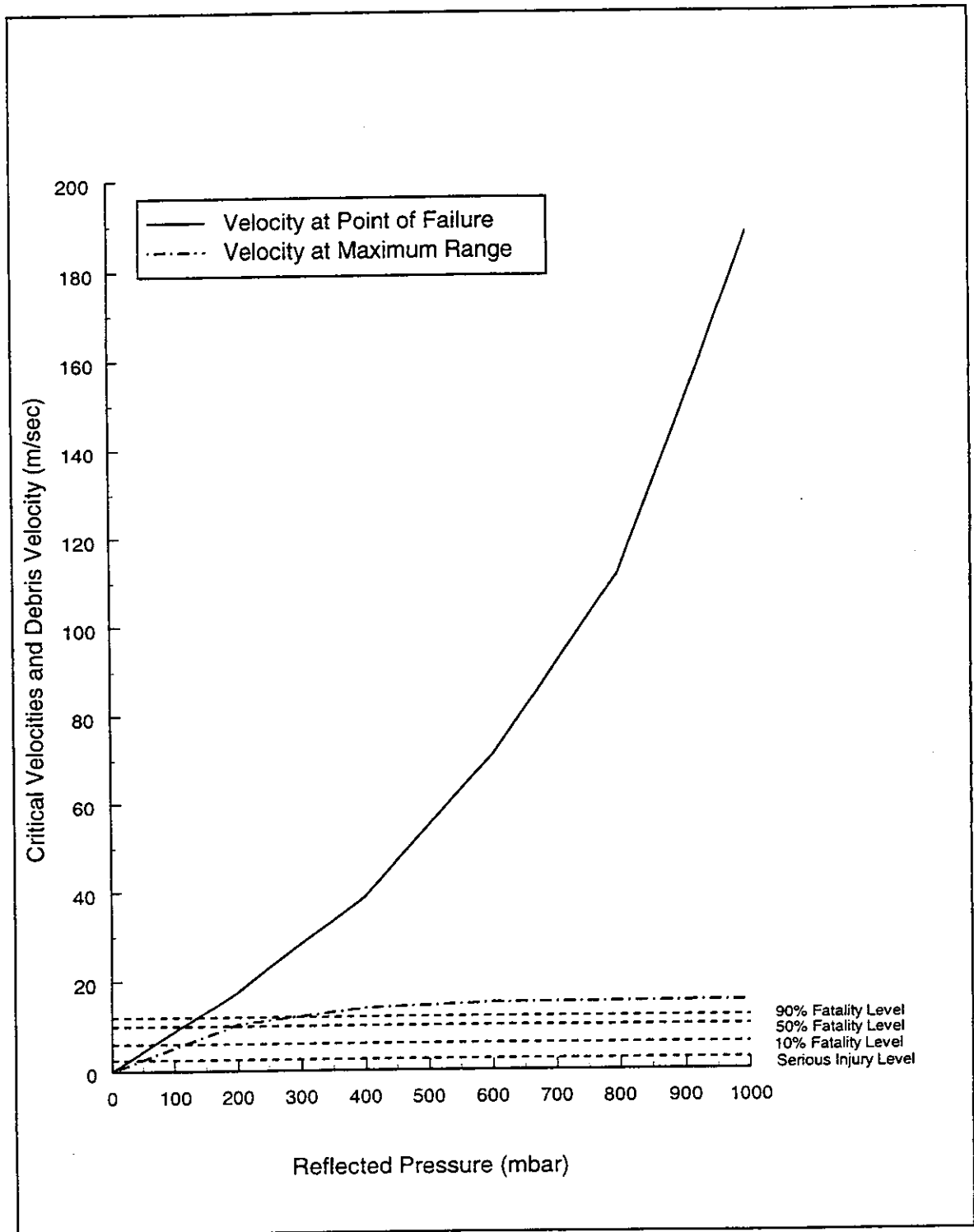


Figure 10.4: Velocity/fatality graph for partitions

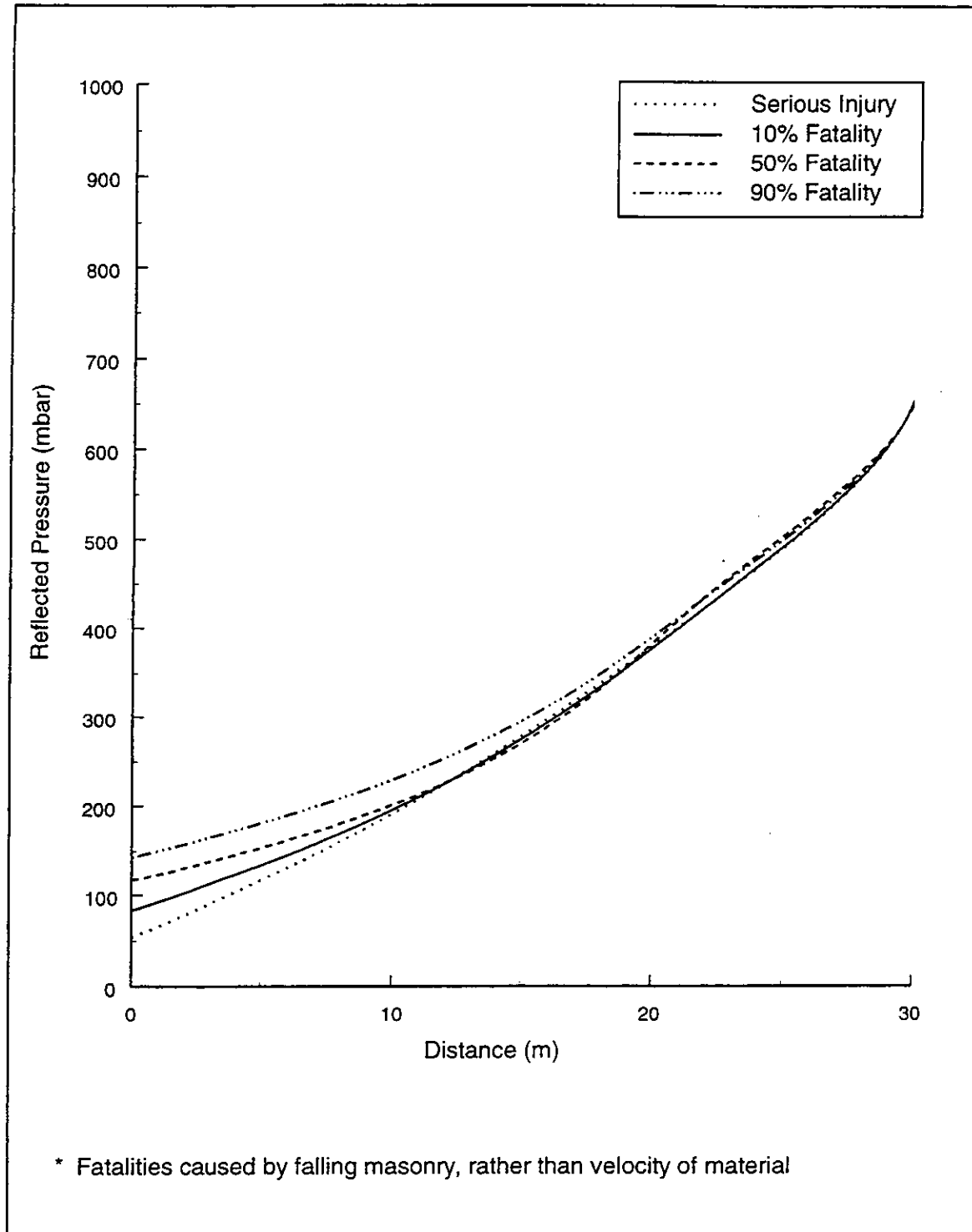
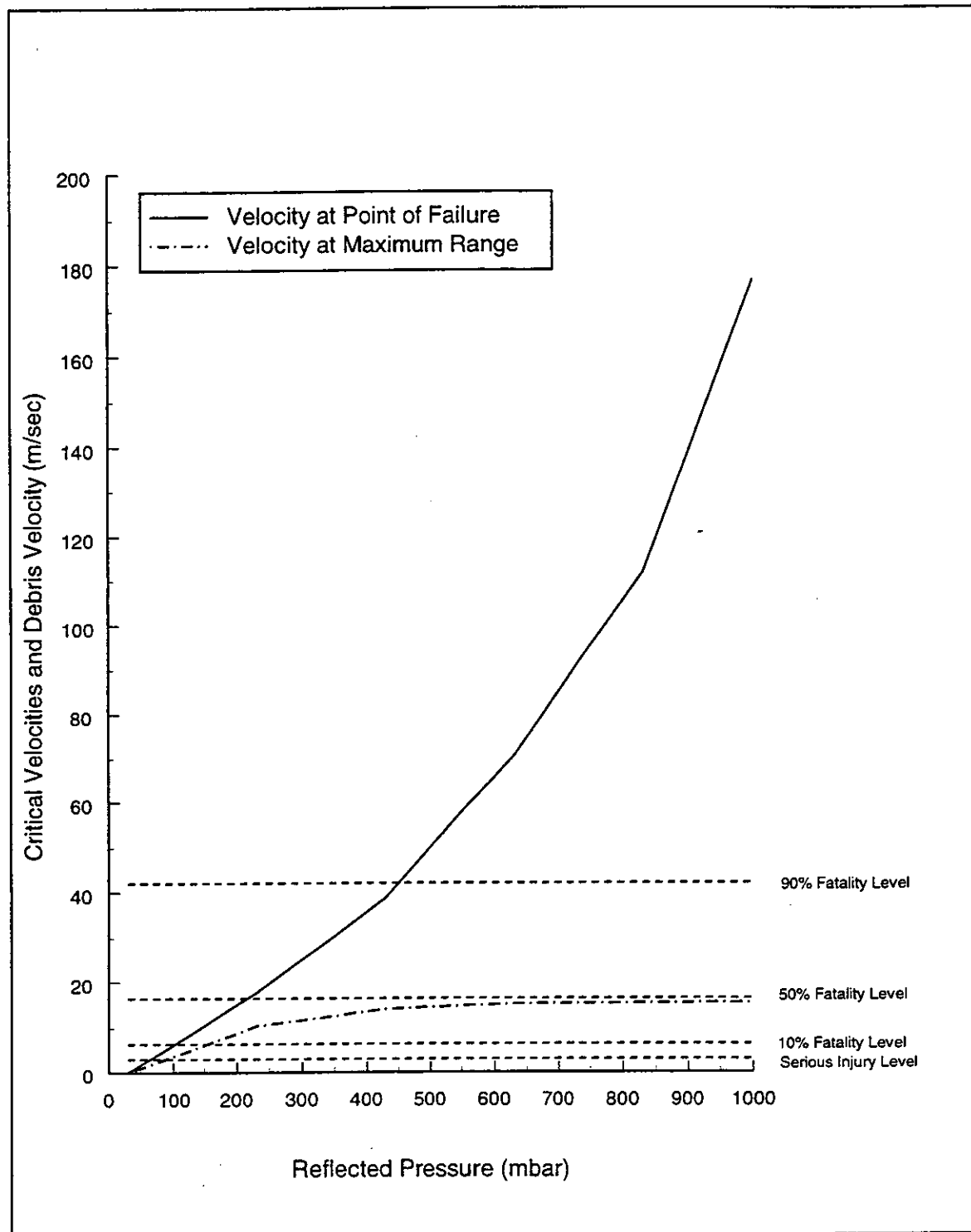
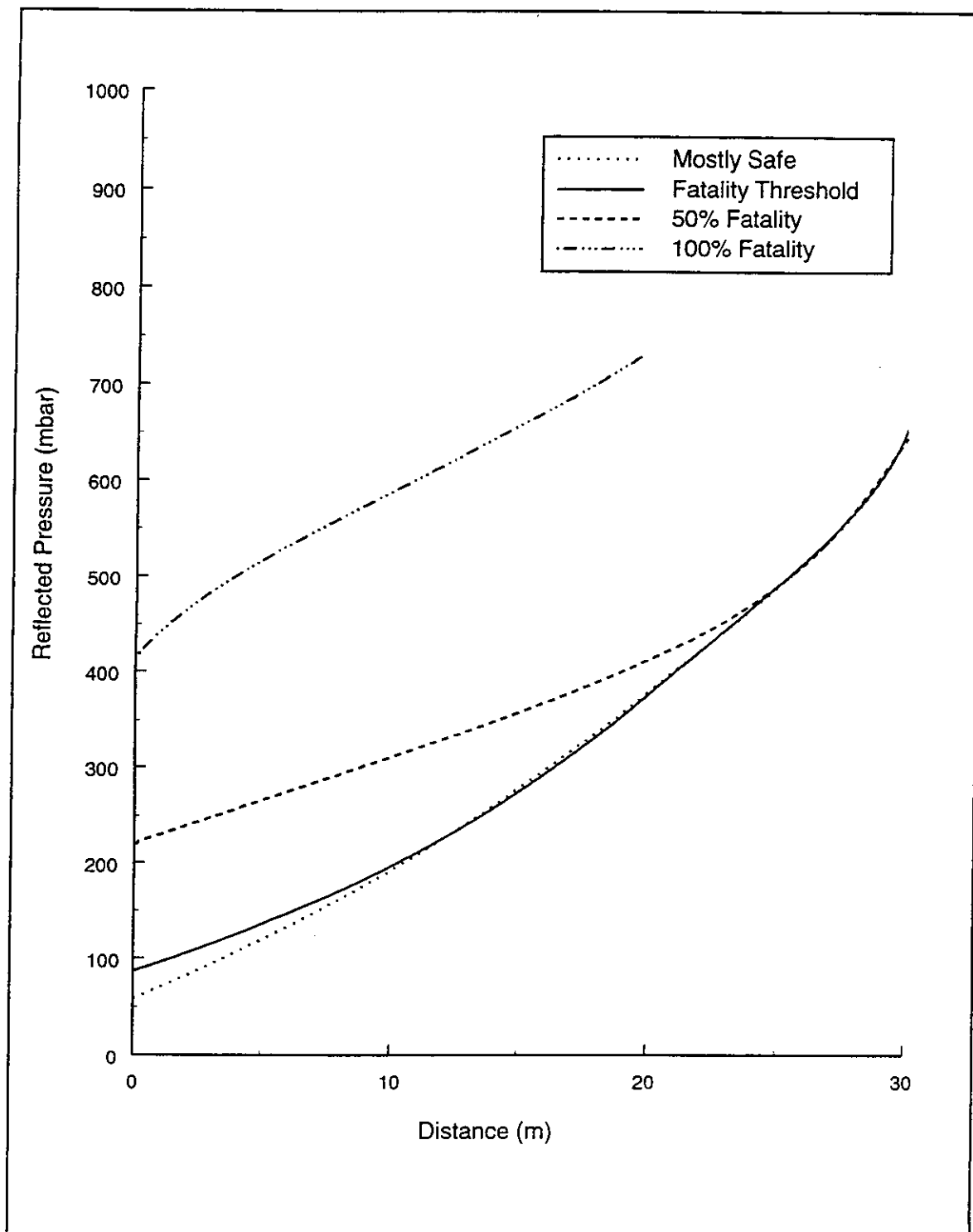


Figure 10.5: Fatalities range for wooden partitions



**Figure 10.6: Velocity/fatality graph for partitions (based on whole body translation)**



**Figure 10.7:** Fatalities range for wooden partitions (based on whole body translation)

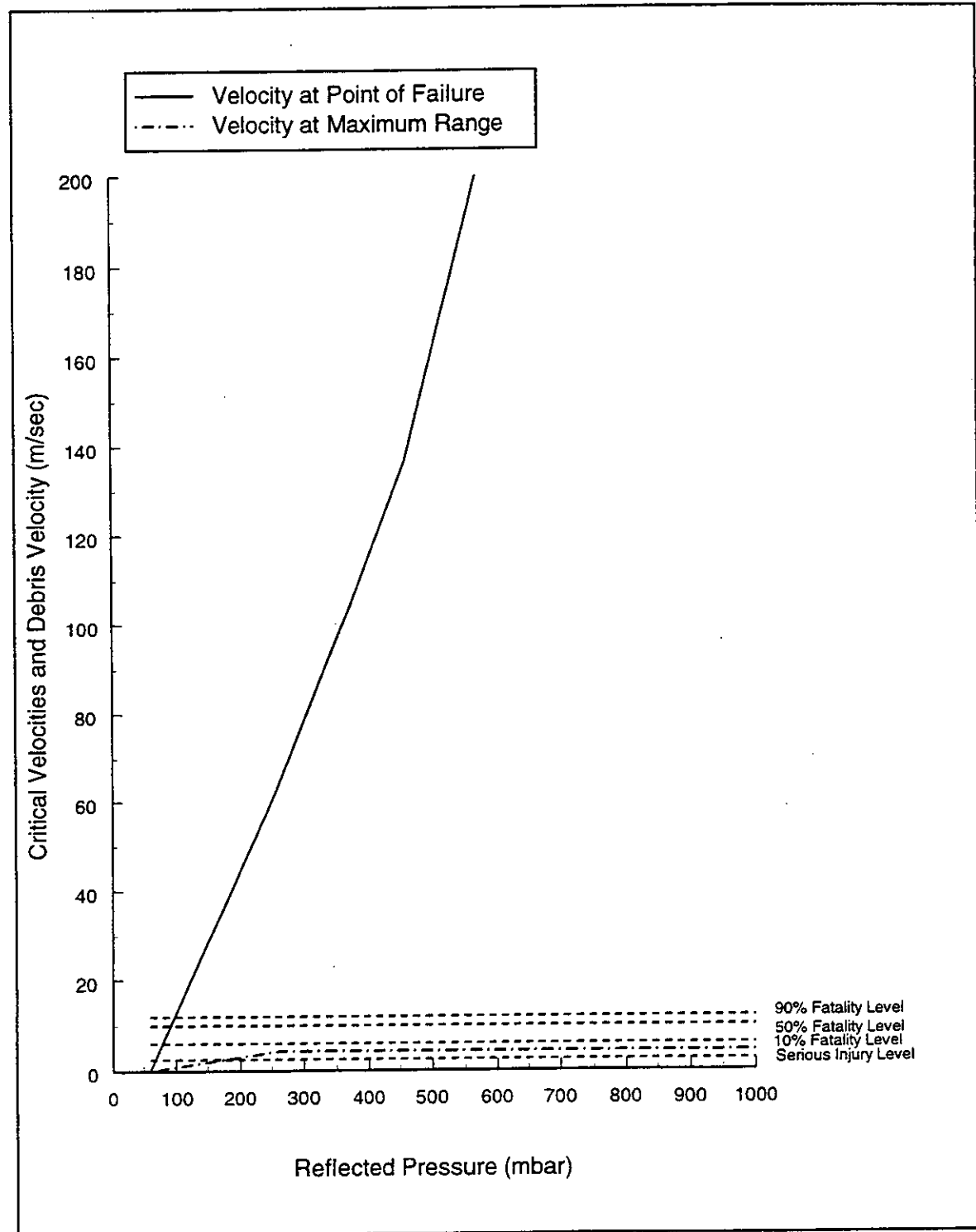
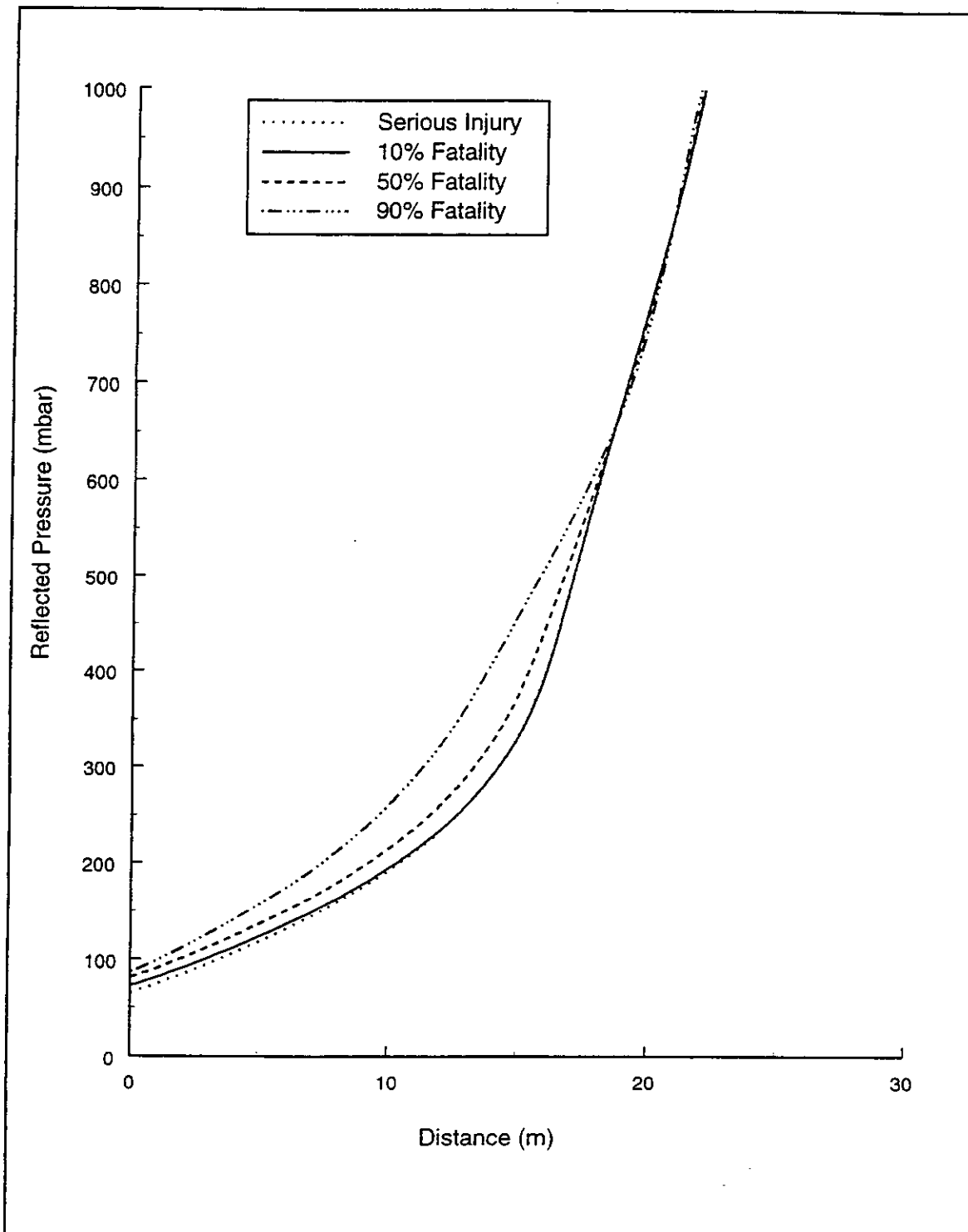
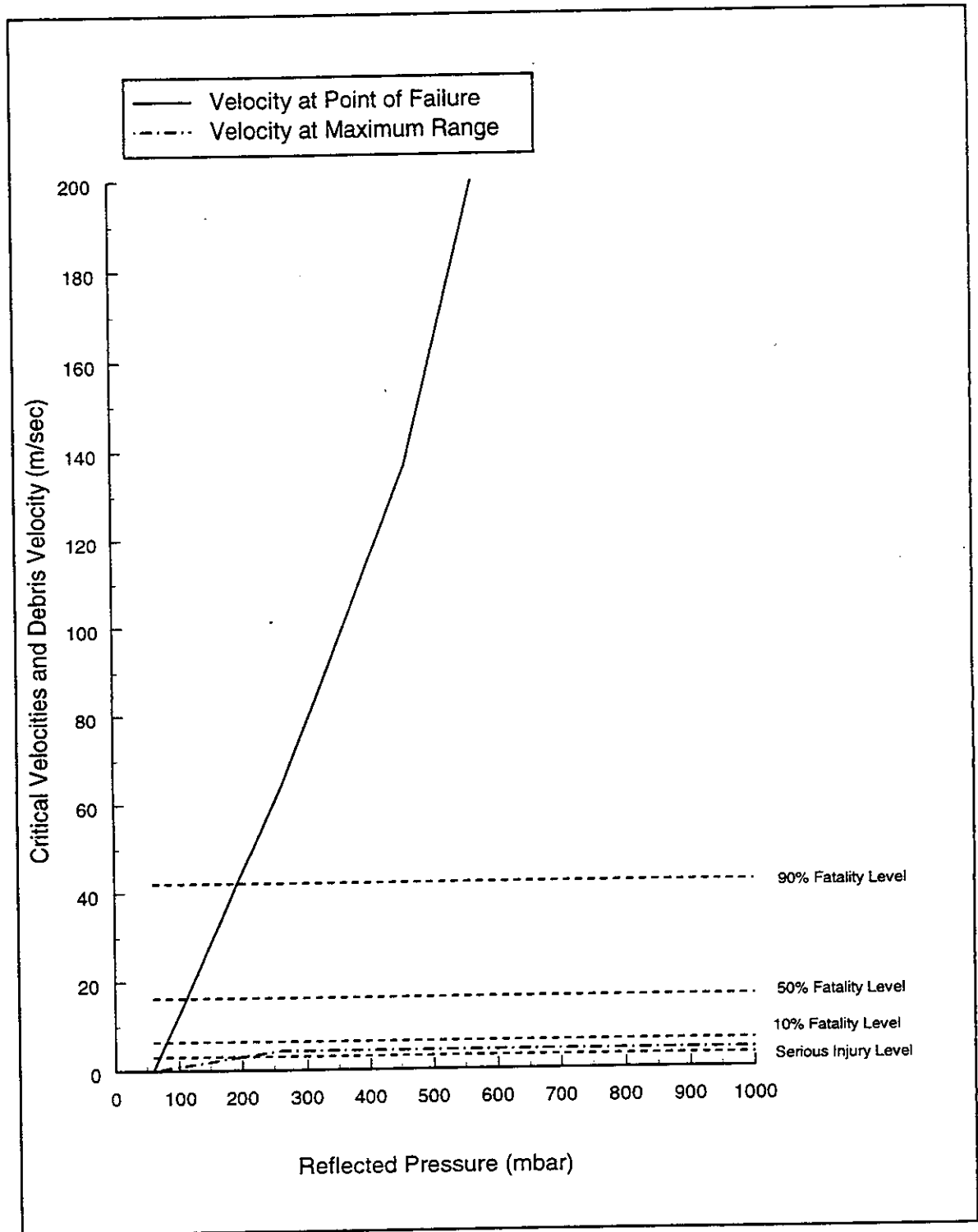


Figure 10.8: Velocity/fatality graph for cladding



**Figure 10.9: Fatalities range for cladding**



**Figure 10.10:** Velocity/fatality graph for cladding (based on whole body translation)



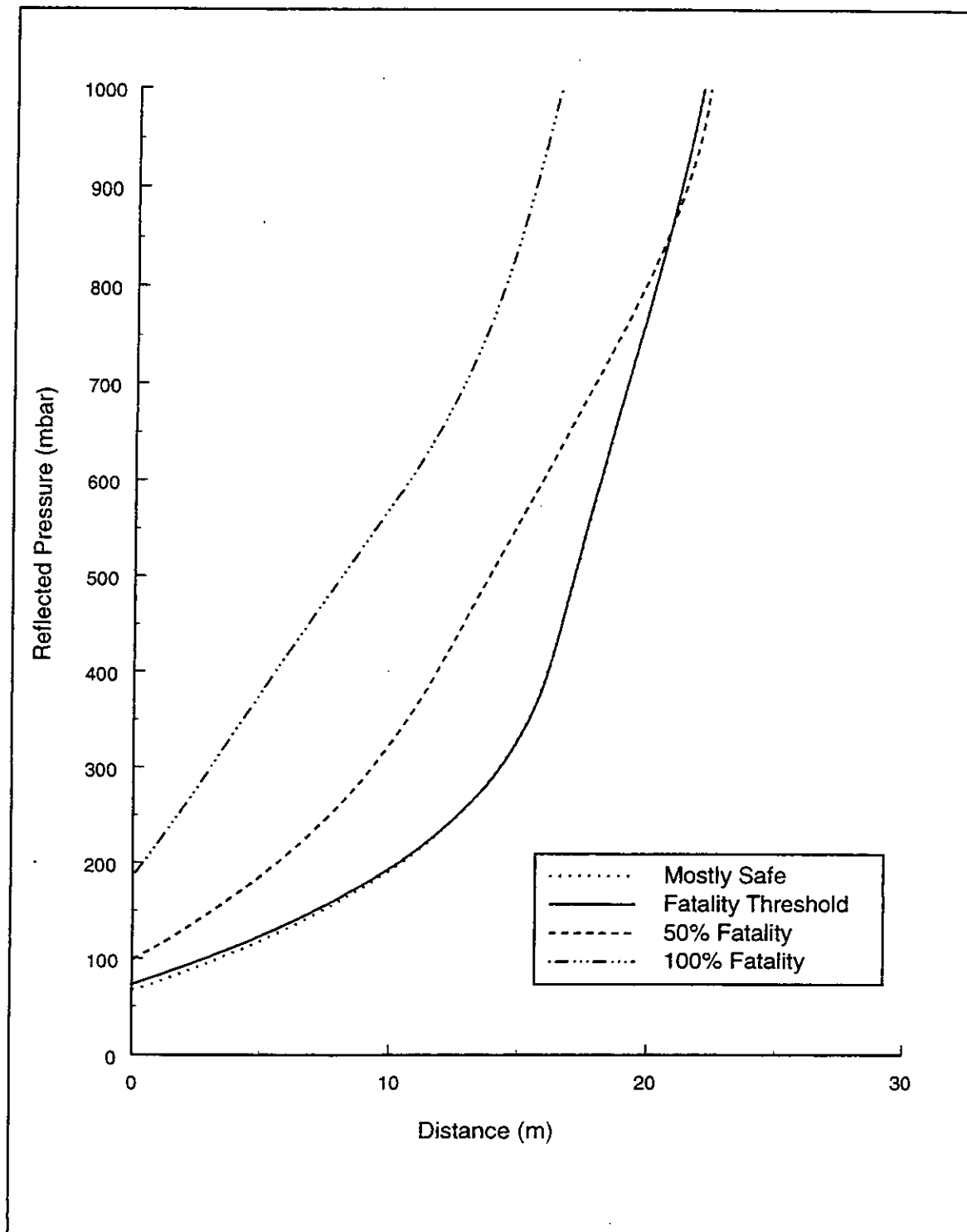


**Figure 10.11: Fatalities range for cladding (based on whole body translation)**

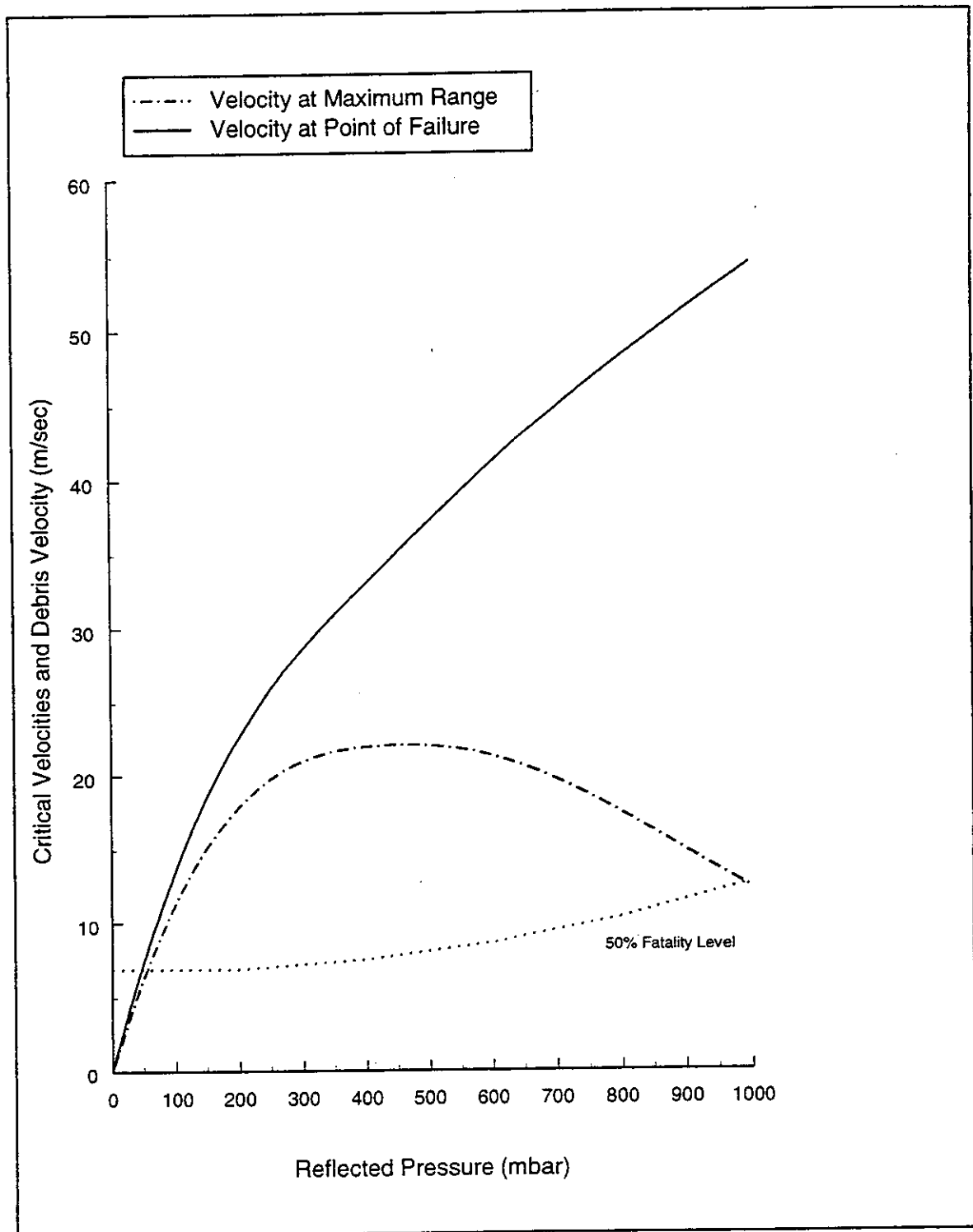
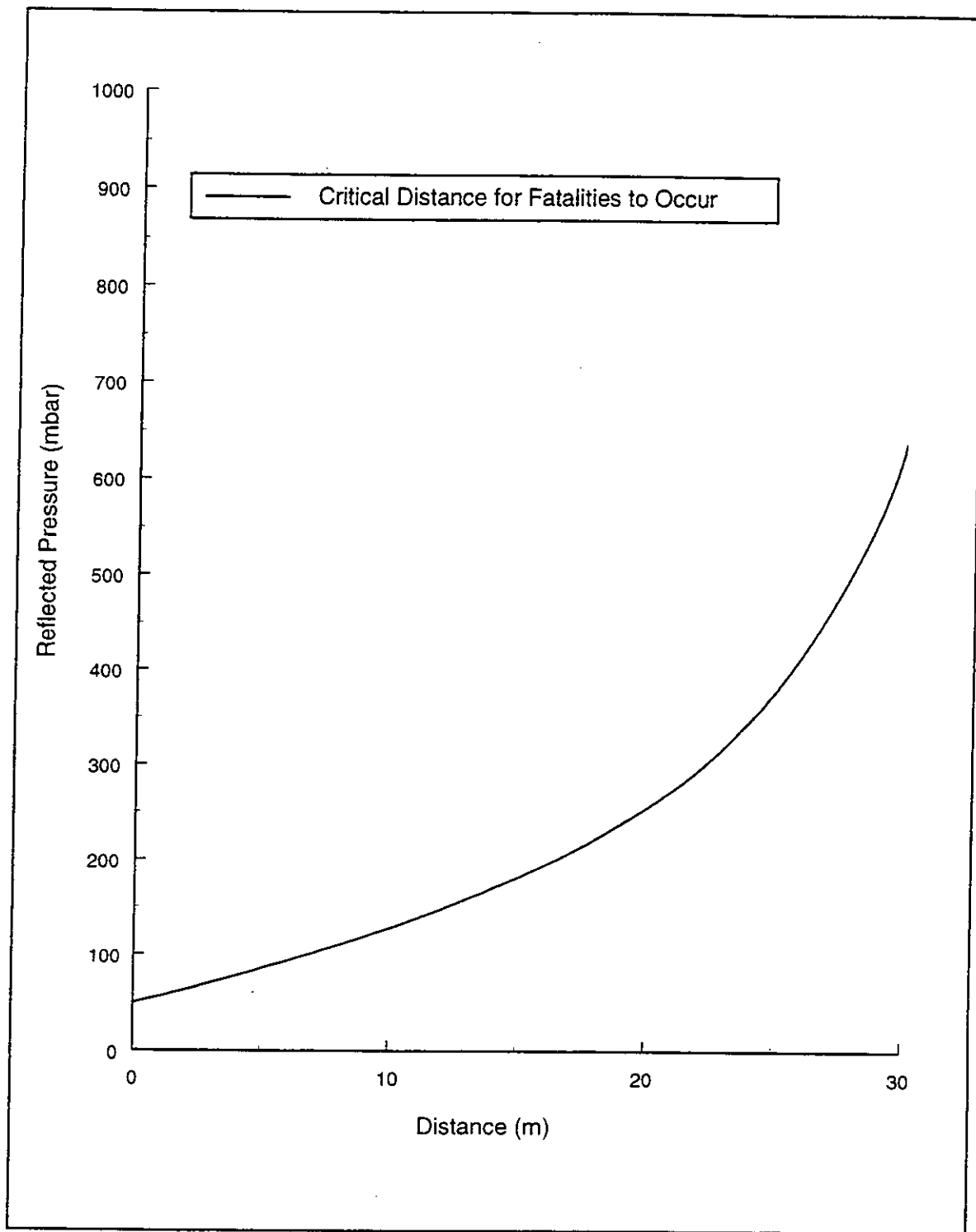
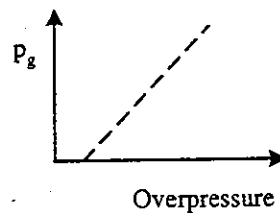
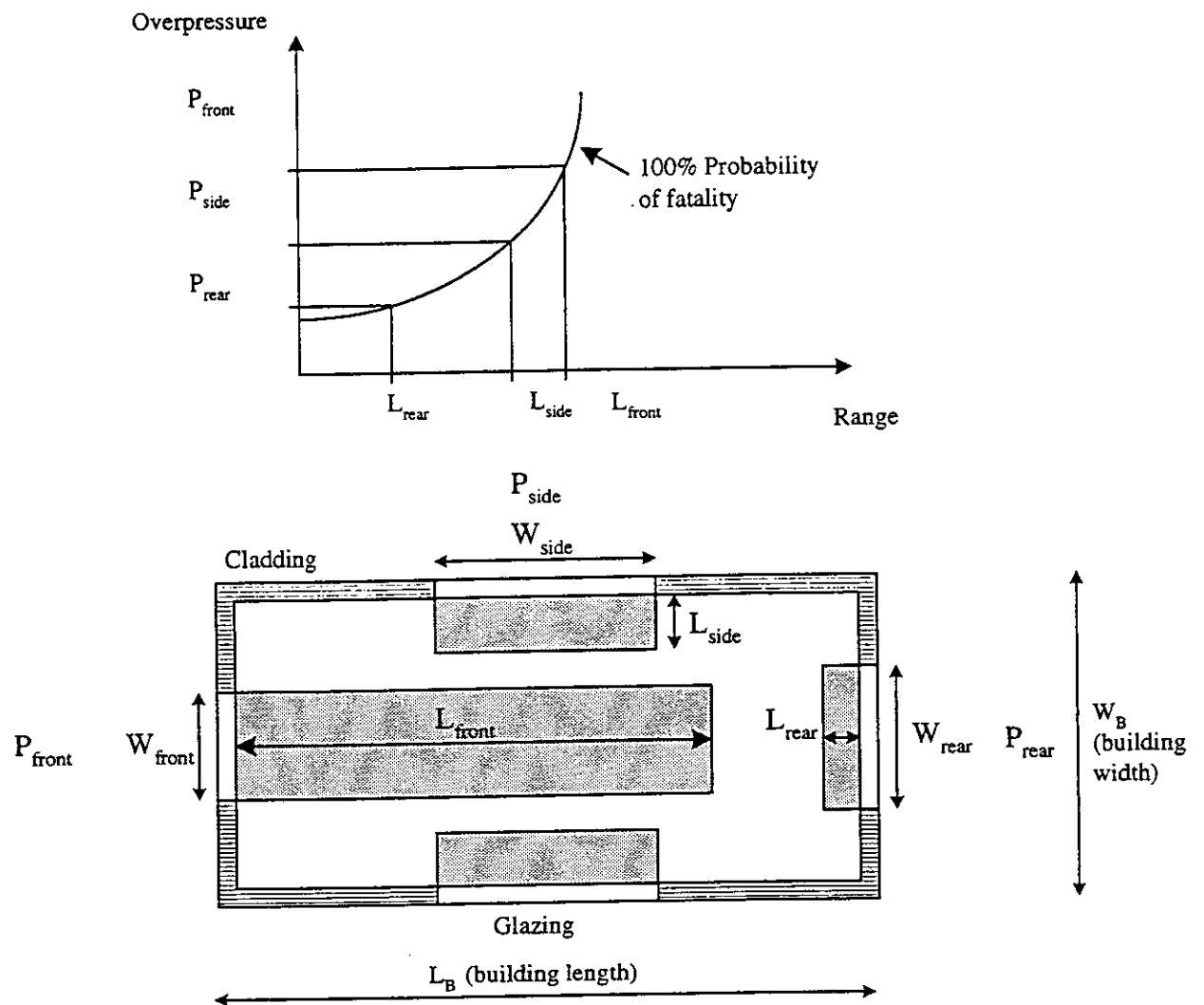


Figure 10.12: Velocity/fatality graph for glazing

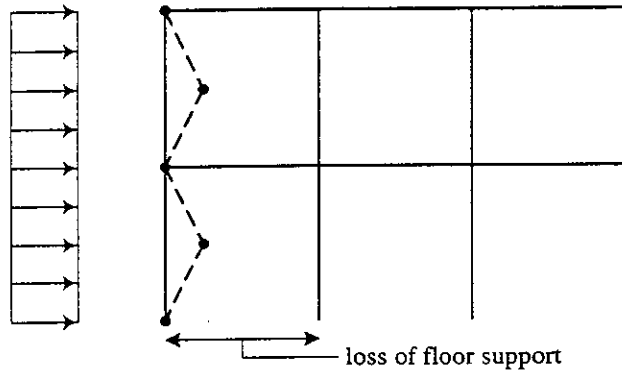


**Figure 10.13: Fatalities range for glazing**



**Figure 10.14:** Fatality probability of building occupants arising from glazing failure

**Partial collapse**



**Total collapse**

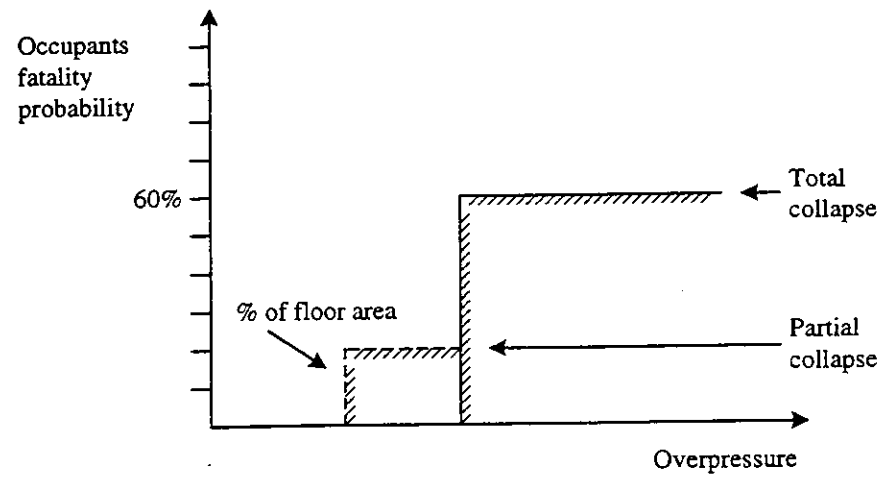
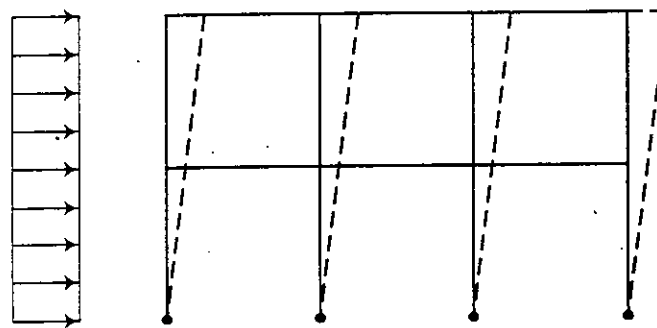
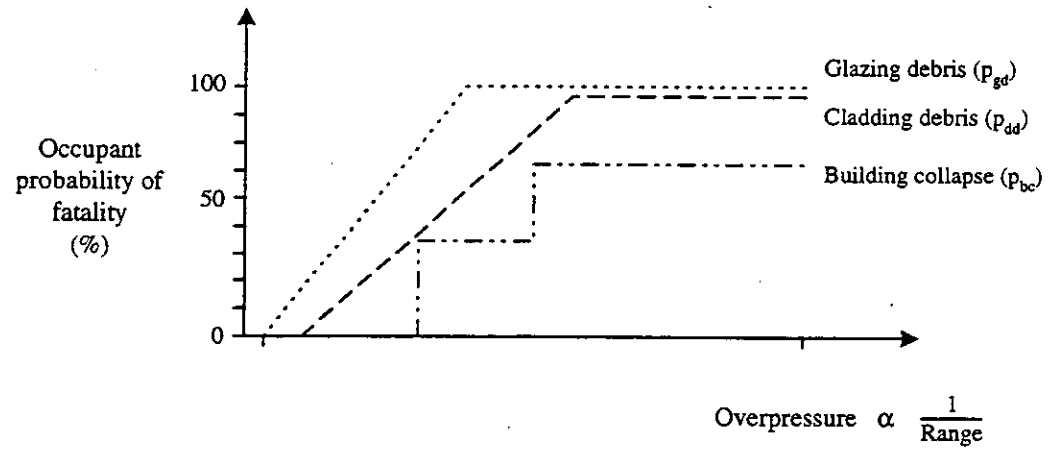


**Figure 10.15: Fatality probability of building occupants arising from building collapse**



Overall Fatality Probability:

$$P = P_{gd} + P_{dd} + P_{bc} \dots\dots$$

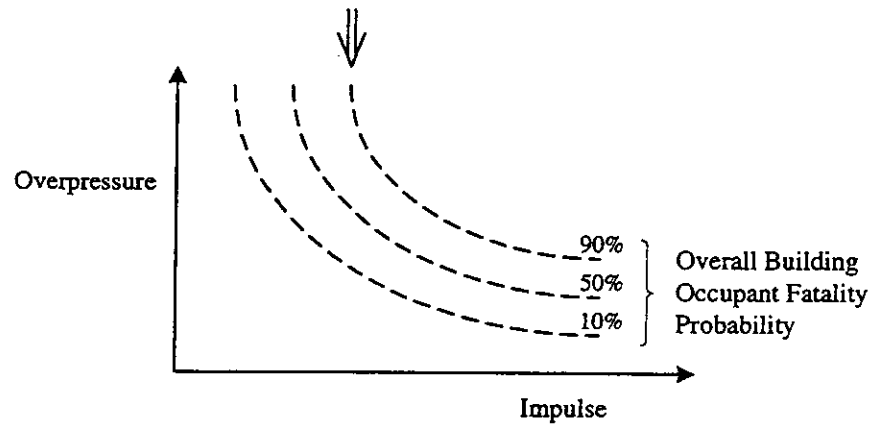


Figure 10.16: Overall building occupant fatality probability

## 11 REFERENCES

1. The Investigation and Control of Gas Explosions in Buildings and Heating Plant. R.J. Harris, British Gas, E & F Spon Ltd. 1983.
2. Methods for the determination of possible damage to people and objects resulting from releases of hazardous materials. CPR 16E, 1st Edition.
3. Loss Prevention in the Process Industries. Volume 1, Frank P. Lees, Butterworths 1989.
4. Explosion hazards and evaluation. W.E. Baker, P.A. Cox, P.S. Westine, J.J. Kulesz, R.A. Strehlow. Elsevier Scientific Publishing Company, Oxford 1983.
5. 'Response of Real Structures to Blast Loadings - the Israeli Experience'. R. Eytan, from Structures Under Shock and Impact II, Editor P.S. Bulson, Computational Mechanics Publications, Thomas Telford.
6. Structure Response and Damage Produced by Airblast from Surface Mining D.E. Siskind, V.J. Stachura, M.S. Stagg & J.W. Kopp, United States Department of the Interior, Bureau of Mines Report on Investigations, 1980.
7. Advisory Committee on Major Hazards. Second Report, Health and Safety Commission, H.M.S.O. 1979.
8. A Simulation Model to Estimate Human Loss for Occupants of Collapsed Buildings in an Earthquake. H.O. Murakami, Hokkaido University, Sapporo, Japan, Earthquake Engineering, Tenth World Conference 1992.
9. New Handbook Planning and Design Data. P. Tutt and D. Adler.
10. Tall Building Data from DOE/PSA Technical Guides 1 and 2 on Shear Walls and Base Frame Design of Buildings.
11. Factors Determining Human Casualty Levels in Earthquakes. Mortality predictions in building collapse. A.W. Coburn, R.J.S. Spence & A. Pomonis. The Martin Centre for Architectural and Urban Studies, University of Cambridge, UK.
12. Design of structures to resist nuclear weapons effects (American Society of Civil Engineers pp 224-225).
13. The Institution of Chemical Engineers Major Hazards Assessment Panel. Overpressure Working Party. The Effects of Explosions in the Process Industries.

- 14 Evaluation of Vapour Cloud Explosions by Damage Analysis. H. Giesbrecht. BASF AG D-6700 Ludwigshafen (Germany) The Journal of Hazardous Materials, 17 (1988) 247-257 Elsevier.
- 15 Earthquake Resistant Design D.J. Dowrick
- 16 Seismic Design of Concrete Structures. T.P. Tassios.
- 17 'Fundamentals of Protective Design for Conventional Weapons', TM 5-855-1, Technical Manual, Headquarters, Department of the Army, November 1986.
- 18 'Glass Fragment Hazard from Windows Broken by Airblast, Fletcher, E.K., Richmond, D.R., and Yelverton, Lovelace Biochemical and Environmental research Institute (1980).
- 19 ASCE - Manuals and Reports on Key Practice - No. 58
- 20 ASCE - Manuals and Reports on Key Practice - No. 42
- 21 Explosive Shocks In Air. G.F. Kinney & K.J. Graham.
- 22 Ultimate Capacity of Blast Loaded Structures Common in Chemical Plants. M.G. Whitney, D.O. Barber & K.H. Syvey. Plant/Operations Progress (Vol.11, No.4) October
- 23 Introduction to Structural Dynamics. John M. Biggs. McGraw-Hill Publishing Company. 1964.
- 24 Explosions - Their types, characteristics, effects, prevention and mitigation. Dr David J. Lewis, Consultant, Liverpool.
- 25 The Response of Glass Windows to Explosion Pressures. I.Chem.E Symposium Series No. 49. R.J. Harris, M.R. Marshall & D.J. Moppett. British Gas Corporation, Midlands Research Centre.
- 26 Engineering Materials M.F Ashby, D.R.H. Jones. Pergamon Press.1980.
- 27 Code of Basic Data for The Design of Buildings. Chapter V Loading. Part 2 Wind Loads. CP3: Chapter V: Part 2: September, 1972
- 28 BS 5950 : Part 1 : 1990 Structural use of Steelwork in Building.
- 29 Glasstone, S. and Dolan, P.J., 1977. 'The Effects of Nuclear Weapons.' 3rd Edition.
- 30 Curtin, W.G., Shaw, G., Beck, J.K., Bray, W.A., 1987. 'Structural Masonry Designer's Manual'. BSP Professional Books.



- 31 'RCCOL - R.C.Column Analysis to BS 5400: Part 4: 1984/1990' Program Version 2.3, WS Atkins Transportation Engineering, July 1992.
- 32 Wilcox, W.W., Botsai, E.E. and Kubler, H., 1991. 'Wood as a Building Material. A guide for Designers and Builders'. John Wiley & Sons, Inc.
- 33 Nowee, J., 1985. 'Dynamic Failure Pressure and Fragmentation of Thermally Hardened Window Panes' PML 1985 - C - 103
- 34 Hurst, N., and Trainor, M., 'Quantified risk assessment for Liquefied Gas Installations', in 'The Safe Handling of Pressure Liquefied Gases - Consequence Analysis and Prevention', Conference Documentation, 26/27 November, 1992, London.
- 35 Curtin, W.G., Shaw, G., Beck, J.K. and Bray, W.A. 'Structural Masonry Designer's Manual' 2nd. Ed. BSP Professional Books, 1987.

**Table 11.1: List of references obtained in literature search**

- Categories**
- 1 Prediction of Blast pressure
  - 2 Global Structural Response
  - 3 Component response
  - 4 Effects on Humans
  - 5 General
- Sources of Reference**
- ICE Institute of Civil Engineers
  - LS Literature Search
  - HSE HSE suggested references
  - Other references held in-house

No:	Author	Reference	Source of reference	Category	Status	Comments
36	Alexander and Hambly.	Design of Structures to Withstand gaseous explosions. Part 1, Concrete, February 1970, Part 2 March 1970	ICE	2	✓	No useful data
37	Mercx, WPM, Weerheijm, J, and Verhagen, ThLA	Some Considerations on the Damage Criteria and Safety Distances for Industrial Explosions. I.Chem.E. Symp. Ser. 124, pp255-275	LS	2	✓	Pressure/damage tables Discussion of blast loading - failure during -ve phase, effects of openings
38		A Manual for the Prediction of Blast and Fragment Loadings on Structures, US Department of Energy, Albuquerque Operations Office. DOE/TIC - 11268	HSE	1/2/3/4	✓	Fatality probability curves for primary and secondary blast damage. Data for damage to buildings from blast, groundshock and fragments
39	Meyers, G.E. and Becker, R.P.	Interim Handbook for Security Glazing', DOE Technical Memorandum 5603 TM., Naval Civil Engineering Laboratory, Port Hueneme, California 93043, USA. September, 1987.	HSE	3	✓	Design parameters and peak blast pressures for polycarbonate glazing (various thicknesses)
40	Meyers, G.E.	Interim Design Criteria and Acceptance Test Specifications for Blast resistant Windows'. The Shock and Vibration Bulletin, Bulletin 56 Part 1, August 1986.	HSE	3	✓	Design parameters and peak blast pressures for tempered glass (various thicknesses) Fragment protection measures
41	Meyers, G.E.	Security Design Criteria for Embassy construction US Department of State Bureau of Diplomatic Security	HSE	3	✓	Peak overpressure capacities for laminated thermally tempered glass
42	Mancini, R.A.	Workshop on Unconfined Vapour Cloud Explosions', Plant Operations Progress, Vol 11 (1), January 1992	HSE	1	✓	Benchmarking different methods
43	Bangash, M.G.H.	Impact and Explosion: Analysis and Design', Oxford, Blackwell Scientific, 1993	HSE	1/2/3	✓	Useful general reference
44	Hadjipavlou, S. and Carr-Hill, G.	A Review of the Blast Casualty Rules Applicable to UK Houses', Home Office Publication 34/86, 1986.	HSE		-	

No:	Author	Reference	Source of reference	Category	Status	Comments
45	Soper	Modelling Laws Related to Target Vulnerability', W.G., US Naval Weapons Laboratory, Technical Memorandum T-9/67, 1967	HSE			
46		Predicting the Consequences of Fire and Explosions', Institute of Mechanical Engineers and Fire Research Station, published by IMechE, 1991	HSE	5	✓	Mainly contained explosions
47		The Effects of Simplification of the Explosion Pressure - Time History', HSE and Steel Construction Institute, HMSO, 1992 (Offshore Technology Information OTI 92-599)	HSE	1	✓	Importance of various aspects of the blast pressure curve for different duration/period ratios
48		Computerised Analysis Tools for Assessing the Response of Structures Subjected to Blast Loading', HSE and Steel Construction Institute, HMSO 1992. (Offshore Technology Information 92 601)	HSE	5	✓	FE analysis techniques
49		The prediction of Pressure Loading on Structures resulting from an explosion' HMSO, Steel Construction Institute, 1992 (OTI 92 594)	ICE	1	✓	Largely theoretical & discussion. Summary of current position as regards prediction of structural loading EFFECTS Package
50		Buildings and the hazard of explosion: symposium, 1972. Building Research Establishment, 1972.	ICE	3	✓	Collection of papers - most relevant 'The breakage of glass windows by gas explosions', Mainstone, 1971. Data on glass strengths and room internal pressures for breakage
51	Singhal, A.C. et al	Simulation of blast pressure on flexible panel - ASCE Journal of Structural Engineering., 1994	ICE	1	✓	Comparison of blast wave forms - triangular overly conservative
52	Philip, E.B.,	Blast Pressure due to explosion: the calculation of their magnitudes and effects. Ministry of Works. 1945	ICE		-	
53	Smith, P.D., and Hetherington, J.G.	Blast and ballistic loading of structures. Oxford: Butterworth-Heinemann Ltd., 1994	ICE	1/2/3/4/5	✓	Useful general reference
54	Ramabhusanam, E., and Lynch, M.	Structural assessment of bomb damage for the World Trade Centre. New York: ASCE, JPCF Nov., 1994.	ICE	5	✓	Description of damage
55	Mainstone, R.J. et al	Structural damage in buildings caused by gaseous explosions and other accidental loadings, 1971 - 1977. London: HMSO, 1978	ICE	2	✓	Survey of accidental structural damage: tables of explosion size and resultant damage

No:	Author	Reference	Source of reference	Category	Status	Comments
56	Astbury, N.F., West, H.W.H., Hodgkinson, H.R., Cubbage, P.A. and Clare, R.	Gas Explosions in load-bearing brick structures. Jan, 1971	ICE	3	✓	Historical pressure - failure data for windows, panelling, walls. Experimental data - explosion within brick building
57		Guidance on the design of domestic accommodation in loadbearing brickwork and blockwork to avoid collapse following an internal explosion. Institution of Structural Engineers, 1969.	ICE	2/3	✓	No relevant data
58	Brown and James	Dust Explosions in factories: a review of the literature. Safety in Mines. Res. Estab. June 19677, Res. Rest., 201	ICE		-	
59		Explosions in Domestic Structures Pt 1 - Rasbash, P2. - Stretch. Struct. Engineer, Oct., 1969.	ICE	2	✓	Pressure relief for explosions within domestic buildings
60	Walley, F.	The effect of explosions on Structures, , ICE Proceedings, Structures and Buildings, Vol 104, Issue 3, Aug 1994, P (26782) Designing for Natural and Man Made Hazards. Predict & Design for Natural and Man Made Hazards, Williamsburg, 9 - 14 September (6317)	ICE	5	✓	List of information available for WW2 Bomb damage from PRO
61	Elliott, C.L. and Mays, G.C.	The protection of Buildings against Terrorism and Disorder., ICE Proceedings, Structures and Buildings, Volume 94, Issue 3, Aug 1992. (20288)	ICE	2/4	✓	P-i curves/isodamage curves for brick-built houses Isodamage curves for human response to blast - primary
62	Elliott, C.L. and Mays, G.C.	The protection of Buildings against Terrorism and Disorder - Discussion., ICE Proceedings, Structures and Buildings, Volume 104, Issue 3, Aug 1994. (26784)	ICE	3	✓	Fig 12 - isodamage diagram Laminated Glass - research at BRE - pane resistance-deflection, P-I curves for laminated glass
63	Jenkins, L.D.	The St. Mary Axe Bomb: Coping with the result of a Large Explosion in a City Centre., AME Annual Conf., Torquay, 28 June - 1 July, 1993 (27224)	ICE	5	✓	Widespread injuries from flying glass
64	Zwoyer, E.,	Design Considerations to resist Blast and Explosions. Predict & Design for Natural and Man Made Hazards, Williamsburg, 9 - 14 September (6316)	ICE		-	
65		'Techniques for assessing industrial hazards: a manual' International Bank for Reconstruction and Development, Washington, DC, 1988	LS	2/4	✓	Damage probabilities for structures and humans

No:	Author	Reference	Source of reference	Category	Status	Comments
66	Massa, R.J.	'The 'secureplan' bomb utility: a PC-based analytic tool for bomb defense', 28. INMM annual meeting on safeguards: a mature technology, Newport Beach CA, USA 12 July 1987.	LS	1/2/3/4	✓	Description of MATHCAD model for estimating bomb effects. Only primary and tertiary effects on humans considered
67	Massa, R.J. and Howard, J.W.	Bomb CAD A CAD based technique for assessing bomb fatality probability and designing and evaluating bomb defense measures. Proceedings of the 1989 Carnahan conference on security technology, Devore, R.W.	LS	1/2/3/4	✓	Similar to above but more advanced - combines with CAD model
68	Longinow, A., Mahammadi, J. and Robinson, R.R.	'Reliability of engineered basements as blast shelters', Illinois Inst. of Tech., Chicago (USA). Dept. of Civil Engineering, 1979	LS	2/3	✓	Probabilistic calculation of structural failure
69	Wilton, C., Zsutty, T.C. and Willoughby, A.B.	'Development of damage and casualty functions for basement shelters: Final report on stage 2', Scientific Service, Inc., Redwood City, CA, September 1983	LS	3/4	✓	Various fatality probability curves for ceiling collapse, debris, translation and direct blast
70		'Assessment of combined effects of blast and fire on personnel survivability', IIT Research Inst., Chicago, June 1982				
71	Fugelso, L.E., Weiner, L.M. and Schiffman, T.H.,	'Explosion Effects Computation Aids', June 1972	LS	4	✓	Data for vulnerability to fragments
72	Iverson, J.H.	'Existing Structures Evaluation. Part II. Window Glass and Applications', , December, 1968.	LS		not yet received	Part 1 sent instead - Walls - resistance functions for different wall types
73		'Blast kills ten (at Angus Chemical Co's nitroparaffins plant), empties town', Angus Chemical Co., IMC Fertilizer Inc., August 1991	LS		Item Not Held	-
74	Eytan, R	'Response of Real Structures to blast loadings - the Israeli experience', ., Proceedings of the Second International Conference on Structures under Shock and Impact II, 1992	LS	5	✓	General paper
75	Longinow, A., et al	'Explosion hazards to urban structures', , Proceedings of the Third Conference on the Dynamic Response of Structures, Los Angeles, 1986	LS	2	✓	Safe separation distances
76	Davies, I.L.I.	'Damaging effects from the impact of missiles against reinforced concrete structures', , Nuclear Energy v 19 n 3 June 1980, pp199 - 205	LS	3	✓	Finite difference model for impact analysis



# **Derivation of fatality probability functions for occupants of buildings subject to blast loads**

## **Phases 2 & 3**

**R M Jeffries & L Gould**  
WS Atkins Science & Technology  
Woodcote Grove  
Ashley Road  
Epsom  
Surrey  
KT18 5BW

The UK Health and Safety Executive (HSE) are often consulted by local planning authorities on the safety aspects of proposed developments in the vicinity of industrial plant and in addition give advice on the siting of new plant with major hazard potential. A quantified risk assessment approach is used, which may include consideration of the effects of explosions which can cause injury to people through direct effects on the body, secondary effects such as the impact of fragments or partial/total building collapse of buildings or tertiary body translation effects. To date the fatalities have been predicted using a probit based on World War II bomb data. The objective of this project is to develop a procedure for assessing the vulnerability of occupants of different types of buildings subject to overpressures produced from vapour cloud explosions. A methodology has been developed for deriving generic fatality probability functions for different building types based on the primary structural characteristics of the building. This report details Phase 2 and 3 of the project in which the methodology developed in Phase 1 was subject to various sensitivity studies in order to refine the approach. Preliminary results, in the form of fatality probability curves, are presented for two typical building types.

This report and the work it describes were funded by the Health and Safety Executive. Its contents, including any opinions and/or conclusions expressed, are those of the authors alone and do not necessarily reflect HSE policy.

## **Note to Readers**

This document is an interim report outlining the results of the second and third phases of an exercise to develop a methodology for estimating the fatality probability for the occupants of buildings subject to explosions. It was written prior to the completion of the final phase of the project and has been issued in order to make the results of the work speedily available to a wider audience, in advance of the publication of the definitive final report produced at the end of the project. Consequently, many of the results and conclusions are presented in a context which lacks the perspective afforded by the final phase of the work. The contents should therefore be viewed as preliminary information and should not be accredited with the authority of a final report.

## CONTENTS

1	INTRODUCTION . . . . .	1
1.1	Summary of Phase 1 . . . . .	1
1.2	Objectives of Phases 2 and 3 . . . . .	2
2	PRESSURE PROFILE AND LOADING EFFECTS . . . . .	5
2.1	Rise time . . . . .	5
2.2	Negative phase . . . . .	7
2.3	Pressure relief due to glazing/cladding failure . . . . .	14
2.4	Aspect ratio . . . . .	16
2.5	Conclusions . . . . .	18
3	STRUCTURAL CAPACITY . . . . .	33
3.1	Brick building type . . . . .	33
3.2	Concrete framed building . . . . .	34
4	GLAZING/DEBRIS EFFECTS . . . . .	42
4.1	Sources of data . . . . .	42
4.2	Glazing failure pressures . . . . .	43
4.3	Glazing velocity/mass distribution . . . . .	44
4.4	Probability of fatality due to glazing fragments . . . . .	46
4.6	Conclusions . . . . .	51
5	ASSESSMENT OF OCCUPANT FATALITY PROBABILITY . . . . .	62
5.1	Brick building type . . . . .	62
5.2	Concrete framed building . . . . .	65
5.3	Comparison with other models/methods . . . . .	67
5.4	Conclusions . . . . .	68
6	CONCLUSIONS AND RECOMMENDATIONS . . . . .	76
7	REFERENCES . . . . .	78

## APPENDICES

A	Summary of literature search
---	------------------------------



## LIST OF TABLES

- 2.1 Typical design positive and negative pressures
- 4.1 Comparison of Mainstone predictions

## LIST OF FIGURES

- 1.1 General Procedure
- 2.1 Schematic Progression of Pulse Shape [7]
- 2.2 Schematic Diagram of Pulse at an Intermediate Distance [8]
- 2.3 Building Response vs. Pressure for Different Pulse Shapes
- 2.4 Pulse Shape Including Negative Phase
- 2.5(a) Building Response without Negative Phase
- 2.5(b) Building Response including Negative Phase
- 2.6 Building Response to Pulse including Negative Phase: No Rear Face Pressure Load
- 2.7 Building Response to Pulse including Negative Phase: Includes Rear Face Pressure Load
- 2.8 Investigation of Negative Phase Response with Aspect Ratio
- 2.9 Building Response vs. Area to Volume Ratio
- 2.10 Effect of Front Face Glazing Failure
- 2.11 Internal Pressure Rise
- 2.12 Rear Face Pressure Load
- 2.13 Building Response vs. Aspect Ratio
- 3.1 Brick Building Dimensions: Elevation at Rear Wall
- 3.2 Brick Building Dimensions: Elevation of Partition Wall (Top) and Elevation of End Wall (Bottom)
- 3.3 Brick Building Dimensions: Internal Plan
- 3.4 Concrete Framed Building Dimensions - Braced Frame
- 3.5 Concrete Framed Building Dimensions - Moment Resisting Frame: General Arrangement - Sections
- 3.6 Concrete Framed Building Dimensions - Moment Resisting Frame: General Arrangement - Plans
- 4.1 Comparison of Glazing Fragment Velocity Calculations
- 4.2 Comparison of Baker Prediction against Experimental Data
- 4.3 Curve Fit to Mass Distribution Data
- 4.4 Methodology for Calculation of Fatality Probability due to Glazing Fragment Impact
- 4.5 Glazing Fatality Curves
- 4.6 Brick Fragment Velocities

- 4.7 Glass Window Fragment Velocities
- 4.8 Fatalities Range for Brickwork (Shock Pulse)
  
- 5.1 Methodology for Global Building Fatality Probability Calculation
- 5.2 Fatality Probability Curve: Brick Building, Short Side Facing, Shock Pulse
- 5.3 Fatality Probability Curve: Brick Building, Long Side Facing, Shock Pulse
- 5.4 Fatality Probability Curve: Brick Building, Short Side Facing, Pressure Pulse
- 5.5 Fatality Probability Curve: Brick Building, Long Side Facing, Pressure Pulse
- 5.6 Fatality Probability Curve: Concrete Building, Short Side Facing, Shock Pulse
- 5.7 Fatality Probability Curve: Concrete Building, Long Side Facing, Shock Pulse
- 5.8 Fatality Probability Curve: Concrete Building, Short Side Facing, Pressure Pulse
- 5.9 Fatality Probability Curve: Concrete Building, Long Side Facing, Pressure Pulse
- 5.10 Comparison of Brick Fatality Probability Curves against Other Models

# 1 INTRODUCTION

The overall objective of this project is to develop a procedure for assessing the fatality probability of occupants of different types of buildings subject to overpressures produced from vapour cloud explosions. This requires the failure sequence of a building subject to increasing blast loads to be determined and the effect on people within the building of either debris generated by the blast load striking them or partial/total collapse of the load bearing structure, to be determined.

This report presents the conclusions from Phases 2 and 3 of the project. Phase 1 is described in the first report of this series and summarised below. The objectives of Phases 2 and 3 are also outlined below.

## 1.1 Summary of Phase 1

Phase 1 involved assessing the general procedure to be used to obtain fatality probability functions for particular buildings and determining the individual functions for glazing failure, cladding failure and building collapse. As such, it included a comprehensive literature search. The search for useful information has been an ongoing part of the project.

The general procedure to be used was reviewed and developed in Phase 1, and is summarised in Figure 1.1. Factors considered included:

- **Building types**

Generic building types were considered, in particular concentrating on types typical of urban residential and commercial areas, with potential high occupancy. Housing, offices, retail and leisure developments, schools and hospitals were all considered in order to identify a range of generic building types and geometries.

- **Pressure loads**

Maximum overpressures, pulse shapes and durations were considered to identify those of most relevance to a vapour cloud explosion scenario.

- **Structural loads**

The structural loads generated by the incident overpressure were considered.

- **Dynamic response**

The response of the building to the dynamic input was considered using a non-linear single degree of freedom elasto-plastic model to predict maximum displacements under prescribed pressure loads.

- **Structural capacity**

The capacities of various structural components under dynamic loading were calculated and compared against historical and experimental data where available.

- **Fatality Probability**

Finally, considering the overall building response and the failure capacities of various components, the probability of fatality of the building occupants was assessed, based on the effects of the individual components such as glazing and cladding together with building collapse.

## 1.2 Objectives of Phases 2 and 3

Having derived the general procedure in Phase 1, Phases 2 and 3 involved assessing the sensitivity of the response of the structure and the corresponding occupant fatality probability to the loading and structural models. The aim was to examine the importance of different aspects of the loading and structural characteristics.

In particular, the following areas were studied:

- the effects of the shape of the pressure pulse on the overall structural response of the building, using representative building sizes.
- the effects of pressure relief due to failure of the windows and wall cladding on the overall response of the building.
- the effects of pressure load on the rear of the buildings.
- the effects of the negative phase of the blast pulse on the global response of the building and its importance for the assessment of occupant fatality probability.
- the structural characteristics of particular generic building types using historical, experimental and analytical data. The differences between the various approaches were reviewed, considering the possible effect of infill wall, etc.

- how the predictions of the model compared against others in the literature, based on historical data.
- the likelihood of fatality as a result of impact by glass and other debris was examined in more detail.

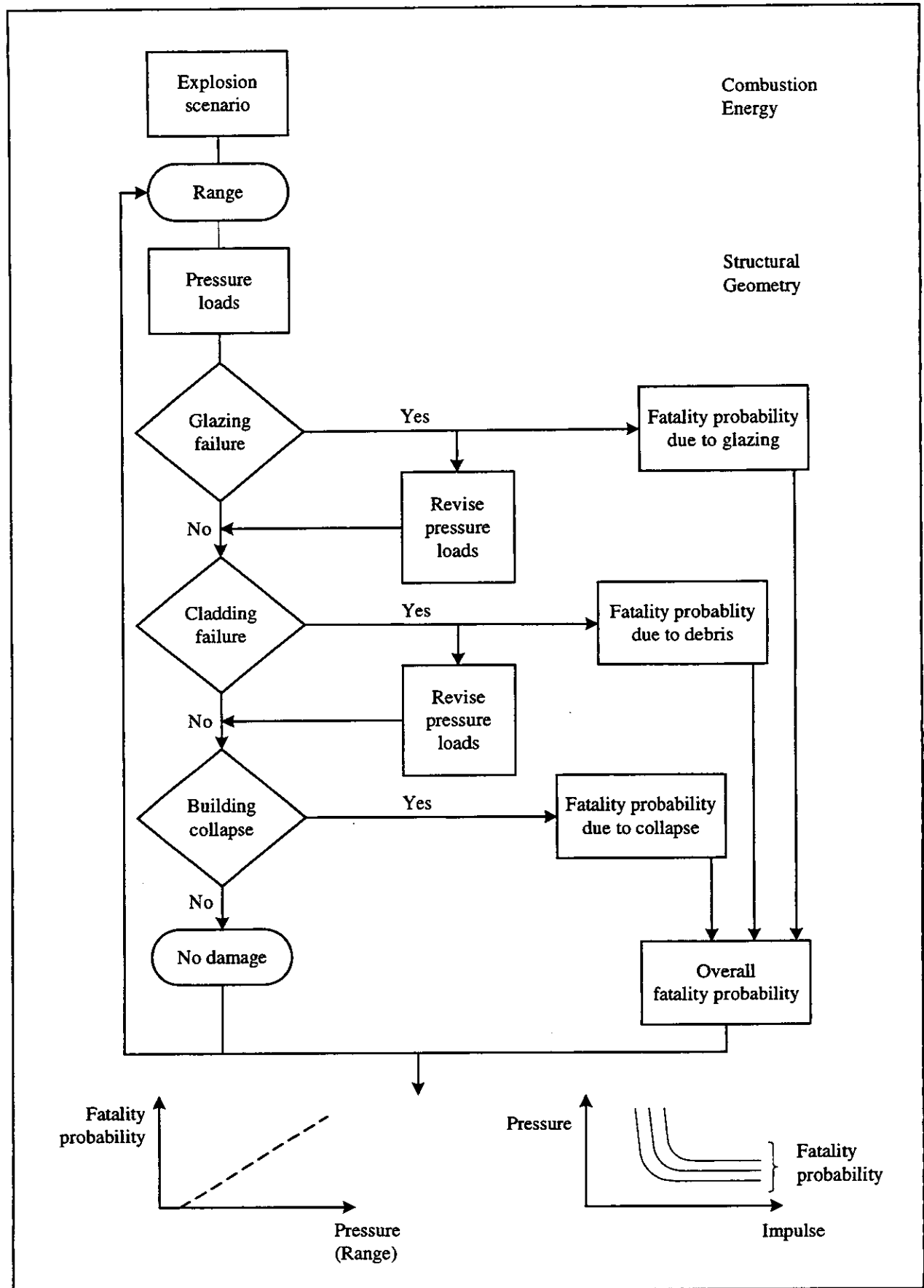


Figure 1.1 General Procedure

## 2 PRESSURE PROFILE AND LOADING EFFECTS

The procedure for deriving fatality probabilities is dependent on a number of factors which cannot be defined exactly, but may be subject to considerable variation. In addition, within the limited scope of this project, several assumptions have to be made which may or may not affect the results. The purpose of this section is to investigate some of these assumptions and determine whether they significantly affect the derived building response and hence the fatality probability.

Four factors have been concentrated on in this section. These are the effects of different rise times, the negative phase, glazing/cladding failure and rear face pressure load. The building chosen as a basis for these calculations is a brick-built house, of dimensions 14m wide x 8.6m long and 8m maximum height.

### 2.1 Rise time

In Phase 1, it was indicated that two pressure profiles would be used, namely the shock wave (zero rise time, decay over the pulse duration  $t_p$ ) and the pressure wave (rise time = decay time =  $t_p/2$ ). For a vapour cloud explosion, the pressure wave relates to locations close to the source and the shock wave to those locations far from the source, although at intermediate distances the wave shape is some combination of the two. Puttock [7] proposes a means of predicting pulse shape at a distance from the source of an explosion, based on experimental results. This defines pulse shape in terms of the ratio of rise time to overall duration i.e. zero for a shock wave and 0.5 for the pressure wave described above. As the pulse travels away from the source, he suggests a shape factor (SF) based on a linear decay with distance, i.e.

$$\frac{\text{rise time}}{\text{pulse duration}} = \max(0.65(1 - 1.25d_f), 0)$$

where  $d_f$  is a distance factor related to the source radius, the peak pressure and the distance from the centre of the explosion. This implies that the pulse is always triangular, as shown on Figure 2.1.

By comparison, the TNO literature [8], suggests that partial shocking-up of the pulse occurs with distance from the source, as shown schematically in Figure 2.2. This is generally accepted to be the case, but the amount of 'partial shocking' i.e. the intercept of the pulse with the pressure axis, cannot at present be quantified. The method given by Puttock gives an approximation to this partially shocked shape.

This difference has implications for our work. In particular, the response of a structure to a blast wave depends on the extent to which the pulse is reflected from the front face. For a shock pulse, the perpendicular reflected pressure can be easily calculated from the equation:

$$P_r = 2P_s + \frac{(\gamma + 1)P_s^2}{(\gamma - 1)P_s + 2\gamma P_o}$$

where  $\gamma$  is the ratio of specific heats at constant pressure and constant volume ( $\sim 1.4$  for air),  $P_s$  is the peak incident overpressure and  $P_o$  is atmospheric pressure. For a pressure pulse, the TNO document [8] indicates that the combined effect of the progressive pressure build up and the rarefaction wave caused by the disturbance of the incident wave by the building is such that the resulting pressure on the surface will not be higher than the incident overpressure plus the dynamic pressure. For an intermediate pulse shape, appropriate reflection factors cannot be calculated unless the shape can be quantified. At present, this is not possible, as outlined above. Consequently, we have concentrated on the two simple pulse shapes, shock wave and pressure wave.

In order to make a comparison of the different effects of the two pulse shapes, we have modelled the effect of pulses of constant impulse ( $2500\text{Ns/m}^2$ ), but varying peak incident overpressures and durations, upon a brick building with representative dimensions as given above. For these calculations, it has been assumed that there is no pressure relief due to glazing or cladding failure, and no pressure on the rear face. The maximum deflection of the building has been calculated using a single degree of freedom non-linear elasto-plastic model, as described in the report on Phase 1. The results of these calculations are shown on Figure 2.3.

It is clear from the graph that the response to the shock pulse is much greater than the response to the pressure pulse. This is principally due to reflection at the front face which has been considered for the shock pulse but not for the pressure pulse, as explained above. However, the reflection factors can be calculated and the dotted line on the graph shows the response to the shock without taking reflection into account. As can be seen, the response to the shock without the reflection is similar to the response to the pressure pulse: at low pressures the response to the shock slightly exceeds the response to the pressure pulse, but at high pressures, the reverse is true, with the cross-over point at  $\sim 260$  mbar. This is in line with the expected behaviour; graphical solutions for the maximum response of a single degree of freedom non-linear elasto-plastic system subject to different pulse shapes are calculated in Biggs [2] and are reproduced widely in the literature [8,1]. From the graphs, for a pulse duration much higher than the natural period, the response predicted by using the graphs is higher for a shock pulse than for a pressure pulse. In this case the loading is quasistatic, and it has been shown that preserving the rise time is very important in modelling the blast pulse in this regime [25]. Conversely, when the pulse duration is much lower than the natural period of the structure, the effect of the rise time is much less, and it is accurate representation of the impulse which is important [25]. In this case, very little difference would be expected between the response to a shock pulse and a pressure pulse if both have the same peak incident overpressure and duration and reflection effects are



ignored. In our calculations, the natural period of the building is  $\sim 0.192\text{s}$ , and for a pulse duration of  $0.192\text{s}$ , the corresponding pressure (for an impulse of  $2500\text{Ns/m}^2$ ) is  $\sim 260\text{mbar}$ . Below this value, the pulse duration is higher than the natural period, and the shock pulse produces a higher response, as expected. The difference in response is large in terms of the percentage difference between the two pulse shapes, but in absolute terms is small, owing to the low value of maximum incident overpressure. Above this value, the converse is true, and the response for both shock and pressure pulses is very similar. This confirms that our model is behaving as expected.

A marked change in gradient can also be seen on the curves at about  $150\text{ mbar}$  for the shock curve (including reflection) and at a slightly higher pressure for the other curves. This marks the onset of plastic behaviour, and shows that some degree of plasticity is to be expected even at fairly low pressures.

The main conclusion from this comparison is that in the absence of experimental data relating to the reflection of partially shocked and pressure pulses, the most conservative assumption for a given pressure and duration is to use a shock pulse and assume that normal front face reflection occurs. This is the case for all distances where the pulse shape is uncertain.

## **2.2 Negative phase**

A full description of the pulse shape would include a phase following the positive phase, in which the pressure falls below ambient and slowly returns to the ambient value. This 'negative phase' is generally ignored in blast calculations, as it tends to have a much smaller magnitude, and the majority of the damaging effects are assumed to occur in the positive phase. The effects of this phase on the overall building response have been calculated here in order to test the validity of this assumption.

For the purposes of these calculations, displacement of the structure in a direction parallel to the direction of travel of the blast wave is referred to as 'positive displacement'. If displacement occurs in the opposite direction, i.e. towards the source of the blast, it is referred to as 'negative displacement'.

### **2.2.1 Brick building response**

Due to the fact that the negative phase tends not to be considered, there is very little in the literature to aid quantification of its magnitude and duration for vapour cloud explosions. Consequently, a representative pulse shape has been selected somewhat arbitrarily for the purposes of these calculations. The peak negative pressure has been chosen to be  $-0.5$  times the peak side-on positive pressure, and the negative phase duration has been chosen as  $3$  times the positive phase duration. This is a fairly large value for the peak negative pressure, and values inferred from plots of pressure against time in the literature are generally smaller than this [7]. However, for the purposes of

these calculations, it is necessary to ensure that any effects are clearly observable, so it is useful to choose a high value. The time taken for the pressure to reach its peak negative value has been based on the rate of pressure drop in the positive phase - i.e. the gradient has been maintained. A schematic view of the pressure pulse is shown in Figure 2.4: for a peak incident overpressure of 500mbar and duration of 0.1s, the corresponding negative phase consists of -250mbar peak pressure and a duration of 0.3s.

The building response has been assessed for the representative brick building using a pulse range similar to that described in Section 2.1, but including the appropriate negative phase. Calculations have been performed for both a pressure pulse and a shock pulse, initially ignoring the effects of rear face pressure and internal pressure. If the negative phase is not included, the response rises to a maximum and oscillates about a constant value (Figure 2.5(a)). By comparison, when the negative phase is included, the building response rises to a peak, but then drops as the negative phase passes and oscillates about a much lower constant value (Figure 2.5(b)). This is corroborated for a range of pressures in Figure 2.6. The figure shows the peak building response at a range of pressures from 0 to 1000 mbar (positive phase pulse duration varies in order to keep the incident positive phase impulse constant at  $2500 \text{ Ns/m}^2$ ) for a shock pulse and a pressure pulse, both including and ignoring the negative phase. As can be seen, the results including the negative phase are consistently lower than the results without the negative phase, the difference increasing with increasing pressure.

These results would suggest that it is conservative to ignore the negative phase of the pulse in this case. A consideration of the loads on the structure however reveals that in some cases this may not always be the most conservative approach: if the time taken for the pressure to reach a peak on the rear face of the building is comparable with the time taken for the negative pressure on the front face to reach its maximum (negative) value, then the resultant negative force on the building may be greater than the initial positive peak force, in which case a greater displacement may result. This is shown in Figure 2.7, in which the results of calculations repeated including the effects of rear face pressure are presented. The peak displacements are very similar, whether or not the negative phase is included, up to a pressure of 800mbar at which point the results start to diverge. At low pressures, the duration of the pulse (chosen to keep the incident impulse constant) is fairly long, so that the negative phase at the front face happens after the rear face load has reached a peak, and the two effects occur effectively independently. At high pressures, however, the pulse duration is very short (62.5ms), and correspondingly the negative phase acts to reinforce the overall negative force on the building. For the shock pulse, this acts to reduce the peak displacement, as the overall positive force is still much greater than the negative force due to the reflection of the incident pulse. For the pressure pulse, at the higher pressures, the resulting negative force from the two combined effects is greater than the positive force; this results in a greater peak displacement in the opposite direction. It should be noted,

however, that this is a theoretical calculation, in which it is assumed that there is no cladding failure and where the magnitude of the negative phase has been exaggerated. In practice, a greater movement in the negative direction will not occur, as at higher pressures glazing and/or cladding will fail under the positive phase pressure and will relieve the subsequent negative force on the building.

### 2.2.2 Variation with aspect ratio

In order to investigate whether the results observed in Section 2.2.1 above are dependent on the aspect ratio selected, a 500mbar peak incident overpressure, 100ms positive phase duration pulse was applied to a building of varying aspect ratio. As in the calculations described above, it has been assumed that there is no glazing and/or cladding failure under this incident load: this is an unrealistic assumption at this pressure, particularly for an incident shock pulse for which the peak reflected pressure will be of the order of 1000 mbar, but it is useful to use a high value of pressure to ensure that any effects are observable. The peak negative pressure of the pulse has again been assumed to be -0.5 times the peak side-on positive pressure, and the negative phase duration has been chosen as 3 times the positive phase duration. As the aspect ratio, B/L, of the building increases where B is the maximum breadth of the building and L is its length, the following parameters of the calculation change:

- The natural frequency increases, and correspondingly the natural period, T, decreases. This implies that for a load duration of  $t_p$  the loading changes from impulsive ( $t_p/T < 0.4$ ) through dynamic ( $0.4 < t_p/T < 2.0$ ) to quasistatic ( $t_p/T > 2.0$ ).
- The building dimension S, increases. S is equal to the lesser of B/2 or H, and relates to the shortest distance that the pulse can travel to reach the rear face. S thus increases until  $2B > H$ , after which time it is constant.
- As S increases, so the time for the pulse to reach a peak at the rear face increases.
- As S increases, for a shock pulse, the time taken for the front face pressure to reduce from the peak reflected value to the incident + dynamic value increases. Thus the impulse at the front face increases with S.
- The building stiffness (K) increases, in proportion to  $B^2$ . Correspondingly, the elastic limit for the building, which is assumed to be proportional to B/K, decreases in proportion to 1/B.

The combination of these features results in the curves shown in Figures 2.8(a) - (d), which imply that the negative phase has a varying significance according to the nature of the pulse and the overall building dimensions. When a pulse hits a building, the subsequent motion is dependent primarily on the ratio of the pulse duration to the natural period of the building (see Phase 1 report). For an

impulsive load without the negative phase included, the building moves first in the positive direction, and then, if the movement has not exceeded the elastic limit, it rebounds to an equal displacement in the negative direction: if there is no damping, this oscillation will continue without any reduction in the peak displacements. The primary effect of including the negative phase is, in this impulsive regime, to reduce the initial positive movement slightly, and to increase the negative rebound slightly, so that the first two peaks in the motion are not quite equal and opposite. Thus in Figure 2.8(a), which shows the results for an incident shock pulse (no rear face pressure included), at an aspect ratio of 0.1, the peak negative displacement is greater than the peak positive displacement when the negative phase is included, whereas they are equal if the negative phase is not included. This imbalance is more significant when the displacements are such that the elastic limit is exceeded. If the initial positive motion does not exceed the limit, but the subsequent rebound does, a much larger negative displacement is observed. This explains the larger increase in the negative displacement than the positive for an aspect ratio of 0.2 in this Figure. Once the initial positive displacement starts to exceed the elastic limit, however, the situation is reversed, and the positive displacement starts to increase at the expense of the negative displacement.

Another feature of Figure 2.8(a) and subsequent figures is that above a certain aspect ratio, the building dimension  $S$  becomes constant. As explained above, this affects the impulse on the front face, and above this point, the impulse is constant. A marked change in the gradient can be observed at this point, i.e. at  $B/L = 2$  in Figure 2.8(a).

The situation is more complex if the effects of rear face pressure are included (Figure 2.8(b)). Firstly, it should be noted that overall displacements are much lower if the rear face pressure is included, with or without the negative phase. This implies that the effect of the force on the rear face is greater than the effect of the negative phase on the front face, which is realistic considering that, using the hypothetical negative phase described above, the peak pressure on the rear face is twice the peak negative pressure at the front face. It should be also noted that for these calculations, the length of the building has been kept constant. The implications of the dimensions chosen are that the load on the rear face always occurs before the negative phase at the front face and the resultant force is effectively a very short positive pulse, followed by a longer, much shallower, negative pulse. This 'reinforcement' of the rear face load by the negative phase at the front face occurs for all aspect ratios if  $L$  is kept constant at the value chosen (8.6m). For a much longer building, this is not the case, and the combined effect of the rear face pressure and the negative phase would be less. For small aspect ratios, the effect of including the negative phase is to increase both the positive and negative displacements. Once plasticity starts to occur, the peak positive displacement is the same whether or not the negative phase is included.

For an incident pressure pulse, the results are different again, although some of the same features can be seen on the plots. Again, if no rear face pressure is included, the peak negative displacement is greater than the peak positive displacement for small aspect ratios, owing to the greater degree of plasticity in the negative direction. In this case, the impulse does not increase with increasing aspect ratio, and the peak positive displacement can be seen to reach a peak at  $B/L = 2.5$ , decreasing thereafter as the aspect ratio increases. This behaviour can be attributed partly to the changing stiffness and natural frequency of the building with the changes in aspect ratio, although this does not explain why the decrease is seen for a pressure pulse but not for a shock pulse. This latter observation is due to the rise time of the pulse: Table 4.5 in the Report on Phase 1 indicates that in the dynamic and quasistatic regime, preserving the rise time of the pulse is important in determining the response of the structure, as the ratio of the rise time to the natural period of the structure determines how quickly the structure responds to the pulse. This can be explained further by using the figures provided in Biggs [2] for the maximum response of elasto-plastic single degree of freedom systems subject to different pulse shapes. For a shock pulse, as the ratio of pulse duration to natural period,  $t_p/T$ , increases, the time to respond decreases, and the maximum displacement increases: conversely, for a pressure pulse, above a value of 2 for  $t_p/T$ , the time to respond and the maximum displacement remain essentially constant as  $t_p/T$  increases. For the structure considered here, an increase in aspect ratio causes the natural period,  $T$ , of the structure to decrease, and hence for a constant pulse duration,  $t_p$ ,  $t_p/T$  increases. Thus an increase in response with increasing aspect ratio would be expected for a shock pulse, and a constant value would be expected for a pressure pulse. However, another feature of the increasing aspect ratio is an increase in stiffness of the structure. This tends to decrease the predicted displacements, according to the equation  $x = F/k$ , where  $x$  is the displacement,  $F$  is the force and  $k$  is the stiffness. The combination of the two effects, decreasing natural period and increasing stiffness, results in a decreasing response with aspect ratio for a pressure pulse in the dynamic and quasistatic regimes, but a constant response for an incident shock pulse.

With the rear face pressure included (Figure 2.8(d)), the situation is again more complex. The peak positive displacement shows similar behaviour to that shown in Figure 2.8(c), again at a smaller absolute value, reflecting the increased negative force on the structure. The exception is the behaviour at an aspect ratio of 0.4 - 0.5, where a big drop in the peak positive displacement can be seen if the negative phase is included. This drop is due to the interaction between plasticity occurring for motion in the negative direction and plasticity occurring for displacement in the positive direction: since the peak negative displacement up to this point is slightly greater than the peak positive displacement, plasticity occurs first in the negative direction, and a drop in the peak positive displacement is observed. As for the shock pulse, however, once plasticity occurs for positive motion, the results are similar whether the negative phase is included or not, primarily because the rear face load occurs

before the negative phase at the front face. The peak negative displacement shows similar behaviour to the peak positive displacement, in that it is dominated by the  $t_p/T$  relationship and the building stiffness, although including the negative phase appears to make a much bigger difference in this case.

Clearly, the effect of inclusion of the negative phase on predicted response depends on the pulse characteristics and the overall building dimensions. The complex nature of the response means that it is difficult to predict whether it is more or less conservative to include the negative phase. In addition, there remains the problem of how to characterise the negative phase in a realistic manner. It should be noted that while this calculation predicts larger negative displacements than positive for some values of aspect ratio, in practice this will not be observed, as at the pressure chosen here, a substantial amount of glazing/cladding failure will occur, giving rise to a certain amount of pressure relief on the structure. Equally, at pressures low enough for the glazing or cladding to remain intact, the cause of the larger negative displacements, i.e. plasticity for motion in the negative direction, will not occur, as the movements will not be large enough to exceed the elastic limit of the structure. In addition, these calculations show that the pressure on the rear face of the building is far more significant than the negative phase pressure, and results in a much greater decrease in overall response.

It may also be concluded that for an incident shock pulse, for aspect ratios greater than 1, it is conservative to ignore the part the negative phase plays in the overall building response, but for smaller aspect ratios, and for an incident pressure pulse, it may be advisable to include it and to consider both the peak positive and the peak negative displacements. However, as outlined above, it is equally important to include realistic assessment of glazing and cladding failure, and it is probable that the greater negative displacements will disappear for a more realistic structural assessment. The inclusion of rear face pressure load in the calculations has been shown to cause a greater drop in structural response than inclusion of the negative phase alone, and it may be that the calculations without the negative phase included are sufficiently representative of the actual structural behaviour that including the negative phase will not add any benefit.

### **2.2.3 Local effects**

In addition to the effect of the negative phase on the global response of the building, it is of interest to consider the effects of negative pressures, i.e. suction, on the individual components of the structure. For example, design positive and negative pressures on structural components due to wind loading can be assessed using the design code CP3 (or the more recent design code BS 6399 [23]). For a typical building, equally permeable to the wind on all four sides, design pressures for different areas of the UK are presented in Table 2.1.

	London Windspeed 38 m/s	Manchester Windspeed 45 m/s	Londonderry Windspeed 52 m/s
Height of Building = 10m			
Peak Positive Pressure	885 Pa	1241 Pa	1658 Pa
Peak Negative Pressure (global i.e. remote from regions of high local turbulence)	-177 Pa	-248 Pa	-332 Pa
Peak Negative Pressure (local to regions of high turbulence)	-797 Pa	-1117 Pa	-1492 Pa
Height of Building = 50m			
Peak Positive Pressure	1171 Pa	1642 Pa	2192 Pa
Peak Negative Pressure (global i.e. remote from regions of high local turbulence)	-234 Pa	-328 Pa	-438 Pa
Peak Negative Pressure (local to regions of high turbulence)	-1054 Pa	-1478 Pa	-1972 Pa

**Table 2.1:**

**Typical design positive and negative pressures**

As can be seen from the table, the peak positive pressures are much greater than the peak suction pressures for most of the wall area. The exception to this is in local areas near to the corners of the wall which experience higher local suction pressures, particularly if other buildings are close by, funnelling wind down the sides of the building. This illustrates the fact that window and cladding fixings tend to be designed for greater wind loads directed into the building than outwards, and hence fixings tend to be stronger in one direction. This may have implications for the internal pressure in the building and the building occupant fatality probability calculations if the negative phase of the blast pulse is included, as the cladding fixings may fail under the negative load even if they don't fail under the initial positive load. The implications for

occupant fatality probability are small, however, as if cladding or glazing fails under the suction pressures it will fall out of the building and will not present a hazard to people inside the building (although it may present a hazard to people outside the building).

### 2.3 Pressure relief due to glazing/cladding failure

The same typical building has been used to investigate the effects of glazing/cladding failure on the overall building response, and the building response as a function of open front face area to volume ratio,  $A/V$ , has been plotted in Figure 2.9. Five different pulse shapes have been used, including:

- Shock Pulse, 500mbar peak incident overpressure, 0.1s duration (SF = rise time/duration = 0);
- Shock Pulse, 400mbar peak incident overpressure, 0.125s duration (i.e. the same overall incident impulse) (SF = 0);
- Pressure Pulse, 500mbar peak incident overpressure, 0.1s duration (SF = 0.5);
- Pressure Pulse, 400mbar peak incident overpressure, 0.125s duration (SF = 0.5); and
- Pressure Pulse with SF = 0.65. This corresponds to a location very close to the source (Puttock, 1995). The peak incident overpressure was 500mbar and total duration 0.1s.

For the shock pulses, it has been assumed that normal reflection occurs at the front face, with the reflected pressure reducing in time to the incident value plus the dynamic pressure, whereas for the pressure pulses and the longer rise time pressure pulse, no reflection has been assumed but the dynamic pressure has been included.

The method for calculating pressure relief due to glazing failure has been described in detail in the report on Phase 1. If the glazing fails the pressure rises within the building, which means that the differential pressure across the walls is lower, reducing the load on the walls. The rate of pressure rise is dependent on the pressure differential across the opening, the area of the opening and the volume of the building.

In performing these calculations, several simplifying assumptions have been made concerning the geometry and other characteristics of the building. In particular, it has been assumed that all glazing/cladding fails at the same overpressure (50mbar), that there are no internal obstructions so that the average pressure increases uniformly throughout the structure and that glazing failure occurs only on the front face. This final assumption means that the



maximum possible open vent area to volume ratio occurs when the front face is fully open and has a numerical value of 0.116 /m. The resultant force on the building is then calculated as shown in Figure 2.10 (Eqn 2) from the resultant of the force on the front face ( $P_o(A-A_g)$ ) plus the net resultant internal force due to the imbalance of areas on the front and rear faces ( $-P_i(A-A_g) + P_iA = +P_iA_g$ ).

Figure 2.9 shows that the response is lower for higher vent areas, but that the glazing makes a much greater difference when the pulse is a shock pulse, Figure 2.9(b) showing the progressively greater effect as the pulse 'shocks up'. There are several reasons for this. At a low open vent area to volume ratio, the response is primarily due to the external pulse and there is very little pressure rise within the building. In this case, the response to the shock pulse is higher due to the reflection of the shock at the front face. At a high open vent area to volume ratio, although the reflection still occurs, there is less frontal area for it to act upon to produce any force, so there is less difference between the response to the different pulse shapes. The reflection also affects the response to the different shock pulses, as although the incident impulses are the same for the two shock pulses, the loads experienced by the building are different as the reflected pressures are different. Similarly for the pressure pulses, the dynamic pressure is lower for the pulse with a lower peak overpressure and hence the response is lower.

In addition to the reflection effects, there is also the effect of pressure relief due to glazing failure to be considered. The rate of pressure rise within the building is dependent on the external pressure (Figure 2.11). For a shock pulse, the external pressure is initially very high, decreasing eventually to zero. The initial rate of pressure increase within the building is consequently also very high, decreasing as the pressure differential decreases. The internal pressure will never reach the maximum peak external pressure, as even for very high area to volume ratios, the internal pressure has a finite rise time, (Figure 2.11(a)). If the incident pulse has a lower peak value, the initial response will be slower and, dependent on the duration, the peak value achieved will generally be lower. The resultant force on the building will thus be lower, as both the external and internal pressures are lower. From Figure 2.9, it does not appear that the size of the opening greatly affects the differences in response to the two different shock pulses (i.e. the difference in response is similar across the whole range of  $A/V$ ).

As a pressure pulse has a finite rise time, it is possible for the internal pressure increase to follow more closely the external pulse provided the vent area is big enough (Figure 2.11(b)). This means that the internal pressure on the rear face is closer to the external pressure on the front face for the pressure pulse, so the response is very similar to that which would be achieved if there were no glazing. This is also true for the response to a pulse shape with a shape factor of 0.65, also shown on the figure: there is very little difference between the response at zero vent area and with the front face fully open.

There are several limitations to the method currently used, the principal one being the assumption that the pressure increases uniformly throughout the building and that there is no time difference between peak pressure being reached at the internal front face and the internal rear face. Without using far more complex methods, at present we cannot achieve a more realistic estimate. However, the approach used is generally conservative; using the average internal pressure overestimates the differential pressure across the front face and if there are no internal obstacles to impede the air flow, it may also underestimate the differential pressure across the rear and side walls. Consequently, the net global force on the building is overestimated which has a corresponding effect on the fatality probabilities due to front face glazing and cladding and global building collapse.

It is clear from Figure 2.9 that the open vent area to volume ratio does affect the building response, although more so for a shock pulse than a pressure pulse. The effects of internal pressure are also important for assessment of side and rear wall failure, which is dependent on the pressure differential across the wall. For an incident pressure pulse in particular, where the internal pressure rise may be quite similar to the external pressure, this can significantly reduce the risk of failure and hence reduce the fatality probability of the building occupants.

#### **2.4 Aspect ratio**

As described earlier, varying the aspect ratio of a building has two effects. Firstly, it changes the building mass and stiffness. Secondly, it changes the loading on the building by changing the length of time taken for an incident shock or pressure pulse to reach the rear face of the building. Two approaches have been used to investigate these effects. The first approach was to vary the length of the building, but keep the mass and stiffness constant, and calculate the overall response. The second was simply to vary the length and then calculate the overall response. It has been assumed, for these calculations, that there is no pressure relief due to glazing failure. As for the previous studies, two different pressure pulses were used, including a shock pulse with 500mbar peak incident overpressure and duration of 0.1s, reflected off the front face and a pressure pulse with the same characteristics but no reflection. A pressure pulse with a shape factor of 0.65 with the same characteristics was also considered, but produced very similar results to the pressure pulse with the 0.5 shape factor. The dynamic pressure was included for both the shock and pressure pulses.

The method for calculating the effects of the pressure on the rear face is based on the TNO document [8], but has been modified to take into account the nature of the pulse, and the motion of the pulse along and around the building. The TNO method states that a shock pulse takes a time of  $L/U$  to reach the rear face, and that it takes an additional time of  $4S/U$  for the average pressure on the rear face to reach a peak, but that the average pressure falls to zero at time

$L/U + t_p$  (where  $t_p$  is the pulse duration). It has been assumed that this generally holds true for a shock pulse, but that if the time to reach the peak is greater than the time for the pulse to travel past the rear face, then the peak is never reached but the pressure falls to zero once the pulse has travelled on. This is shown schematically in Figure 2.12(a). The condition for the peak average pressure not to be achieved on the rear face is thus that  $4S/U > t_p$ . Since  $S$  is equal to half the building breadth or the building height, whichever is the smaller, this puts constraints on the building dimensions, beyond which the full effect of pressure on the rear face is not felt.

For a pressure pulse, again it is assumed that the pulse takes a time of  $L/U$  to reach the rear face, but in this case it has been assumed that the time for the average pressure to reach a peak is  $4S/U + t_p/2$ , i.e. it includes the rise time of the pulse itself. Again, the average pressure falls to zero at time  $L/U + t_p$ , but the same cut-off constraint has been imposed (Figure 2.12(b)). In this case, the constraint corresponds to  $4S/U > t_p/2$ , so it is more likely that the peak average pressure will not be achieved for a pressure pulse than for a shock pulse with the same duration.

The results of the assessment are shown in Figure 2.13, in which building response is plotted as a function of the quantity  $L/S$  where  $S=B/2$  i.e.  $L/S$  is twice the aspect ratio.

If the mass and stiffness of the building are kept constant, the response shows a steady increase up to a constant value above a value of  $L/S=7.5$  for the pressure pulse and  $L/S=12.5$  for the shock pulse. For a very long building, the time for the pulse to reach the rear face is very long, and in effect, the building is responding to two pulses - the incident pulse on the front face, followed at some time later by a pressure pulse on the rear face. There is thus no overlap between the two pulses, and effectively no relief given by the rear face pressure. Consequently, for such a long building, the response to the same pulse is the same irrespective of the length. By comparison, for a very short building, the time taken to reach the rear face is very short, so there is considerable overlap in time between forces on the front and rear faces and the resultant net force on the building is much smaller, causing a much smaller overall response. This is true for both the shock and pressure pulses, although for a shock pulse, the front face pressure is much higher than the rear face pressure due to reflection, so the resultant force is always much higher than for an incident pressure pulse, where the front and rear pressures are of similar magnitude (only differing by the dynamic pressure on the front face,  $Q$ ).

If the mass and stiffness of the building are allowed to vary, however, the curves show quite different characteristics. The empirical calculations based on Lees [9] use the height and breadth of a building to calculate the natural period, which means that although as the length changes the mass and stiffness vary, they vary in the same proportion, and the natural frequency does not change. However, as the length increases, the mass and the stiffness both increase, so

a smaller response would be expected for the same input: conversely as the length decreases, a larger response would be expected for the same input. This has to be combined with the fact that as described above, the overlap between the front and rear pressures significantly affects the response. If an extremely short building were considered, such that the time of travel to the rear face was insignificant, for the pressure pulse the net resultant force on the building would be almost zero (the actual value depends on the building dimension,  $S$  (equal to the smaller of  $B/2$  or  $H$ ), and the consequent rise time on the rear face ( $4S/U + t_p/2$ )). Consequently the response is very small at very low values of  $L$ . By comparison, because the front and rear pulse shapes are different for the shock pulse, and reflection is taken into account at the front face, the resultant force is never zero and the response stays correspondingly high at low values of  $L$ . The balance between this overlap effect, and the effect of the changing mass and stiffness results in the curve shapes as shown in the figure.

## 2.5 Conclusions

From this sensitivity study it is clear that the factors affecting the building response are complex. Of primary importance appears to be the shape of the blast pulse: while the pulse shape on its own seems to be of less importance perhaps than some of the other parameters, the amount of reflection or non-reflection makes a big difference to the response of the building. This is clear from both the response to rear face pressure load and the response to glazing failure, in which the increased impulse due to reflection plays an important part. This is not surprising, since in estimating the reflected pressure for the shock pulse, the peak incident overpressure is multiplied by a factor which in most cases exceeds 2, and the corresponding impulse that the building experiences is greatly increased. Clearly the extent to which the pulse is reflected is very important and it would be useful to be able to quantify it for situations other than the perpendicular reflection of a shock pulse (i.e. for partially shocked pressure waves).

The internal pressure rise is also important, but it appears that for a pressure pulse in particular, the effect on the building response is more obvious at low values of the open vent area to volume ratio. The effects of internal pressure are important for assessment of side and rear wall failure, which is dependent on the pressure differential across the wall. For an incident pressure pulse, where the internal pressure rise may be quite similar to the external pressure, this can significantly reduce the risk of failure and hence reduce the fatality probability of the building occupants.

In the calculations performed here, the negative phase of the pulse has been shown in most cases to reduce the peak structural displacement, but to a lesser extent than including the pressure on the rear face of the building. For some combinations of building dimensions, it may be conservative to ignore its effects, but it is difficult to predict when this is the case. In particular, for

small aspect ratios and high pressures, the combination of effects from the negative phase and the pressure on the rear face of the building may give rise to a greater deflection in the negative direction than in the positive direction, although it should be noted that in practice this is unlikely to be observed, as glazing and cladding failure will restrict the load that the structure actually experiences. However, negative pressures may affect those structural components which are designed to resist a larger pressure into the building than outwards, and may cause them to fail, when they would not do so under the positive pressures alone. It is thus generally desirable to include the negative phase of the pulse for the structural calculations, although at present it is not clear how this phase may be accurately characterised.

The effect of loading on the rear of the building is dependent on the building dimensions and has a much more beneficial effect for small buildings than for large ones. This is because of the time taken for the pulse to travel around and past the building; for a small building, the rear face load may significantly oppose the front face load if the time of travel to the rear face is short, whereas for a large building, the load at the front face will generally have finished by the time the load on the rear face starts to increase. For very long buildings (i.e. long compared with the distance over which the pressure decays) it may also be necessary to take into account the fact that the incident overpressure will have decayed significantly by the time the wave reaches the rear face. In addition, for a wide or tall building, the time taken for the pulse to travel along the building may be sufficiently great that the rear face does not experience the maximum average pressure over its full width or height, but only over part of it. In this case, the average pressure on the rear face is reduced. However, this effect, which tends to increase the building response, is outweighed by the increased mass and stiffness of large buildings which tend to reduce the building response.

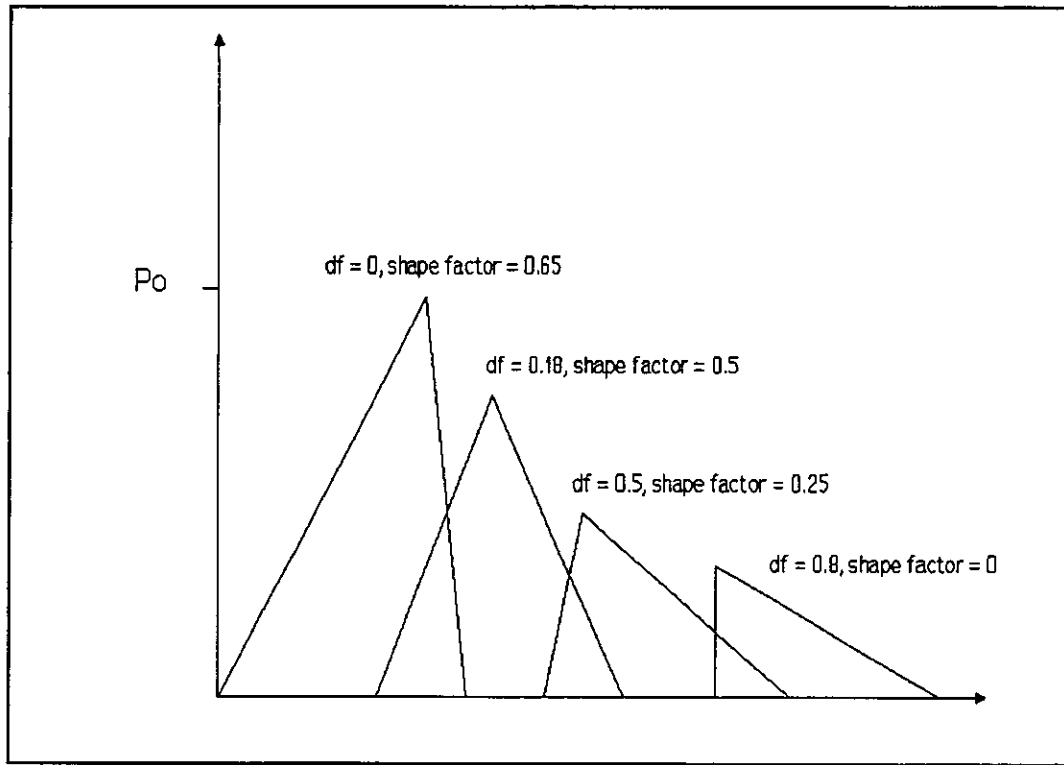


**Figure 2.1: Schematic Progression of Pulse Shape [7]**

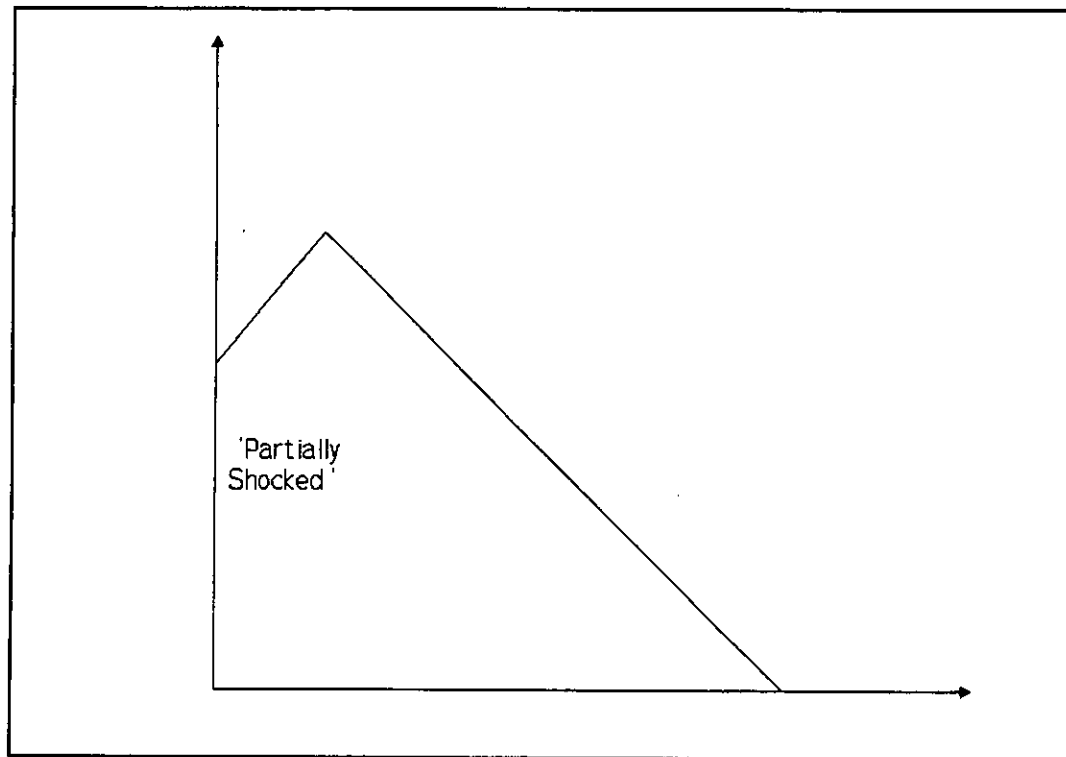


**Figure 2.2 Schematic Diagram of Pulse at an Intermediate Distance [8]**

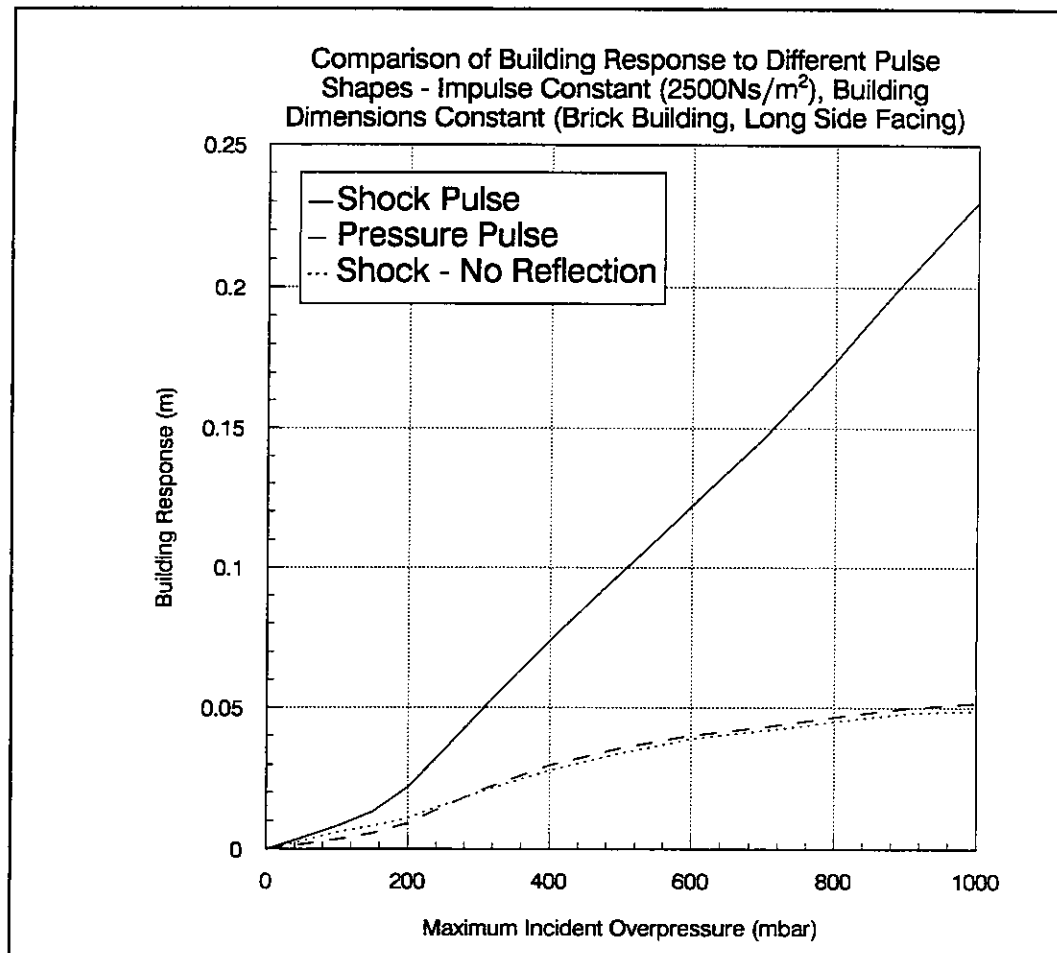


**Figure 2.3 Building Response vs. Pressure for Different Pulse Shapes**

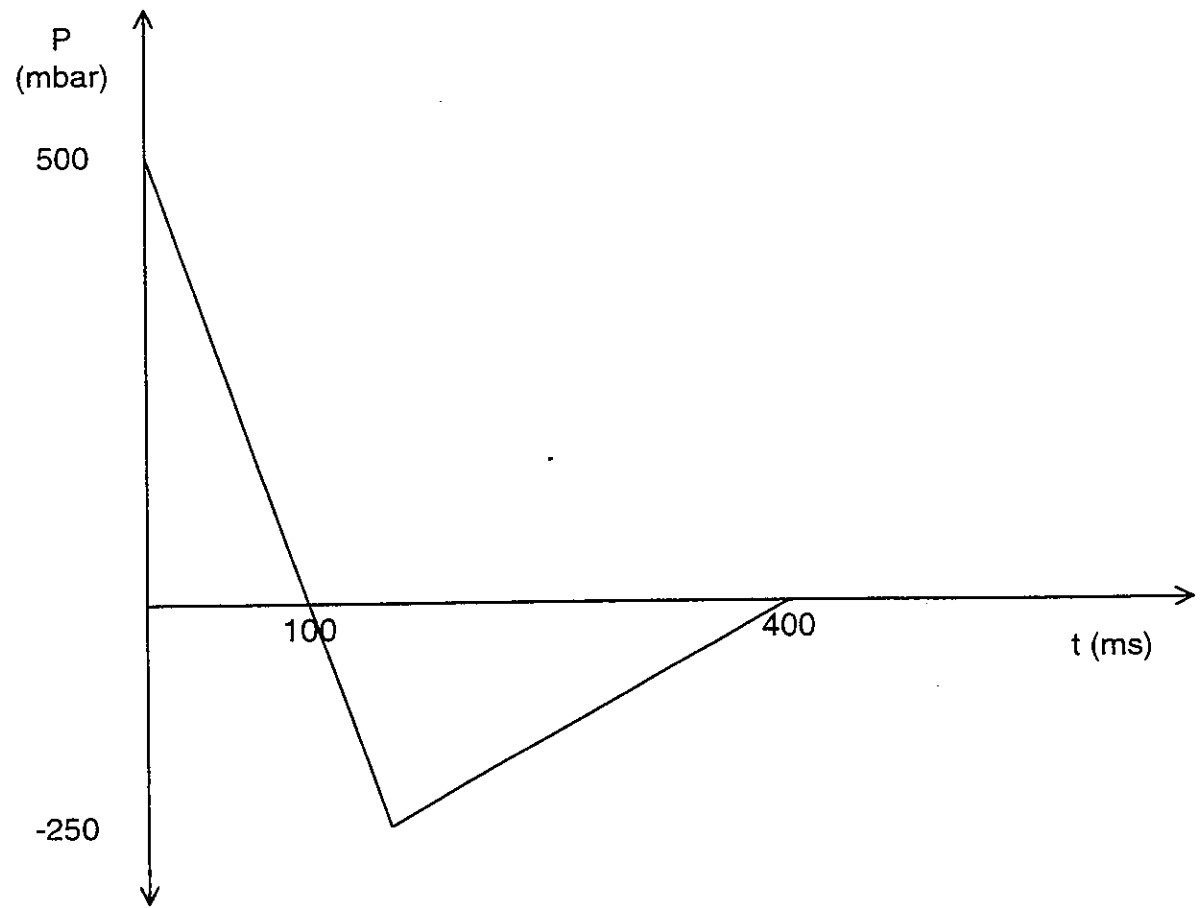


**Figure 2.4: Pulse Shape Including Negative Phase**



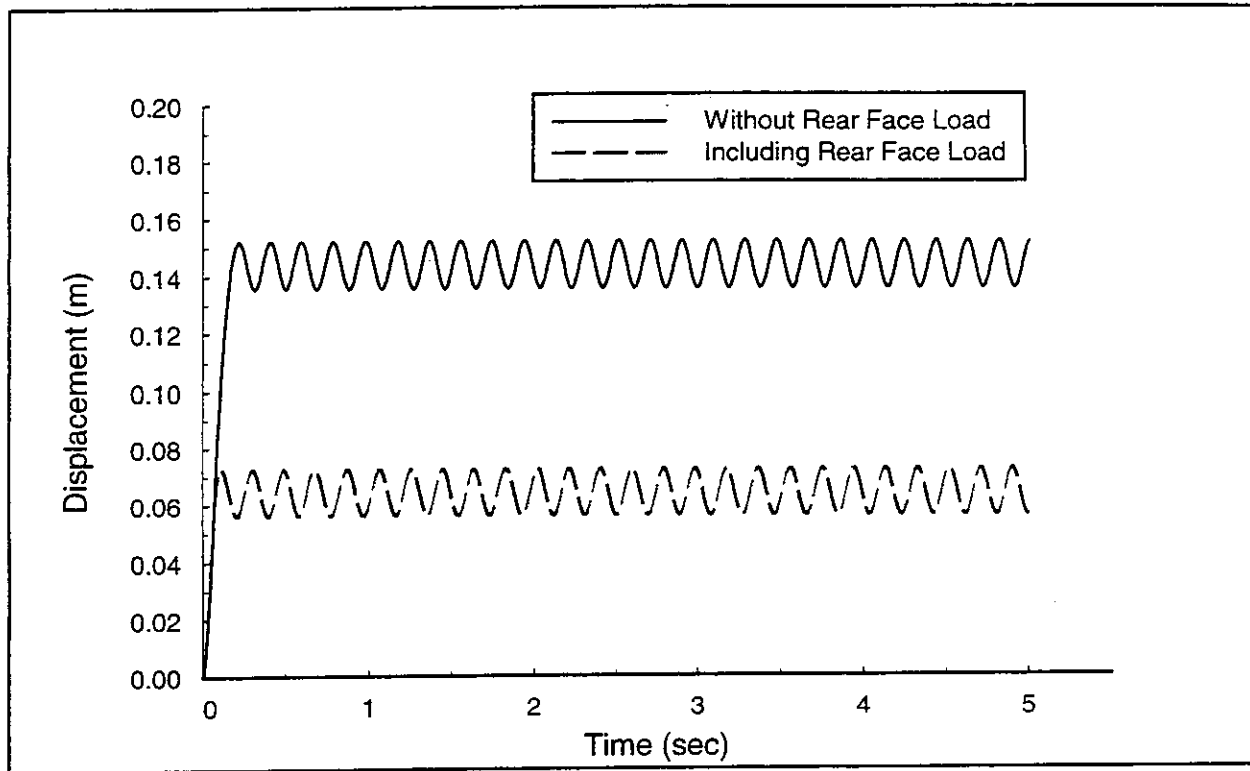


**Figure 2.5(a): Building Response without Negative Phase**

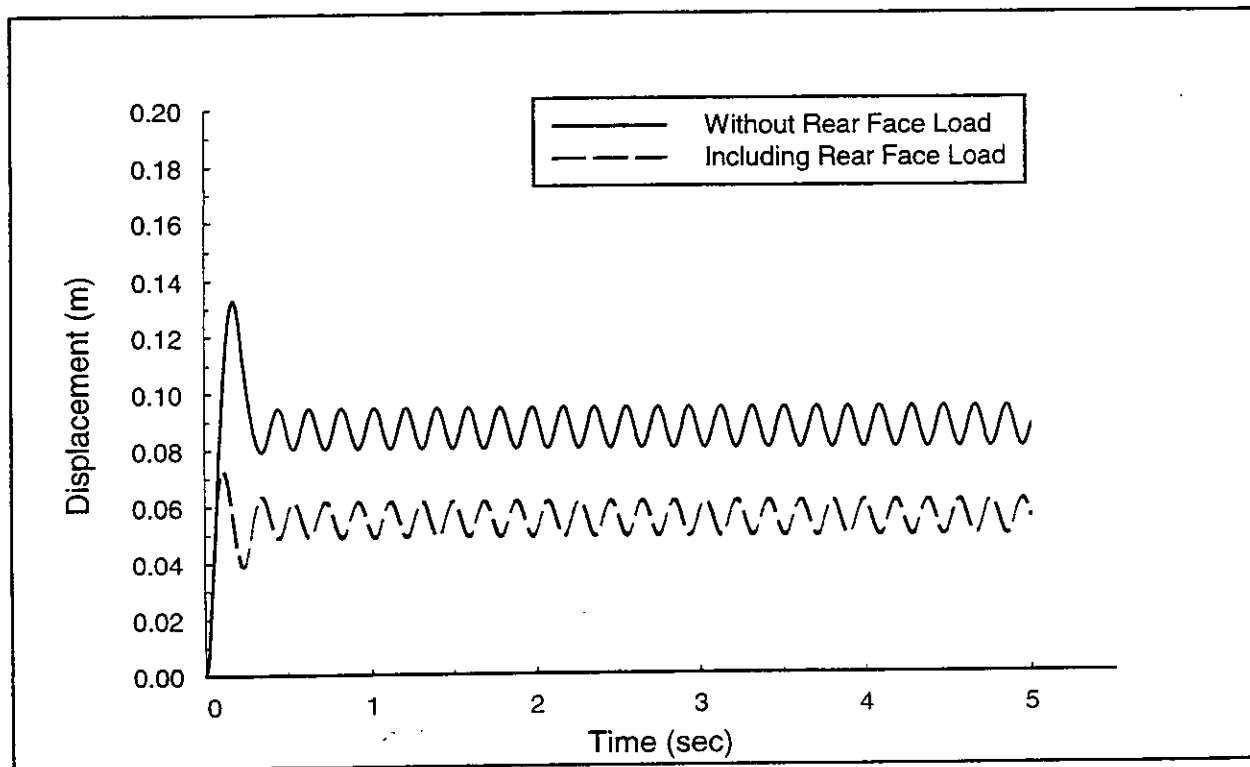


**Figure 2.5(b): Building Response Including Negative Phase**

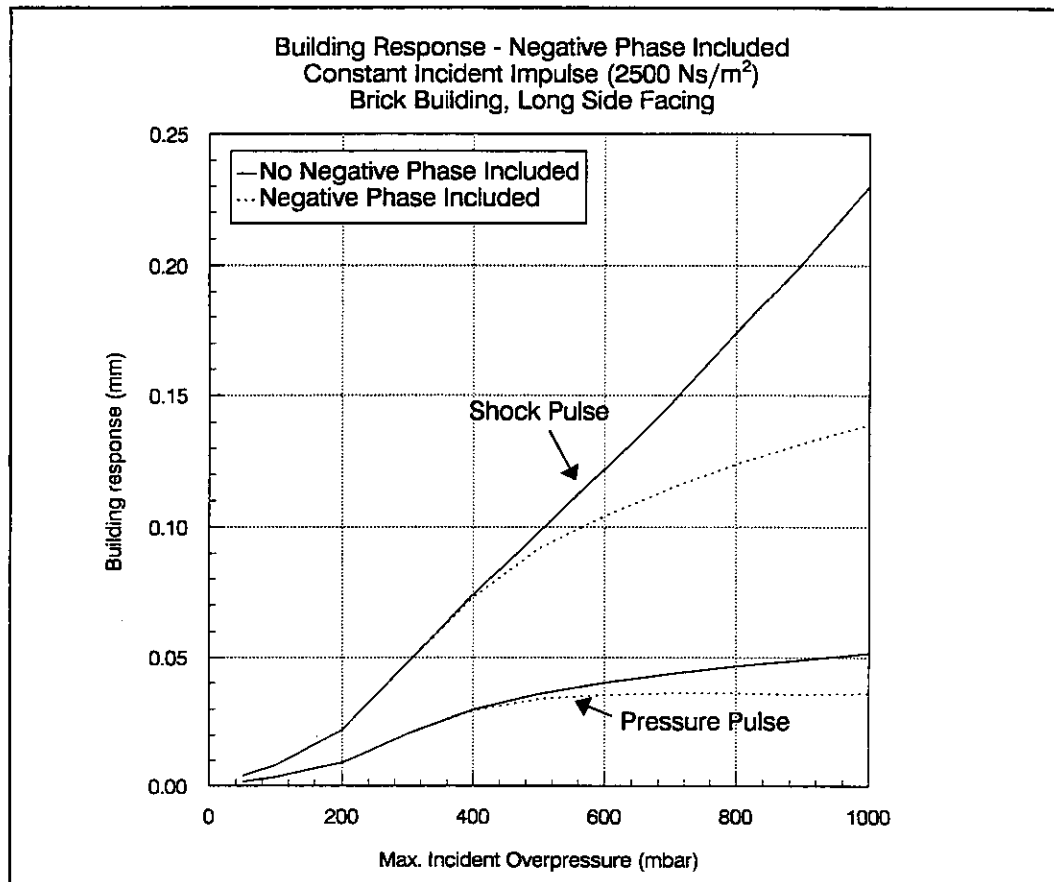


**Figure 2.6 Building Response to Pulse Including Negative Phase  
 No Rear Face Pressure Load**

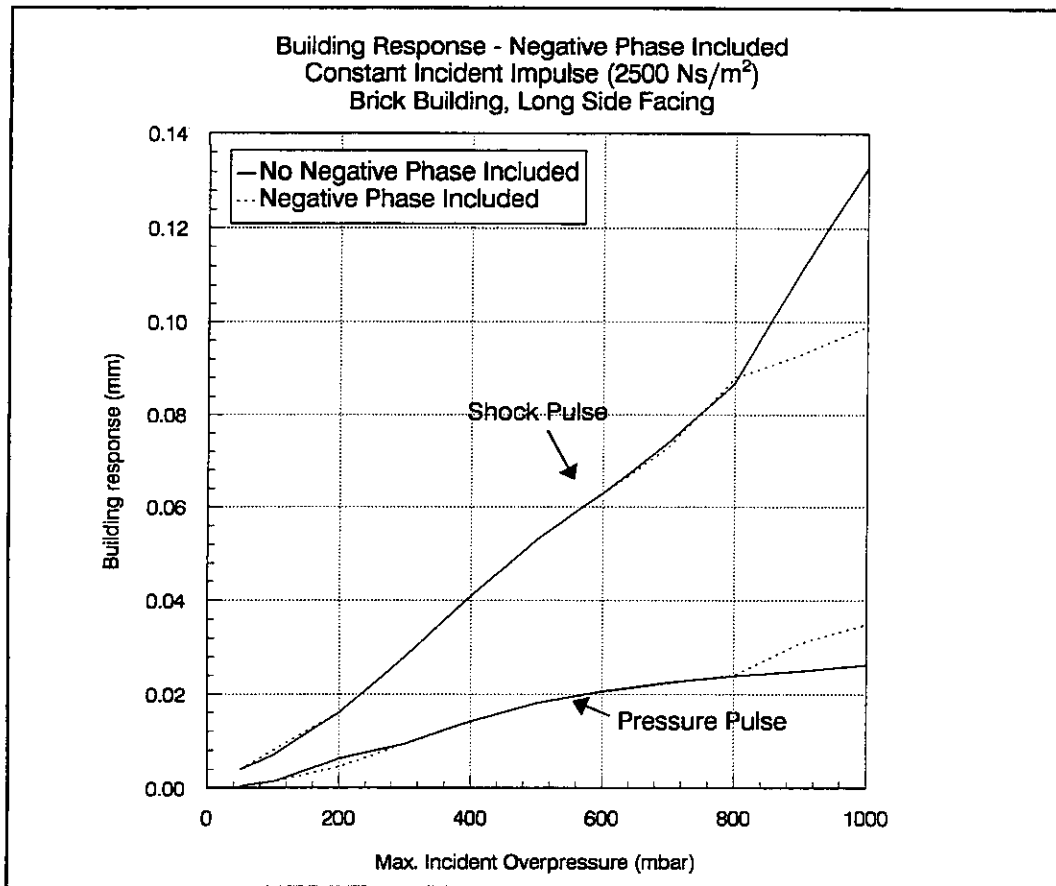
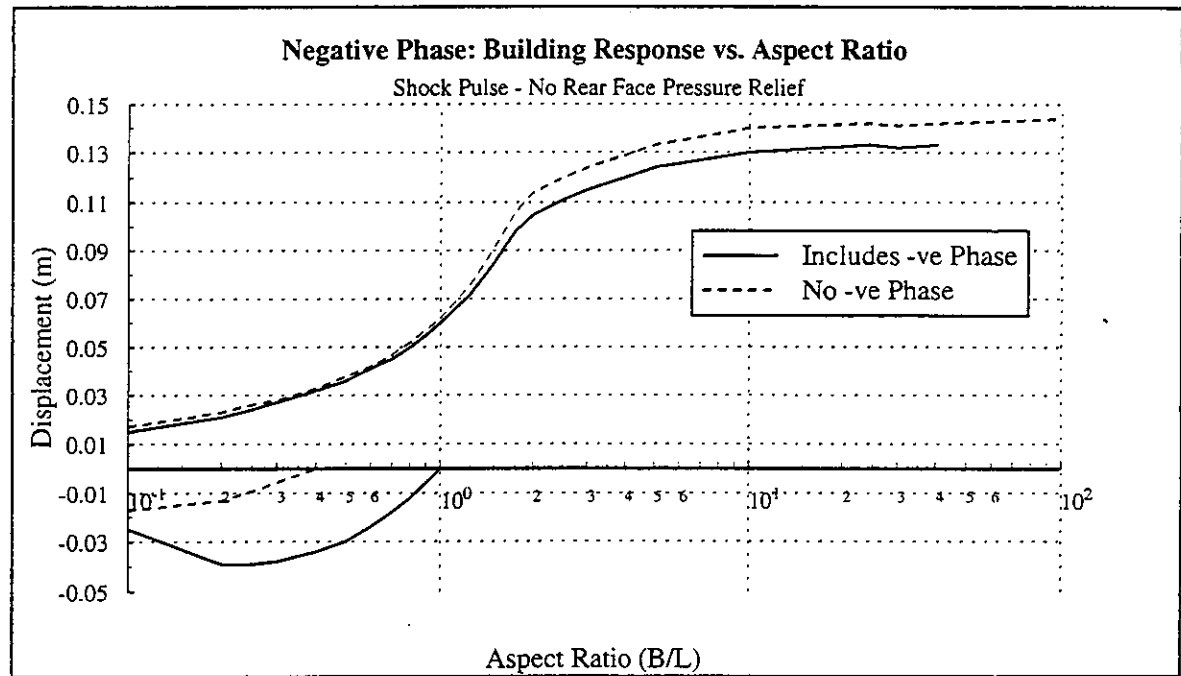
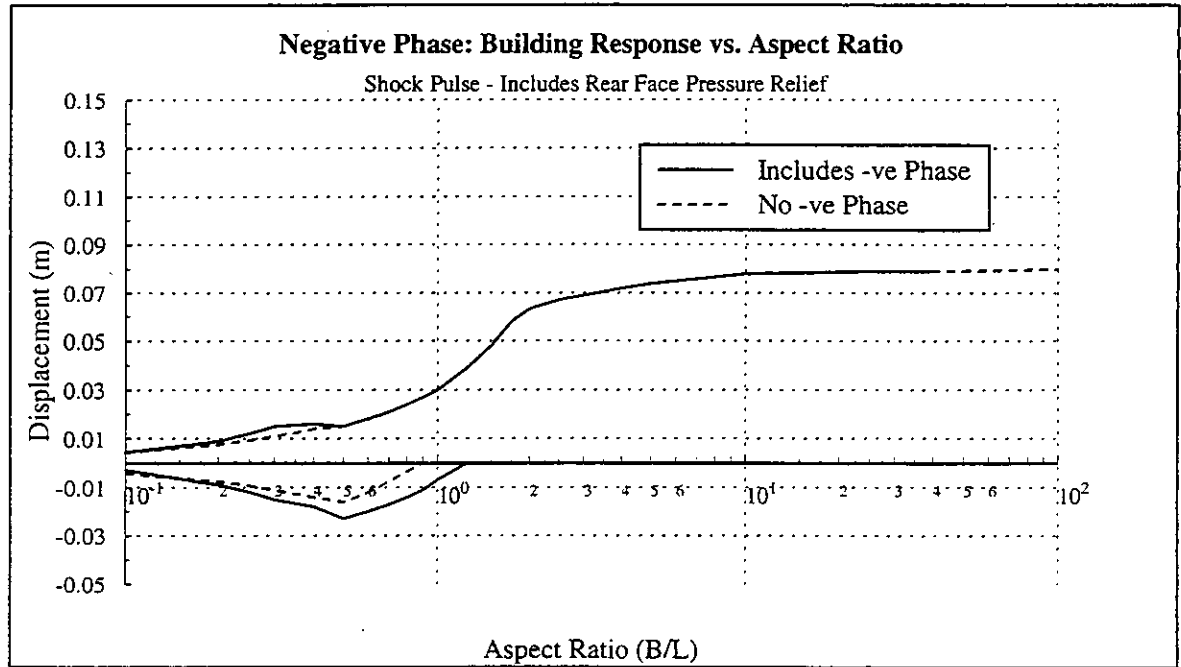


**Figure 2.7 Building Response to Pulse Including Negative Phase  
 Includes Rear Face Pressure Load**

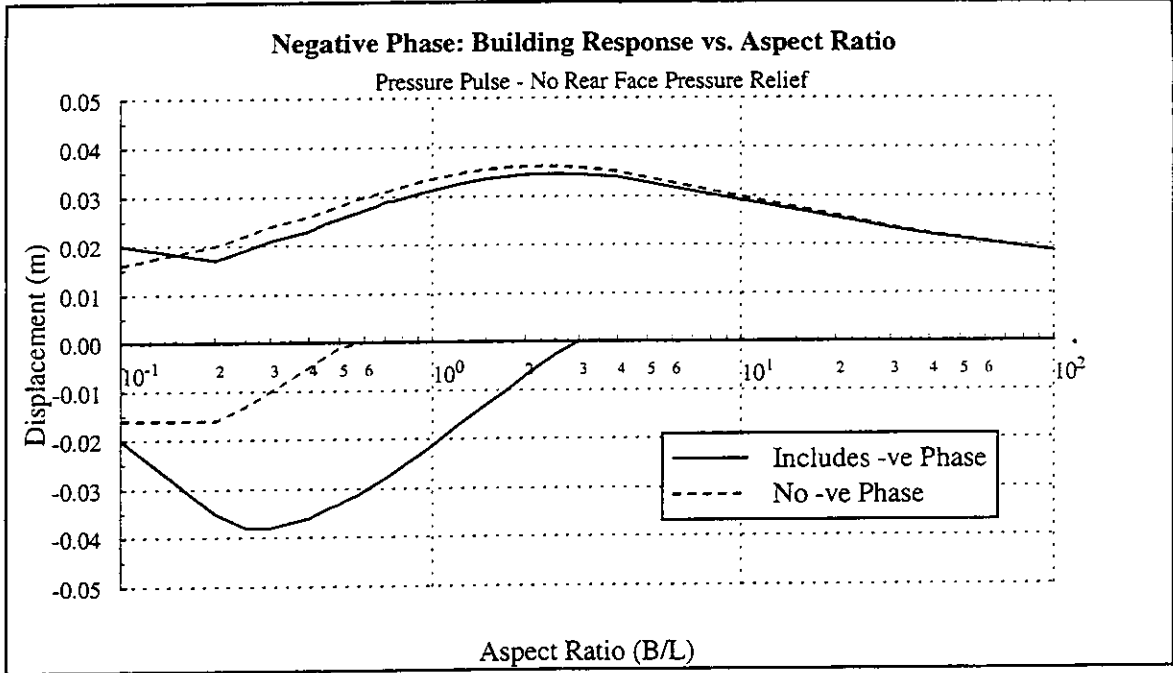


a) Shock Pulse: no rear face pressure relief

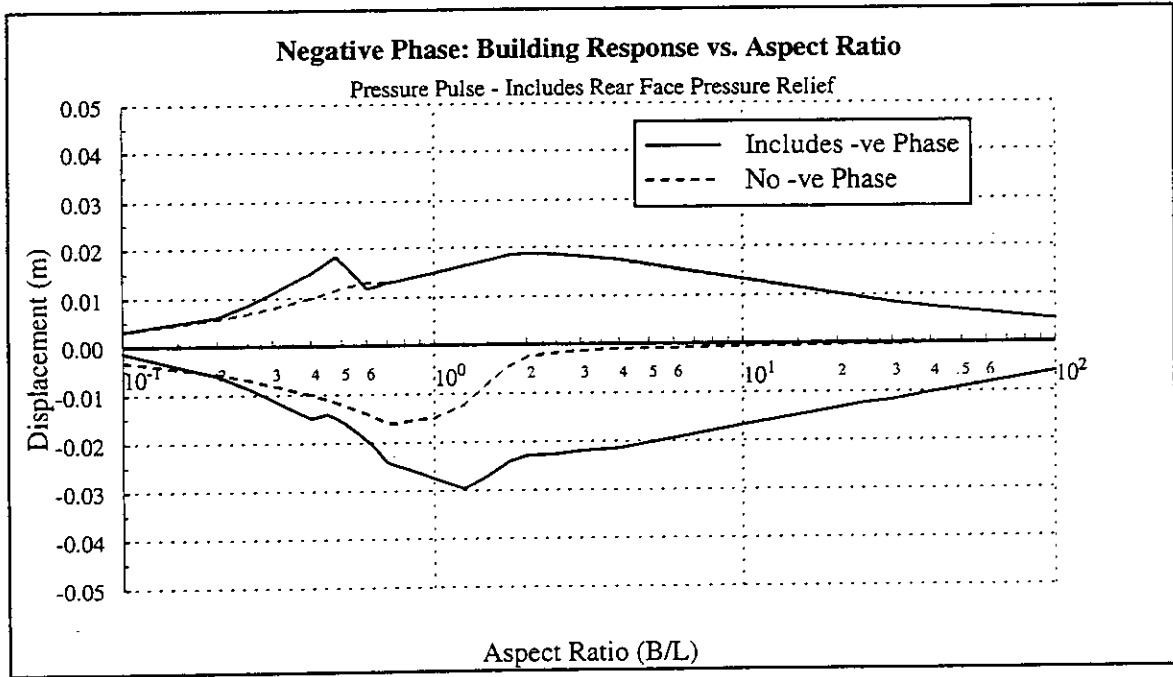


b) Shock Pulse: includes rear face pressure relief

**Figure 2.8: Investigation of Negative Phase Response with Aspect Ratio**

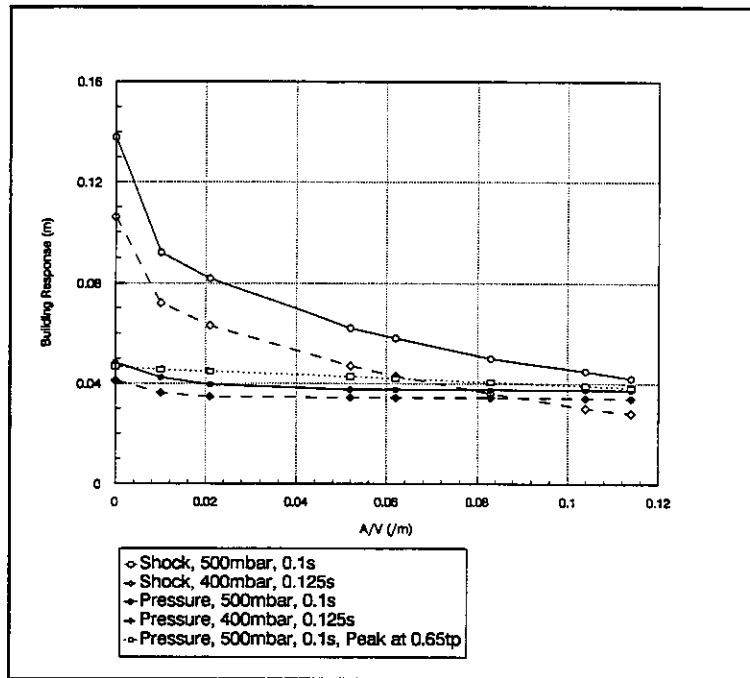


c) Pressure Pulse: no rear face pressure relief

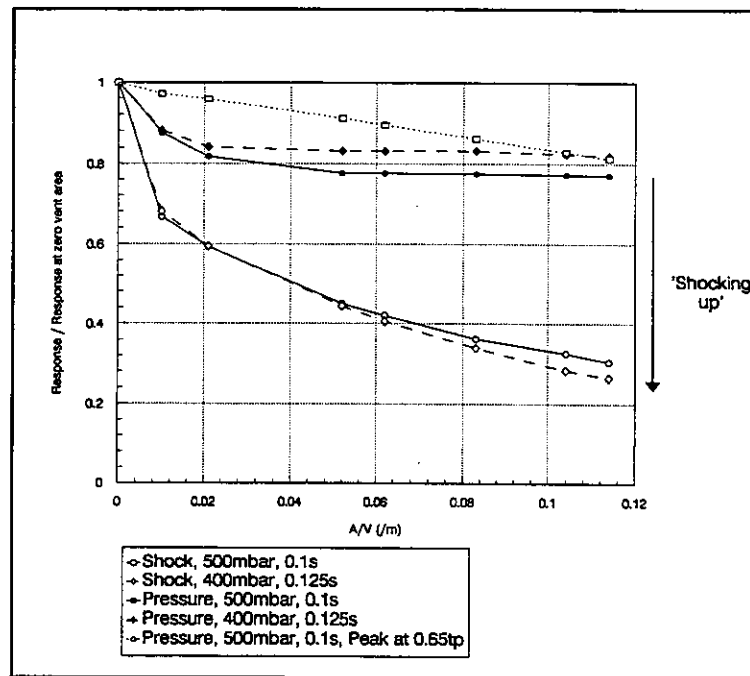


d) Pressure Pulse: includes rear face pressure relief

**Figure 2.8: Investigation of Negative Phase Response with Aspect Ratio**



a) Building Response



b) Response over response at zero vent area

Figure 2.9 Building Response vs. Area to Volume Ratio

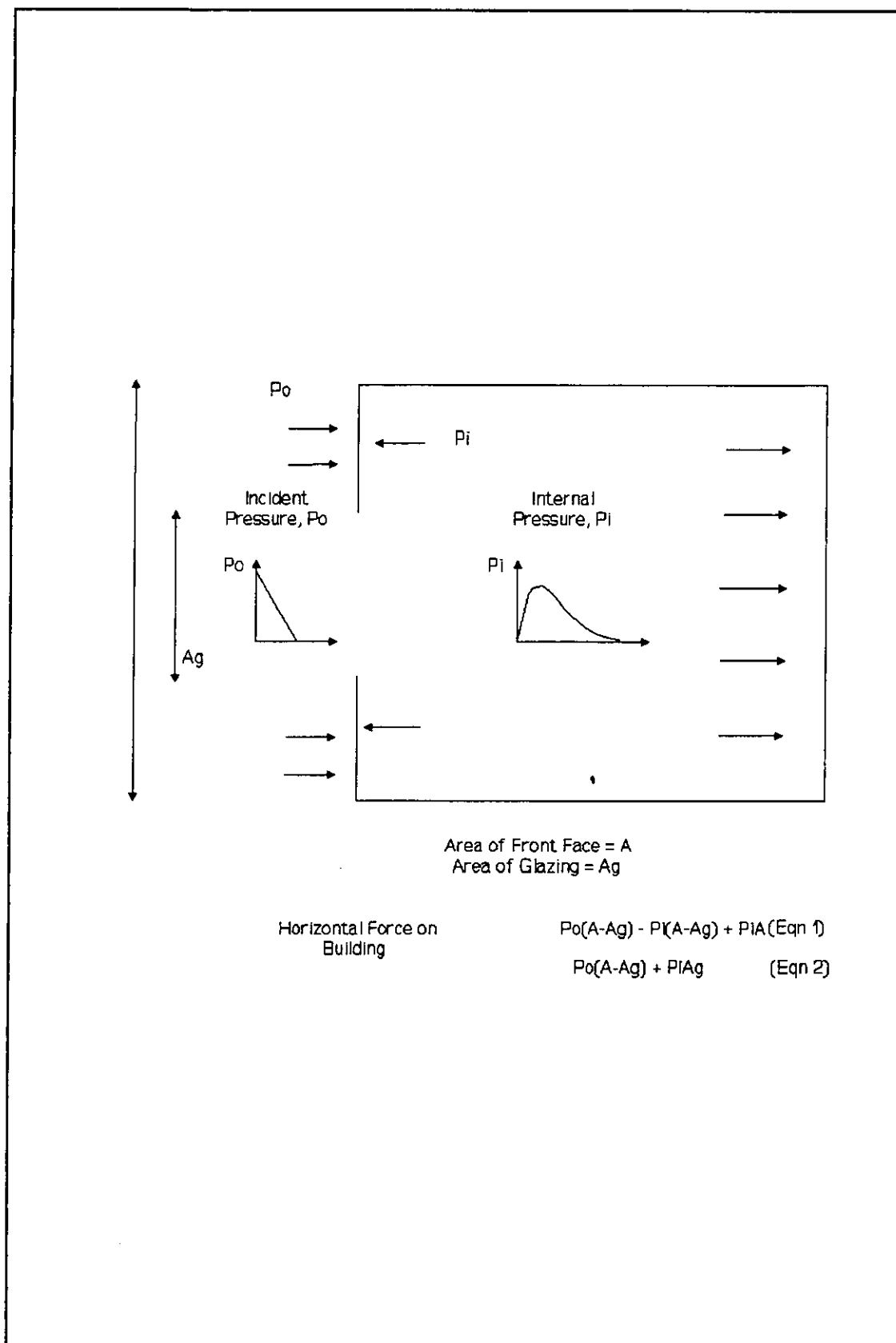


**Figure 2.10 Effect of Front Face Glazing Failure**

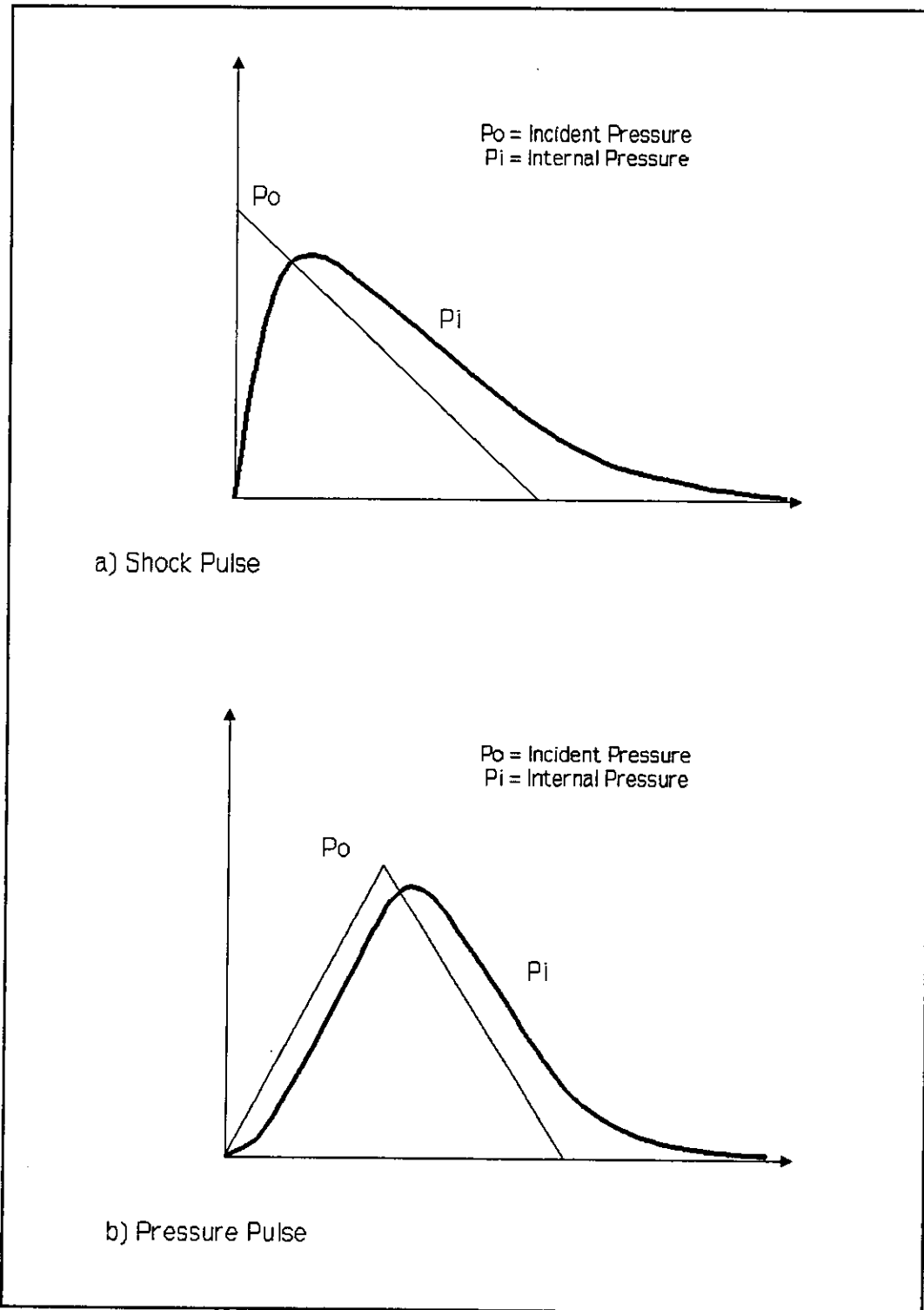
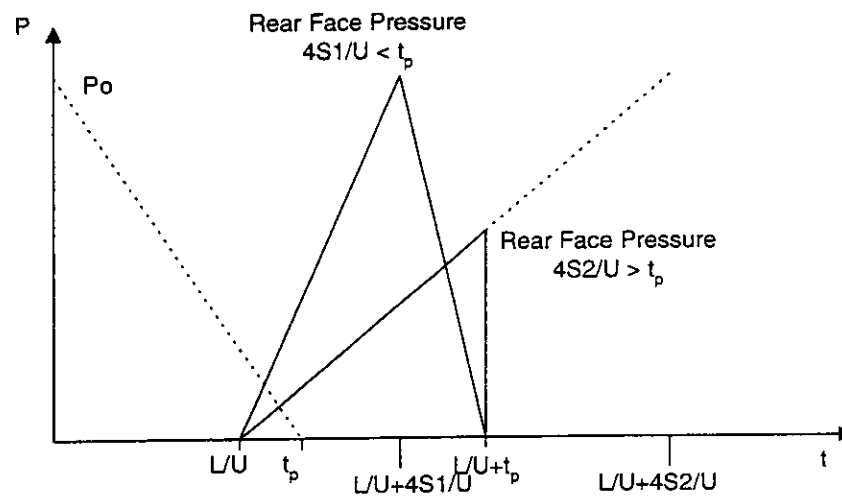
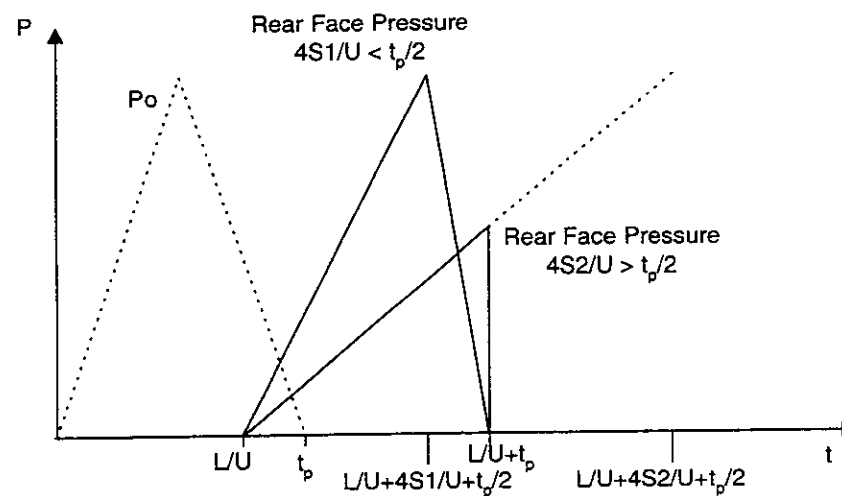


**Figure 2.11 Internal Pressure Rise**





a) Shock Pulse



b) Pressure Pulse

Key:  
 L = Building Length  
 U = Wave Speed  
 Po = Incident Pressure  
 S1 = Building Dimension (smaller of breadth/2 or height) for full rear face load  
 S2 = Building Dimension (smaller of breadth/2 or height) for partial rear face load  
 tp = incident pulse duration

**Figure 2.12: Rear Face Pressure Load**

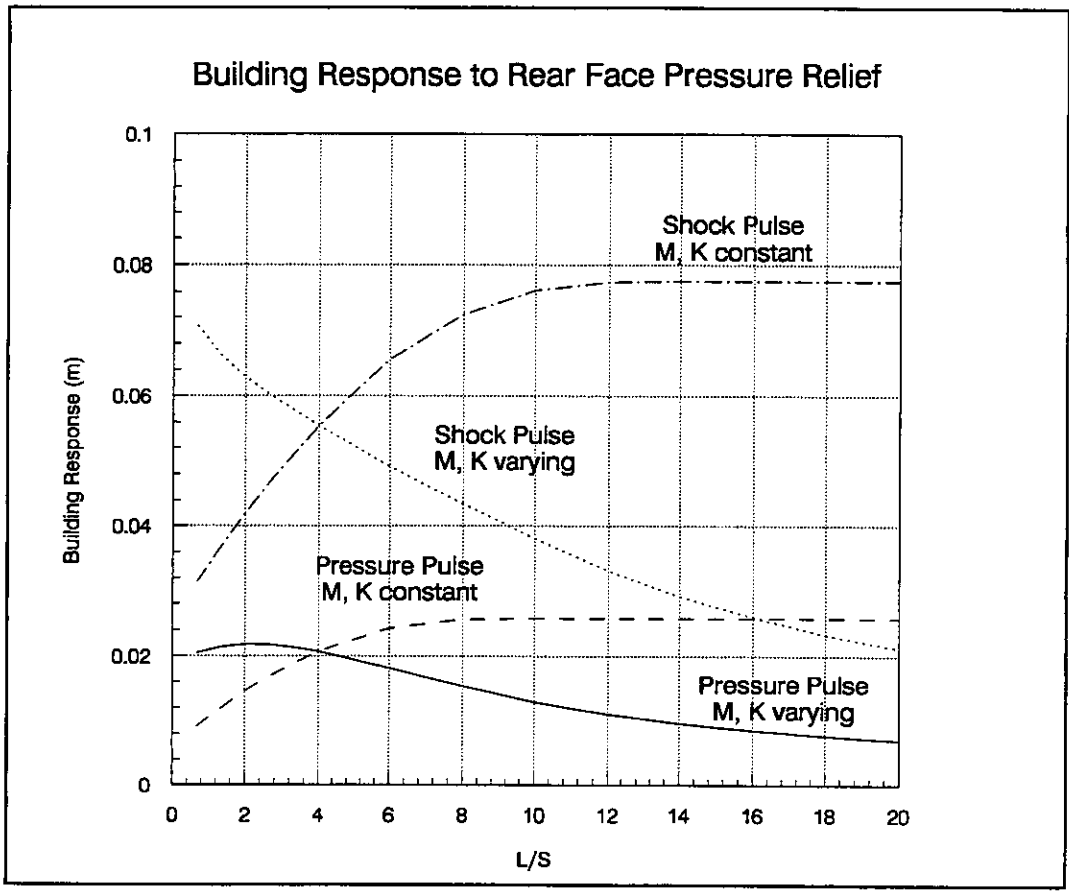


**Figure 2.13 Building Response vs. Aspect Ratio**

### 3 STRUCTURAL CAPACITY

In Phase 1, the structural performance of both load-bearing frames and non load-bearing external cladding was examined to assess typical failure pressures under dynamic loading. In Phases 2 and 3, this has been extended to look at two actual building designs to derive structural capacities for use in the fatality probability calculations.

The two building types chosen for consideration are a brick-built house and a concrete framed office building. The brick house is based on two construction examples for a typical semi-detached two-storey house, one from the 1930's and one of a more recent construction. Two examples have also been used for the concrete framed office building, one of which uses a braced frame, and the other of which makes use of a moment resisting frame.

The geometrical and constructional details of the buildings assessed and the calculations performed are outlined in the following two sections.

#### 3.1 Brick building type

The floor plans and cross section of a typical semi-detached two storey house are shown in Figures 3.1 - 3.3. Two typical constructional types have been assessed. The older 1930's example has solid facing brick external walls with internal load-bearing partitions of 100mm blockwork and the party wall is also a solid brick wall. The recent construction example has 280mm thick external cavity walls with a facing brick outer leaf, a 100mm lightweight block inner leaf and cavity insulation. The party wall is a 280mm cavity brick wall and the internal load bearing partitions are 100mm blockwork. The floor construction for both examples is timber boarding on timber joists either built into the masonry or supported on joist hangers. The roof construction is tiles and battens on timber trussed rafters supported on wall plates on the front and rear walls or on the inner leaf of the front and rear walls. The overall dimensions of the house are 14m x 8.6m plan area, with a maximum height of 8m. Glazing areas are 7.6 x 2 m<sup>2</sup> on the front face, 11.2 x 2 m<sup>2</sup> on the rear face and 2.6 m<sup>2</sup> on each side.

Several assumptions have been made concerning the structural design of the building. In particular it has been assumed for the recently constructed building that the roof is adequately braced and acts as a rigid diaphragm to resist horizontal loads, and that the floors and roof are adequately fixed to the masonry with connections capable of providing at least simple resistance to lateral movement in accordance with BS 5628: Part 1: 1978 Appendix C. For the older style building this is less likely to be true.

For this type of building, with a traditional design where horizontal and vertical spanning of wall panels is small and where internal walls are properly bonded at right angles between the external walls, the critical walls are those external

wall panels on the upper floors. At the upper level, only limited precompression from the roof is present to enhance the walls' horizontal loading capacity. The worst case is the gable wall where there is no precompression from the roof. It is assumed for the purpose of these calculations that the gable wall is tied back to the trussed rafter roof structure at the eaves and ceiling levels. The wall is considered to be simply supported top and bottom, but continuous at the corners of the building.

Assessment of the capacity of the external walls to resist loading has been based on design principles for masonry buildings (BS 5628: Part 1 'Structural Use of Reinforced Masonry'). The static collapse load for the wall panels has been assessed using material and load factors of 1.0 to give the load to initiate cracking in the wall. This gives, for the cavity wall, a combined resistance of 59.3 mbar, and for the solid wall a resistance of 168 mbar.

For accidental wind loading, the static collapse load may be increased by a factor of  $\sim 1.6$  in order to derive the collapse load under dynamic loads [22]. This gives a dynamic failure pressure of 96.9 mbar for the cavity wall and 275 mbar for the solid wall. It should be noted that these values are very much for the worst case scenario, i.e. the gable end where there is no precompression in the wall to enhance the capacity. These values are, however, in reasonably good agreement with the historical data identified in Phase 1.

### **3.2 Concrete framed building**

Two types of concrete frames have been considered, a braced frame and a moment resisting frame. The geometries for the two types are different, as described below. In these calculations, attention has been focused on failure of the frame itself, and its static load capacity. The dynamic load capacity can then be calculated from a knowledge of the dynamic characteristics of the cladding.

#### **3.2.1 Reinforced concrete braced frame building**

A typical floor plan, cross section and typical member sizes for the reinforced concrete frame are shown in Figure 3.4. It is a 4-storeyed building, with overall dimensions of 40m x 14m x 16m high. Along the long side, there are 8 bays of 5m each, divided by reinforced concrete columns 300 x 300mm area. The short side comprises two unequal bays, one of 8m and one of 6m. The floors are designed as a monolithic beam and slab construction with solid slabs spanning one way and supported on beams which are framing into the concrete. The columns are designed to transfer all vertical loads to the foundations and any moments arising from the framing of unequal beams into any one particular column. The external horizontal wind loading in the transverse direction is resisted by end shear walls and in the longitudinal direction resistance is provided by the staircase and infill masonry panels in the side walls.

For the purposes of these calculations, it has been assumed that the structure is tied together in accordance with BS 8110: Part 1: 1985, and the static collapse load for the column supports has been assessed using material and load factors of 1.0.

The calculated static column collapse load is 118.6 - 162.5 mbar, dependent on the assumed load distribution: the lower value assumes that on the short side, both of the spans are fully loaded, whereas the higher value assumes that one span is fully loaded and the other is subject to dead load alone. These values also assume that the wall cladding is capable of transferring this load to the columns. In reality, some or all of the glazing or cladding will fail at a lower pressure than this. A similar calculation assuming no load transfer from the walls to the frame gives a static collapse load of 1976 - 2708 mbar.

### **3.2.2 Reinforced concrete moment resisting frame building**

The geometry of this example building is slightly different from the previous one, and a typical floor plan, cross section and member sizes of the frame are shown in Figures 3.5 and 3.6. The building is a seven-storeyed office block, extending from an underground basement to 5th floor, with additional tank rooms at roof level. The overall height of the building is 25.75m from ground level, with a basement height of 3.15m. Plan dimensions are 29.25m x 15.45m and bays are approximately equal width: 5 bays longitudinally of length 5.625m or 6.0m, and 3 bays in the transverse direction of length 5.0m or 5.225m.

The floors are designed as monolithic beam and slab construction with solid slabs spanning one way and supported on secondary beams which in turn are carried by main beams framing into the columns. The columns are designed to transfer all vertical and horizontal loading to the foundations. It is assumed that the frame has been designed in accordance with the provisions of BS 8110: Part 1: 1985.

The column dimensions in this example are not uniform up the height of the column. At ground floor level, the dimensions are 300mm x 500mm and the calculated static collapse load is calculated as 144 - 150 mbar. In this case the range is based on the maximum and minimum loads on the column. The first floor columns have dimensions of 300mm x 300mm, and a corresponding static load capacity of 135 - 154 mbar. Again, the calculations assume that the load can be transferred from the walls into the column.

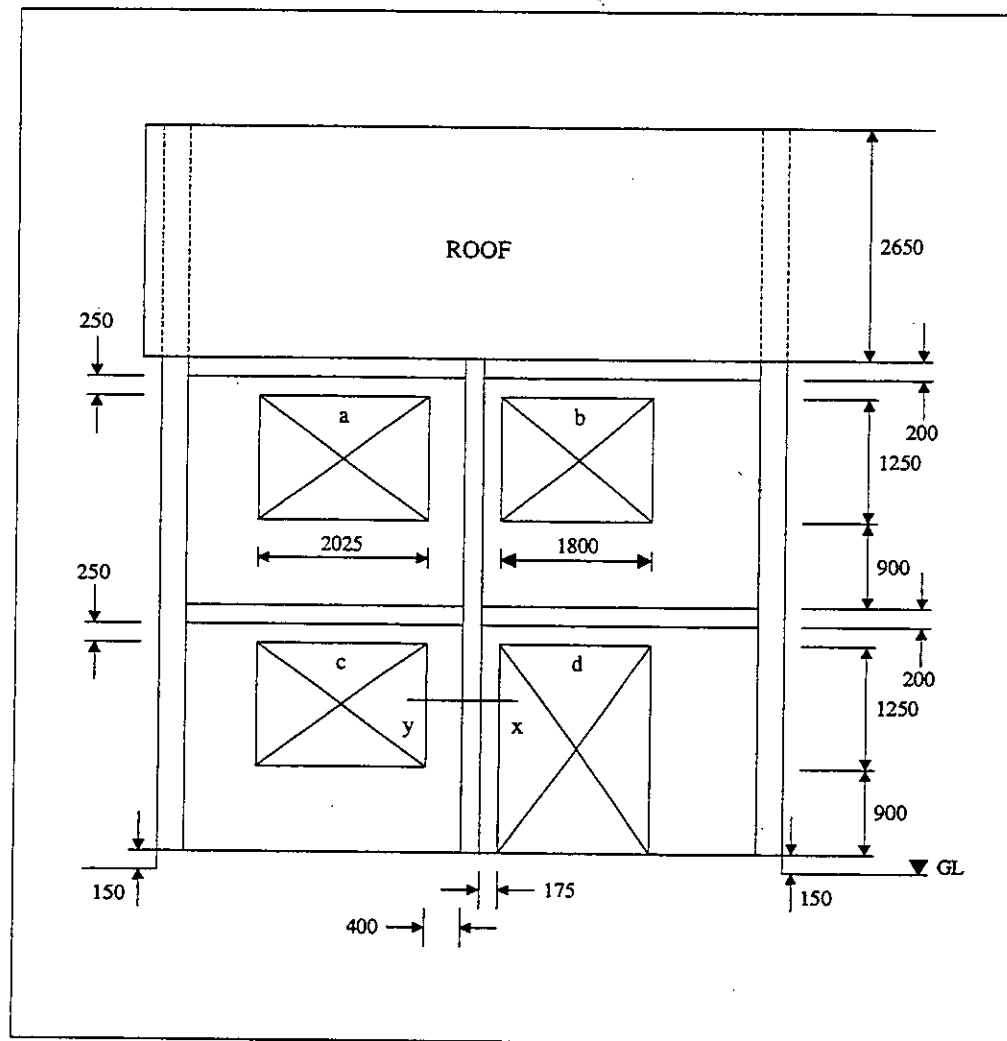


**Figure 3.1 Brick Building Dimensions: Elevation at Rear Wall**

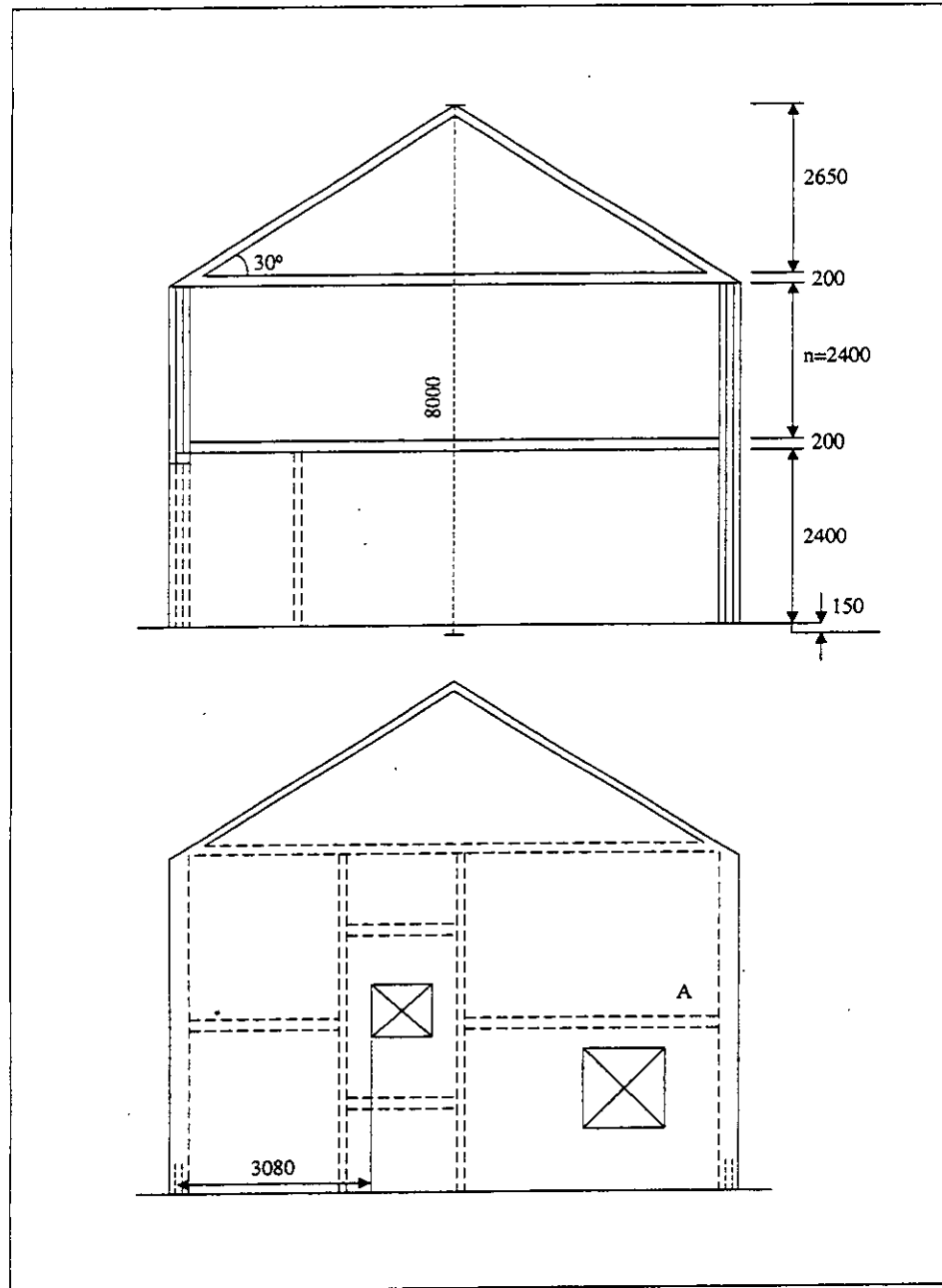


**Figure 3.2 Brick Building Dimensions: Elevation of Partition Wall (top) and Elevation of End Wall (bottom)**

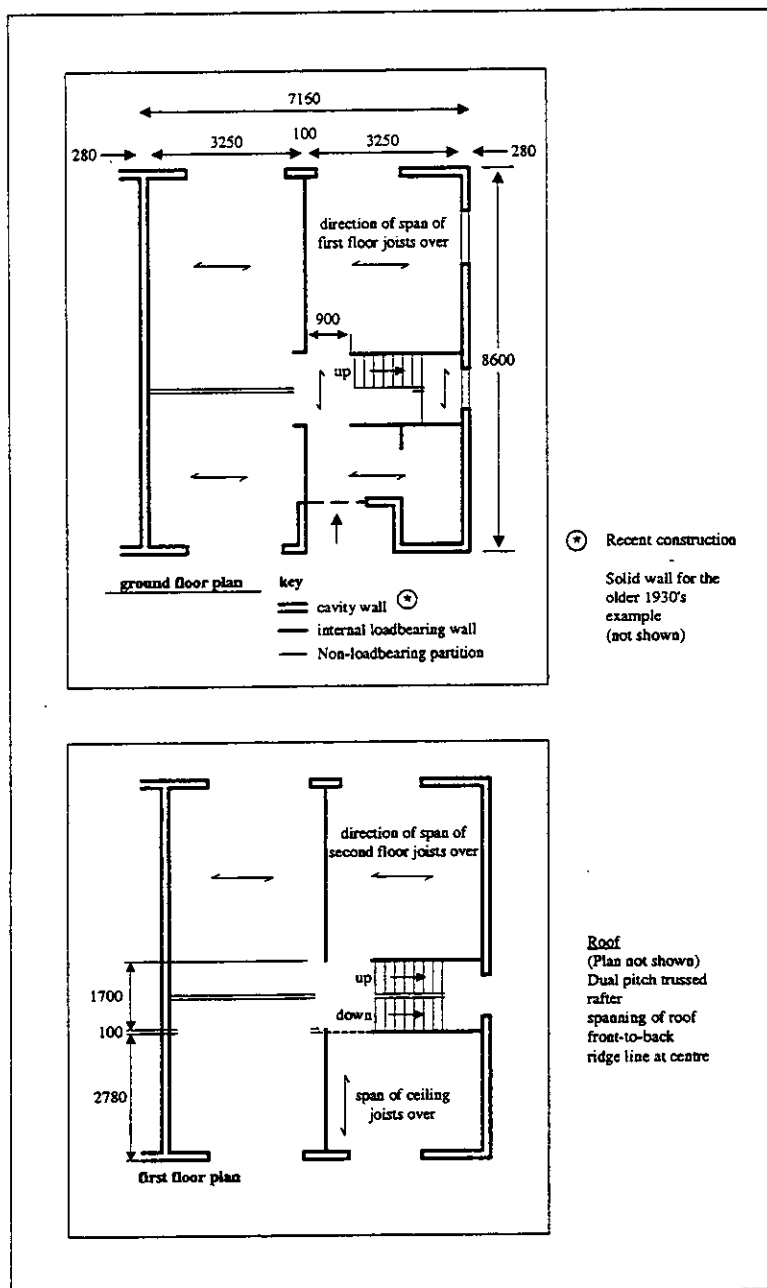
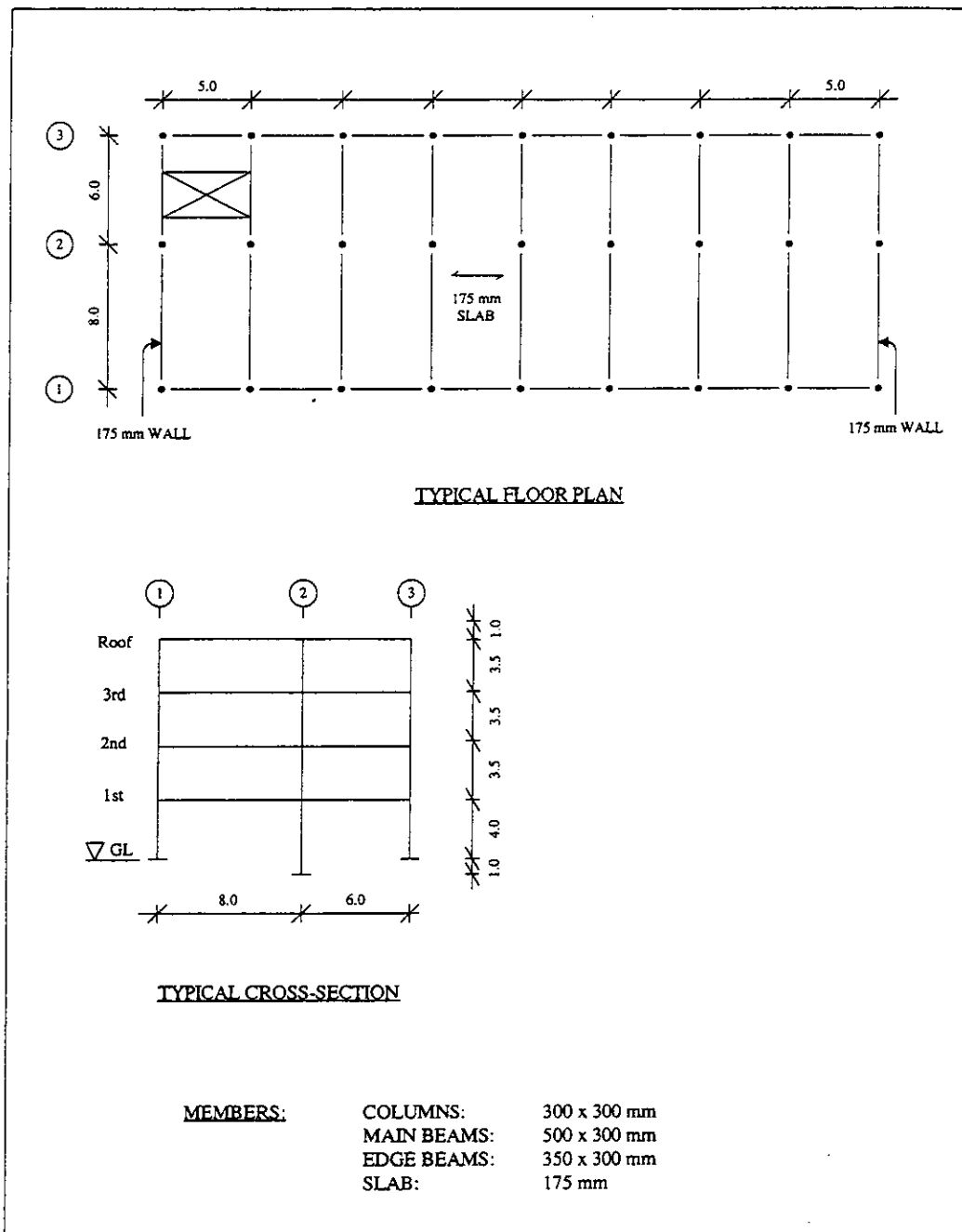


Figure 3.3 Brick Building Dimensions: Internal Plan





**Figure 3.4 Concrete Framed Building Dimensions - Braced Frame**

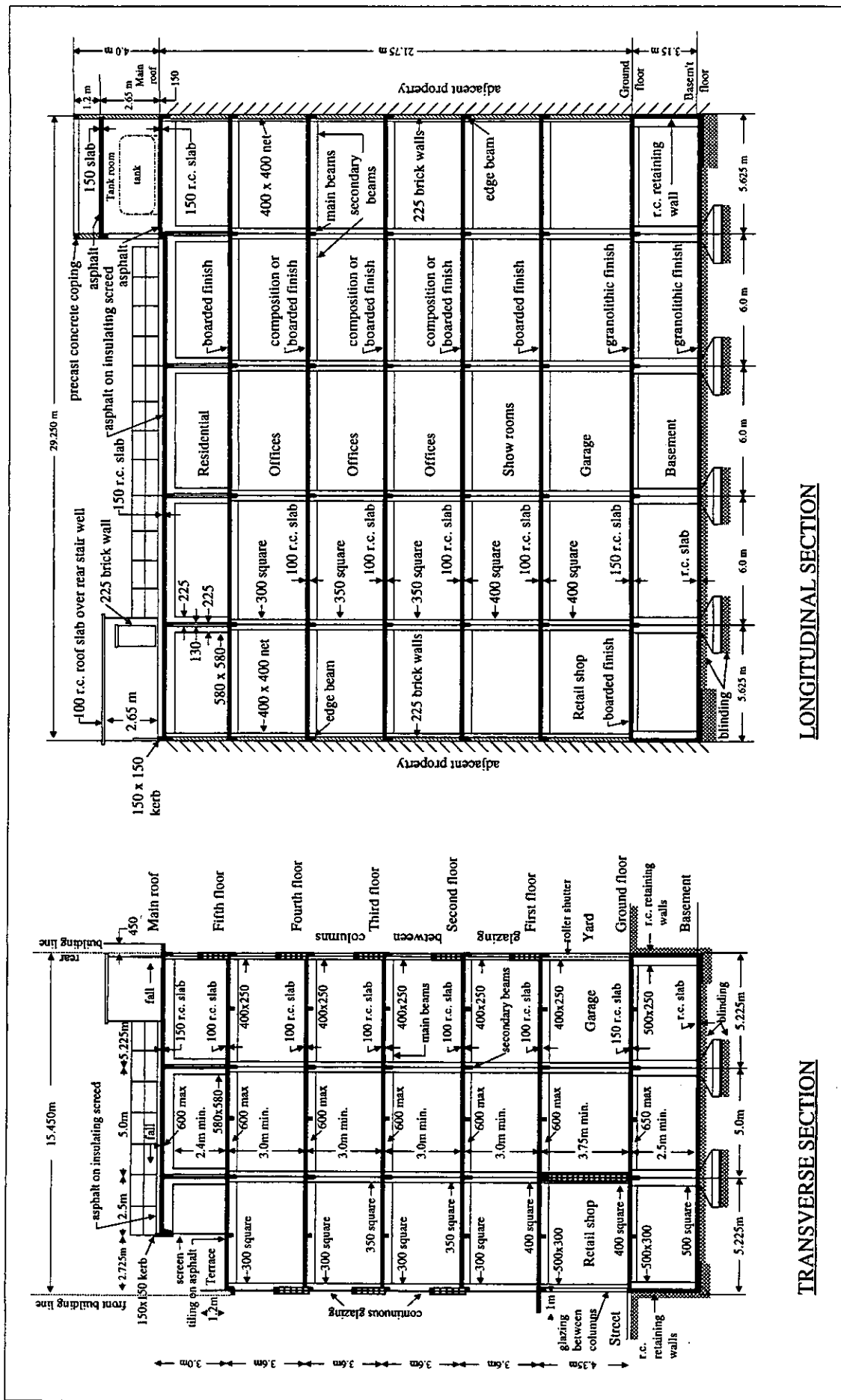


Figure 3.5 Concrete Framed Building Dimensions - Moment Resisting Frame: General Arrangement -Sections

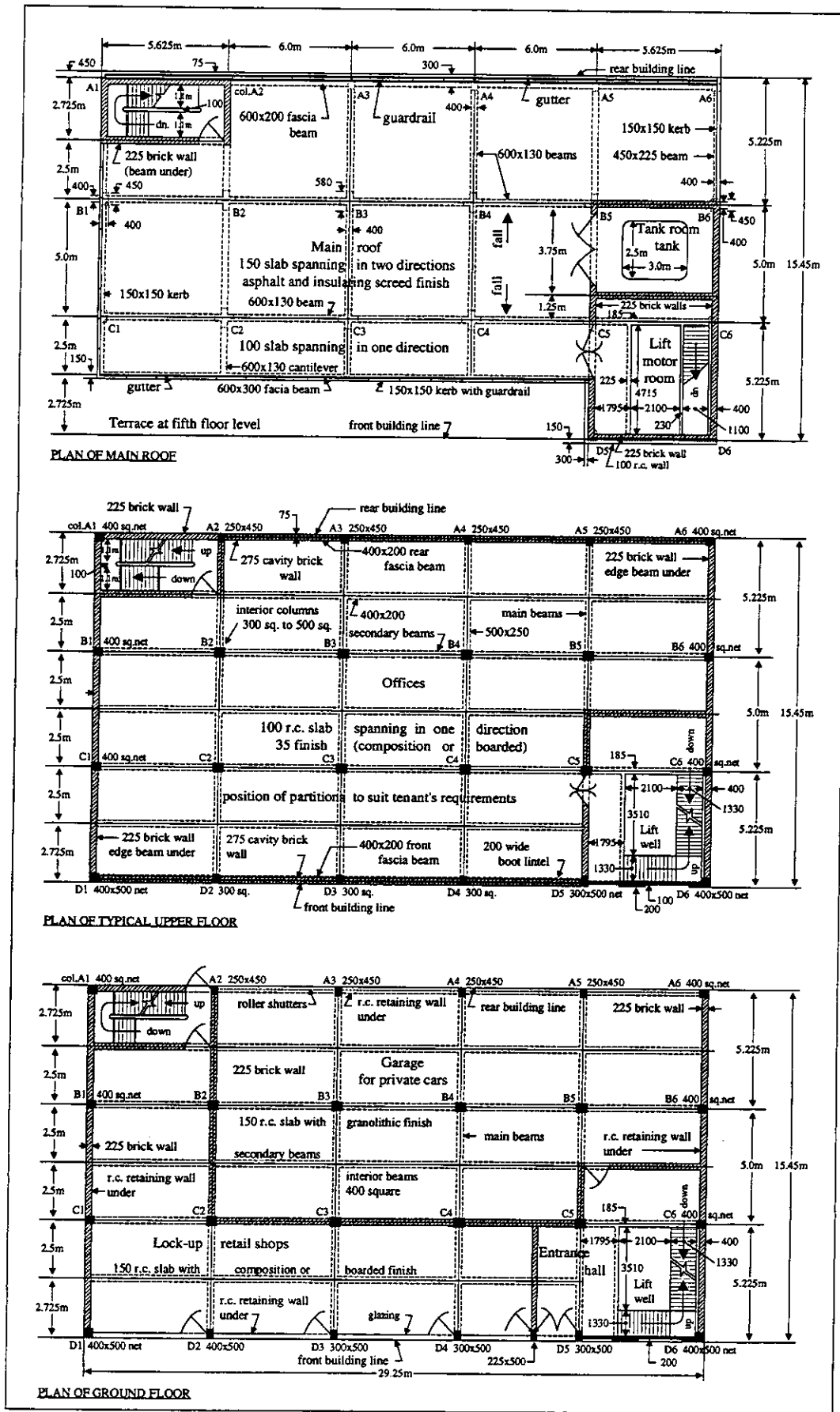


Figure 3.6 Concrete Framed Building Dimensions - Moment Resisting Frame: General Arrangement - Plans

## 4 GLAZING/DEBRIS EFFECTS

One outstanding item from Phase 1 was the fatality probability of humans to glazing fragments: there appeared to exist two approaches for assessing the fatality probability, one based on skin penetration and one based on skull fracture, which presented very different estimates of fatality. This discrepancy, and the uncertainty in the prediction of glazing fragment size and velocity have been investigated in more detail, as described below.

### 4.1 Sources of data

As part of Phase 3, a literature search has been performed in order to identify any additional data specifically relating to fragment mass and velocity distributions and lethality curves for glazing and debris fragments. Sources of data include:

- Computer database searches: the databases searched include MEDLINE, FLAIR/BRIX, EMBASE, Occ Saf. And Health, and MHIDAS.
- Contacts with a number of organisations have been made, requesting the availability of any suitable fatality probability curves or fragment mass/velocity distribution data. Organisations contacted have been:
  - Defence Evaluation and Research Agency - Trauma Injuries and Fort Halstead
  - Northern Ireland Forensic Laboratories
  - DEO (Works) (Including Special Security Group)
  - Institute of Explosives Engineers
  - Royal Military College of Science Shrivenham
- US Department of Defence Explosives Safety Board: the Minutes of the Explosives Safety Seminars have been searched for any relevant data.
- The Internet has been searched for data relating to skull fracture and blast hazard to humans.

A number of references were identified as being potentially useful, as outlined in Appendix A. Unfortunately, however, while many of the references obtained included material of general interest, there was little of specific use. In addition, some references which are directly relevant are provided by the military establishments and contain classified information. The references of particular use identified previously and as part of this search included:

1. Baker et al [1] provides equations for predicting the mean mass and velocity of glazing fragments and vulnerability criteria for injury from penetrating and non-penetrating fragments. It also includes a method for

assessing the velocity of an unconstrained debris fragment subject to a blast overpressure, which was used for calculating debris vulnerabilities.

2. Feinstein [10] provides a general description of the background behind the debris fatality probability curves presented in Baker et al [1].
3. Experimental data for glazing fragment masses and velocities following failure of a window under blast loading is contained in several papers by Fletcher et al [3, 14, 15] Nowee, [4] and Pritchard [13]. Harris et al [16] contains experimental data for glazing fragment velocities following failure of a window under blast loading.
4. Glaister [17] provides general information relating to skull fracture and fatality probabilities.

#### 4.2 Glazing failure pressures

There are several sources of data for glazing failure pressures including both experimental and theoretical models. Forsen, R. and Selin, B. [19] includes a comparison of experimental data and theoretical predictions and shows that the method proposed by Mainstone [18] agrees quite well with experimental results. From other experimental data available, we can produce the following comparative table:

Source of data	Pane dimensions (m)	Pane thickness (mm)	Experimental failure pressure (mbar)	Mainstone prediction (mbar)
Nowee [4]	1.65 x 1.1	6	56	50 - 60
Fletcher, E.R., Richmond, D.R. and Jones, R.K. [14]	0.86 x 1.22	5.6	57.2	60 - 75
	1.1 x 1.1	5.8	57.2	55 - 65
Fletcher, E.R., Richmond, D.R. and Richmond, D.W.[15]	0.86 x 1.22	6.0	82.74	60 - 75
	1.1 x 0.51	3.15	68.95	80 - 85

**Table 4.1:**

#### **Comparison of Mainstone predictions**

Based on this comparison, and the work of Forsen, R. and Selin, B. [19], we have decided to use the graphs presented in Mainstone [18] as a guideline to typical failure pressures.

### 4.3 Glazing velocity/mass distribution

In Phase 1, the equations provided in Baker [1] for calculating the mean mass and velocity distributions for glazing fragments were proposed. These equations estimate the mean frontal area of the fragments as:

$$A = 6.4516 \times 10^{-4} e^{[2.4 - (12.5 + (5.8566 \times 10^{-5} P_e)^2)^{1/2}]} m^2$$

for the peak effective pressure,  $P_e$  in the range 0 to 96.5 kPa. The corresponding mean velocity is given as:

$$V = [0.2539 + 1.826 \times 10^{-4} (h - 7.62 \times 10^{-4})^{-0.928}] \times [0.3443 P_e^{0.547}] m/s$$

for  $P_e$  in the range 690 Pa to 689 kPa and the thickness of the glass,  $h > 7.62 \times 10^{-4} m$ .

These equations make no reference to the pulse duration, only to the peak overpressure and the glazing thickness. They also do not include the dynamic failure pressure of the glazing. There are two options for including the failure pressure: either shift the curve along by a pressure equivalent to the failure pressure, or impose a cut off on the curve at the failure pressure of the glazing. Given that the curve is based on experimental data the latter method is considered more appropriate, as it means that the curve still passes through the experimental data points at high pressures.

It was found in Phase 1 that using these equations directly predicted very small fragment masses at the pressures of interest: so small, in fact, that the derived vulnerabilities based on the skull fracture criterion were very small and using the penetration criterion resulted in no fatalities at all. Consequently it was assumed in Phase 1 that the worst case would be for the mass to be 10 times greater than the calculated mean, but the mean velocity to be the same. This assumption corresponded approximately to the heaviest fragment with the highest velocity observed by Fletcher.

In order to investigate the above equations and assumptions, the paper by Fletcher et al [3], on which the above equations were based and further experimental work by Nowee [4], Harris, Marshall and Moppett [16] and the Eskimo II and III experiments [14, 15] were studied. All of these papers present results of experimental work on glazing failure and fragment generation. In the experiments reported in Fletcher et al [3], which relate to the Eskimo III experiments, two 107 x 51 x 0.317cm glass panes were exposed face on to a large high explosive detonation at an incident overpressure of 40 mbar with a duration of 250 msec. The mean mass and velocity of the ensuing fragments were 1.06g and 22.6m/s. This can be compared with the predictions using the expression given in Baker et al [1] for this scenario of 1.57g and 14.5m/s. By comparison, in the TNO experiments [4], panes of unhardened glass,

glass, dimensions 1.679m x 1.129m with a nominal thickness of 6mm were loaded with a peak overpressure of 130 mbar, which was approximately twice the dynamic failure pressure of the pane. The pulse duration in this case was 30ms. The mean measured fragment mass and velocity were 80g and 12m/s, which again can be compared with the predictions of 3g and 17.0 m/s using the expression given in Baker et al [1]. Thus the TNO experiments produced much larger, slower fragments than the experiments described in Fletcher et al [3]. Clearly the Baker equations alone cannot fully predict the apparent outcome of these experiments.

Baker [1] also includes equations and graphs for calculating the velocity of an unconstrained fragment subject to a blast overpressure: this was used in Phase 1 for assessing debris velocities for brickwork and other cladding. This method was applied to a fragment of glazing in order to compare the prediction of velocity for an unconstrained fragment against the Baker glazing velocity calculation. In addition, the velocity was calculated based on the total impulse applied to a glazing fragment from the equation:

$$v = \frac{A}{M}(I_a - I_f)$$

where  $I_a$  is the applied impulse and  $I_f$  is the impulse required to cause failure. The area to mass ratio,  $A/M$  was taken as  $1/h\rho$  where  $h$  is the glazing thickness and  $\rho$  is the glass density. The Baker predictions, and the results of the debris calculation and the impulse calculations are shown on Figure 4.1, together with points corresponding to the Fletcher and the TNO experiments [3, 4].

Several points can be observed from the graph. First, concerning the impulse calculation, the duration of the assumed pulse greatly affects the slope of the curve. For the 6mm glazing, the impulse calculation has been performed for durations of 30ms, corresponding to the TNO experiment and 170ms, corresponding to the average duration of the Eskimo II and III experiments and on which the Fletcher paper [3] and the Baker equations [1] are based. While the 30ms impulse line appears to agree quite well with the TNO data point, the slope of the 170ms impulse line agrees very well with the initial velocity predicted by using the Baker curve. It appears that at pressures close to the failure pressure of the glazing, the impulse equation predicts quite well the expected fragment velocity. The curve calculated using the unconstrained fragment approach has been plotted for 170ms pulse duration, and shows a different form from the impulse line. It appears that the Baker equations predict a velocity distribution which is some combination of the impulse and debris curves: at pressures close to the glazing failure pressure, the distribution is similar to the impulse calculation and corresponds to all of the impulse which exceeds the required impulse to cause failure being converted into forward motion. At much higher pressures, the failure impulse is a much smaller proportion of the incident impulse, failure occurs relatively quickly compared with

the pulse duration, and much less of the incident force is able to be translated into forward motion.

The curve presented in Baker for the velocity distribution is plotted in Figure 4.2 together with experimental data for internal explosions from Harris, Marshall and Moppett [16], and from the Eskimo II and III experiments [14, 15]. Although the scatter in the data is broad, the Baker curve appears to agree reasonably with the other data, and hence the Baker equation has been used to predict glazing fragment velocities for the fatality probability calculations.

The mass distribution appears to show far more spread than the velocity distribution. In particular, for thick glass (i.e.  $t > 6.0\text{mm}$ ), Fletcher notes that at overpressures below 100mbar the measured frontal areas in his experiments were considerably larger than predicted from his derived regression equation (which is the basis for the Baker equation). For the TNO experiments [4] the average mass was also much greater than would have been predicted from the Baker equations. One reason for this could be the method for collecting the fragments: the TNO experiments used photography to measure velocities and masses, while in the experiments reported in Fletcher et al [3], the fragments were collected in a polystyrene witness plate. The first method may be biased towards identification of large fragments as they are easier to track on film, while the second method could reduce the apparent average mass as fragments can break on impact with the plate. In order to obtain a better estimate for the fragment mass distribution, particularly at low pressures, a curve has been fitted to the data available, including that presented in Fletcher et al [3], including the additional data which was not included in the data analysis used to create the Baker curves (Figure 4.3), and the TNO experiments [4]. A simple polynomial fit has been used, giving a curve equation:

$$\text{Fragment mean area} = 834.16 \times (100 \times P_e)^{-1.1772} \text{ cm}^2$$

where  $P_e$  is the effective pressure in Pa (i.e. reflected pressure for a normally incident shock pulse, or side-on pressure for a pressure pulse). This equation for mean fragment area can then be used in conjunction with the glass thickness and density to calculate a mean fragment mass. The curve fit predicts slightly higher masses at lower pressures than the curve given in Baker, but similar masses at higher pressures.

#### 4.4 Probability of fatality due to glazing fragments

Having calculated the fragment mass and velocity, it is necessary to identify the relevant criteria for human fatality probability. There are several different criteria available: in Fletcher et al [3], criteria for a 50% probability of skull fracture and a 50% probability of skin penetration are presented, based on in vivo experiments on sheep and dogs. The TNO paper [4] indicates that of these criteria, it is the criterion for skull fracture which is the most conservative. However, it should be noted that although the data exists to identify a velocity



limit for a certain probability of skull fracture or skin penetration, at present no data have been identified which enable us to predict the conditional probabilities of these injuries giving rise to fatality. This is subject of further literature surveys. Nowee [4] appears to assume that in an explosion incident there will be so many fragments generated that an exposed person will receive several hits from fragments, which individually would have a 50% probability of causing skull fracture, and that the net effect of these multiple impacts is fatality. However, there is little in the literature considered to date to directly relate skull fracture to fatality, and it is possible that use of this criterion may lead to a too onerous fatality probability, particularly at low pressures. The criteria presented in Fletcher et al [3] do not extend below masses of  $\sim 0.4\text{g}$  or above masses of  $\sim 200\text{g}$ , and extrapolation is necessary for smaller and larger masses. In extrapolating, the gradient of the line has been maintained, although the lines in Baker et al [1] for debris fatality probability indicate that the curves flatten out for low or high masses.

The alternative approach is to use the probability of skin penetration as a vulnerability criterion. Data are provided in both Fletcher et al [3] and in Feinstein [10]: the latter reference forms the basis for the curves presented in Baker for a penetrating injury, and has been chosen for use in these calculations, as it incorporates data from a wider range of sources. The criterion is based on a mass x velocity<sup>4</sup> relationship, and assumes that for an incident fragment with  $mv^4 = 4910 \text{ kg m}^4/\text{s}^4$ , there is a 10% probability of an incapacitating skin penetration injury. Inherent in this criterion is the assumption that if the fragment penetrates the skin, its residual velocity is sufficient to cause severe damage. This criterion requires greater velocities for fatality and is thus considerably less conservative than the skull fracture approach.

A combined approach has been derived using the two criteria for skull fracture and skin penetration, based on the average area of a human head and body and the fragment density from the broken window. The derived approach is as follows and illustrated in Figure 4.4.

- The fragment spatial density from Fletcher et al [3] has been used to derive the number of fragments per square foot with pressure:

$$\text{Fragment density} = (e^{(3.1037+0.05857P_e)} - 22.28) \cdot 4.910e^{-5.012t_w}$$

where  $P_e$  is the peak effective pressure in Pa and  $t_w$  is the glazing thickness in cm. Hence the number of fragments hitting the head,  $N_{fh}$ , and the number of fragments hitting the body,  $N_{fb}$ , can be calculated, for a particular pressure, assuming an average head area of  $0.031\text{m}^2$  and an average body area of  $0.359\text{m}^2$ . For double glazed windows, the fragment density is assumed to be double the value given by the above equation.

- The average fragment mass and initial velocity for a particular pressure are calculated from the mass distribution based on the curve fit to the Fletcher data, and the velocity curve presented in Baker [1] i.e.

$$\text{Fragment mass} = \text{Fragment mean area} \times t_w \times \rho$$

$$\text{Initial velocity} = (0.2539 + 1.826 \times 10^{-4} (\frac{t_w}{100} - 7.62 \times 10^{-4})^{-0.928}) \times (0.3443 P_e^{0.547})$$

- The typical range of fragment masses and initial velocities corresponding to the average values at that pressure are calculated. The heaviest, slowest fragment is assumed to have 10 times the average mass, and 0.6 x 1.5 times the average velocity: conversely, the lightest, quickest fragment is assumed to have 0.1 times the average mass and 1/0.6 x 1.5 times the average velocity. These assumptions are based on the upper bound of the spread of fragment masses and velocities observed in the experiments described in Fletcher et al [3].
- Having calculated the initial fragment velocity, the distance travelled and the change in velocity with distance can be calculated taking the drag on the fragment and acceleration due to gravity into account. Once a fragment falls below a height of 0.5 m above the floor, it is deemed to be no longer hazardous.
- A uniform distribution of fragment masses and velocities is assumed, between the heaviest, slowest fragment and the lightest, quickest fragment at a given pressure. The probability of a single fragment hit being able to cause injury can then be calculated from the proportion of fragments whose mass and velocity exceed the relevant criterion at the given pressure and for a range of distances from the window (i.e. reduced velocity). Thus for hits to the head, the fraction of fragments exceeding the criterion for a 50% probability of skull fracture can be calculated ( $f_{injh}$ ). The number of potentially injurious fragments,  $N_{injh}$ , for a given pressure and distance from the window, is then calculated from the number of fragments hitting the head and the percentage exceeding the criterion. i.e.

$$N_{injh} = f_{injh} \times N_{fh}$$

A similar calculation is performed for hits to the body, based on the skin penetration criterion.

- Even if fragment masses and velocities exceed the injury criterion, each potentially injurious hit only has a certain probability of causing that injury i.e. 50% for skull fracture, and 10% for skin penetration ( $p_{ig}$ ).

In addition, each injury only has a certain probability of causing fatality. This has been assumed to be 10% for a skull fracture and 50% for skin penetration ( $p_{fh}$ ). These are somewhat arbitrary assumptions, and may be changed in the light of further data as and when it becomes available.

- The overall probability of fatality is then calculated for a given pressure and a given distance from the window from:

$$\text{Probability of fatality} = 1 - (1 - p_{ig} \times p_{fh})^{N_{inj}}$$

for skull fracture, and a similar equation for skin penetration. The two fatality probabilities are then combined to obtain the overall fatality probability for glazing. This calculation is then repeated for a range of pressures and distances from the window to derive the fatality probability as a function of pressure and distance. This can then be used to assess the fatality probability of building occupants to glazing failure, using the methodology outlined in the report on Phase 1.

The fragment fatality probability curves for an incident shock pulse can be seen in Figure 4.5. The curves are based on this modified approach, with distributions of fragment mass calculated from our fit to the data presented in Fletcher et al [3], and distributions of velocity at different pressures calculated from the equations given in Baker et al [1]. The glazing failure pressure has been taken as 69mbar, based on data from Mainstone [18], for a 1.25m x 1.025m pane of glass, 4mm thick, and a pulse duration of 100ms. As can be seen, the fatality probability is zero until the effective pressure reaches ~ 300mbar. This is due to the fact that although the glazing has failed, the fragments are not travelling fast enough to cause serious injury. The curves will change for different window dimensions and failure pressures, and they are also sensitive to the assumed probability of a single injurious hit being fatal.

#### 4.5 Debris velocity/mass distributions

The investigation into the applicability of the Baker equations for predicting glazing mass and velocity distributions has highlighted the difference between velocity predictions based on the impulse transmitted to the fragment and those based on the motion of an unconstrained fragment, particularly at pressures far in excess of the failure pressure. This has implications for the prediction of debris velocities and hence vulnerabilities. In Phase 1, the unconstrained fragment approach was used to predict velocities. This may significantly underestimate the velocity, particularly at low pressures. It appears that a combination of the two approaches may provide a better estimate. As part of Phase 3, the method for predicting debris fragment velocities has been revised. The following procedure has been used:

- Step 1:** The load on the wall has been calculated for a specified incident pulse shape. This includes reflection of the incident pulse where necessary, but does not include any pressure-relieving mechanisms.
- Step 2:** The natural frequency of the wall and its maximum elastic displacement and ductility have been estimated, based on empirical data and analytical formulae.
- Step 3:** A single degree of freedom system based on the dynamic characteristics of the wall has been set up, and the time it takes for the wall to fail for that particular incident pulse have been calculated.
- Step 4:** Two approaches have been used for calculating the initial velocity. First, the initial velocity of the fragment has been estimated by assuming that the impulse up to the time of failure is completely transformed into forwards motion of the fragment. The remaining impulse in the incident pulse has been assumed to act on an unconstrained fragment, and an additional contribution to the velocity is calculated from the equations given in Baker et al [1]. The second approach is to calculate the velocity of the whole panel at failure and to assume that the debris fragment has this initial velocity, plus the velocity of an unconstrained fragment subject to the remainder of the incident pulse. A third approach considered is to assume that the strain energy stored due to the deformation of the panel is completely converted into kinetic energy and use this to calculate the initial velocity. However, the calculations showed that the panels considered were failing before the maximum displacement (and hence the maximum strain energy) was achieved, and hence that this approach may significantly overestimate the initial velocity.

The calculated fragment velocities for a single brick are shown in Figure 4.6. As can be seen, the method using an initial velocity based on the panel velocity at failure produces lower overall velocities, but the difference is small.

As a means of checking the above method, the velocity of a glazing fragment has been calculated and compared against the equivalent prediction using the equations given in Baker et al [1]. The comparison was based on the Eskimo II and III experiments [14, 15], as these form the basis for the equations presented in Baker et al [1]. Consequently, the pane sizes, thicknesses and pulse durations were assumed to be similar to the experimental layout, and in addition, the difference in time between the fragment hitting the witness plate and the pulse passing the witness plate was taken into account. The implication of this latter assumption is that the fragment does not experience the full impulse contained within the pulse, as it hits the witness plate before the pulse

has completely passed the fragment: consequently a reduced contribution from the unconstrained fragment calculation is calculated. This is particularly important for the Eskimo II and III calculations as the pulse durations are very long (~250msec), and hence it is highly likely that the fragment will not experience the full force of the incident pulse. The fragment velocity was based on the second approach outlined above. The comparison is shown in Figure 4.7, for an incident shock pulse for glass of thickness 2.64mm, 4.0mm and 6.0mm. The agreement is quite good for the thicker glazing, but our method shows a wider range as the glazing thickness changes. In the absence of further data, it seems that this is an appropriate technique to use for debris velocities.

It should be noted that as part of this calculation the dynamic failure pressure of the brick wall is calculated for the different pulse shapes. The calculations for a wall typical of the brick-built house result in a failure pressure of 407mbar for an incident shock pulse (reflected value) and 320mbar for an incident pressure pulse, based on the static values given in Section 3.1.

The vulnerability criterion used for debris is based on that presented in Baker et al [1] for non-penetrating fragments, although the fragment size used is such that the fatality probability is independent of increasing mass, and depends only on the velocity i.e. for a mass greater than 3kg, the critical velocity is constant. For a single brick, dimensions 200 x 100 x 75mm, the mass is ~3.75kg, and hence the critical velocity is in the constant region. The calculated fatality curves are shown in Figure 4.8 for an incident shock pulse, using the velocity profile given in Figure 4.7 for a single brick, together with the assumption that if wall failure occurs, a 60% probability of fatality exists in the region directly behind the wall due to collapse of the wall itself.

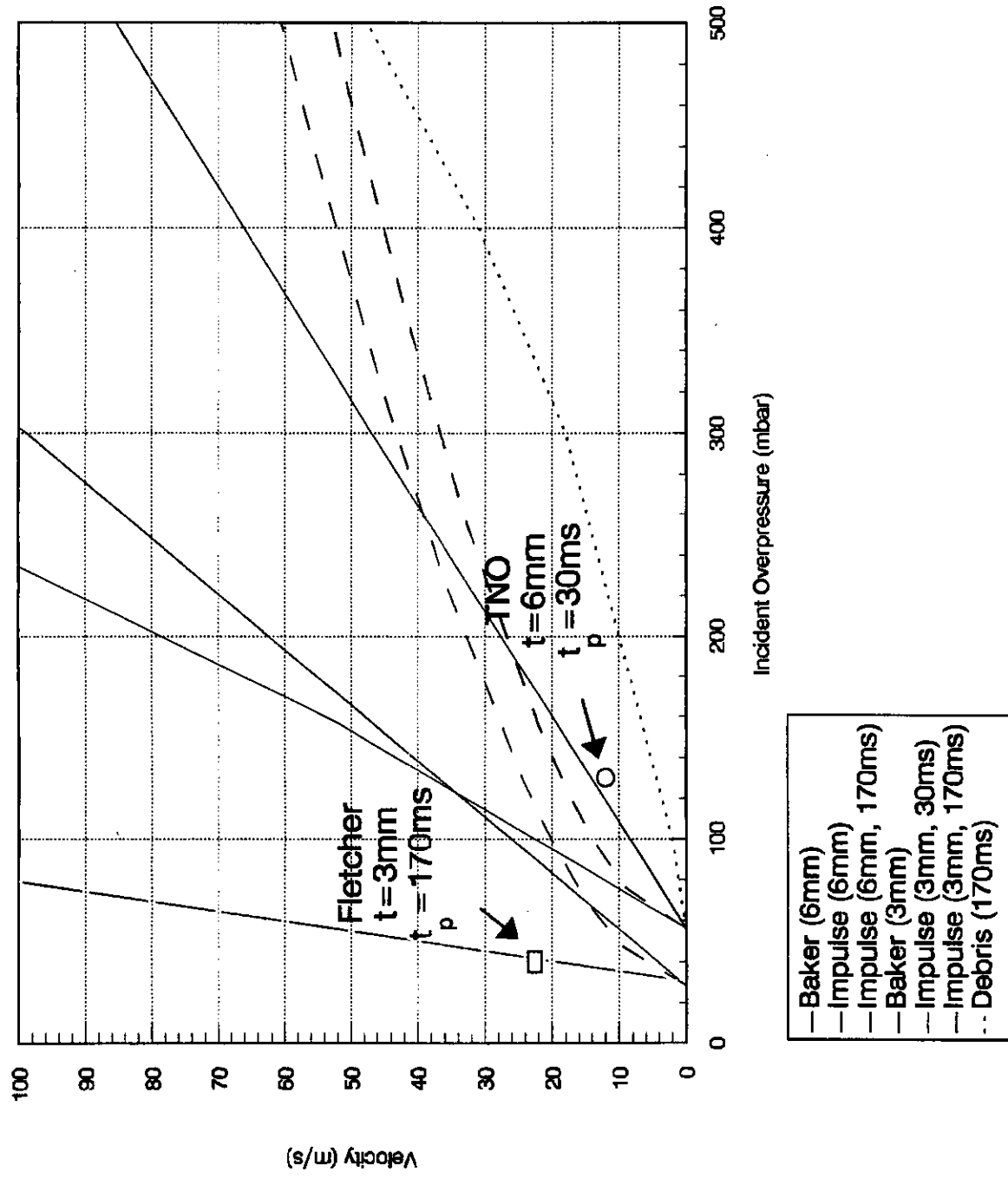
Finally, the method for estimating the area affected by debris generation has been revised. In Phase 1, we assumed that glazing and debris were distributed on a perimeter basis, i.e. the area affected by glazing was calculated from the amount of glazing on the perimeter of the building and the area affected by debris was estimated from the remaining perimeter length. This is felt to be non-conservative, as for most buildings any glazing is surrounded by supporting framework and cladding. Consequently, 100% of the building perimeter has been assumed to be a potential source of debris for the fatality probability calculations.

#### **4.6 Conclusions**

The vulnerability of humans to glazing and debris are highly important issues in the calculation of overall building fatality probability curves, and it has been necessary to make several assumptions in order to try and quantify the limits of fatality probability. Specific areas of uncertainty include:

- Fragment mass and velocity distributions arising from the failure of a panel subject to a blast load. There are some discrepancies between the different experimental results for glazing failure which indicate that the Baker equations for fragment mass may not be applicable in all cases. The principal differences appear to be at low pressures, and an attempt has been made to modify the equation used for mass distribution to better represent the observed higher masses at low pressures. The previous calculations of debris velocities, based on the velocity of an unconstrained fragment, also appear to underestimate the velocity at low pressures, and a method has been proposed to rectify this, based on a combination of the velocity of the panel at the point of failure and the velocity of an unconstrained fragment.
  
- Criteria for human vulnerability to fragments. The glazing criterion based on skull fracture as the critical injury seems to predict high levels of fatality for relatively low fragment masses and velocities, particularly if skull fracture is taken to imply 100% fatality. By contrast, the criterion based on skin penetration requires much higher velocities for fatality, which do not seem to be consistent with the velocities required for skull fracture. It is important to select a criterion which best represents reality, based on historical and/or experimental data where available. A combined approach has been derived which makes use of the relative areas of the head and the body, and the fragment spatial density arising from the failed window. This takes no account of any protection that may be offered to the body by clothing. Further searches of the literature have been undertaken.

# Figure 4.1: Comparison of Glazing Velocities



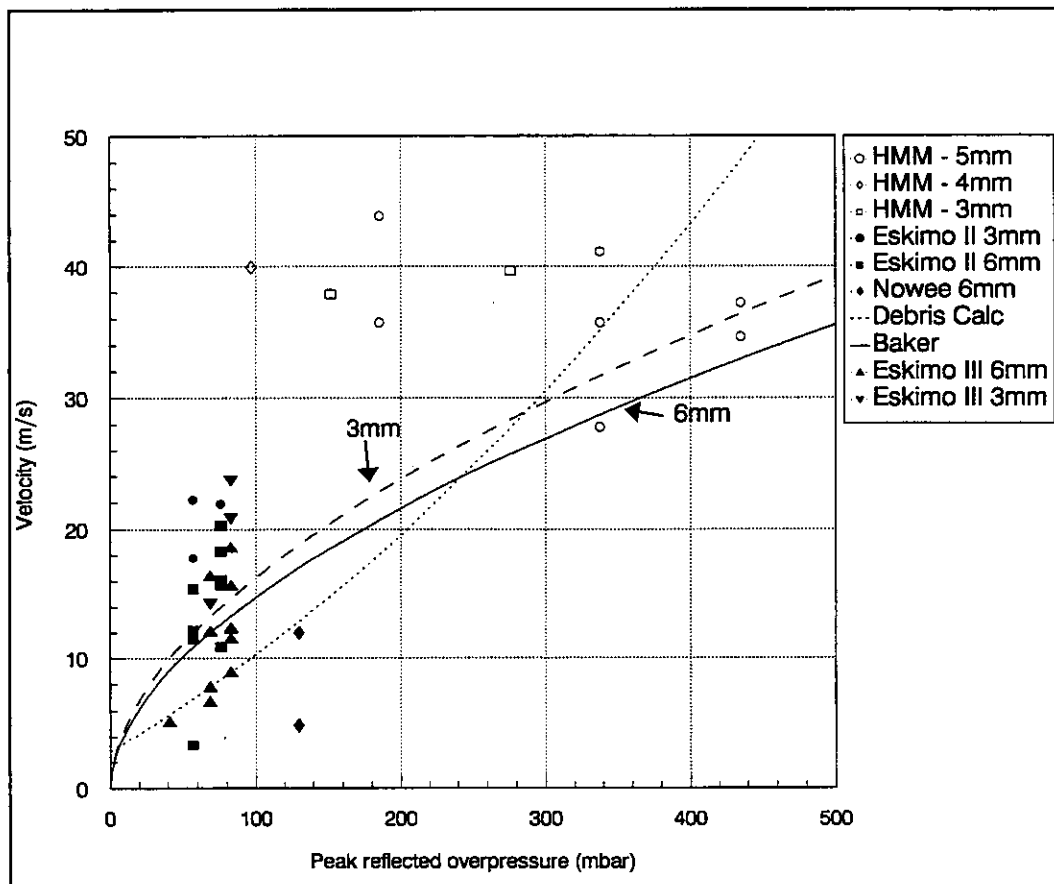


**Figure 4.2 Comparison of Baker Prediction against Experimental Data**



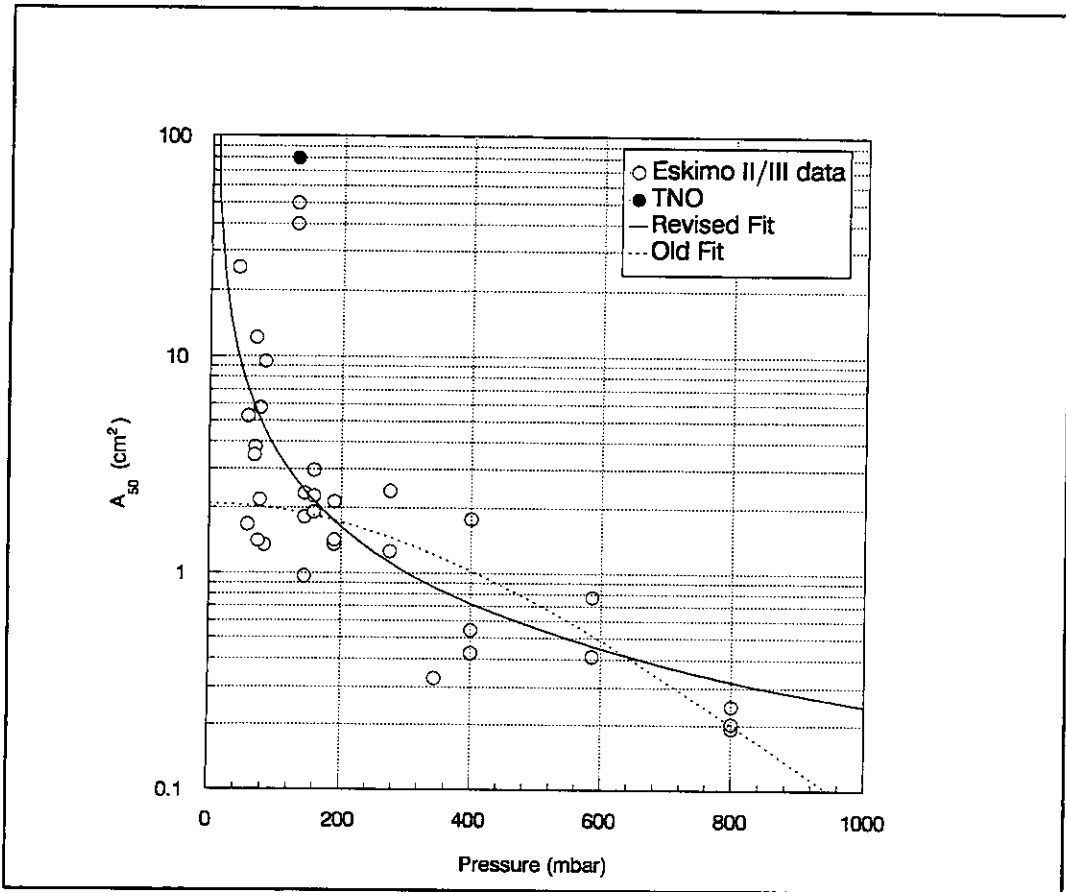


**Figure 4.3 Curve Fit to Mass Distribution Data**

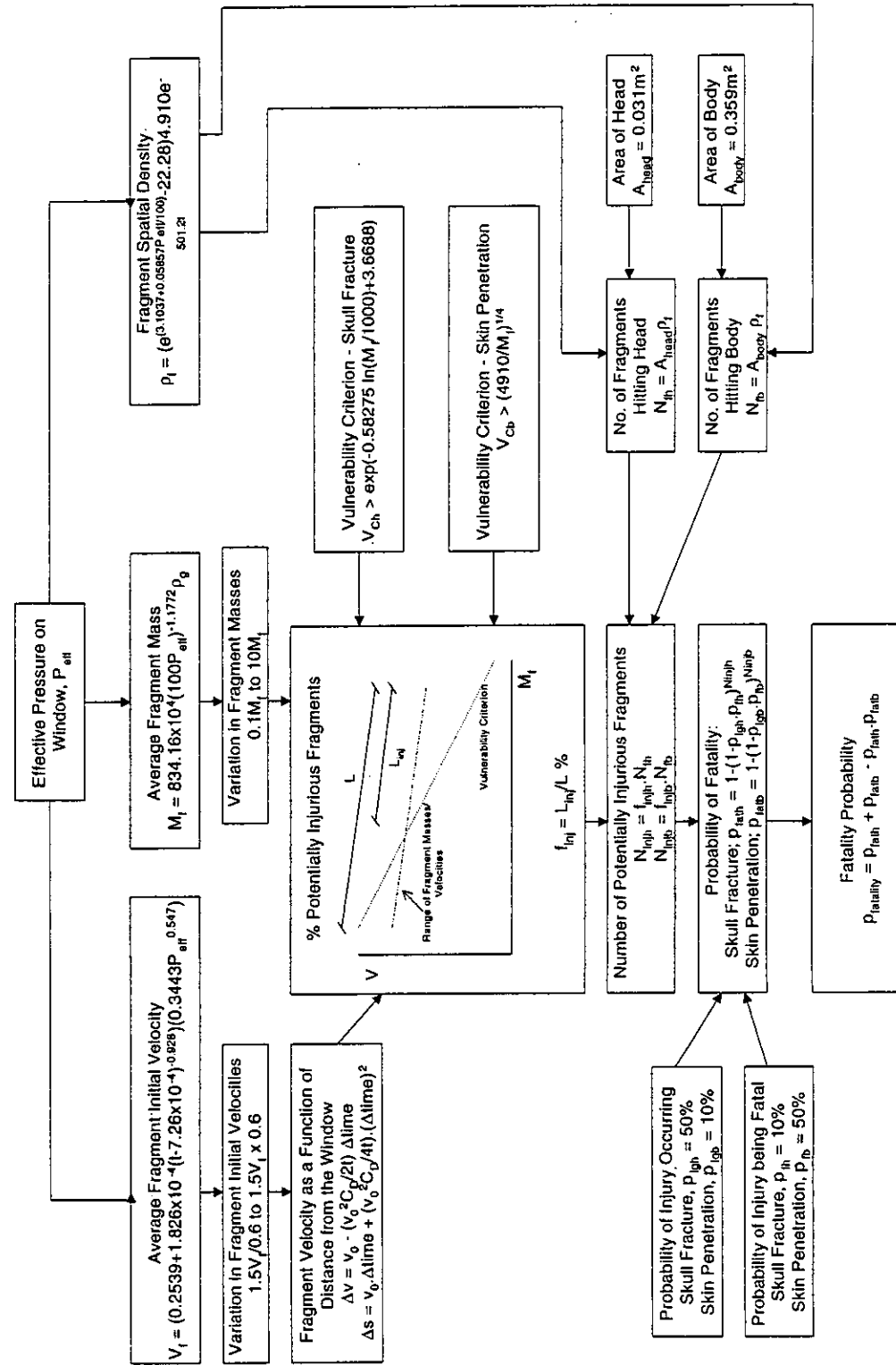


Figure 4.4: Methodology for Calculation of Fatality Probability due to Glazing Fragment Impact

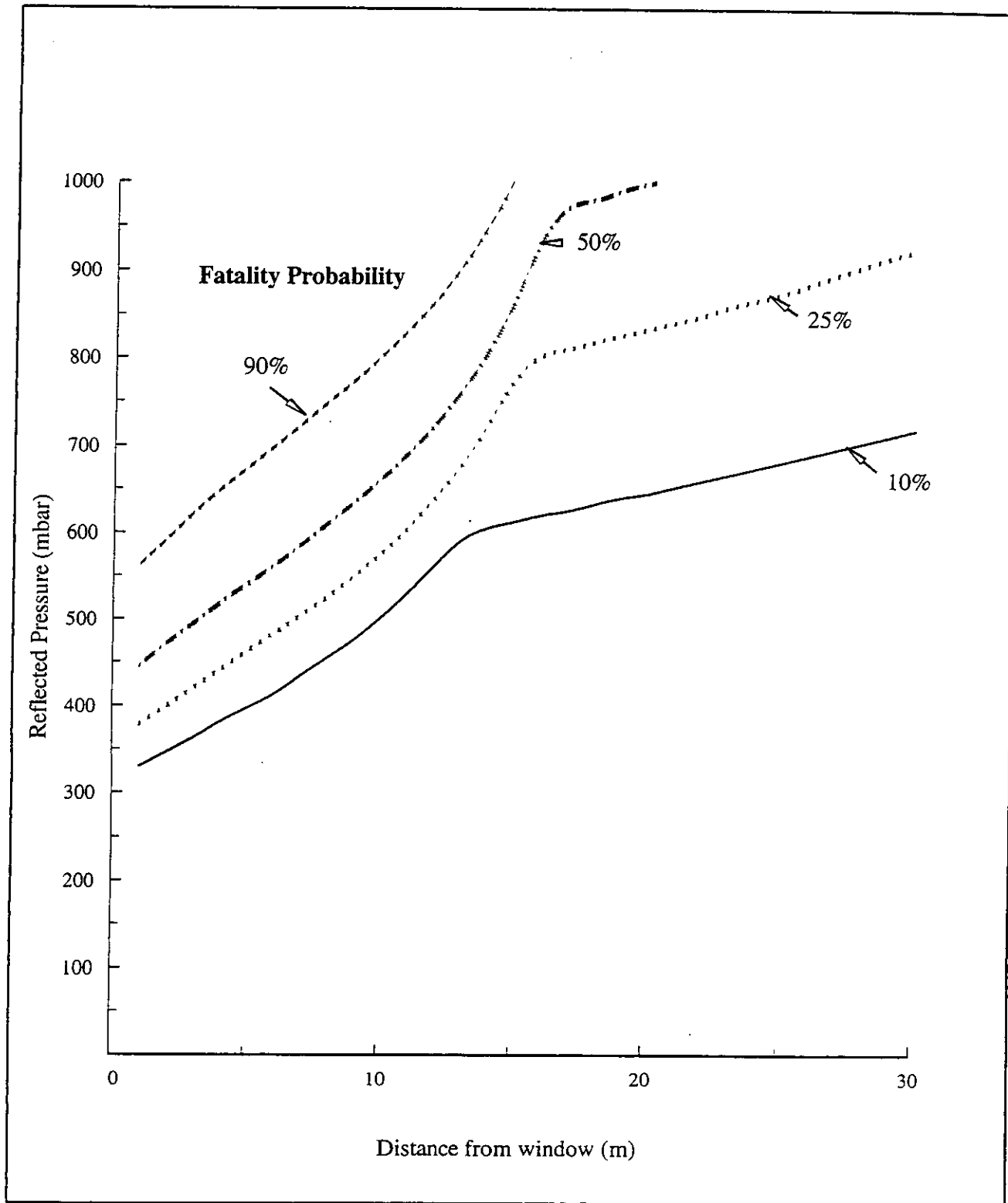


Figure 4.5: Glazing Fatality Curves

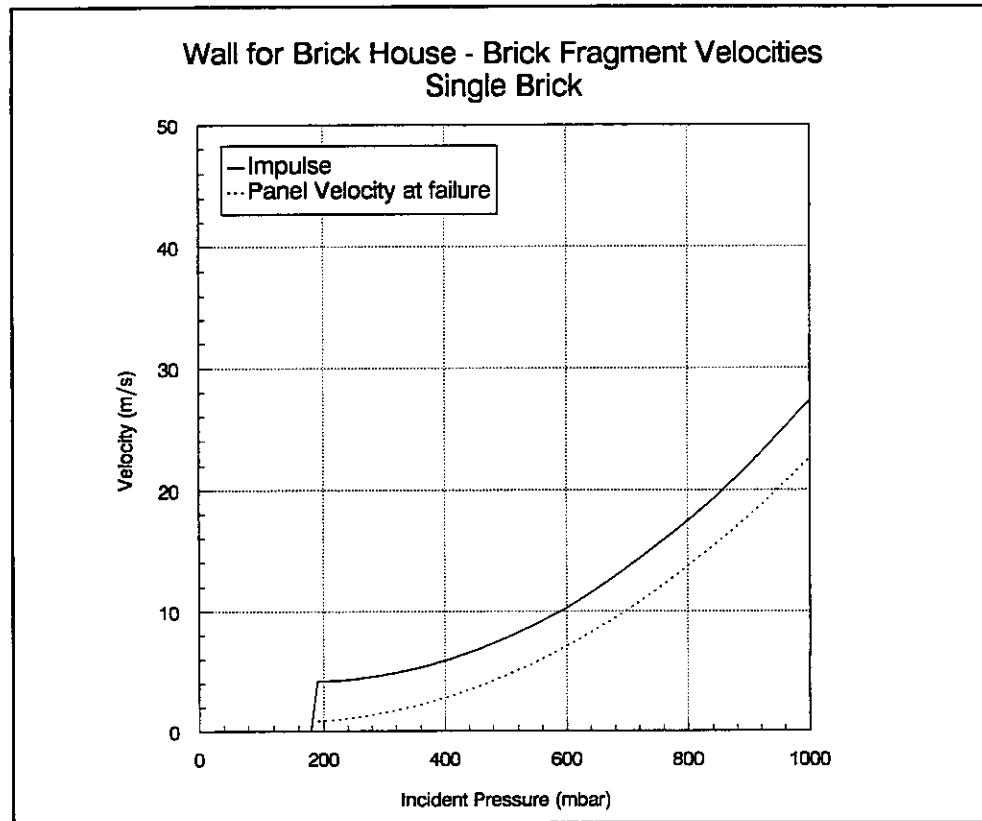
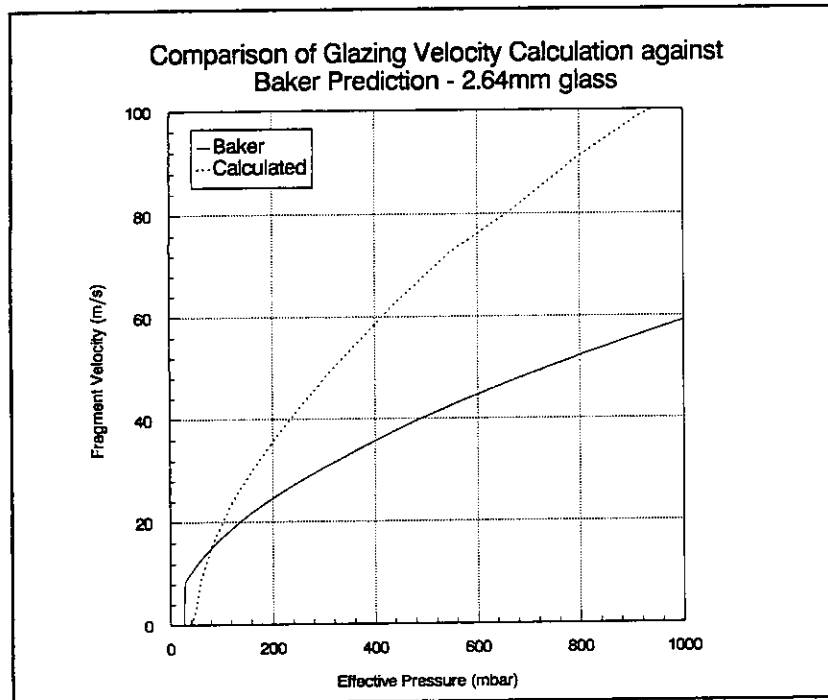
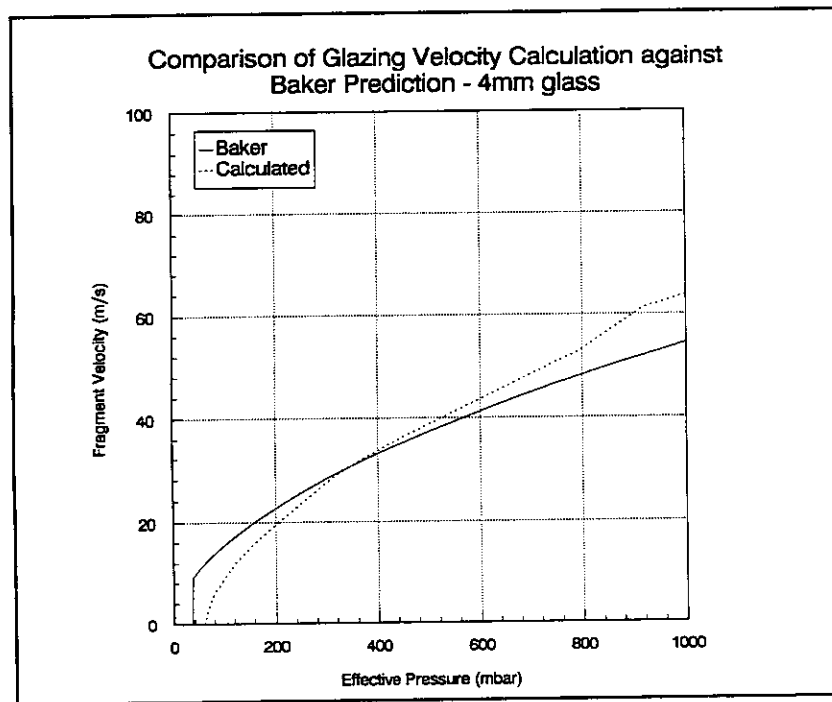


Figure 4.6 Brick Fragment Velocities

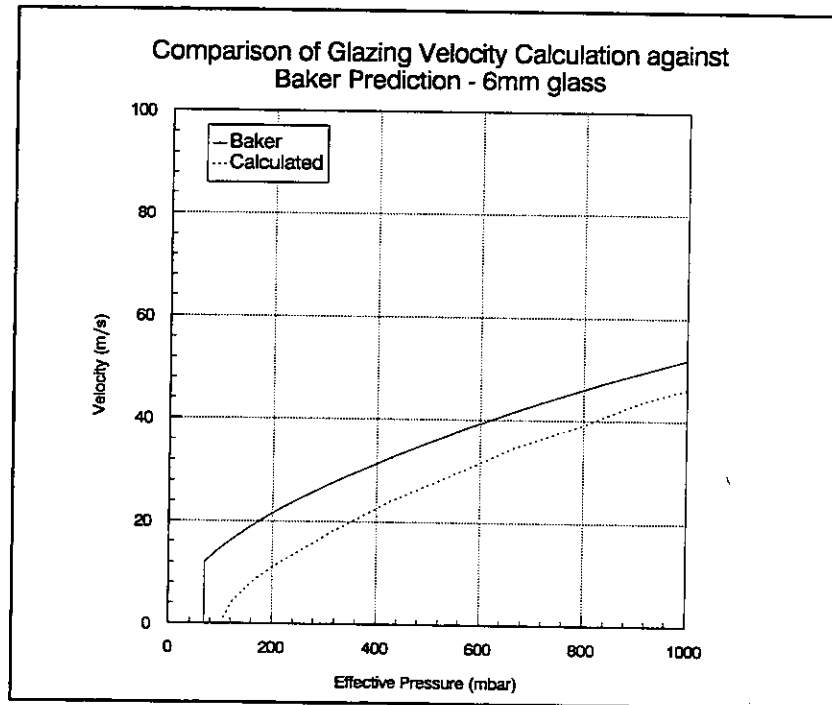


a) Glass Window Fragment Velocities: 2.64mm glass



b) Glass Window Fragment Velocities: 4mm glass

**Figure 4.7 Glass Window Fragment Velocities**



c) Glass Window Fragment Velocities: 6.0mm glass

Figure 4.7 (cont'd) Glass Window Fragment Velocities

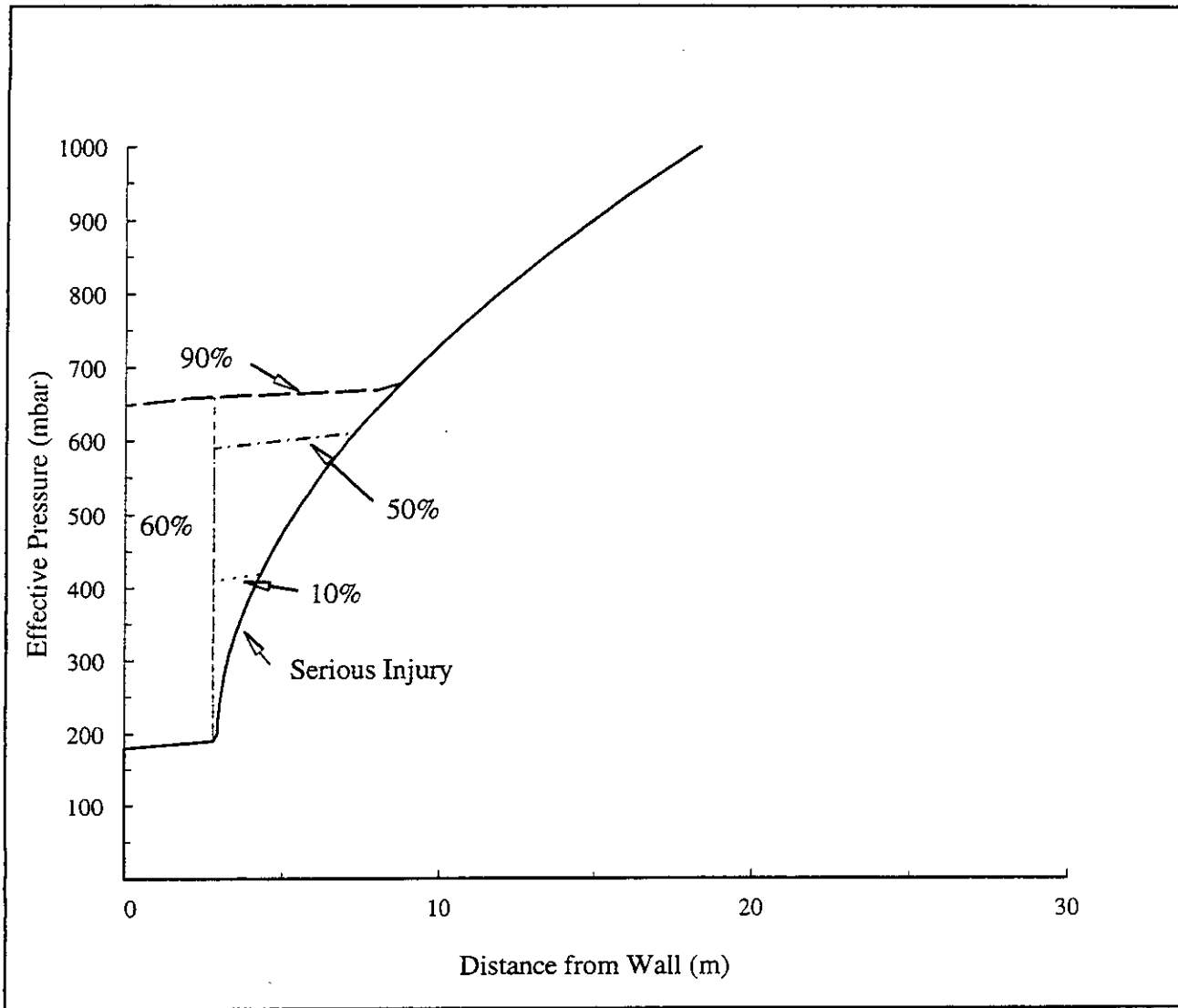


**Figure 4.8: Fatalities range for Brickwork (Shock Pulse)**

## 5 ASSESSMENT OF OCCUPANT FATALITY PROBABILITY

The methodology derived in Phase 1 and revised during the course of Phases 2 and 3 has been applied to two typical building types in order to assess the fatality probability under blast loading. Each building type has been assessed for two different orientations, i.e. long side and short side facing the blast, and two different pulse shapes, i.e. a shock pulse and a pressure pulse, both of varying peak overpressure, but 0.1s duration.

The buildings assessed are as follows:

- Brick-built house: a 1930s semi-detached brick house, as described in Section 3.1 was assessed. The overall dimensions of this building are 14.0m x 8.6m with a maximum height of 8.0m.
- Concrete Framed Office Building: the braced frame building described in Section 3.2.1 was assessed. This is a 4 storey office building with overall dimensions 40m x 14m x 16m high

The assessment of fatality probability has incorporated the effects of front face glazing failure and rear face pressure relief, but the negative phase of the pulse has not been included.

The fatality probability assessments are described below, and a diagram illustrating the approach is presented in Figure 5.1.

### 5.1 Brick building type

In order to make an assessment of the brick building, several assumptions have to be made concerning the building orientation and internal layout, the glazing and brickwork failure pressures and the fatality probability on collapse. First, it has been assumed that the building corresponds to the layout shown in Figures 3.1 - 3.3, with the exception that one of the windows on the short side of the building has been removed to ensure that there is no overlap between the fatality probability due to glazing impact from the two different directions. This is purely a simplifying assumption for the purposes of these calculations. The internal walls are assumed to provide a barrier to glazing and debris from the external walls, but are not considered in any other way i.e. they do not contribute to internal debris, nor do they affect the internal pressure build up. The orientation of the building has been chosen to provide the worst fatality scenario. In this case, if the long side faces the blast, the rooms are longer at the rear of the building, so for glazing failure and debris, there is a greater range possible at the rear. Thus the building has been orientated so that the rear



faces the blast. For the side-on orientation, the building is symmetrical, so the choice of orientation is immaterial.

The failure sequence proposed is as follows:

- Front face glazing fails at an effective front-face pressure (i.e. reflected pressure for a shock pulse or incident plus dynamic pressure for a pressure pulse) of 69 mbar. This value comes from Mainstone (1971) for a pane size of 1.25 x 1.025m, 4mm thick, and a pulse duration of 100ms.

The glazing failure enables pressure to build up within the building and relieve the pressure on the external walls. The probability of failure due to glazing failure starts to increase in the front rooms.

- Front face wall fails at a reflected pressure of 407 mbar for a shock pulse and a resultant differential pressure (i.e. front face pressure minus the internal pressure) of 320mbar for a pressure pulse. These values are based on the debris velocity calculations which include an assessment of the dynamic failure pressure of the wall based on its static failure pressure and dynamic characteristics.

Front face wall failure causes the rate of internal pressure rise to increase, and causes an increase in fatality probability due to debris impact in the front rooms.

- Side and rear wall glazing fails when the differential pressure across the rear wall reaches 69 mbar.

It is assumed that the pressure at the sides is the same as that at the rear. The differential pressure is the rear face pressure less the internal pressure in the building. An increase in fatality probability due to glazing impact occurs in the rear and side rooms. Side and rear wall glazing failure is assumed not to affect the internal pressure.

- Side and rear walls fail when the differential pressure across the rear wall reaches 320 mbar. This is the same for both incident shock and pressure pulses as the rear face pressure in both cases resembles a pressure pulse.

All the walls are assumed to fail at the same time. If the walls fail, the building occupants become vulnerable both to debris from the walls and building collapse. In this case, the probability of fatality due to collapse is assumed to be 60%, based on earthquake data and the likelihood of rapid emergency service response in the case of an accidental explosion.

- Global building collapse occurs at an effective front-face pressure between 495 mbar and 1100 mbar, dependent on the building orientation and pulse shape, if the rear and side walls have not already collapsed.

The potential for overlapping areas of fatality probability have been included such that occupants cannot be 'killed twice'. In addition, the direction of the resultant pressure across the walls has been taken into account, such that if the windows or walls are blown outwards by the internal pressure, the occupants of the building are not vulnerable to the glazing fragments or debris generated.

Four fatality probability curves are presented in Figures 5.1 to 5.4, corresponding to different building orientations and incident pressure pulse shapes.

Figure 5.1 shows the calculated fatality probability for a shock pulse incident on the short side of the building. The dotted line shows the glazing fatality probability, the dashed line shows the probability of fatality due to debris impact and the dash-dot line shows the probability of fatality due to collapse. The solid line is the overall combined fatality probability. It should be noted that the ordinate axis is peak incident overpressure, but for the shock pulse this is reflected, so the pressure experienced by the front face is considerably higher. As can be seen from the figure, for this orientation the probability of fatality due to glazing impact is very low, and the overall value is dominated more by debris and building collapse. This is primarily because there is very little glazing on the short side of the building to give rise to glazing hazard. The long sides have a lot more glazing, but the failure sequence is such that the front wall fails before the side wall glazing: this gives rise to a higher pressure inside the building than outside, and the model predicts that the side wall glazing is blown out of the building. This does not therefore contribute to the probability of fatality of the occupants. Similarly, if the walls fail, they are assumed to only contribute to the debris hazard if they are blown inwards. In this case, side wall failure occurs at an incident pressure of  $\sim 500$ mbar, but there is no increase in the debris fatality probability, which implies that again, the walls are being blown out, not in. The building is assumed to have collapsed once all four walls have failed. In this case, the walls collapse at an incident overpressure of  $\sim 490$ mbar, and 60% fatality probability is assumed.

The model prediction that walls or glazing debris could be projected outwards instead of inwards is thought to represent a real effect that has been observed experimentally by some workers [21].

Figure 5.2 shows the results for a shock pulse incident on the long side of the building. In this case the glazing and debris effects are higher because the front-face area presented to the blast is greater, and this is reflected in the overall fatality probability. In particular, the amount of glazing on the long faces gives rise to a much higher glazing hazard, although again, this is only due to front face glazing, as the rear face glazing and walls are blown out of the building.

For an incident pressure pulse, the results are slightly different, primarily because there is a much smaller pressure differential between the front and rear faces of the building, and hence failure tends to occur on all four walls at the same time. Consequently in Figures 5.3 and 5.4, the onset of debris fatality probability corresponds very closely to the building collapse, and a large step is seen in the overall fatality probability. For the short side facing the blast, a peak is seen in the probability of fatality due to glazing at 400mbar. This is because at pressures lower than this, the differential pressure across the side and rear walls is such that the windows are blown into the building once they have failed, whereas at higher pressures the windows are blown out of the building and the hazard level drops. This is also seen in the probability of fatality due to debris for the long side facing the pressure pulse (Figure 5.4), at pressures in excess of 600mbar.

## **5.2 Concrete framed building**

In a similar manner to the assessment of the brick building, assumptions have to be made concerning specific details of the concrete framed building in order to allow an assessment of the occupant fatality probability. The building geometry is assumed to correspond to that shown in Figure 3.4. The end walls are assumed to have no glazing. 90% of the perimeter length and 50% of the external area on the side walls has been assumed to be glazed. The failure pressure of the glazing has been assumed to be somewhat higher than that for the house, at 105 mbar, based on a slightly smaller pane size than used in the house and double glazed bonded units, but the failure pressure of the cladding has been assumed to be the same as the house. It has been assumed to be an open plan structure, such that the only impediments to debris are the external walls themselves, although in order to simplify the calculations it has been assumed that if the short side is facing the blast the glazing cannot travel further than half-way through the building. This is because for this orientation the glazing will be coming in an equal amount from each side of the building; ignoring the overlap makes the calculations much simpler and is only slightly non-conservative.

The failure sequence proposed is as follows:

- Front face glazing fails at an effective front-face pressure of 105 mbar.

This enables pressure to build up within the building and relieve the pressure on the external walls. Glazing hazard occurs up to a maximum range defined by the length of the building.

- Front face wall fails at a resultant differential pressure of 407 mbar for a shock pulse and 320mbar for a pressure pulse.

This causes the rate of internal pressure rise to increase, and causes some debris hazard again up to a maximum range defined as above.

- Side and rear wall glazing fails when the differential pressure across the rear wall reaches 105 mbar.

As for the brick building, it is assumed that the pressure at the sides is the same as that at the rear. The differential pressure is the rear face pressure less the internal pressure in the building. Glazing hazard occurs up to the maximum range. Side and rear wall glazing failure is assumed not to affect the internal pressure.

- Side and rear walls fail when the differential pressure across the rear wall reaches 320 mbar.

All the walls are assumed to fail at the same time. For such a long building, this is probably not a realistic assumption, but at present there is no way of estimating the travelling pressure along the long face. If the walls fail, the building occupants become vulnerable to debris from the walls.

- Building collapse starts to occur once the incident effective pressure reaches the dynamic failure pressure of the concrete columns. This has been assumed to be 1976 mbar based on the calculations in Section 3. If column failure occurs, it has been assumed that the front bay collapses, and for the purposes of this Phase, it has been assumed that 100% fatality probability occurs within that bay. For the pulse incident on the short side of the building, this corresponds to a fatality probability of 100% in 12.5% of the building, i.e. a collapse fatality probability of 12.5%. The corresponding figure for the long side facing the blast is 57%, assuming that the longer of the two bays is the one that collapses.

The potential for overlapping hazard areas has again been taken into account such that occupants cannot be 'killed twice'. This is particularly important for such an 'open plan' arrangement. In addition, the direction of the resultant pressure across the walls has been taken into account, such that if the windows or walls are blown outwards by the internal pressure, the occupants of the building are not vulnerable to the glazing fragments or debris generated.

The four calculated fatality probability curves are presented in Figures 5.5 to 5.8. As for the brick building assessment, the overall fatality probabilities are highly dependent on the direction of the resultant pressure across the rear and side walls. This is highlighted in Figure 5.5 which shows the effect of an incident shock pulse on the short side of the building. For such a highly glazed and open building, it would be expected that the fatality probability would be dominated by glazing effects. However, as there is no glazing on the short side of the building, this is not the case, and the glazing fatality probability for this orientation is actually zero. Although the glazing fails at a fairly low pressure, it does not start to be hazardous until a much higher pressure. Before this

higher pressure is reached on the sides of the building, the front face fails, and the internal pressure starts to increase. Thus the glass starts to be blown outwards, before it reaches a sufficiently high inwards velocity to cause injury. The overall fatality probability for this orientation is thus dominated by the debris hazard. The onset of fatality probability due to debris is at  $\sim 200$ mbar, when the front wall starts to fail. The fatality probability is initially flat, representing the vulnerability of occupants in the region directly behind the wall. As the pressure increases, however, the velocity of the debris increases and the fatality probability starts to increase. The side walls start to fail at  $\sim 400$ mbar, and a corresponding increase in fatality probability is observed. The directional effect of the resultant pressure is visible in the debris curve at 900mbar, with the sudden drop being attributable to a change in the direction of failure of the walls. Collapse of the building plays a small part in the overall curve at high pressures: in this case, collapse is assumed to be progressive, with only a small proportion of the frame collapsing (12.5%), as outlined above.

With the long side facing the pulse (Figure 5.6), the glazing curve is dominant, with the fatality probability reaching  $\sim 80\%$  at 400mbar. For this orientation, and these building dimensions, the direction of the pressure across the rear and side walls is almost immaterial, as the curves are dominated by glazing and debris from the front face. Although the side and rear walls are blown outwards, the front face glazing and debris on their own lead to a very fatality probability level. Intuitively this is sensible, as with the long side facing the blast, the maximum distance of building occupants from the failed window or wall is just 14m as opposed to 40m for the blast incident on the short side of the building. Collapse for this orientation results in a higher degree of fatality probability, as outlined above.

These two plots indicate the importance of the orientation of the building with respect to the incident pulse. The same is also true for an incident pressure pulse (Figures 5.7 and 5.8). Again, for the pulse incident on the short side of the building, glazing does not contribute to the overall fatality probability, and only the debris is important. The debris fatality probabilities show similar characteristics to those observed for the incident shock pulse, although generally at slightly higher pressures due to the fact that reflection has not been considered for the pressure pulse. Column collapse also does not occur at the pressures under consideration. With the long side of the building facing the pulse, the fatality probability is again dominated by the glazing hazard, although the onset of the probability of fatality is at a higher pressure due to the assumed effective lack of reflection of the pressure pulse.

### **5.3 Comparison with other models/methods**

Figure 5.9 shows a comparison of the fatality probability curves for the brick house together with data from Jarrett [9] and military data from Hewkin [5]. The Hewkin data is a summary of data from accidental and military explosions

and is not solely for brick buildings. The Jarrett data actually relate to building damage, and occupant fatality probabilities have been inferred from the damage description. Also shown are the current API guidelines for a brick building [24]: It should be noted that the pulse shapes used in this document correspond approximately to those for an explosion equivalent to 3 tonne propane based on curve 7 of the TNO multi-energy method.

As can be seen from the figure, at high pressures, i.e. close to the source of the explosion, the calculated curves for a shock pulse on a brick building predict very similar fatality probabilities to those predicted by models based on historical data. It is also clear that the API guidelines are highly conservative. It appears that the methodology used in this assessment leads to appropriate fatality probability levels, at least for brick buildings.

#### **5.4 Conclusions**

The fatality probability curves for both building types have been shown to be highly dependent on the resultant pressure across the building walls, and in particular to the direction of that pressure i.e. inwards or outwards. This seems to be a reasonable deduction, as experimental data show that external explosions can result in walls being blown outwards. This is confirmed in the work by Mercx, Weerheijm and Verhagen [21], in which a series of experiments were performed to investigate the effect of openings in a structure on the blast load. They reported loads directed outwards from the chamber, and corresponding walls falling outwards on full-scale tests on houses. The calculations of external and internal pressure in the model presented here are quite simplistic, in that the internal pressure in this model is based on the average pressure build up within a box, and the external pressure calculations assume that the pressure reaches a peak on the side walls at the same time as the rear walls. However, these two simplifications are consistent with each other, and ensure that the average effect is consistent.

The results for different building orientations are quite different, particularly when there are different quantities of glazing on the different faces of the building. It is clearly important to take building orientation into account when calculating generic building fatality probability curves. When large quantities of glazing are present, the glazing fatality probability dominates the overall fatality probability curve, a factor which needs to be studied closely when looking at modern office buildings which tend to be very highly glazed. It may be that the tougher glass used in these building types will reduce the probability of fatality.

The assessment for the brick building has been compared against alternative models proposed by Hewkin and Jarrett. The methodology does not predict 100% fatality probability at high pressures, primarily because this assessment is based on purely structural considerations, and at the very high pressures, alternative human biological factors need to be taken into account such as lung

failure due to direct blast effects. However, it does appear to give a reasonable agreement for lower and mid-range pressures. Thus the agreement with the alternative models is sufficiently good to provide some confidence in the methodology used.

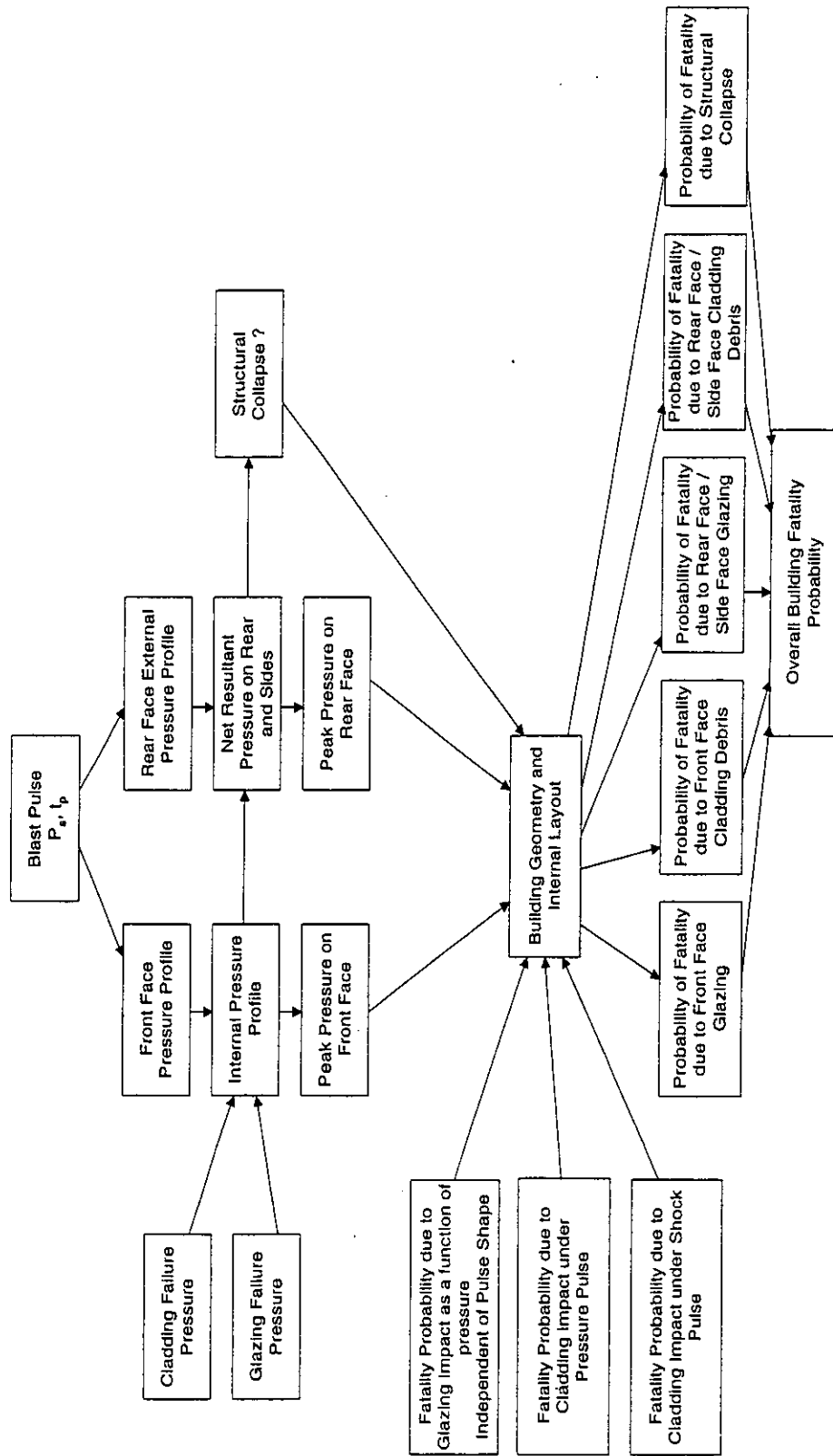


Figure 5.1: Methodology for Global Building Fatality Probability Calculations



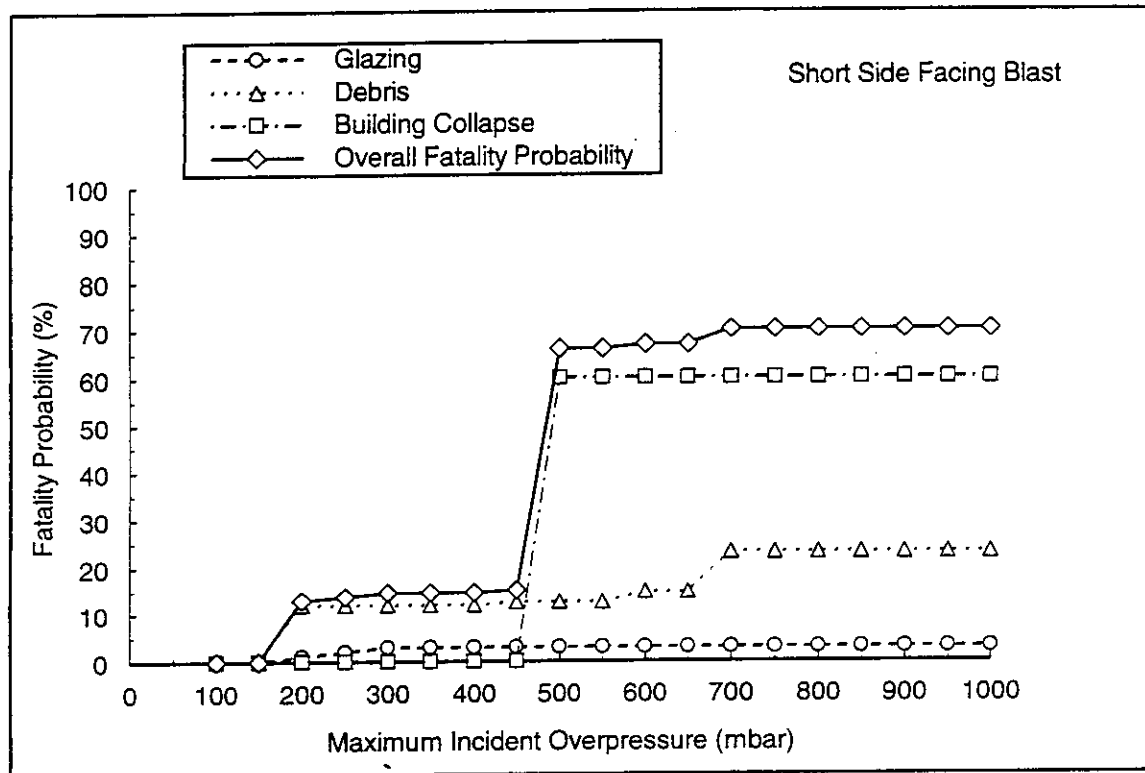


Figure 5.2 Fatality Probability Curve: Brick Building, Short Side Facing, Shock Pulse

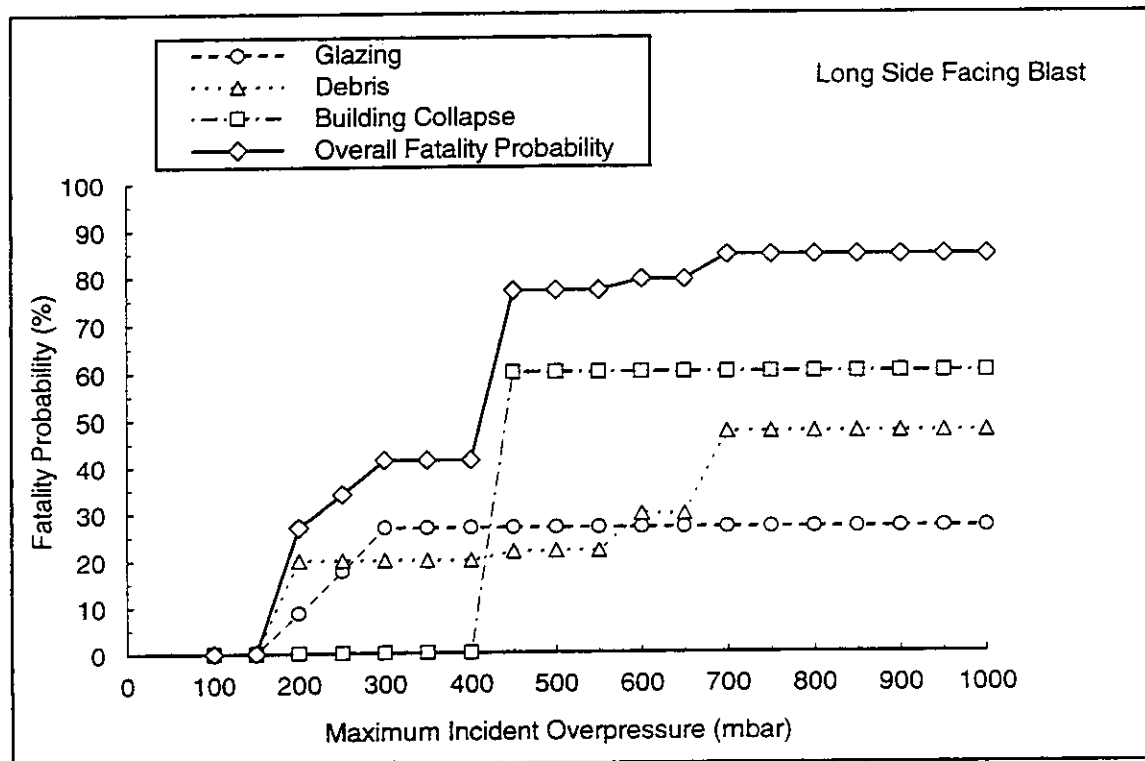


Figure 5.3 Fatality Probability Curve: Brick Building, Long Side Facing, Shock Pulse

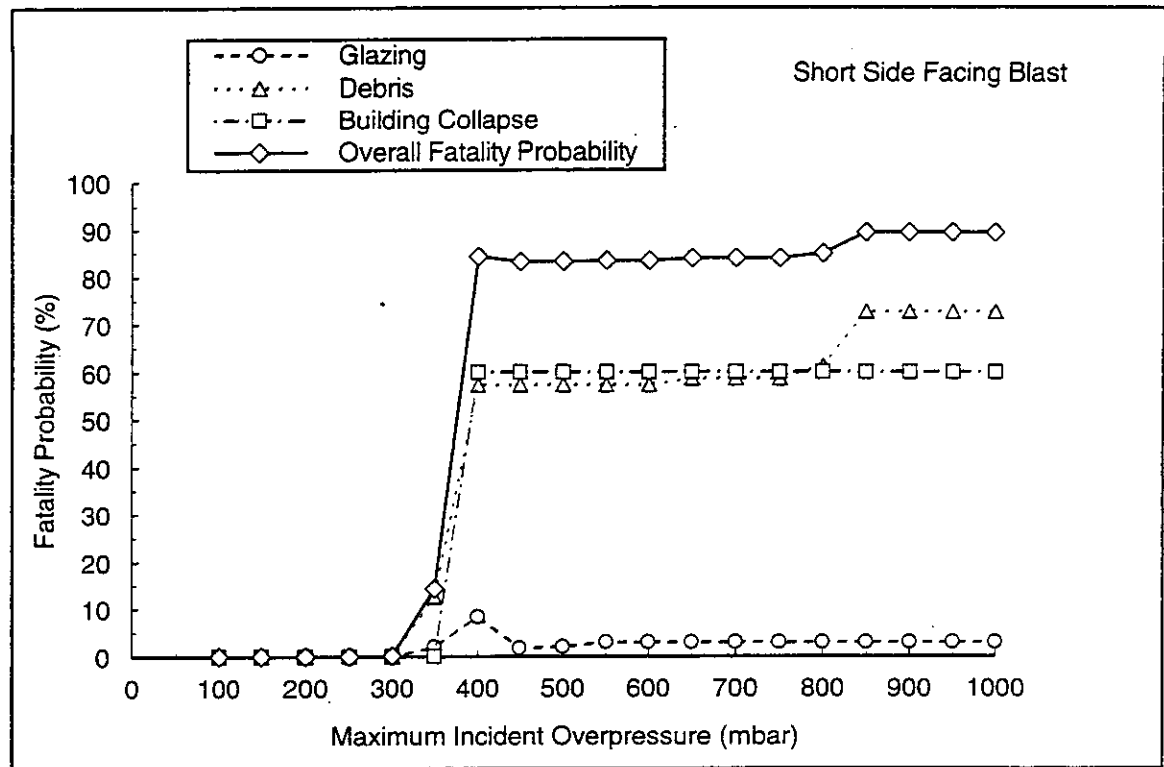


Figure 5.4 Fatality Probability Curve: Brick Building, Short Side Facing, Pressure Pulse

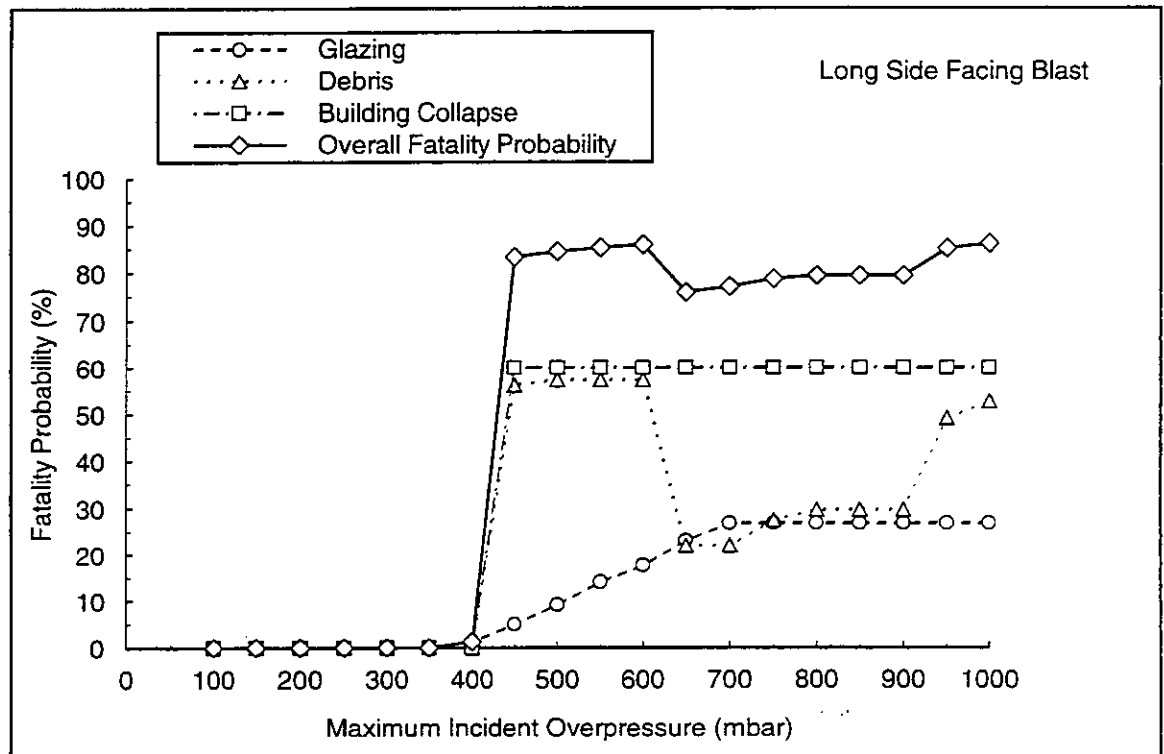


Figure 5.5 Fatality Probability Curve: Brick Building, Long Side Facing, Pressure Pulse

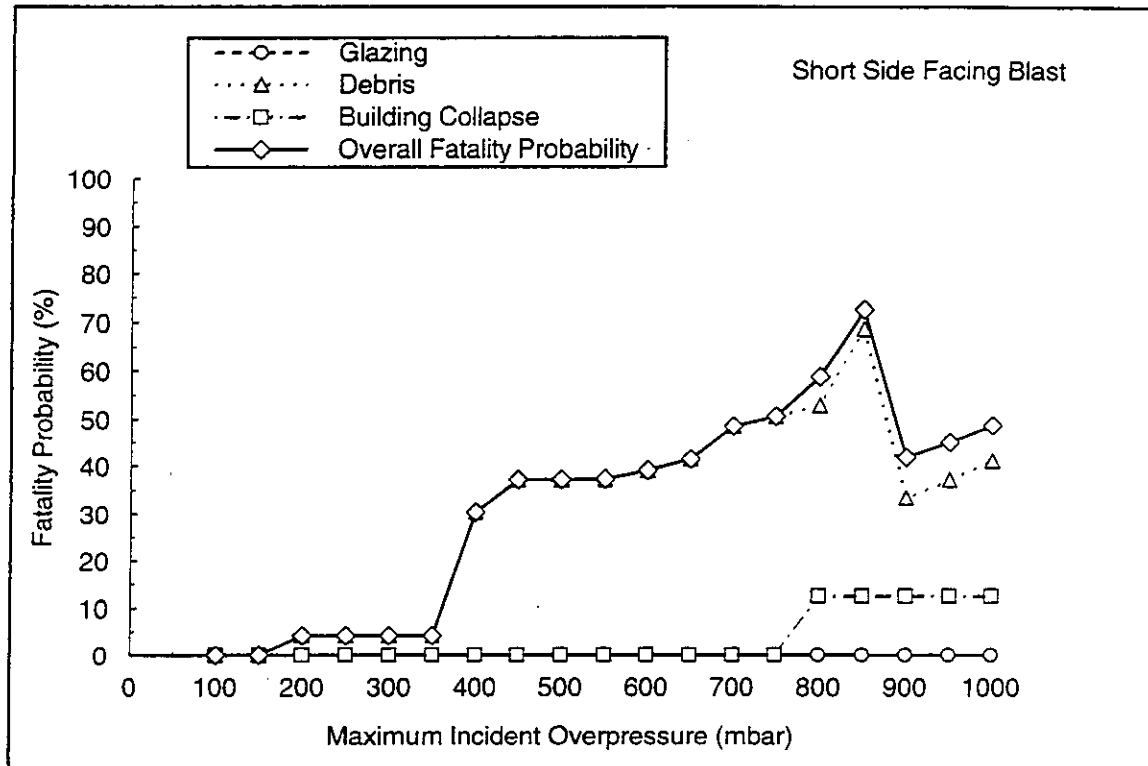


Figure 5.6 Fatality Probability Curve: Concrete Building, Short Side Facing, Shock Pulse

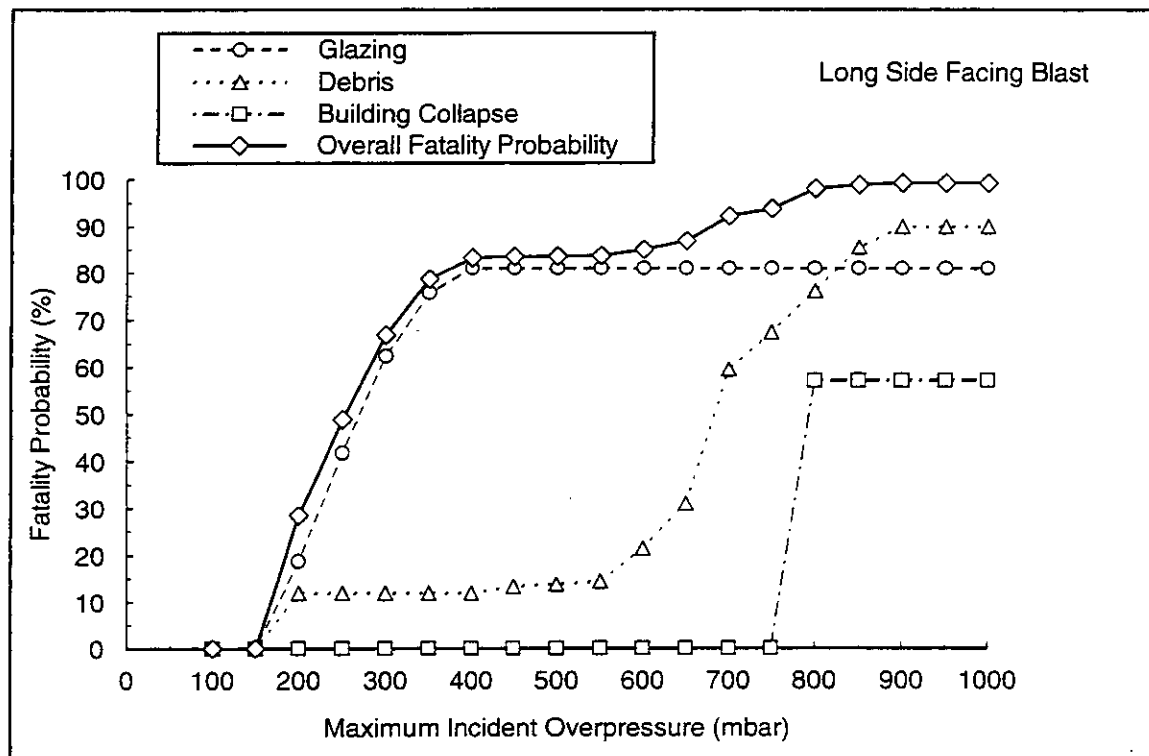


Figure 5.7 Fatality Probability Curve: Concrete Building, Long Side Facing, Shock Pulse

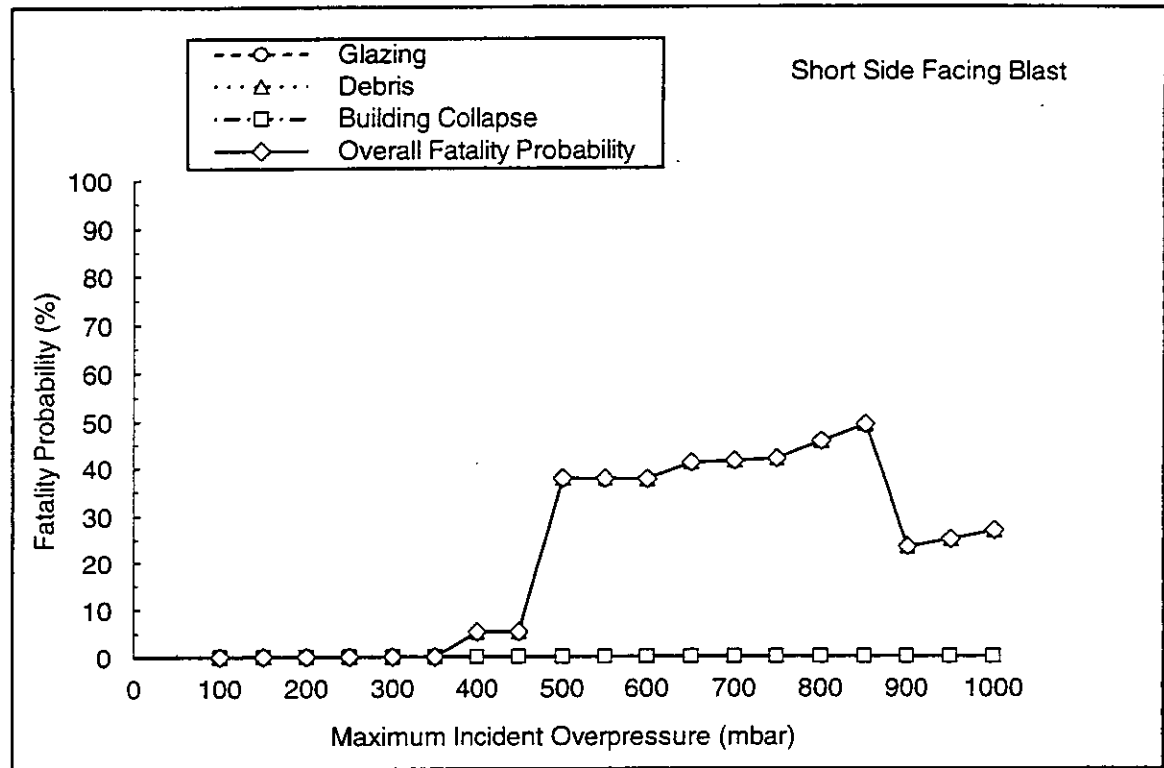


Figure 5.8 Fatality Probability Curve: Concrete Building, Short Side Facing, Pressure Pulse

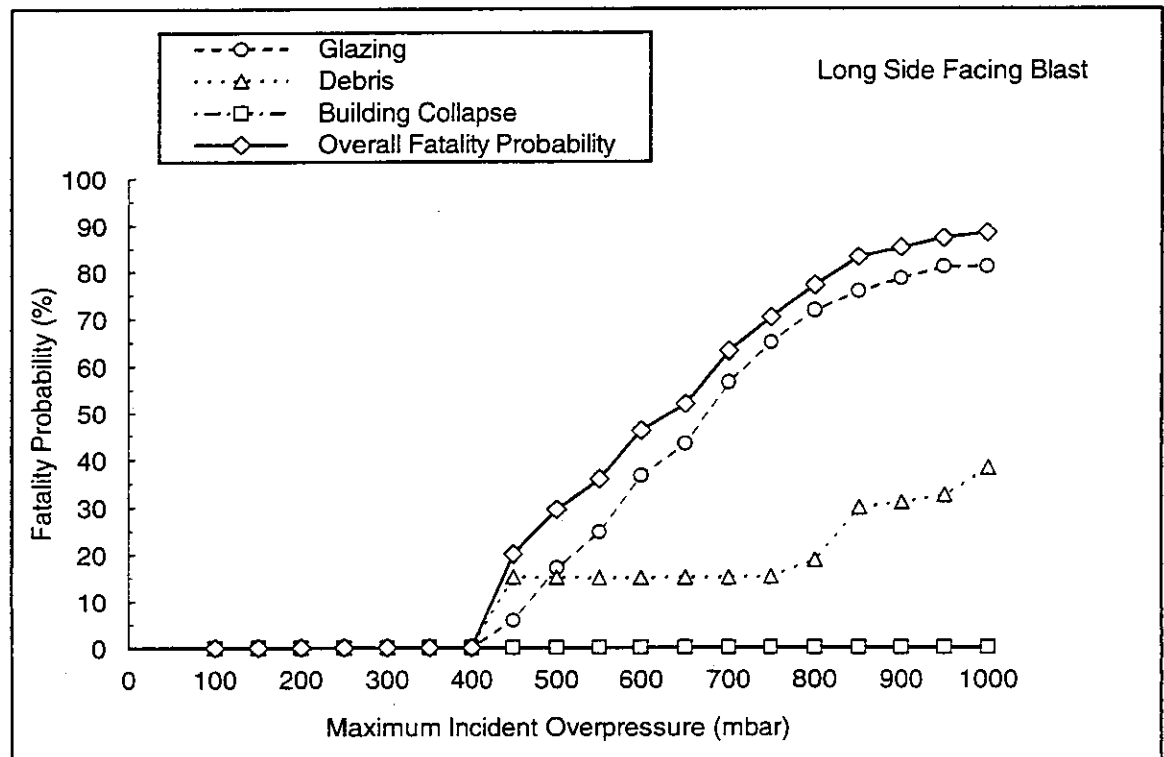
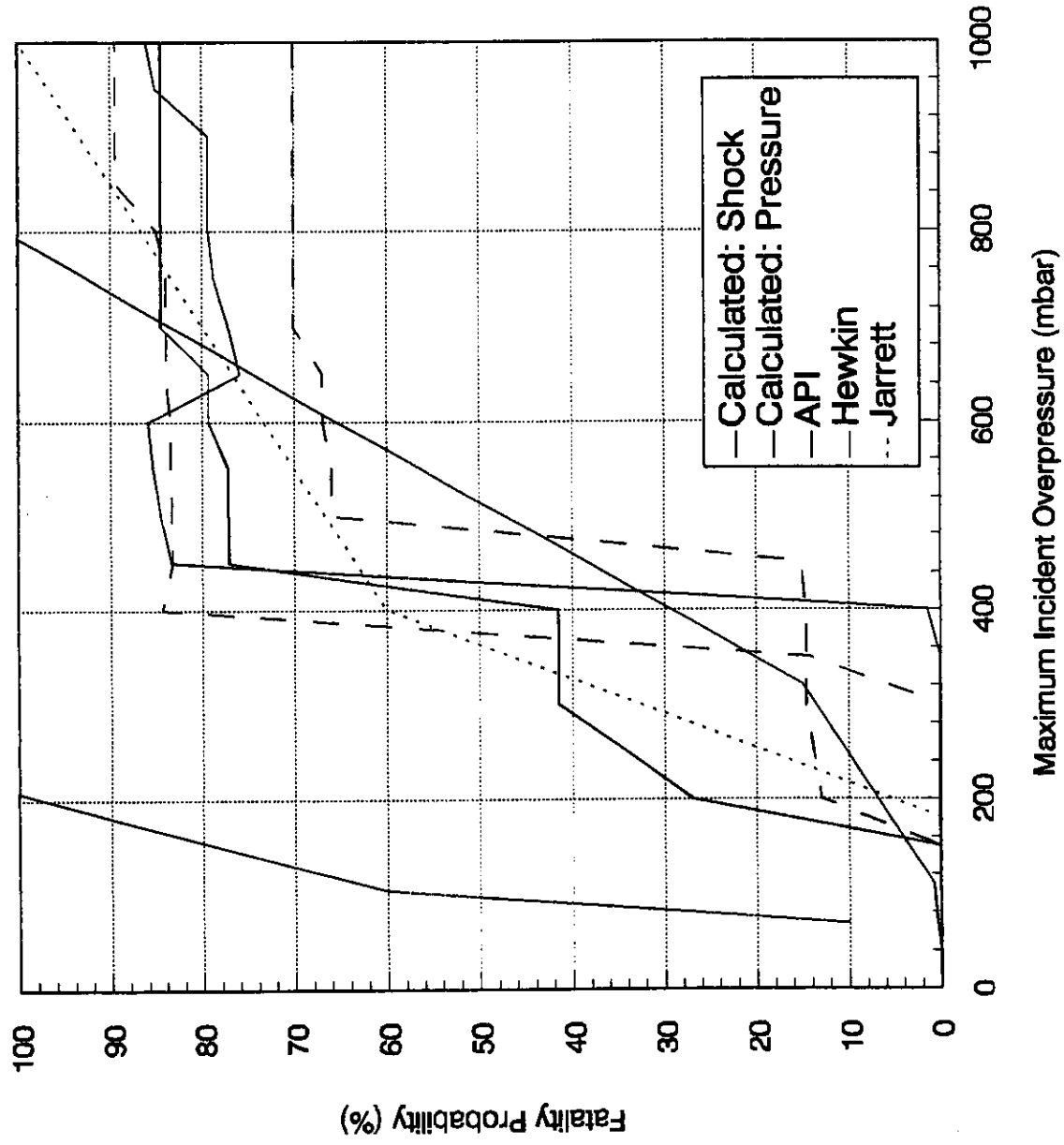


Figure 5.9 Fatality Probability Curve: Concrete Building, Long Side Facing, Pressure Pulse

Figure 5.10 Fatality Probability Curves  
 Comparison of Brick Building Curves against Other Models



## 6 CONCLUSIONS AND RECOMMENDATIONS

Phases 2 and 3 have concentrated on further developing the methodology for assessing the probability of fatality of building occupants, and on applying the methodology to two typical building types.

A lack of information has been identified concerning the reflection characteristics of pulse shapes other than the pure shock or the pure pressure pulse. While the shape of the pulse at intermediate distances is recognised to be 'partially shocked', no method for quantifying the shape or the reflection characteristics has been identified. It has been shown to be conservative to assume that for intermediate shapes the pulse is a shock pulse which is fully reflected from the front face of the building. The negative phase of the pulse has also been shown to be important, although the effect is dependent on the building aspect ratio, and for some cases, it is conservative to ignore it. However, it is possible that the negative phase may reinforce the effects of the load on the rear face, and can generate displacements which are greater in the negative direction than in the positive direction. This needs to be considered carefully in calculating the collapse load of the structure.

The methodology for predicting building response has been tested for sensitivity to the shape of the incident blast pulse, the effect of glazing failure, and the effects of rear face pressure relief. Individually, pressure relief due to glazing/cladding failure and due to pressure on the rear face both affect the overall response of the building, but the extent of the effect is dependent on the building geometry and its orientation with respect to the blast load. The effect on overall response of pressure relief due to glazing failure appears to be less noticeable for a pressure pulse than a shock pulse, as for an incident pressure pulse the calculated internal pressure shows a similar profile to the external pressure, and the resultant force on the building is not significantly different from that for zero vent area. Rear face pressure relief is dependent on the building length; if the length is greater than a certain value, such that the time taken for the pulse to reach the rear face is greater than the duration of the incident pulse, then the rear face pressure does not serve to reduce the load experienced at the front face. The combination of the two effects is most important from the point of view of occupant fatality probability, as failure of the side and rear walls of a building has been assumed to be a function of the differential pressure across the wall.

The methods for estimating the variation of the mean glazing fragment velocity distribution with pressure have been investigated. The Baker equation appears to represent a realistic prediction of velocity distribution for glazing, although it would be useful to obtain more experimental data. A comparison of the Baker prediction against the velocities calculated by assuming that all of the incident impulse is transmitted to the fragment and those predicted by considering the velocity of an unconstrained fragment, reveals that the Baker curve lies between the two extremes: at pressures close to failure, the impulse

calculation is close to the Baker prediction, while at high pressures the unconstrained fragment approach appears to be more appropriate. Consequently, a combined approach has been developed to predict debris velocities: whereas previously the unconstrained fragment approach has been used on its own, this has now been combined with the velocity of the panel at the point of failure to produce an appropriate velocity profile.

The mean glazing fragment mass predicted by Baker appears to be low for low incident pressures when compared against experimental data other than that on which the equations were based. The curve has been modified to try and improve the approximation at low pressures, by fitting a curve to the experimental data, including the data which were measured after the curve presented in Baker had been derived. This produces slightly higher masses at low pressures, but it is acknowledged that some of the fragments observed in experiment are considerably larger than even this equation would predict. Consequently a range of mass-velocity pairs have been used for generating the fragment hazard curves, in order to try and identify the most hazardous combination.

Structural calculations have been performed for two typical building types to assess static and dynamic structural failure pressures. The building types selected were a typical brick-built semi-detached house, and a reinforced concrete framed office building. For each type, two different typical constructional techniques were assessed to gain some idea of the range of capacities possible. The two building types have then been assessed in terms of occupant fatality probability. A combined glazing fatality probability criterion has been used based on the relative areas of the head and the body and the estimated fragment density distribution.

When subject to a shock pulse, the brick building showed lower levels of fatality than the concrete building, principally due to the greater extent of glazing in the concrete building. The response to the different pulse shapes has been shown to be highly dependent on the rates of pressure build up on the inside and outside of the building, which in turn is dependent on the building dimensions, glazing characteristics and orientation. It is thus necessary to consider all possible orientations in order to derive a generic curve for a specific building type.

The calculated fatality probability curves have been compared against other predictions. The agreement with the models of Jarrett and Hewkin is sufficiently good to provide some confidence in the methodology used.

## 7 REFERENCES

1. Baker, W.E., Cox, P.A., Westine, P.S., Kulesz, J.J. and Strehlow, R.A. 'Explosion Hazards and Evaluation'. Elsevier Scientific Publishing Company, Oxford, 1983.
2. Biggs, J.M., 'Introduction to Structural Dynamics', McGraw Hill Book Company, New York, 1964.
3. Fletcher, E.R., Richmond, D.R. and Yelverton, J.T. 'Glass Fragment Hazard from Windows Broken by Airblast'. Lovelace Biomedical and Environmental Research Institute, 1980.
4. Nowee, J. 'Dynamic Failure Pressure and Fragmentation of Thermally Hardened Window Panes', TNO Report No. PML 1985 - C - 103, 1985.
5. Hewkin, D.J. 'Consequences of Pressure Blast - the probability of fatality inside buildings' US DoD Explosives Safety Seminar, Anaheim, CA-18-20 August 1992.
6. 'Derivation of Fatality Probability Functions for Occupants of Buildings Subject to Blast Loads. Interim Report (Phase 1)', WS Atkins Science and Technology, Report No. AM5033.003-R01
7. Puttock, J.S. 'Fuel Gas Explosion Guidelines - the Congestion Assessment Method', ICHME Symposium Series No 139, 1995.
8. 'Methods for the Determination of Possible Damage', CPR 16E, TNO, 1992.
9. Lees, F.P. 'Loss Prevention in the Process Industries. Volume 1.', Butterworths, 1989.
10. 'Fragment Hazard Criteria', Feinstein, D.I. from Minutes of the Explosives Safety Seminar (1971)
11. 'Glass Fragment Hazard from Windows Broken by Airblast' Fletcher, Richmond and Yelverton (1980)
12. 'Dynamic Failure Pressure and Fragmentation of Thermally Hardened Window Panes', Nowee, 1985 PML 1985-C-103, Prins Maurits Laboratorium, TNO, Technological Research
13. 'Breakage of Glass Windows by Explosions' D.K.Pritchard (1980),
14. 'Airblast Effect on Windows in Buildings and Automobiles on the Eskimo II event', Fletcher, E.K., Richmond, D.R. and Jones, R.K. Minutes of the Department of Defence Explosives Safety Seminar (15th), 1973.



15. 'Airblast Effect on Windows in Buildings and Automobiles on the Eskimo III event', Fletcher, E.K., Richmond, D.R. and Richmond, D.W. Minutes of the Department of Defence Explosives Safety Seminar (16th), September, 1974.
16. 'The response of glass windows to explosion pressures', Harris, R.J., Marshall, M.R. and Moppett, D.J. I.Chem.E.Symposium Series No. 49
17. 'Head Injury and Protection', D.H.Glaister from 'Aviation Medicine' Ernsting, J and King, P eds. Butterworths, 1988. ISBN 0-407-01470-5
18. 'The Breakage of Glass Windows by Gas Explosions' Mainstone, R.J., Building Research Station Current Paper, CP 26/71, September 1971.
19. 'Damage to glass panes from high explosive detonations', Rickard Forsen and Borje Selin, National Defence Research Establishment (FOA) February 1991. Report No. C 20832-2-3
20. 'Management of Hazards Associated with Location of Process Plant Buildings', API Health and Environmental Affairs Department, CMA Regulatory Affairs Department. API Recommended Practice 752 CMA Manager's Guide, First Edition, May 1995
21. 'Some Considerations on the Damage Criteria and Safety Distances for Industrial Explosions', Mercx, W.P.M., Weerheijm, J. and Verhagen, Th.L.A., TNO. Icheme Symposium Series No.124.
22. 'Structural Masonry Designer's Manual', Curtin, W.G., Shaw, G., Beck, J.K. and Bray, W.A. BSP. 2nd Ed., 1987.
23. British Standard 'Design Loading for Buildings. Part 1. Code of Practice for dead and imposed loads'. BS 6399: Part 1: 1984.
24. 'Management of Hazards Associated with Location of Process Plant Buildings'. API Recommended Practice 752, First Edition, May 1995.
25. 'The Effects of Simplification of the Explosion Pressure - Time History'. HSE & Steel Construction Institute, HMSO, 1992 (Offshore Technology Information 92 601).

**APPENDIX A**  
**SUMMARY OF LITERATURE SEARCH**

### HSE Blast Probits: Phase 3 Literature Search

Databases searched include: EMBASE  
MEDLINE  
Occ. Saf. & Health  
BRIX/FLAIR  
MHIDAS

Document Reference	Source	Obtained - Date
Pounds, CA and Smalldon, KW 'The distribution of glass fragments in front of a broken window and the transfer of fragments to individuals standing nearby' J Forensic Sci Soc Jul-Oct 1978, 18(3-4) p197-203	Database	2/4/96
Locke, J and Scranage, JK 'Breaking of Flat Glass - Part 3: Surface Particles from Windows' Central Research Establishment, Home Office Science Service, Aldermaston, Reading, UK Forensic Sci Int (Ireland), 1992, 57/1 (73-80)	Database	2/4/96
Locke, J and Unikowski, JA 'Breaking of Flat Glass - Part 1: Size and Distribution of Particles from Plain Glass Windows' Forensic Sci Int (Ireland), 1991, 51/2 (251-262)	Database	2/4/96
Luce, RJW, Buckle, JL and McInnes, I 'A study on the backward fragmentation of window glass and the transfer of glass fragments to individual's clothing' J Can Soc Forensic Sci (Canada), 1991, 24/2, (79-89)	Database	2/4/96
Lawrence, WE and Johnson, EE 'Design for limiting explosion damage' Chemical Engineering, Vol 81, No 1, pp96 - 104	Database	2/4/96
Lynn Beason, W, Meyers, GE and James, RW 'Hurricane related window glass damage in Houston' ASCE Journal of Structural Engineering, 1984, v110(12), 2843 - 57	Database	2/4/96
Pantelides, CP, Horst, AD and Minor, JE 'Postbreakage behaviour of heat strengthened laminated glass under wind effects' ASCE Journal of Structural Engineering, 1993, v119(2), 454-467	Database	2/4/96

Document Reference	Source	Obtained - Date
Pantelides, CP, Horst, AD and Minor, JE 'Postbreakage behaviour of architectural glazing in windstorms' Journal of Wind Engineering and Industrial Aerodynamics, 41-44 (1992) 2425 - 2435	Database	26/3/96
Ahsan Kareem 'Performance of cladding in Hurricane Alicia' ASCE Journal of Structural Engineering, 1986, v112(12), 2679 - 2694	Database	2/4/96
Mercz, WPM 'The effects of explosions on humans' Europex Newsletter. Sep 1990. no 13, Page 1 - 6		
Grossman, PUA and Mackenzie, CE 'Resistance of House Wall Sheeting to Flying debris' Division of Building Research Technical Paper No 15, Commonwealth Scientific and Industrial Research Organization, Melbourne, CSIRO 1977	Database	2/4/96
Ernsting, J and King, P 'Aviation Medicine' Butterworths, 1988. ISBN 0-407-01470-5	RAeSoc Library	2/4/96
DoD Explosives Safety Board. Minutes of the Explosives Safety Seminar (14th) February 1973		2/4/96
DoD Explosives Safety Board. Minutes of the Explosives Safety Seminar (13th) September 1971		2/4/96
DoD Explosives Safety Board. Minutes of the Explosives Safety Seminar (12th) August 1970		2/4/96
DoD Explosives Safety Board. Minutes of the Explosives Safety Seminar (11th) September 1969		2/4/96
Clancey, VJ 'The effects of explosions' I.Chem.E.Symposium Series No 71, pp 87-108	SG	2/4/96
Hunt, DLM and Wood, AJ 'The estimation of missile velocities following the failure of a vessel containing high temperature pressurised water' UKAEA Safety and Reliability Directorate report, SRD R 341, August 1987	SG	2/4/96

Document Reference	Source	Obtained - Date
Brighton, PWM 'Pressure produced by Instantaneous Chlorine Releases inside Building' UKAEA Safety and Reliability Directorate report, SRD R 467, March 1988	SG	2/4/96
Fletcher, ER, Richmond, DR and Jones, RK 'Airblast effects on windows in buildings and automobiles on the Eskimo II event' DDESB Seminar Minutes, 1973	HSE	3/96
Woodward, JL and Crossthwaite, PJ 'How to set explosion protection standards' Hydrocarbon Processing, December 1995	HSE	3/96
Baker, QA, Tang, MJ, Scheier, E and Silva, GJ 'Vapour cloud explosion analysis' AIChE 28th Annual Loss Prevention Symposium, Atlanta, Georgia, April 17-21 1994	Ref from Above	
Becht, C and Benteftifa, CA 'Improve building performance to survive vapor-cloud explosions' Hydrocarbon Processing, October 1995	Ref from Above	
Cates, A 'A non-specialist guide to semi-confined vapour cloud explosion' Int Conf Fire and Explosion Hazards; Energy Utilization, Gloucestershire, UK, May 1991	Ref from Above	



**MAIL ORDER**

HSE priced and free  
publications are  
available from:  
HSE Books  
PO Box 1999  
Sudbury  
Suffolk CO10 6FS  
Tel: 01787 881165  
Fax: 01787 313995

**RETAIL**

HSE priced publications  
are available from  
good booksellers

**HEALTH AND SAFETY ENQUIRIES**

HSE InfoLine  
Tel: 0541 545500  
or write to:  
HSE Information Centre  
Broad Lane  
Sheffield S3 7HQ

HSE home page on the World Wide Web:  
<http://www.open.gov.uk/hse/hsehome.htm>

**CRR 147**

**£72.00 net**

ISBN 0-7176-1434-4



9 780717 614349